APPENDIX A

WSMR TEST DETAILS

TABLE OF CONTENTS

LIST OF FIGURES

LIST OF TABLES

REFERENCES

There are no sources in the current document.

APPENDIX

Appendix A. WSMR Test Details

This Appendix provides a review of important aspects related to SPIGAT, the GNSS signal generation, and activities performed during the DOT test week at WSMR. Included are descriptions for generating the LTE signals, adjusting the mapping data to provide power measurements across the equipment test area, analysis demonstrating measured vs. expected power on the antenna floor, stability of power measurements over the test week, linearity of power over test limits, system calibration, antenna and cable measurements used in these analyses, and lastly, a summary of activities for the entire month at WSMR.

A.1   Interference System Development Considerations

The high level specifications for development of the SPIGAT capability are shown in Table A-1. These specifications and the test configuration at the EMVAF drove several critical decisions in development of SPIGAT. Three key issues were ensuring the maximum interference power could be achieved across the entire test area, automating the interference tests as well as system calibration and mapping, and lastly, ensuring interference signals were conditioned properly so GNSS equipment degradation could be attributed to the fundamental signal being generated and not unwanted emissions. Achieving the maximum power required a HPA that ultimately was provided by the support engineers at WSMR. Additionally, satisfying maximum power also required careful consideration of component insertion losses and ultimately sourcing a standard gain horn designed for the interference frequency range to be tested. The desire to complete the test effort in a single week dictated automation and sourcing an RF switch capable of handling these power levels and frequencies to be tested. And lastly, the filters required performance characteristics to sufficiently attenuate OOBE when generating LTE signals and led to development of 22 RF passband cavity filters specifically for this test effort. Each of these areas is touched on in later sections of this Appendix.

Table A-1: Interference Transmitter Specifications

Name	Value	Unit
Range of selectable center frequencies	[1475, 1490, 1505, 1520, 1525, 1530, 1535, 1540, 1545, 1550, 1555, 1575, 1595, 1615, 1620, 1625, 1630, 1635, 1640, 1645, 1660, 1675]	MHz
Automation capability	Software controlled selection of center frequency, signal type, and transmit power	N/A
Interference signal generation capability	White noise or LTE	N/A

Number of selectable bandwidths	2	N/A
3 dB bandwidth (Signal Type-1)	1	MHz
3 dB bandwidth (Signal Type-2)	Consistent with LTE	N/A
Maximum power the setup is capable of delivering at any receiver location	≥ -10	dBm

Another consideration for this testing was the LTE waveforms to be used for the downlink and uplink signals. The LTE package offered by Keysight for its VSG products was considered originally but ultimately it was determined the MATLAB emulation, which also adheres to the LTE standard, had sufficient fidelity for this test effort. MATLAB generated time series representation of the downlink and uplink signals and these were converted so they could be loaded into the VSG for continuous replay. The actual MATLAB commands used to generate the downlink and uplink waveforms are shown below in respective order.

```
[rmcwaveform_DL,rmcgrid_DL,rmccfgout_DL] =
lteRMCDLTool(rmcconfig_DL,rand([1,10000]));
    [rmcwaveform_UL,rmcgrid_UL,rmccfgout_UL] =
lteRMCULTool(rmcconfig_UL,rand([1,10000]));
```

The associated configuration MATLAB structures used in the commands above are shown in Table A-2. The duration of the uplink and downlink files was two seconds each and these were played out continuously end to end from VSG memory.

Table A-2: LTE Parameters definition for the downlink and uplink signals

Downlink Parameters Definition	Uplink Parameters Definition
Rmcconfig_DL.RC='R.2'	Rmcconfig_UL.RC = 'A3-5'
Rmcconfig_DL.NDLRB=50	Rmcconfig_UL.NULRB = 50
Rmcconfig_DL.CellRefP=1	
Rmcconfig_DL.NCellID=0	Rmcconfig_UL.NCellID = 0
Rmcconfig_DL.CyclicPrefix='Normal'	Rmcconfig_UL.CyclicPrefixUL = 'Normal'
Rmcconfig_DL.CFI=2	
Rmcconfig_DL.Ng='Sixth'	
Rmcconfig_DL.PHICHDuration='Normal'	
Rmcconfig_DL.NFrame=0	Rmcconfig_UL.NFrame = 0
Rmcconfig_DL.NSubframe=0	Rmcconfig_UL.NSubframe = 0
Rmcconfig_DL.TotSubframes=2000	Rmcconfig_UL.TotSubframes = 2000
	Rmcconfig_UL.CyclicShift = 0
	Rmcconfig_UL.Shortened = 0
	Rmcconfig_UL.Hopping = 'Off'
Rmcconfig_DL.OCNG = 'On'	Rmcconfig_UL.SeqGroup = 0

Rmcconfig_DL.Windowing = 16	Rmcconfig_UL.Windowing = 16
Rmcconfig_DL.DuplexMode = 'FDD'	Rmcconfig_UL.DuplexMode = 'FDD'
	Rmcconfig_UL.NTxAnts = 1
Rmcconfig_DL.SerialCat = 1	
Rmcconfig_DL.SamplingRate = 15360000	Rmcconfig_UL.SamplingRate =15360000
Rmcconfig_DL.Nfft = 1024	Rmcconfig_UL.Nfft = 1024
Rmcconfig_DL.PDSCH.TxScheme = 'Port0'	
Rmcconfig_DL.PDSCH.Modulation = {'QPSK'}	Rmcconfig_UL.PUSCH.Modulation = 'QPSK'
Rmcconfig_DL.PDSCH.NLayers = 1	Rmcconfig_UL.PUSCH.NLayers =1
Rmcconfig_DL.PDSCH.Rho = 0	
Rmcconfig_DL.PDSCH.RNTI = 1	Rmcconfig_UL.RNTI = 1
Rmcconfig_DL.PDSCH.RVSeq = [0 1 2 3]	Rmcconfig_UL.PUSCH.RVSeq = [0 2 3 1]
Rmcconfig_DL.PDSCH.RV = 0	Rmcconfig_UL.PUSCH.RV = 0
Rmcconfig_DL.PDSCH.NHARQProcesses = 8	Rmcconfig_UL.PUSCH.NHARQProcesses = 8
Rmcconfig_DL.PDSCH.NTurboDecIts = 5	Rmcconfig_UL.PUSCH.NTurboDecIts = 5
	Rmcconfig_UL.PUSCH.DynCyclicShift =0
	Rmcconfig_UL.PUSCH.NBundled =0
	Rmcconfig_UL.PUSCH.BetaACK =2
Rmcconfig_DL.PDSCH.CSIMode = 'PUCCH 1-1'	Rmcconfig_UL.PUSCH.BetaCQI = 2
Rmcconfig_DL.PDSCH.PMIMode = 'Wideband'	Rmcconfig_UL.PUSCH.BetaRI = 2
Rmcconfig_DL.PDSCH.PRBSet = [0:49]	Rmcconfig_UL.PUSCH.PRBSet = [0:49]
Rmcconfig_DL.PDSCH.TrBlkSizes = [4392 4392 4392 4392 4392 0 4392 4392 4392 4392]	Rmcconfig_UL.PUSCH.TrBlkSizes = [5160 5160 5160 5160 5160 5160 5160 5160 5160 5160]
Rmcconfig_DL.PDSCH.CodedTrBlkSizes = [12960 13800 13800 13800 13800 0 13800 13800 13800 13800]	Rmcconfig_UL.PUSCH.CodedTrBlkSizes = [14400 14400 14400 14400 14400 14400 14400 14400 14400 14400]
	Rmcconfig_UL.PUSCH.PMI = 0
	Rmcconfig_UL.PUSCH.OrthCover = 'On'

A.2   Chamber Mapping

8

Chamber mapping determined RF power across the chamber floor and was ultimately used to adjust SPIGAT test event summary files to establish power incident at each device tested. Mapping was also accomplished with the GNSS signal generation system to demonstrate power uniformity over the test area. The approach for mapping was to first establish a grid that encompassed equipment placed in the test area. Figure A-1 shows the grid utilized in this effort with 45 measurement points (blue diamonds) spaced approximately four feet apart. The mapping grid origin for purposes of labeling points is at the bottom left corner of this figure (point X=0 and Y=0). Each axis spanned values from 0 to 6. For reference, the mapping point at the center of the grid was identified as P33 and was directly below the interference transmit and GNSS antennas and P03 as will be described in a later section was the reference point used for system calibrations. The red rectangles represent the area used for equipment under test.

The mapping and calibration procedure used a cavity backed spiral antenna mounted on a tripod, calibrated RF cable, and a spectrum analyzer. The characteristics of the cavity backed spiral are provided in a later section along with cable and transmit antenna characterizations. Power measurements were made by positioning the tripod over a designated mapping point, boresighting the cavity backed spiral on the transmit antenna using a laser pointer attached to the antenna, having the interference generation and GNSS systems generate tones at each required frequency, and lastly, having the spectrum analyzer step through each frequency and measure the power of these tones. The interference signal generation system used the system calibration file (described in a later section) to target a power level of -40 dBm as measured at the spiral antenna. Measurements were taken with analyzer settings; auto-calibration disabled, preamplifier ON with internal attenuation fixed at 6 dB (lowest available), span of 1 MHz using 1001 points centered at the measurement frequency with resolution and video bandwidths of 5 kHz, averaging ON and set to four frames, and using the RMS detector (see Table A-3).
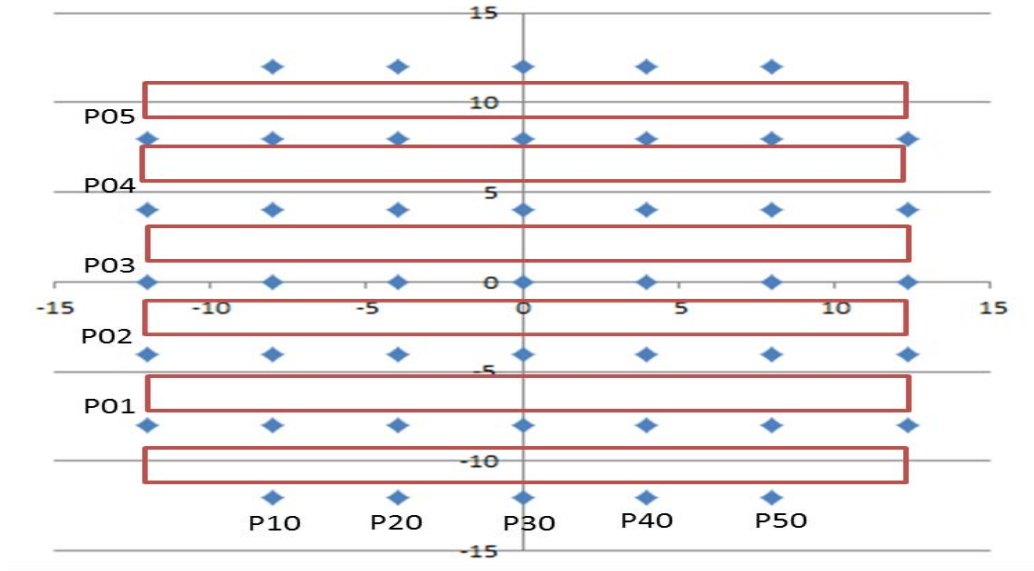
Figure A-1: Chamber Mapping Grid

Table A-3: Example of Instrument settings for 1675 MHz

att:	+6.00E+00	mkx:	+1.6750000000000000E+009
autoatt:	0	mky:	-5.38870E+01
autocal:	OFF	pdiv:	+1.000E+01
avgstate:	1	peaky:	0
cont:	0	points:	+1001
det:	AVER	preamp:	1
fcent:	+1.6750000000000000E+009	rbw:	+5.10000000E+003
fref:	EXT	reflev:	-3.400E+01
fspan:	+1.0000000000000000E+006	sweep:	+1.46600000E-001
fstart:	+1.6745000000000000E+009	trace:	WRIT
fstop:	+1.6755000000000000E+009	vavg:	+4
		vbw:	+5.10000000E+003

A.3   Chamber Mapping Comparison and Stability

Chamber mapping at all 45 points was accomplished at the beginning (4/25) and end (4/28) of DOT testing with all equipment installed in the test area. Mapping was also accomplished with all equipment removed during the prior week (4/22) to establish variation introduced with GNSS equipment in the test area. (Section A.8 provides a high level review of activities conducted for the entire month of April at WSMR). For processing the mapping data, the power at each frequency was adjusted for the target power of -40 dBm, spiral antenna gain at boresight and calibration cable loss. Additionally, the calibration antenna was approximately 1.5 feet above the blue absorbing material where GNSS equipment was placed for test. To account for this difference, an additional 0.5 dB was included for this height differential to reflect the additional free space loss. (Note the face of the transmit horn antenna was 25 feet above the blue absorbing material so at these frequencies the difference of 1.5 feet equates to approximately 0.5 dB less power received for equipment on the absorber compared with cavity backed spiral measured power.) Ultimately, the corrected mapping measurements are interpolated to each equipment test location and added to the interference system control file to determine the unique power received at each of these locations.

The mappings performed on 4/25 and 4/28 were compared and found to be very consistent. Figure A-2 shows a scatter plot of mapping location differences per frequency and demonstrates the variation across these dates was within plus or minus approximately 0.5 dB. When the differences are histogrammed by magnitude however (see Figure A-3), it can be observed that over 98% of the mapping points agreed to within plus or minus 0.25 dB. Figure A-4 further compares the power differences spatially and shows the lower left and upper right corners had the largest variations. The final corrected mapping values provided for DOT receiver processing represented the average of mapping from 4/25 and 4/28.

A mapping comparison was also made between 4/22 when no equipment was installed in the test area and 4/25 to get a sense for how much the equipment affected received power. This can be seen in Figure A-5 with a scatter plot of these differences. Notice the scale is double in this figure compared with the previous scatter plot and differences were as large as plus or minus 1 dB. Figure A-6 shows the histogram of the differences and in this comparison approximately 75% of the mapping points agreed to within plus or minus 0.25 dB. The spatial comparison is shown in Figure A-7. The largest differences are generally in the upper left corner which could be due to concentration of equipment towards this end of the chamber. It should be noted that increased variation between a clean chamber test area and one populated with over 80 pieces of equipment under test is not surprising. This level of variation is actually considered very good and was confirmed by the WSMR test engineers based on their experience with this chamber.
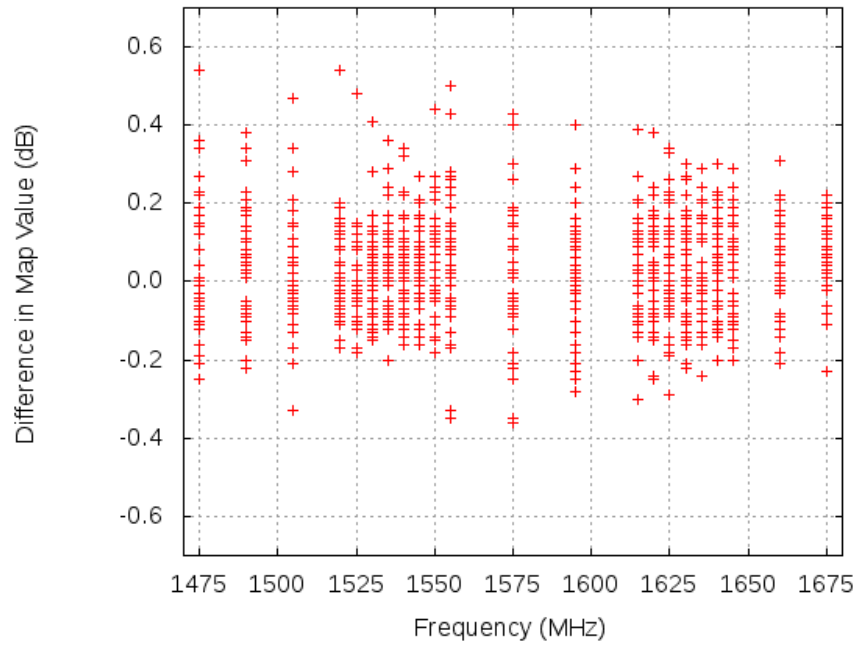
Figure A-2: Mapping Point differences between April 25th and April 28th
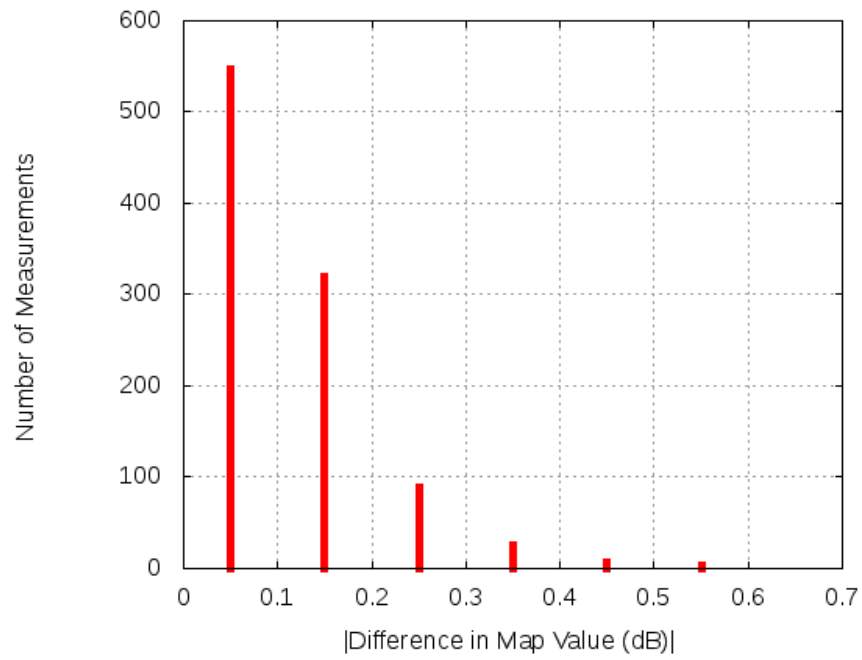
Figure A-3: Histogram of Differences between April 25th and April 28th Mappings
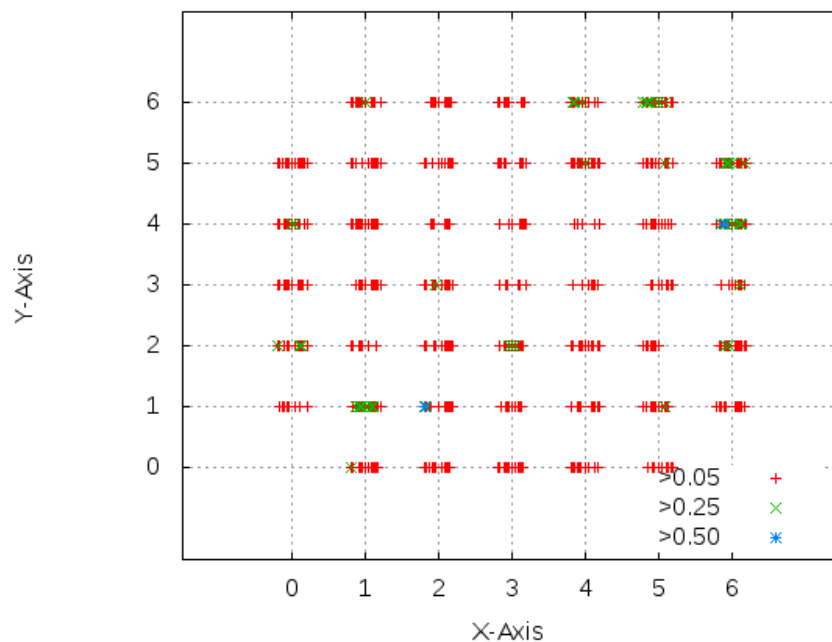
Figure A-4: Power Differences across the Test Grid between April 25th and April 28th Mappings (freqs. run from 1475 to 1675 at each point from left to right)
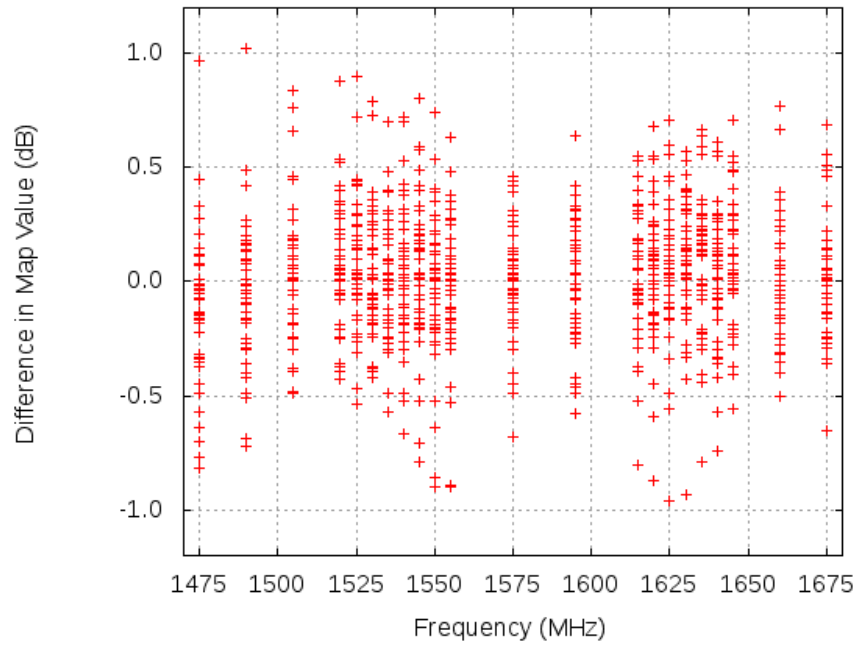
Figure A-5: Mapping Point differences between April 22nd and April 25th
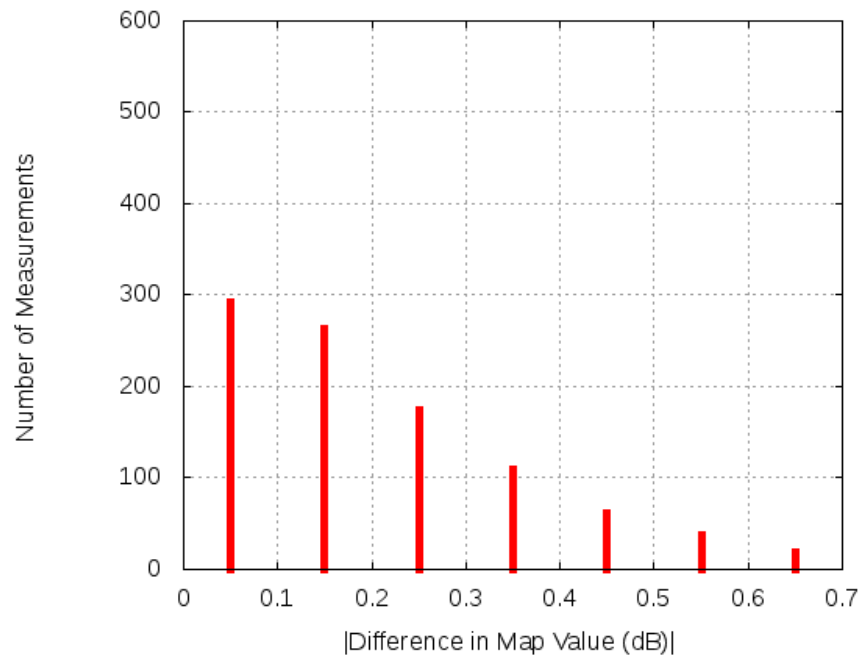
Figure A-6: Histogram of Differences between April 22nd and April 25th Mappings
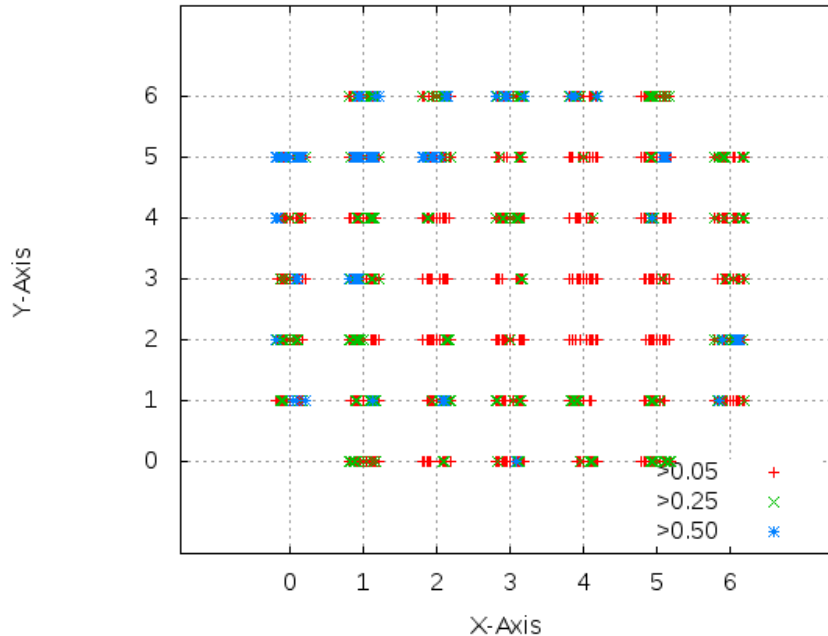
Figure A-7: Power Differences across the Test Grid between April 22nd and April 28th Mappings (freqs. run from 1475 to 1675 at each point from left to right)

One additional comparison noteworthy from mapping is how interference power varied over the course of the DOT test week. The previous analysis demonstrated the variation for all 45 mapping locations at the start and end of testing. During the test week, a mapping procedure was generally executed at reference location P03 in the AM and PM of each day as a confidence check on test stability. Figure A-8 shows all P03 mappings during DOT week after being corrected for target power, cavity backed spiral gain, calibration cable and the same 0.5 dB mentioned above for height differential of the calibration antenna. The variation from morning to evening and day to day was extremely well behaved with all measurements agreeing within 0.4 dB. For comparison purposes, the mapping at the reference location was also provided for 4/22 when no equipment was present in the test area. It is important to note that the calibration antenna was moved numerous times over each day either for full mapping or to allow participants access to the test area. Temperature was also recorded over the course of the one month test effort and observed to vary by as much as 6 degrees C. This temperature variation would be another source influencing daily power measurement variation.

17
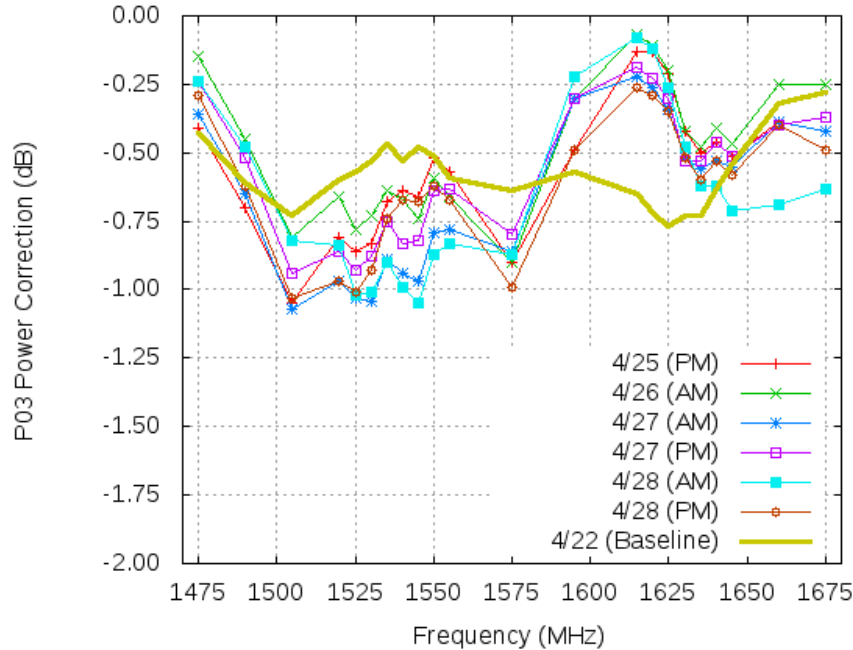
Figure A-8: Comparison of Mapping Corrections from DOT Test Week

A.4 System Calibration

Calibration of the interference and GNSS systems were handled differently. This section describes the interference system calibration only. The calibration procedure determined the reference point on the grid as well as VSG settings to achieve desired power for each of the 22 interference test frequencies. The reference point for system calibration was determined by finding the location receiving the least power from among grid points P03, P30, P36, and P63. These peripheral points represent roughly the 3 dB beamwidth of the transmit antenna and therefore selecting the location with the least received power ensures the majority of the test area will receive the desired interference power or higher. Location P03 was determined as this point and was used as the reference throughout all chamber testing. The calibration procedure was very similar to mapping except it used a notional VSG setting as a starting point and then computed power corrections per frequency to achieve -40 dBm at P03. This calculation used the notional VSG setting, cavity backed spiral antenna gain, and calibration cable loss. During the two week check out period prior to the formal test numerous system calibrations were executed. Based on consistency of these measurements it was decided to take the linear average of these

values to fix the calibration table. The dates used in this average are provided below. Table A-4 provides the average calibration values.

cal_p03_20160408_144622, cal_p03_20160411_144033, cal_p03_20160412_142537, cal_p03_20160413_131930, cal_p03_20160415_180323

Table A-4: Calibration Values inserted into measlabtable.cfg:

Frequency (MHz)	Cal. Value (dB)	Cal. Value (dB)	Frequency (MHz)
1475	-3.30	1575	-4.90
1490	-3.21	1595	-5.29
1505	-3.34	1615	-6.08
1520	-3.69	1620	-6.03
1525	-3.50	1625	-6.27
1530	-3.61	1630	-6.11
1535	-3.59	1635	-6.01
1540	-3.70	1640	-6.22
1545	-3.78	1645	-6.52
1550	-4.09	1660	-6.53
1555	-4.28	1675	-6.71

One additional consideration for compensation of calibration values was use of a CW tone at center frequency versus the LTE signal. The concern was the LTE signal would have additional signal attenuation at filter edges due to roll-off vice the CW tone at center frequency. The signal power loss for the LTE signal versus the single-tone was analyzed for each of the filters (6 and 8 section filters) and the maximum difference was 0.17 dB. Given this small value it was decided adding a compensation term for LTE signal attenuation was not warranted.

A.5   Interference System Linearity

The interference linearity procedure measured interference power over the entire range for each test frequency. This procedure was executed from P03 and stepped through the full range of power in 2 dB steps with a CW tone. For the interference frequencies furthest from the RNSS band the range was -80 to -10 dBm, for the three frequencies closet to and just above and below the RNSS band the range was -100 to -30 dBm, and lastly, for the two frequencies in the RNSS band the range was -130 to -60 dBm. As with calibration and mapping, the spiral antenna, calibration cable and spectrum analyzer were used to measure and record each power measurement. Figure A-9 shows measured power corrected for spiral antenna gain and cable loss

versus target power commanded by the interference system. This figure shows all frequency and power measurements together and demonstrates the expected linear relationship from approximately -100 dBm and higher. Below -100 dBm, the spectrum analyzer was not able to accurately resolve the tone being received due to the measurement system noise floor. To further demonstrate interference system performance, Figure A-10 shows the difference between targeted and measured power for select frequencies. These figures show that over the power range tested the interference system faithfully delivered intended power to within approximately 0.5 dB.
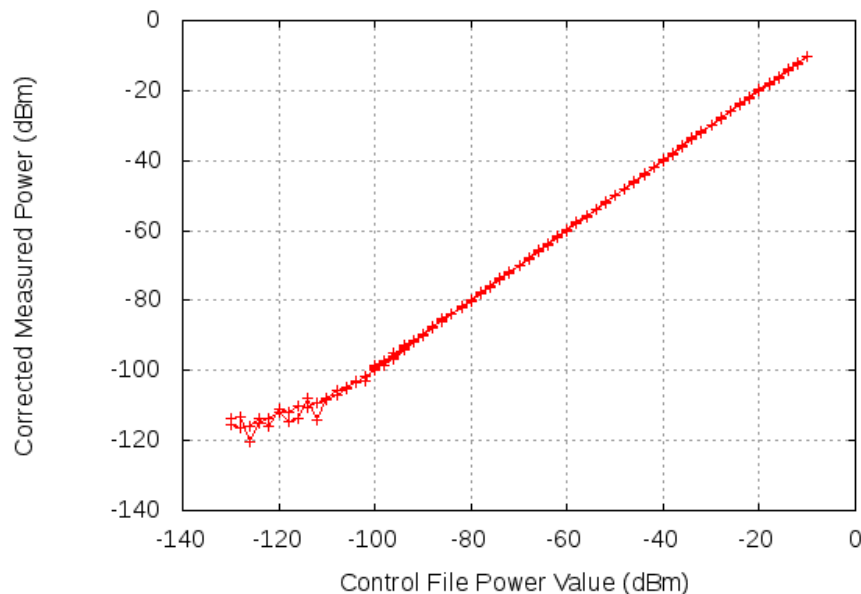
Figure A-9: Comparison of Targeted Power (Recorded in Control File) and Measured Power corrected for Spiral Antenna Gain and Cable Loss
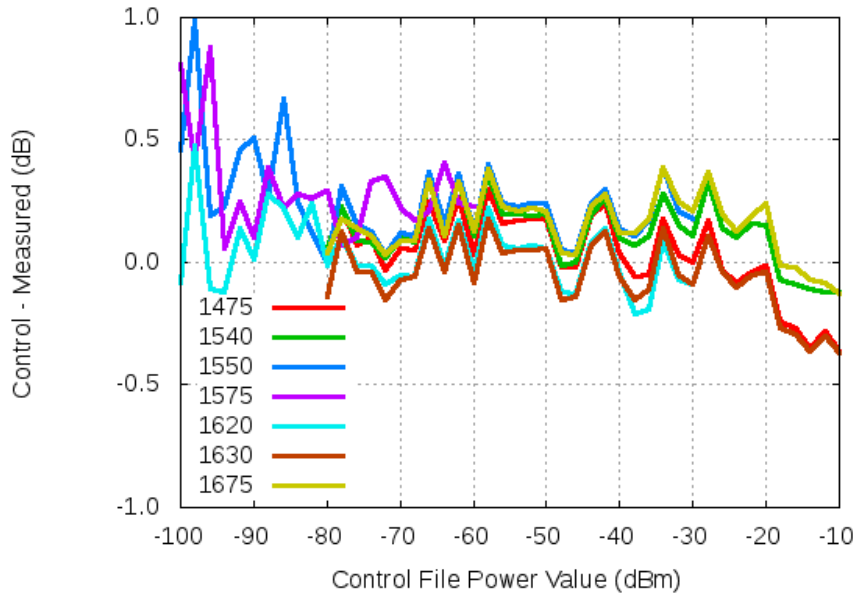
Figure A-10: Comparison of Targeted Power (Recorded in Control File) Differenced from Measured Power for Select Frequencies

A.6 Comparison of Measured vs. Predicted Power

The measured power versus predicted power was estimated by making a special calibration of the SPIGAT system. In this instance, interference system output was routed through a 60 dB attenuator and into the spectrum analyzer used with the cavity backed spiral for making measurements on the chamber floor. Therefore, cable/antenna to the transmit antenna and cable/antenna from the receive antenna were bypassed (see Figure A-11) to obtain a direct power measurement at the output of the interference system. The mapping procedure was executed as if the calibration antenna was being utilized in the test area. The predicted power was then computed using measured power from the spectrum analyzer corrected for the 60 dB attenuator and associated cables, cable loss to the transmit antenna, transmit antenna gain, and free space loss to the calibration antenna. This predicted power was then compared with measurements made with the calibration antenna located at P33 which is directly below the transmit antenna (peak beam).

$$FSL = -27.55 + 20 \log (f_{MHz}) + 20 \log (R_{meter})$$

21

R_{meter} = 7.16m (WSMR indicated face of horn to top of blue absorbing material directly below is 25'. Calibration antenna is 1.5' above absorbing material.)

Figure A-12 shows the result of the comparison using mapping data from 4/22 when the chamber was clear of any test equipment. The figure demonstrates very good agreement between predicted and measured power within approximately 0.5dB.
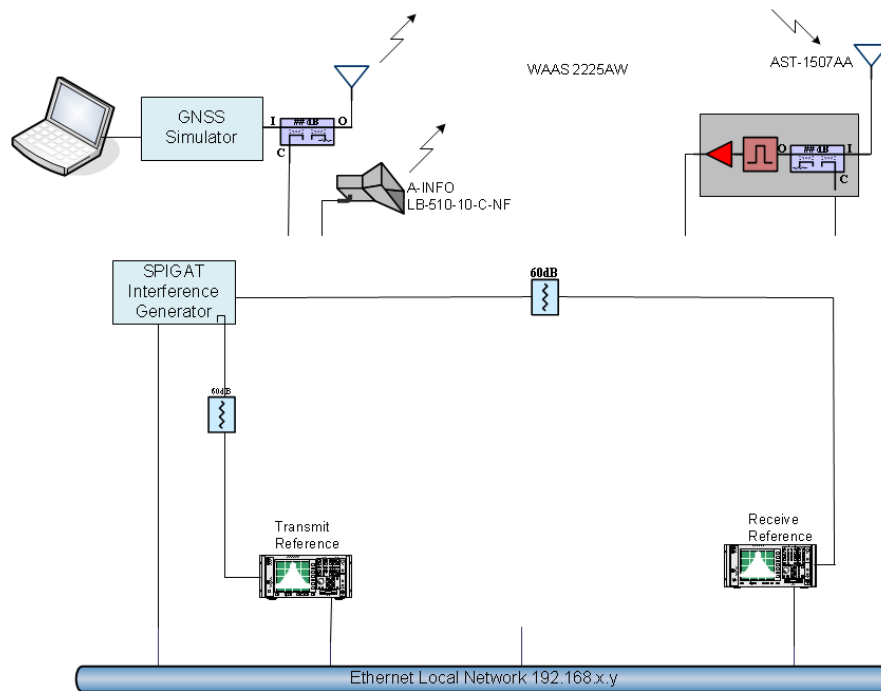
Figure A-11: Diagram of Special Test where Transmit and Receive Antenna Paths were Bypassed
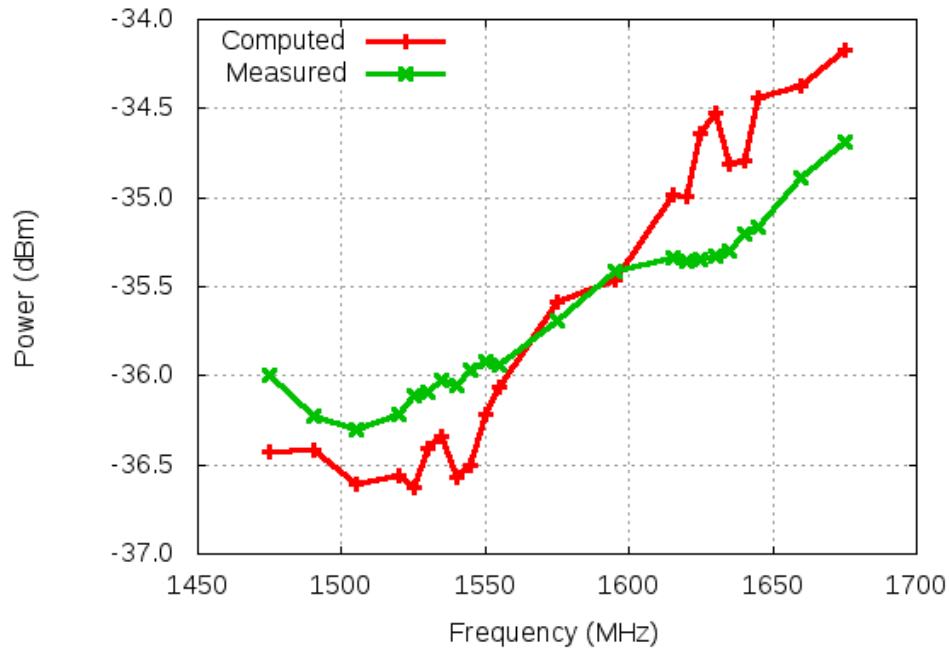
Figure A-12: Measured Power at P33 (corrected for spiral gain and calibration cable) compared with Predicted Power (interference system output power, horn antenna gain, horn cable loss, and Free Space Loss)

A.7   SPIGAT Antenna Characterizations

The Cavity Backed Spiral (Cobham AST-1507AA) and Standard Gain Horn (A-Info LB-510-10-C-NF) antennas used in the test effort were provided to Leading Systems Technologies (LST) of Fairfax, VA in March 2016 for gain and pattern characterizations. Characterization of the spiral is key since it is required to calibrate received power of interference and GNSS signals across the chamber test area while characterization of the horn is also desired to validate A-info's product data sheet and assist with link budget computations.

A.7.1   AST-1507AA

The critical estimates from the LST characterization in support of the ABC test effort are measurements when the spiral is boresighted on the source. The orientation of the Cobham spiral for testing at LST is provided in Figure A-13. The Figure represents the view from the back of the antenna in the LST anechoic chamber and in this illustration the green dashed line and the green arrow represent the axis of rotation for beam pattern observations. The beam pattern measurements off boresight are not provided in this note but the 3 dB beamwidth was determined to be approximately 80 degrees. For boresight characterization, the spiral antenna was rotated sequentially from 0, 30, 45, 60, 90, 120, 135 and 150 degrees about the axis directed toward the source. The orange rectangle represents the TNC female connector, which was positioned facing up with respect to the ground as shown for the 0 degree orientation. The source antenna was vertically polarized for these measurements due to better performance in this chamber for the frequencies of interest. The frequency response of the spiral was measured from 800 to 2000 MHz inclusive of the frequencies of interest for ABC testing from 1227 to 1675 MHz.

Figure A-14 provides spiral antenna gain characteristics when boresighted at the source. The similar response for each orientation of this antenna demonstrates its excellent axial ratio properties. It is also interesting to note that variation with respect to antenna orientation above 1450 MHz is on the order of 0.25 dB which is reportedly approaching the accuracy limits for the LST chamber. Table A-5 provides average gain and axial ratio versus frequencies required in the ABC test effort. There are 22 frequencies utilized for interference generation and three specified for GNSS antenna mapping. For purposes of completeness, the insertion loss of the RF cable used at WSMR between the cavity backed spiral and the spectrum analyzer for mapping and calibration acitivies has been included in this same table.
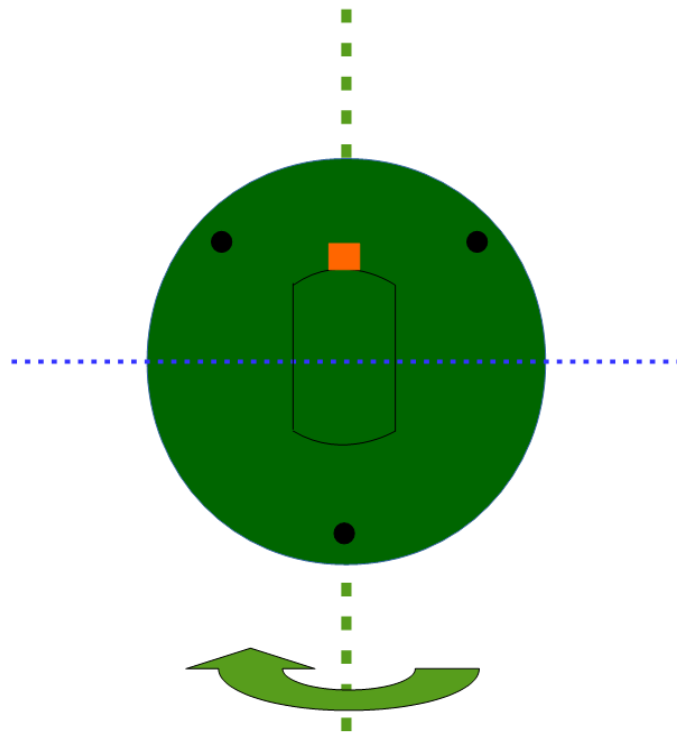
Figure A-13: AST-1507AA Positioning; Back View
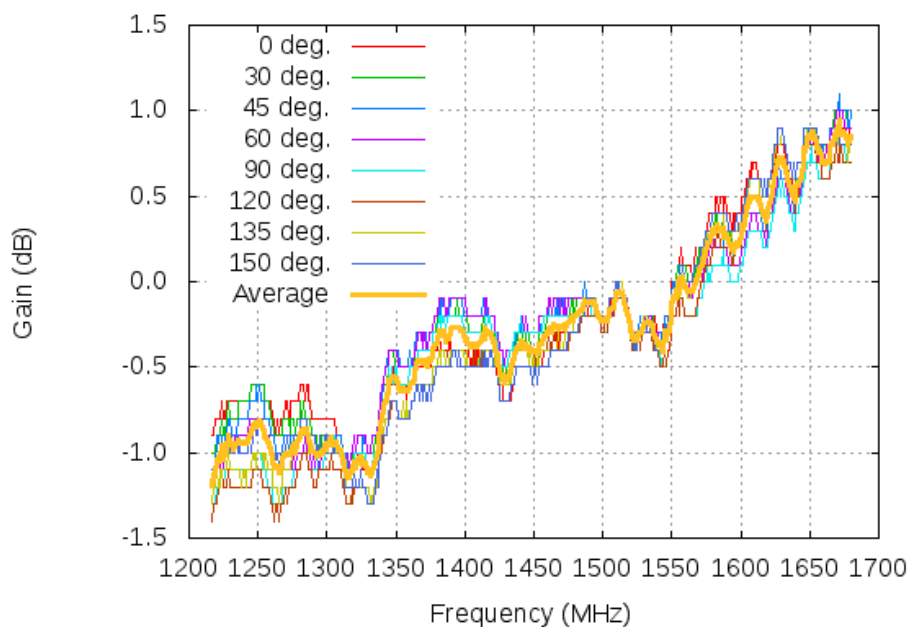
Figure A-14: AST-1507AA Boresight Measurements

Table A-5: AST-1507AA, Serial #174

Frequency (MHz)	Gain @ Boresight (dBil)	Axial Ratio (dB)	Cable Loss (dB)
1227*	-0.98	0.50	7.76
1475.	-0.24	0.20	8.44
1490.	-0.11	0.10	8.42
1505.	-0.18	0.10	8.45
1520.	-0.28	0.10	8.52
1525.	-0.34	0.10	8.54
1530.	-0.24	0.10	8.57
1535.	-0.25	0.10	8.60
1540.	-0.35	0.10	8.63
1545.	-0.29	0.20	8.64
1550.	-0.16	0.20	8.66
1555.	-0.07	0.30	8.72
1561*	-0.06	0.30	8.74
1575.	0.21	0.30	8.76

1595.	0.17	0.30	8.78
1605*	0.45	0.40	8.76
1615.	0.44	0.30	8.75
1620.	0.41	0.30	8.75
1625.	0.65	0.30	8.77
1630.	0.73	0.30	8.79
1635.	0.56	0.30	8.83
1640.	0.54	0.20	8.87
1645.	0.69	0.20	8.88
1660.	0.70	0.20	9.00
1675.	0.86	0.30	9.08

*GNSS Antenna Mapping Frequencies for ABC Test

A.7.2 LB-510-10-C-NF

The A-Info horn antenna gain and pattern performance were characterized at two source antenna orientations. For this testing, the source antenna and A-info polarizations were matched and the horn was rotated to measure pattern response. Figure A-15(a) shows the A-Info position for horizontal polarization measurements and (b) shows the position for vertical polarization measurements. The frequency response of the horn was measured from 800 to 2000 MHz but the frequencies of interest are primarily 1475 to 1675 MHz. Figure A-16 shows the horn gain at boresight for vertical polarization and Figure A-17 shows beam pattern response for the same polarization. Comparing these measurements with the A-Info product specification show a reasonably good match.

(a)   (b)
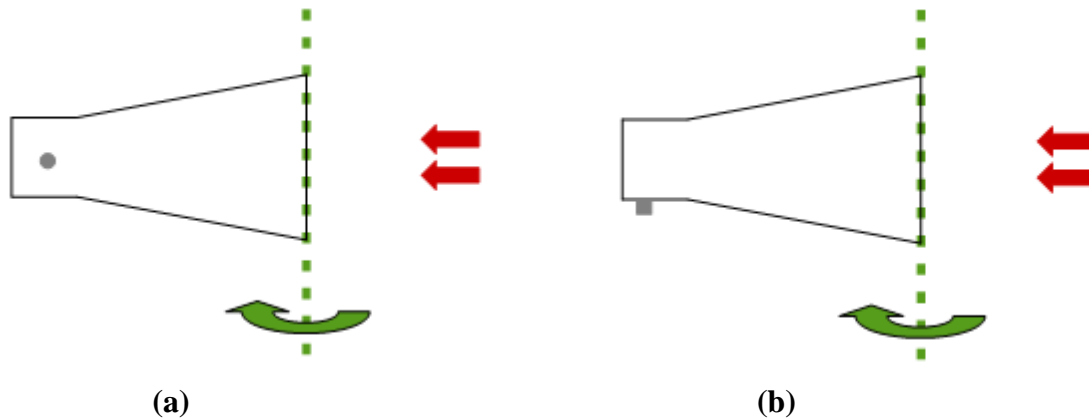
**Figure A-15: (a) A-Info Horizontal Position Side View,
(b) A-Info Vertical Position Side Vie**
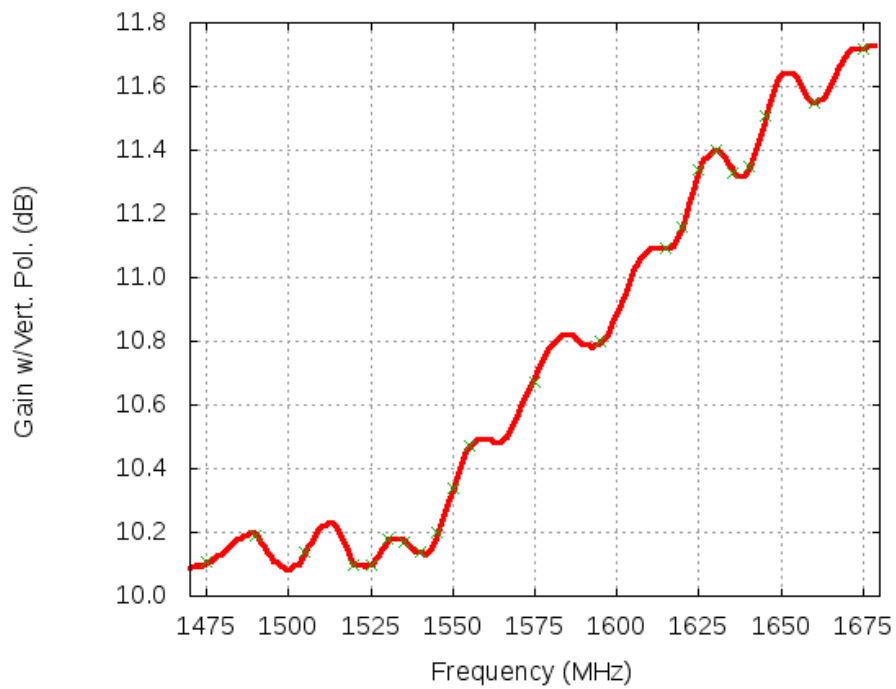
Figure A-16: LB-510-10-C-NF Vertical Gain @ Boresight vs. Frequency
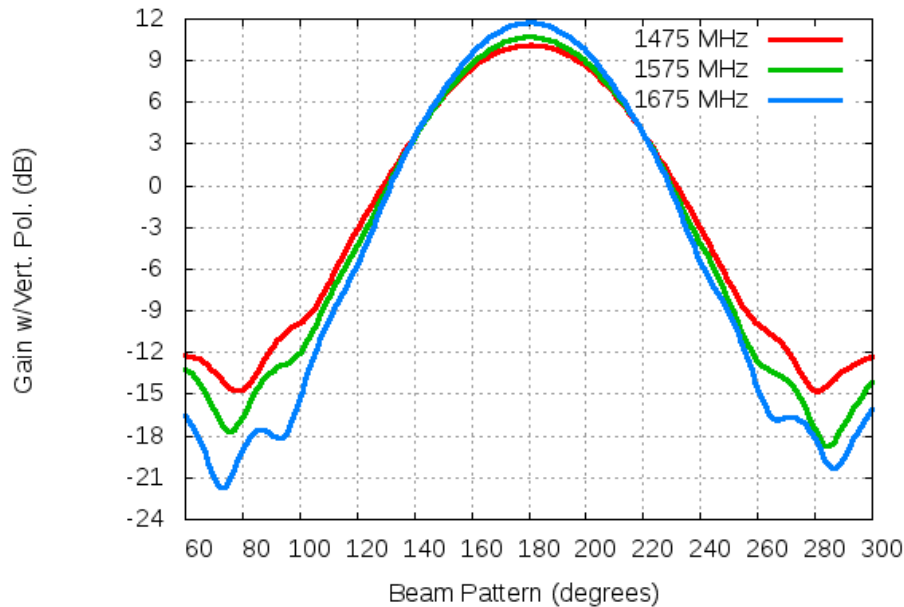
Figure A-17: LB-510-10-C-NF Vertical Pattern @ 1475, 1575 and 1675 MHz

A.8 WSMR Activity Summary

Table A-6 summarizes the activities for the entire month spent at WSMR. "F-Map" was a complete 45 point mapping used in the final corrections of SPIGAT event summary files.

Table A-6: Summary of WSMR Activities for April ABC Testing (4/4-4/28)

Day	AWGN	LTE	In-band	IMD	C/No	5-Map	A-Map	F-Map	P03 Cal/ Map	Set-up/ Remove
M T W Th	Arrived, unpacked equipment, installed transmit antennas, established grid, characterized HPA and cables, dry-ran calibration and mapping, calibrated GNSS signals. Determined 1575 and 1595 MHz AWGN tests needed separate runs due to inherent noise of HPA in-band. Adjusted GNSS antenna lower at end of the 7th to address reflections off horn (final location).									
F M[2]		4/08[1]	4/11	4/11	4/08		4/08 4/11		4/08 4/11	

29

T		4/12		4/12	4/12	4/12	4/12		4/12	
W	4/13							4/13	4/13(2)	
Th										Set-up
F								4/15	4/15[4]	
M	4/18		4/18		4/18				4/18(2)	
T	4/19	4/19							4/19(2)	
W		4/20		4/20	4/20	4/20			4/20	
Th		4/21[3]		4/21	4/21	4/21			4/21	
F								4/22	4/22	Remove
M					4/25			4/25	4/25	Set-up
T	4/26	4/26							4/26	
W	4/27	4/27							4/27	
Th			4/28	4/28	4/28			4/28	4/28	Remove

1-"Eared" version of Type 2 LTE signal. All other Type-2 runs were with no "Ears".
2-Characterization (system linearity) test run on 4/11.
3-No L2 signals.
4-Final calibration table established for all follow-on testing. Full mapping on 4/15 used this table.

Checkout
DOD
Civil

A.9   Chamber OOBE

The fundamental components of the SPIGAT include a VSG to generate interference signals and an HPA to provide sufficient amplification to achieve desired test levels. Given the limited ACLR of a typical VSG and the potential for spectral regrowth due to HPA nonlinearity at high input power, bandpass cavity filters were specified for SPIGAT with sufficient out of band rejection to ensure that receiver CNR measurements would reflect degradation caused by the fundamental of the interference, exclusive of any OOBE produced. The following test data and analysis demonstrate that the OOBE suppression provided by SPIGAT during LTE radiated tests performed at WSMR was sufficient to prevent receiver CNR degradation due to OOBE in the RNSS band.

In SPIGAT the interference signal passes from the VSG through a programmable attenuator and into the HPA. The amplified signal then passes through a bandpass cavity filter (specific to the signal frequency and selected by RF switch) before being directed to devices under test. At

WSMR the signal was routed through a long cable to the transmit antenna where it was radiated toward antennas on the chamber floor.

To assess the adequacy of OOBE suppression, spectra at the output of the HPA were recorded via spectrum analyzer (connected through a 60 dB pad). Spectra were recorded for a range of input power levels by fixing the signal power at the VSG while adjusting the programmable attenuator in 2 dB increments over the desired range. These measurements were taken while generating the downlink signal at 1550 MHz as this is the LTE test signal closest to the RNSS band and, therefore, most relevant to the OOBE question. The expansion of spectral regrowth as signal power increases is apparent from a suite of such measurements shown in Figure A-18.
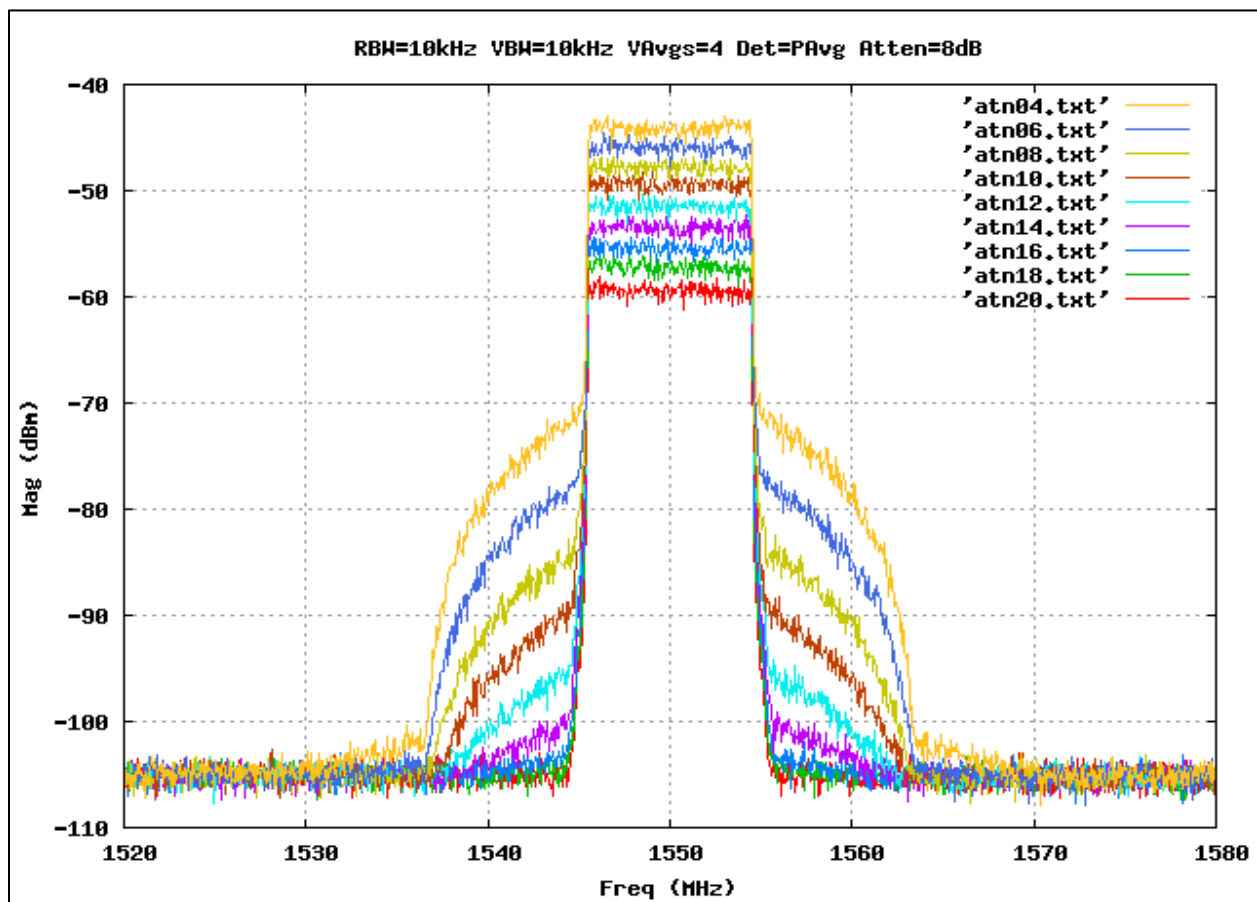
Figure A-18: Spectra Showing Expanding Regrowth for Increasing HPA Input Power

The spectra thus recorded with the 60 dB pad are mapped to test levels by comparing VSG and attenuator settings with those set during radiated tests. Table A-7 shows the correspondence. Given VSG power fixed at 0 dBm (for regrowth spectra), the spectrum that corresponds to a

radiated test level is the one with attenuation nominally equal to the test attenuation less the test VSG power. As an example, radiated tests of the 1550 MHz signal at -30 dBm are achieved with VSG power of -5.91 dBm and 20 dB attenuation. Given VSG power fixed to 0 dBm, the corresponding regrowth measurement has nominal attenuation of 26 dB.

Table A-7: Attenuation for Regrowth Spectra to Correspond to Radiated Tests

	radiated tests				regrowth measurements		
	A	B		C=A-B	D	E=D-C=B-A	~E
	test	VSG		attenuated	VSG	required	nominal
frequency	level	power	Attenuation	power	power	attenuation	attenuation
[MHz]	[dBm]	[dBm]	[dB]	[dBm]	[dBm]	[dB]	[dB]
1550	-30	-5.91	20	-25.91	0	25.91	26
1620	-30	-3.97	20	-23.97	0	23.97	24
1550	-10	-5.91	0	-5.91	0	5.91	6
1620	-10	-3.97	0	-3.97	0	3.97	4
1535	-10	-6.41	0	-6.41	0	6.41	6
1630	-10	-3.89	0	-3.89	0	3.89	4

As noted above, regrowth spectra were recorded only for interference at 1550 MHz. In the following, results presented for 1620 MHz (and other frequencies) were achieved by shifting data taken at 1550 MHz. This seems appropriate because even though 1550 and 1620 MHz interference signals were distinctly generated during radiated tests using the LTE downlink and uplink signals, respectively, both signals produce a flat 9 MHz wide pedestal with steep roll off. Given this similar energy distribution, the spectral regrowth for 1620 MHz interference is expected to have similar shape. On the other hand, the HPA gain at 1620 MHz is about 0.5 dB lower than at 1550 MHz. Therefore, regrowth at 1550 MHz may be slightly more severe than at 1620 MHz for a given input power since the higher gain at 1550 MHz moves the HPA farther into compression. In summary, the 1550 MHz spectra applied to 1620 MHz may be slightly pessimistic there (i.e. regrowth overstated).

For reference in the remaining discussion, the measured filter gain response of the 1550 and 1630 MHz filters are shown in Figure A-19 in the same scale as the figures that follow. The 1550 MHz filter is representative of the set of filters (including 1620 MHz) having narrow rolloff constraints while the 1630 MHz filter is representative of the set having more relaxed parameters.

Figure A-20 and Figure A-21 represent the 1550 and 1620 MHz LTE interference signals (blue curves) as seen at the chamber floor for the -30 dBm test level (Figure A-20) and the -10 dBm test level (Figure A-21). These two signals are selected because they are at the tested LTE

32

frequencies closest to and on either side of the RNSS band of interest. The curves were obtained as follows. Spectra were selected with appropriate nominal attenuation for correspondence with the target test level (see Table A-7). The measured filter response (1550 or 1620 MHz) was added to the spectra to produce the composite post-filter signal shape. This approach of measuring the HPA output and applying the filter response allows inspection of OOBE that may otherwise be lost to the instrument noise floor if measured directly at the filter output, due to steep rolloff of the cavity filters and limited dynamic range of the measuring device. Each composite curve was then adjusted to the test level by subtracting the average of all points within the 9 MHz pedestal and adding back the value of the test level (-30 or -10 dBm). Finally, the curve was converted from units of dBm/9MHz to dBW/Hz by adding factors of -69.54 (to convert /9 MHz to /Hz) and -30 (to convert dBm to dBW).

Regarding other figure elements, the vertical black lines mark the edges of the RNSS band. The horizontal orange line is the ambient noise floor density, defined as $N_0 = kT$, for $T = 290\,K$, which is approximately -204 dBW/Hz. The size of additive OOBE relative to the ambient noise floor determines the magnitude of C/N_0 degradation experienced by a receiver. For example, the horizontal yellow line, which is 16.3 dB lower than the orange line, is the level for additive noise of constant density across the full receiver bandwidth which would produce 0.1 dB degradation in the receiver. This is so merely because it is the noise density that when added to the ambient noise density, raises the floor by 0.1 dB. OOBE is not likely to be of constant density, but the line is included to serve as a useful reference. Receiver degradation is negligible (i.e less than 0.1 dB) for OOBE with density below the yellow line. Thus OOBE suppression can be assessed by comparing the magnitude of OOBE with this reference.

Figure A-20 represents the interference signals at the -30 dBm test level using the 26 dB regrowth spectra for 1550 MHz and the 24 dB spectra for 1620 MHz. This is the highest level reached in radiated tests for these inner frequencies. By inspection of the plot the OOBE in the RNSS band is below the yellow reference line, thereby causing negligible degradation. The darker blue curve shows the portion of the regrowth spectra that was dominated by the noise floor of the measuring instrument. From other measurements taken with better instrument settings at higher HPA input power (less signal attenuation), it is known that the instrument noise floor can be reduced by at least 12 dB without exposing any spectral regrowth at this power level. For this reason a shadow noise floor (light grey) has been represented on the plot to demonstrate that for the -30 dBm test level there is exceptional margin. This result also applies to the other signals that are tested only to this level but farther from the RNSS band, namely the signals at 1545 and 1625 MHz. In summary, OOBE suppression is more than adequate to prevent receiver CNR degradation due to OOBE from the four LTE signals closest to the RNSS band at their levels of test.

Figure A-21 represents the interference signals at the -10 dBm test level using the 6 dB regrowth spectra for 1550 MHz and the 4 dB spectra for 1620 MHz. This level is above the test range for

these inner signals but was the original level used to specify filter attenuation and rolloff performance to satisfy OOBE requirements. In this case, some OOBE within the RNSS band rises above the yellow reference line, but it is in the extreme frequencies of the band, narrower than 2 MHz between 1559 and 1561 MHz and narrower than 3 MHz between 1607 and 1610 MHz. The innermost signals tested at the -10 dBm level are at 1540 and 1630 MHz, each of which is a full 10 MHz farther from the RNSS band. This additional separation is more than enough for the 1540 MHz signal to shift the 2 MHz of OOBE to be outside the RNSS band, since this signal uses a filter having the same narrow rolloff constraints as the 1550 and 1620 MHz filters. However, application to the 1630 MHz signal is less apparent since this filter has more relaxed parameters.

Figure A-22 represents the 1535 and 1630 MHz interference signals at the -10 dBm test level using the 6 dB regrowth spectra for 1535 MHz and the 4 dB spectra for 1630 MHz. These two frequencies are the innermost signals using filters having the more relaxed parameters. As depicted, OOBE is well below the yellow 0.1 dB reference line, indicating receiver degradation is negligible. This result also applies to the other signals that use filters having the relaxed parameters, all of which are tested to this level but are farther from the RNSS band, namely 1475 through 1530 and 1635 through 1675 MHz.

In summary, the analysis demonstrates that OOBE suppression at WSMR was sufficient for all levels of test at each LTE frequency. Figure A-20 demonstrates that OOBE is sufficiently suppressed for all narrow-filter signals up through the -30 dBm test level (i.e. the full test range for 1545, 1550, 1620 and 1625, but only up to -30 dBm for 1540); Figure A-21 demonstrates this at the -10 dBm test level for all narrow-filter signals that run to this level (i.e. 1540; but also 1545 and 1625 although these are not actually tested at this level); and Figure A-22 demonstrates this for all relaxed-filter signals up to the -10 dBm test level (i.e. the full test range for 1475 through 1535 and 1630 through 1675).
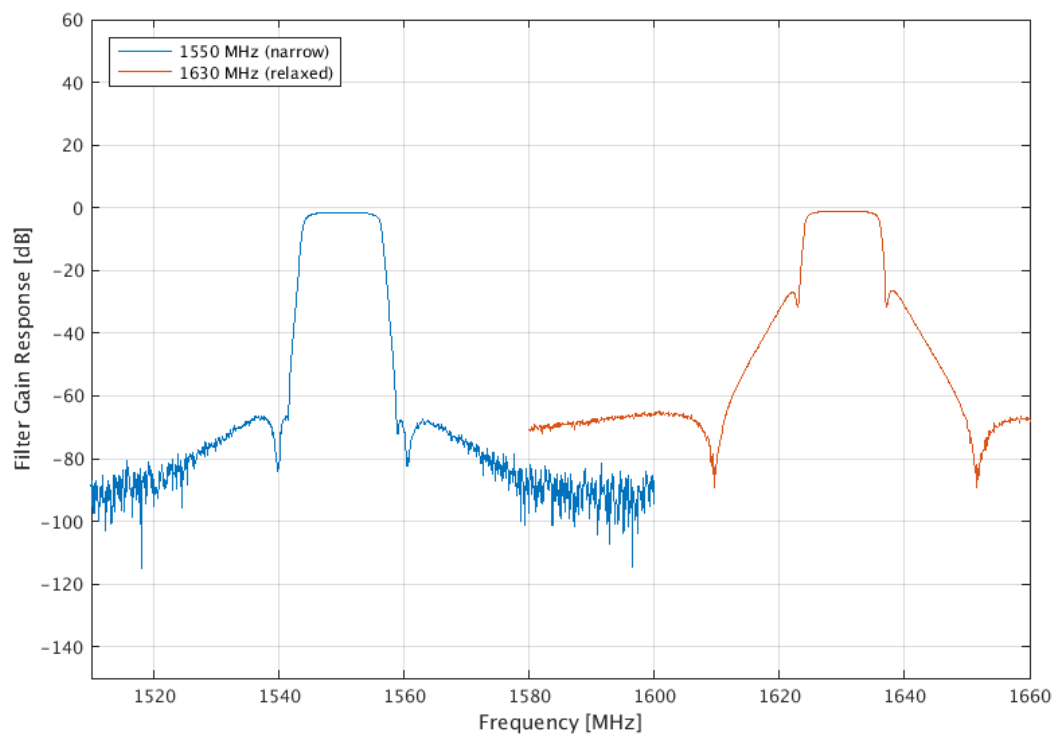
Figure A-19: Example Gain Response of Narrow and Relaxed Filters
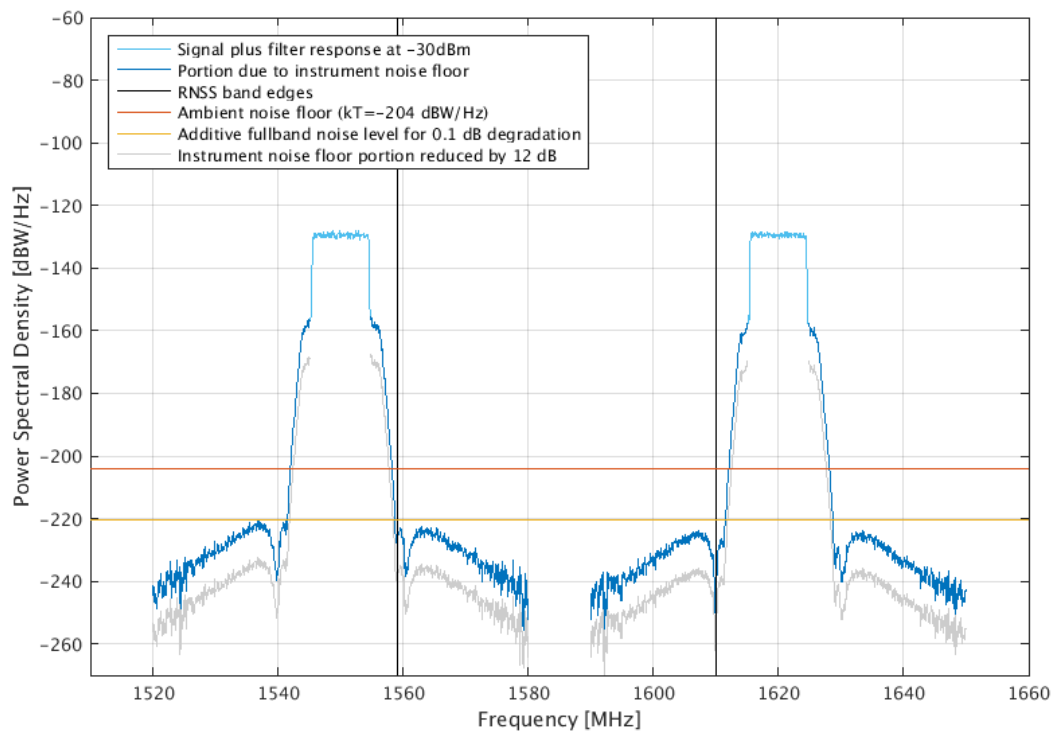
Figure A-20: Composite PSDs for Innermost LTE Signals at -30 dBm
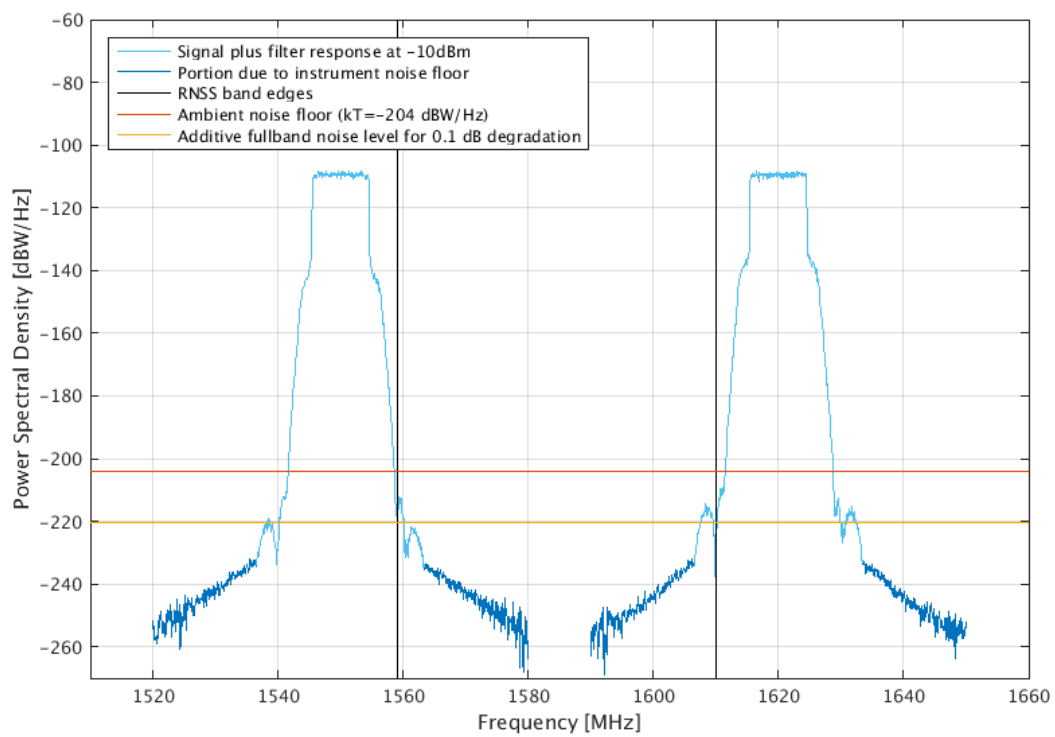
Figure A-21: Composite PSDs for Innermost LTE Signals at -10 dBm
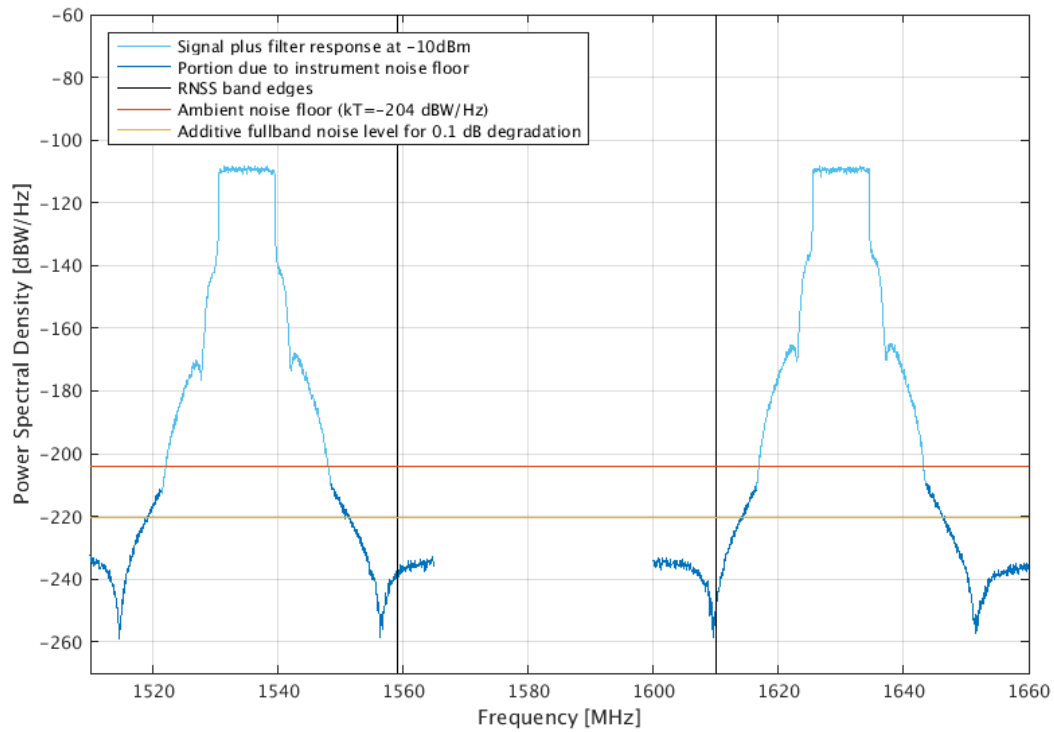
Figure A-22: Composite PSDs for the Innermost Relaxed-filter LTE Signals at -10 dBm

A.10 GNSS Signal Generation

This section provides some details of the GNSS signal generation system.

A.10.1.1   Transmit antenna characterization

The gain patterns of the GNSS transmitting antenna at various center frequencies are shown in Figure A-23. At boresight, this antenna provides RHCP gains of ~0.1 dBic (1227 MHz), 4.4 dBic (1572 MHz), and 4.0 dBic (1602 MHz).

(a) 1227.6 MHz (b) 1563 MHz

(c) 1575 MHz (d) 1602 MHz
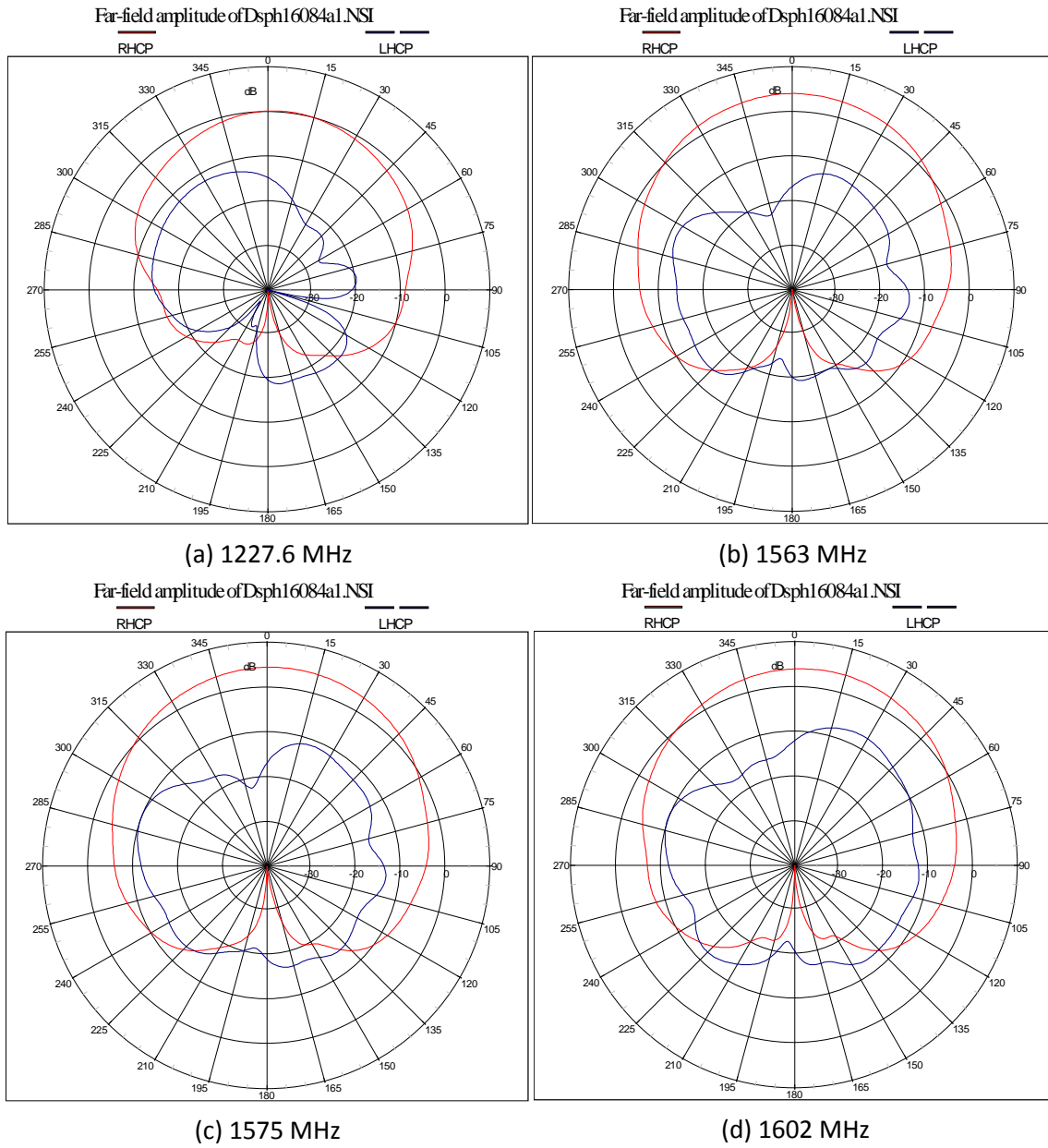
Figure A-23: GNSS Signal Generator Transmit Antenna Gain Patterns

A.10.2 Almanacs

A.10.2.1   GPS Almanac

PRN-24 was generated at -10 dB and PRN-29 at -20 dB relative to the nominal received power levels (see Table 7). Both of these satellites are visible throughout the entire 6 hour simulation time. Using the GNSS generation equipment (see Section 4.3.3.1), due to a limitation on the number of available channels the Spirent signal generator limits the number of emulated GPS satellites to no more than ten based upon dilution of precision (DOP) (with PRN-24 and PRN-29 forced to always be present).

```
******** Week 869 almanac for PRN-01 ********
ID:                      01
Health:                  0
Eccentricity:            0.00000000000000e+000
Time of Applicability(s): 144000
Orbital Inclination(rad): 9.59931088700065e-001
Rate of Right Ascen(r/s): 0.00000000000000e+000
SQRT(A)  (m 1/2):        5.15370081099980e+003
Right Ascen at Week(rad): 2.74046301800000e+000
Argument of Perigee(rad): -1.20197773000000e+000
Mean Anom(rad):          -2.25293839000000e+000
Af0(s):                  0.00000000000000e+000
Af1(s/s):                0.00000000000000e+000
week:                    869


******** Week 869 almanac for PRN-02 ********
ID:                      02
Health:                  0
Eccentricity:            0.00000000000000e+000
Time of Applicability(s): 144000
Orbital Inclination(rad): 9.59931088700065e-001
Rate of Right Ascen(r/s): 0.00000000000000e+000
SQRT(A)  (m 1/2):        5.15370081099980e+003
```

```
Right Ascen at Week(rad):       1.59598827400000e+000

Argument of Perigee(rad):       2.71410071800000e+000

Mean Anom(rad):                 -1.21557569500000e+000

Af0(s):                         0.00000000000000e+000

Af1(s/s):                       0.00000000000000e+000

week:                           869


******** Week 869 almanac for PRN-03 ********

ID:                             03

Health:                         0

Eccentricity:                   0.00000000000000e+000

Time of Applicability(s):       144000

Orbital Inclination(rad):       9.59931088700065e-001

Rate of Right Ascen(r/s):       0.00000000000000e+000

SQRT(A)  (m 1/2):               5.15370081099980e+003

Right Ascen at Week(rad):       4.49386715899998e-001

Argument of Perigee(rad):       8.89944077000001e-001

Mean Anom(rad):                 -1.57409238800000e+000

Af0(s):                         0.00000000000000e+000

Af1(s/s):                       0.00000000000000e+000

week:                           869


******** Week 869 almanac for PRN-04 ********

ID:                             04

Health:                         0

Eccentricity:                   0.00000000000000e+000

Time of Applicability(s):       144000

Orbital Inclination(rad):       9.59931088700065e-001

Rate of Right Ascen(r/s):       0.00000000000000e+000

SQRT(A)  (m 1/2):               5.15370081099980e+003
```

```
Right Ascen at Week(rad):       1.61451172800000e+000

Argument of Perigee(rad):       4.73291158999999e-001

Mean Anom(rad):                 1.62043118500000e+000

Af0(s):                         0.00000000000000e+000

Af1(s/s):                       0.00000000000000e+000

week:                           869


******** Week 869 almanac for PRN-05 ********

ID:                             05

Health:                         0

Eccentricity:                   0.00000000000000e+000

Time of Applicability(s):       144000

Orbital Inclination(rad):       9.59931088700065e-001

Rate of Right Ascen(r/s):       0.00000000000000e+000

SQRT(A)  (m 1/2):               5.15370081099980e+003

Right Ascen at Week(rad):       -5.81213951099999e-001

Argument of Perigee(rad):       1.29498612900000e+000

Mean Anom(rad):                 1.22770595600000e+000

Af0(s):                         0.00000000000000e+000

Af1(s/s):                       0.00000000000000e+000

week:                           869


******** Week 869 almanac for PRN-06 ********

ID:                             06

Health:                         0

Eccentricity:                   0.00000000000000e+000

Time of Applicability(s):       144000

Orbital Inclination(rad):       9.59931088700065e-001

Rate of Right Ascen(r/s):       0.00000000000000e+000

SQRT(A)  (m 1/2):               5.15370081099980e+003
```

```
Right Ascen at Week(rad):      5.16054987899998e-001

Argument of Perigee(rad):      -1.46300911900000e+000

Mean Anom(rad):                9.50933694800001e-001

Af0(s):                        0.00000000000000e+000

Af1(s/s):                      0.00000000000000e+000

week:                          869


******** Week 869 almanac for PRN-07 ********

ID:                            07

Health:                        0

Eccentricity:                  0.00000000000000e+000

Time of Applicability(s):      144000

Orbital Inclination(rad):      9.59931088700065e-001

Rate of Right Ascen(r/s):      0.00000000000000e+000

SQRT(A)  (m 1/2):              5.15370081099980e+003

Right Ascen at Week(rad):      -1.53364002700000e+000

Argument of Perigee(rad):      2.92355132100000e+000

Mean Anom(rad):                -3.03474617000000e+000

Af0(s):                        0.00000000000000e+000

Af1(s/s):                      0.00000000000000e+000

week:                          869


******** Week 869 almanac for PRN-08 ********

ID:                            08

Health:                        0

Eccentricity:                  0.00000000000000e+000

Time of Applicability(s):      144000

Orbital Inclination(rad):      9.59931088700065e-001

Rate of Right Ascen(r/s):      0.00000000000000e+000

SQRT(A)  (m 1/2):              5.15370081099980e+003
```

```
Right Ascen at Week(rad):       -1.47555172400000e+000

Argument of Perigee(rad):        2.97652006100000e+000

Mean Anom(rad):                  2.57835054400000e+000

Af0(s):                          0.00000000000000e+000

Af1(s/s):                        0.00000000000000e+000

week:                           869


******** Week 869 almanac for PRN-09 ********

ID:                             09

Health:                         0

Eccentricity:                    0.00000000000000e+000

Time of Applicability(s):       144000

Orbital Inclination(rad):        9.59931088700065e-001

Rate of Right Ascen(r/s):        0.00000000000000e+000

SQRT(A)  (m 1/2):                5.15370081099980e+003

Right Ascen at Week(rad):       -1.56848144500000e+000

Argument of Perigee(rad):        1.45941114400000e+000

Mean Anom(rad):                  2.32180273500000e+000

Af0(s):                          0.00000000000000e+000

Af1(s/s):                        0.00000000000000e+000

week:                           869


******** Week 869 almanac for PRN-10 ********

ID:                             10

Health:                         0

Eccentricity:                    0.00000000000000e+000

Time of Applicability(s):       144000

Orbital Inclination(rad):        9.59931088700065e-001

Rate of Right Ascen(r/s):        0.00000000000000e+000

SQRT(A)  (m 1/2):                5.15370081099980e+003
```

44

```
Right Ascen at Week(rad):      2.67993223700000e+000

Argument of Perigee(rad):      5.90835452000001e-001

Mean Anom(rad):               -3.54773163799999e-001

Af0(s):                        0.00000000000000e+000

Af1(s/s):                      0.00000000000000e+000

week:                          869


******** Week 869 almanac for PRN-11 ********

ID:                            11

Health:                        0

Eccentricity:                  0.00000000000000e+000

Time of Applicability(s):      144000

Orbital Inclination(rad):      9.59931088700065e-001

Rate of Right Ascen(r/s):      0.00000000000000e+000

SQRT(A)  (m 1/2):              5.15370081099980e+003

Right Ascen at Week(rad):      1.40136146500000e+000

Argument of Perigee(rad):      6.84068560999999e-001

Mean Anom(rad):                3.11031377300000e+000

Af0(s):                        0.00000000000000e+000

Af1(s/s):                      0.00000000000000e+000

week:                          869


******** Week 869 almanac for PRN-12 ********

ID:                            12

Health:                        0

Eccentricity:                  0.00000000000000e+000

Time of Applicability(s):      144000

Orbital Inclination(rad):      9.59931088700065e-001

Rate of Right Ascen(r/s):      0.00000000000000e+000

SQRT(A)  (m 1/2):              5.15370081099980e+003
```

```
Right Ascen at Week(rad):        -4.82020854899998e-001

Argument of Perigee(rad):        -8.12766790000000e-001

Mean Anom(rad):                  -2.84381163100000e+000

Af0(s):                          0.00000000000000e+000

Af1(s/s):                        0.00000000000000e+000

week:                            869


******** Week 869 almanac for PRN-13 ********

ID:                              13

Health:                          0

Eccentricity:                    0.00000000000000e+000

Time of Applicability(s):        144000

Orbital Inclination(rad):        9.59931088700065e-001

Rate of Right Ascen(r/s):        0.00000000000000e+000

SQRT(A)  (m 1/2):                5.15370081099980e+003

Right Ascen at Week(rad):        -2.52682590500000e+000

Argument of Perigee(rad):        1.50618374300000e+000

Mean Anom(rad):                  -5.35064935699999e-001

Af0(s):                          0.00000000000000e+000

Af1(s/s):                        0.00000000000000e+000

week:                            869


******** Week 869 almanac for PRN-14 ********

ID:                              14

Health:                          0

Eccentricity:                    0.00000000000000e+000

Time of Applicability(s):        144000

Orbital Inclination(rad):        9.59931088700065e-001

Rate of Right Ascen(r/s):        0.00000000000000e+000

SQRT(A)  (m 1/2):                5.15370081099980e+003
```

46

```
Right Ascen at Week(rad):        -2.54563283900000e+000

Argument of Perigee(rad):        -2.09949839100000e+000

Mean Anom(rad):                  -9.34581875800001e-001

Af0(s):                          0.00000000000000e+000

Af1(s/s):                        0.00000000000000e+000

week:                            869


******** Week 869 almanac for PRN-15 ********

ID:                              15

Health:                          0

Eccentricity:                    0.00000000000000e+000

Time of Applicability(s):        144000

Orbital Inclination(rad):        9.59931088700065e-001

Rate of Right Ascen(r/s):        0.00000000000000e+000

SQRT(A)  (m 1/2):                5.15370081099980e+003

Right Ascen at Week(rad):        -2.59459817400000e+000

Argument of Perigee(rad):        -7.41997718999999e-001

Mean Anom(rad):                  -4.29327011100000e-001

Af0(s):                          0.00000000000000e+000

Af1(s/s):                        0.00000000000000e+000

week:                            869


******** Week 869 almanac for PRN-16 ********

ID:                              16

Health:                          0

Eccentricity:                    0.00000000000000e+000

Time of Applicability(s):        144000

Orbital Inclination(rad):        9.59931088700065e-001

Rate of Right Ascen(r/s):        0.00000000000000e+000

SQRT(A)  (m 1/2):                5.15370081099980e+003
```

47

```
Right Ascen at Week(rad):        -4.65248584700001e-001

Argument of Perigee(rad):        -3.85978222000000e-001

Mean Anom(rad):                  9.20198559800000e-001

Af0(s):                          0.00000000000000e+000

Af1(s/s):                        0.00000000000000e+000

week:                            869


******** Week 869 almanac for PRN-17 ********

ID:                              17

Health:                          0

Eccentricity:                    0.00000000000000e+000

Time of Applicability(s):        144000

Orbital Inclination(rad):        9.59931088700065e-001

Rate of Right Ascen(r/s):        0.00000000000000e+000

SQRT(A)  (m 1/2):                5.15370081099980e+003

Right Ascen at Week(rad):        5.76244592700001e-001

Argument of Perigee(rad):        -2.75002646400000e+000

Mean Anom(rad):                  -1.65793895700000e-001

Af0(s):                          0.00000000000000e+000

Af1(s/s):                        0.00000000000000e+000

week:                            869


******** Week 869 almanac for PRN-18 ********

ID:                              18

Health:                          0

Eccentricity:                    0.00000000000000e+000

Time of Applicability(s):        144000

Orbital Inclination(rad):        9.59931088700065e-001

Rate of Right Ascen(r/s):        0.00000000000000e+000

SQRT(A)  (m 1/2):                5.15370081099980e+003
```

48

```
Right Ascen at Week(rad):        2.68705499200000e+000

Argument of Perigee(rad):        -2.43825757500000e+000

Mean Anom(rad):                  1.04815793000000e+000

Af0(s):                          0.00000000000000e+000

Af1(s/s):                        0.00000000000000e+000

week:                            869


******** Week 869 almanac for PRN-19 ********

ID:                              19

Health:                          0

Eccentricity:                    0.00000000000000e+000

Time of Applicability(s):        144000

Orbital Inclination(rad):        9.59931088700065e-001

Rate of Right Ascen(r/s):        0.00000000000000e+000

SQRT(A)  (m 1/2):                5.15370081099980e+003

Right Ascen at Week(rad):        6.32605314300000e-001

Argument of Perigee(rad):        -3.91284585000001e-001

Mean Anom(rad):                  -9.07470583900000e-001

Af0(s):                          0.00000000000000e+000

Af1(s/s):                        0.00000000000000e+000

week:                            869


******** Week 869 almanac for PRN-20 ********

ID:                              20

Health:                          0

Eccentricity:                    0.00000000000000e+000

Time of Applicability(s):        144000

Orbital Inclination(rad):        9.59931088700065e-001

Rate of Right Ascen(r/s):        0.00000000000000e+000

SQRT(A)  (m 1/2):                5.15370081099980e+003
```

49

```
Right Ascen at Week(rad):       2.63330423800000e+000

Argument of Perigee(rad):       1.31460762000000e+000

Mean Anom(rad):                 1.19534623600000e+000

Af0(s):                         0.00000000000000e+000

Af1(s/s):                       0.00000000000000e+000

week:                           869


******** Week 869 almanac for PRN-21 ********

ID:                             21

Health:                         0

Eccentricity:                   0.00000000000000e+000

Time of Applicability(s):       144000

Orbital Inclination(rad):       9.59931088700065e-001

Rate of Right Ascen(r/s):       0.00000000000000e+000

SQRT(A)  (m 1/2):               5.15370081099980e+003

Right Ascen at Week(rad):       1.62840294800000e+000

Argument of Perigee(rad):       -2.64889907800000e+000

Mean Anom(rad):                 2.32440674300000e+000

Af0(s):                         0.00000000000000e+000

Af1(s/s):                       0.00000000000000e+000

week:                           869


******** Week 869 almanac for PRN-22 ********

ID:                             22

Health:                         0

Eccentricity:                   0.00000000000000e+000

Time of Applicability(s):       144000

Orbital Inclination(rad):       9.59931088700065e-001

Rate of Right Ascen(r/s):       0.00000000000000e+000

SQRT(A)  (m 1/2):               5.15370081099980e+003
```

50

```
Right Ascen at Week(rad):      2.69298374700000e+000

Argument of Perigee(rad):      -1.82339680200000e+000

Mean Anom(rad):                -7.65956640200001e-002

Af0(s):                        0.00000000000000e+000

Af1(s/s):                      0.00000000000000e+000

week:                          869


******** Week 869 almanac for PRN-23 ********

ID:                            23

Health:                        0

Eccentricity:                  0.00000000000000e+000

Time of Applicability(s):      144000

Orbital Inclination(rad):      9.59931088700065e-001

Rate of Right Ascen(r/s):      0.00000000000000e+000

SQRT(A)  (m 1/2):              5.15370081099980e+003

Right Ascen at Week(rad):      -2.57619190200000e+000

Argument of Perigee(rad):      2.88240265800000e+000

Mean Anom(rad):                -1.44661092800000e+000

Af0(s):                        0.00000000000000e+000

Af1(s/s):                      0.00000000000000e+000

week:                          869


******** Week 869 almanac for PRN-24 ********

ID:                            24

Health:                        0

Eccentricity:                  0.00000000000000e+000

Time of Applicability(s):      144000

Orbital Inclination(rad):      9.59931088700065e-001

Rate of Right Ascen(r/s):      0.00000000000000e+000

SQRT(A)  (m 1/2):              5.15370081099980e+003
```

51

```
Right Ascen at Week(rad):        1.65867066400000e+000

Argument of Perigee(rad):        -6.39523148999999e-001

Mean Anom(rad):                  1.03374876339972e+000

Af0(s):                          0.00000000000000e+000

Af1(s/s):                        0.00000000000000e+000

week:                            869


******** Week 869 almanac for PRN-25 ********

ID:                              25

Health:                          0

Eccentricity:                    0.00000000000000e+000

Time of Applicability(s):        144000

Orbital Inclination(rad):        9.59931088700065e-001

Rate of Right Ascen(r/s):        0.00000000000000e+000

SQRT(A)  (m 1/2):                5.15370081099980e+003

Right Ascen at Week(rad):        -1.62840080300000e+000

Argument of Perigee(rad):        -1.22941148300000e+000

Mean Anom(rad):                  1.46781361100000e+000

Af0(s):                          0.00000000000000e+000

Af1(s/s):                        0.00000000000000e+000

week:                            869


******** Week 869 almanac for PRN-26 ********

ID:                              26

Health:                          0

Eccentricity:                    0.00000000000000e+000

Time of Applicability(s):        144000

Orbital Inclination(rad):        9.59931088700065e-001

Rate of Right Ascen(r/s):        0.00000000000000e+000

SQRT(A)  (m 1/2):                5.15370081099980e+003
```

```
Right Ascen at Week(rad):      -2.52893137900000e+000

Argument of Perigee(rad):       9.67672229000000e-001

Mean Anom(rad):                -1.88577055900000e+000

Af0(s):                         0.00000000000000e+000

Af1(s/s):                       0.00000000000000e+000

week:                           869


******** Week 869 almanac for PRN-27 ********

ID:                             27

Health:                         0

Eccentricity:                   0.00000000000000e+000

Time of Applicability(s):       144000

Orbital Inclination(rad):       9.59931088700065e-001

Rate of Right Ascen(r/s):       0.00000000000000e+000

SQRT(A)  (m 1/2):               5.15370081099980e+003

Right Ascen at Week(rad):      -1.59251999900000e+000

Argument of Perigee(rad):      -1.65117299600000e+000

Mean Anom(rad):                 5.39627194399999e-001

Af0(s):                         0.00000000000000e+000

Af1(s/s):                       0.00000000000000e+000

week:                           869


******** Week 869 almanac for PRN-28 ********

ID:                             28

Health:                         0

Eccentricity:                   0.00000000000000e+000

Time of Applicability(s):       144000

Orbital Inclination(rad):       9.59931088700065e-001

Rate of Right Ascen(r/s):       0.00000000000000e+000

SQRT(A)  (m 1/2):               5.15370081099980e+003
```

53

```
Right Ascen at Week(rad):        -4.56912398300000e-001

Argument of Perigee(rad):        -2.05713677400000e+000

Mean Anom(rad):                  2.58443236400000e-001

Af0(s):                          0.00000000000000e+000

Af1(s/s):                        0.00000000000000e+000

week:                            869


******** Week 869 almanac for PRN-29 ********

ID:                              29

Health:                          0

Eccentricity:                    0.00000000000000e+000

Time of Applicability(s):        144000

Orbital Inclination(rad):        9.59931088700065e-001

Rate of Right Ascen(r/s):        0.00000000000000e+000

SQRT(A)  (m 1/2):                5.15370081099980e+003

Right Ascen at Week(rad):        5.84426879900000e-001

Argument of Perigee(rad):        -1.34343349900000e+000

Mean Anom(rad):                  2.46437074459972e+000

Af0(s):                          0.00000000000000e+000

Af1(s/s):                        0.00000000000000e+000

week:                            869


******** Week 869 almanac for PRN-30 ********

ID:                              30

Health:                          0

Eccentricity:                    0.00000000000000e+000

Time of Applicability(s):        144000

Orbital Inclination(rad):        9.59931088700065e-001

Rate of Right Ascen(r/s):        0.00000000000000e+000

SQRT(A)  (m 1/2):                5.15370081099980e+003
```

54

```
Right Ascen at Week(rad):        -5.27972102200001e-001

Argument of Perigee(rad):        1.41317498700000e+000

Mean Anom(rad):                  6.90480113000000e-001

Af0(s):                          0.00000000000000e+000

Af1(s/s):                        0.00000000000000e+000

week:                            869


******** Week 869 almanac for PRN-31 ********
ID:                              31

Health:                          0

Eccentricity:                    0.00000000000000e+000

Time of Applicability(s):        144000

Orbital Inclination(rad):        9.59931088700065e-001

Rate of Right Ascen(r/s):        0.00000000000000e+000

SQRT(A)  (m 1/2):                5.15370081099980e+003

Right Ascen at Week(rad):        -1.53629112200000e+000

Argument of Perigee(rad):        -1.19382882100000e+000

Mean Anom(rad):                  -3.10803759100000e+000

Af0(s):                          0.00000000000000e+000

Af1(s/s):                        0.00000000000000e+000

week:                            869
```
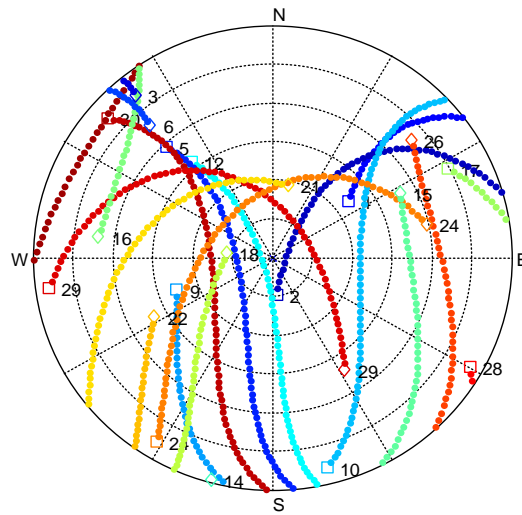
GPS Satellite Visibility
(PRN-24 at -10 dB,
PRN-29 at -20 dB)

A.10.2.2   GLONASS Almanac

SV-01 was generated at -10 dB and SV-02 at -20 dB relative to the nominal received power levels (see Table 7). Both of these satellites are visible throughout the entire 6 hour simulation time.

```
******** Week 869 almanac for SV-01, slot 1 ********

ID:                     101

Health:                 32

Eccentricity:           2.80435376435597e-004

Time of Applicability(s):   144000

Orbital Inclination(rad):   1.12033508367946e+000

Rate of Right Ascen(r/s):   0.00000000000000e+000

SQRT(A)  (m 1/2):       5.05032756696999e+003

Right Ascen at Week(rad):   7.40792320628956e-001
```

```
Argument of Perigee(rad):      1.04180853107395e-001

Mean Anom(rad):                1.15091734896345e+000

Af0(s):                        -1.45391561091000e-004

Af1(s/s):                      0.00000000000000e+000

week:                          869


******** Week 869 almanac for SV-02, slot -4 ********

ID:                            2-4

Health:                        32

Eccentricity:                  1.33246975536473e-003

Time of Applicability(s):      144000

Orbital Inclination(rad):      1.12862364314003e+000

Rate of Right Ascen(r/s):      0.00000000000000e+000

SQRT(A)  (m 1/2):              5.05064077398080e+003

Right Ascen at Week(rad):      7.47441593549524e-001

Argument of Perigee(rad):      -2.20437677064413e+000

Mean Anom(rad):                -2.59971956740604e+000

Af0(s):                        1.79462134838000e-004

Af1(s/s):                      1.81898940355000e-012

week:                          869


******** Week 869 almanac for SV-03, slot 5 ********

ID:                            305

Health:                        32

Eccentricity:                  1.32498816166167e-003

Time of Applicability(s):      144000

Orbital Inclination(rad):      1.12566875527212e+000

Rate of Right Ascen(r/s):      0.00000000000000e+000

SQRT(A)  (m 1/2):              5.05066930031813e+003

Right Ascen at Week(rad):      7.48675234560466e-001
```

57

```
Argument of Perigee(rad):      -2.05289822822853e+000

Mean Anom(rad):                1.69623491824316e+000

Af0(s):                        6.39893114567000e-005

Af1(s/s):                      9.09494701773000e-013

week:                          869


******** Week 869 almanac for SV-04, slot 6 ********

ID:                            406

Health:                        32

Eccentricity:                  4.07477957999495e-004

Time of Applicability(s):      144000

Orbital Inclination(rad):      1.12598979849155e+000

Rate of Right Ascen(r/s):      0.00000000000000e+000

SQRT(A)  (m 1/2):              5.05036637505249e+003

Right Ascen at Week(rad):      7.47210497782127e-001

Argument of Perigee(rad):      -2.31046441525516e+000

Mean Anom(rad):                1.15466300306374e+000

Af0(s):                        1.59780494869000e-004

Af1(s/s):                      9.09494701773000e-013

week:                          869


******** Week 869 almanac for SV-05, slot 1 ********

ID:                            501

Health:                        32

Eccentricity:                  5.25326160780691e-004

Time of Applicability(s):      144000

Orbital Inclination(rad):      1.12011662854620e+000

Rate of Right Ascen(r/s):      0.00000000000000e+000

SQRT(A)  (m 1/2):              5.05034296657956e+003

Right Ascen at Week(rad):      7.39644393530448e-001
```

58

```
Argument of Perigee(rad):      1.23200649291355e+000

Mean Anom(rad):                3.13126501826303e+000

Af0(s):                        -3.61446291208000e-006

Af1(s/s):                      -9.09494701773000e-013

week:                          869


******** Week 869 almanac for SV-06, slot -4 ********

ID:                            6-4

Health:                        32

Eccentricity:                  8.53360015146096e-004

Time of Applicability(s):      144000

Orbital Inclination(rad):      1.12005137128198e+000

Rate of Right Ascen(r/s):      0.00000000000000e+000

SQRT(A)  (m 1/2):              5.05065643919592e+003

Right Ascen at Week(rad):      7.39560464322004e-001

Argument of Perigee(rad):      2.45142186808776e+000

Mean Anom(rad):                1.08577069852623e+000

Af0(s):                        8.49086791277000e-005

Af1(s/s):                      0.00000000000000e+000

week:                          869


******** Week 869 almanac for SV-07, slot 5 ********

ID:                            705

Health:                        32

Eccentricity:                  1.10069518293223e-003

Time of Applicability(s):      144000

Orbital Inclination(rad):      1.12581361051808e+000

Rate of Right Ascen(r/s):      0.00000000000000e+000

SQRT(A)  (m 1/2):              5.05066586996986e+003

Right Ascen at Week(rad):      7.49361979736101e-001
```

```
Argument of Perigee(rad):        -2.09985541861908e+000

Mean Anom(rad):                  -1.40932465105142e+000

Af0(s):                          -6.72508031130000e-006

Af1(s/s):                        -0.00000000000000e+000

week:                            869


******** Week 869 almanac for SV-08, slot 6 ********

ID:                              806

Health:                          32

Eccentricity:                    1.69977794661984e-003

Time of Applicability(s):        144000

Orbital Inclination(rad):        1.12591505648484e+000

Rate of Right Ascen(r/s):        0.00000000000000e+000

SQRT(A)  (m 1/2):                5.05037218492650e+003

Right Ascen at Week(rad):        7.49133082568086e-001

Argument of Perigee(rad):        -1.40947614523548e+000

Mean Anom(rad):                  -2.86620078192880e+000

Af0(s):                          -2.71061435342000e-005

Af1(s/s):                        0.00000000000000e+000

week:                            869


******** Week 869 almanac for SV-09, slot -6 ********

ID:                              9-6

Health:                          32

Eccentricity:                    1.49164382262733e-003

Time of Applicability(s):        144000

Orbital Inclination(rad):        1.12887573482007e+000

Rate of Right Ascen(r/s):        0.00000000000000e+000

SQRT(A)  (m 1/2):                5.05029813945331e+003

Right Ascen at Week(rad):        2.87210862370048e+000
```

```
Argument of Perigee(rad):       -2.17340232687494e+000

Mean Anom(rad):                 -2.65756649912442e+000

Af0(s):                         8.67033377290000e-005

Af1(s/s):                       7.27595761418000e-012

week:                           869


******** Week 869 almanac for SV-10, slot -7 ********

ID:                             10-7

Health:                         32

Eccentricity:                   1.64202181019619e-003

Time of Applicability(s):       144000

Orbital Inclination(rad):       1.14681706329809e+000

Rate of Right Ascen(r/s):       0.00000000000000e+000

SQRT(A)  (m 1/2):               5.05053138049315e+003

Right Ascen at Week(rad):       2.85464671037023e+000

Argument of Perigee(rad):       2.65732697939073e+000

Mean Anom(rad):                 -1.96468327760479e+000

Af0(s):                         1.51759013534000e-005

Af1(s/s):                       9.09494701773000e-013

week:                           869


******** Week 869 almanac for SV-11, slot 0 ********

ID:                             1100

Health:                         32

Eccentricity:                   1.96070028249679e-003

Time of Applicability(s):       144000

Orbital Inclination(rad):       1.14010497737022e+000

Rate of Right Ascen(r/s):       0.00000000000000e+000

SQRT(A)  (m 1/2):               5.05072659215691e+003

Right Ascen at Week(rad):       2.84299979611610e+000
```

61

```
Argument of Perigee(rad):      6.59073671346432e-002

Mean Anom(rad):               -1.57173974293076e-001

Af0(s):                        2.48514115810000e-005

Af1(s/s):                     -0.00000000000000e+000

week:                          869


******** Week 869 almanac for SV-12, slot -4 ********

ID:                            12-4

Health:                        32

Eccentricity:                  3.29010000000000e-003

Time of Applicability(s):      144000

Orbital Inclination(rad):      1.13279198837290e+000

Rate of Right Ascen(r/s):      0.00000000000000e+000

SQRT(A)  (m 1/2):              5.05054067518879e+003

Right Ascen at Week(rad):      3.09690261246385e+000

Argument of Perigee(rad):      2.95384060463576e+000

Mean Anom(rad):                1.79044601315838e-001

Af0(s):                        5.00000000000000e-004

Af1(s/s):                      0.00000000000000e+000

week:                          869


******** Week 869 almanac for SV-13, slot -2 ********

ID:                            13-2

Health:                        32

Eccentricity:                  7.99396667097814e-004

Time of Applicability(s):      144000

Orbital Inclination(rad):      1.13983784832610e+000

Rate of Right Ascen(r/s):      0.00000000000000e+000

SQRT(A)  (m 1/2):              5.05028282604365e+003

Right Ascen at Week(rad):      2.84230006542228e+000
```

```
Argument of Perigee(rad):       1.44672167995213e+000

Mean Anom(rad):                 3.13950706608156e+000

Af0(s):                         1.00303441286000e-005

Af1(s/s):                       -0.00000000000000e+000

week:                           869


******** Week 869 almanac for SV-14, slot -7 ********

ID:                             14-7

Health:                         32

Eccentricity:                   1.55466745629980e-003

Time of Applicability(s):       144000

Orbital Inclination(rad):       1.14654884486877e+000

Rate of Right Ascen(r/s):       0.00000000000000e+000

SQRT(A)  (m 1/2):               5.05056499236033e+003

Right Ascen at Week(rad):       2.85343237647763e+000

Argument of Perigee(rad):       2.62825282626368e+000

Mean Anom(rad):                 1.14646984845523e+000

Af0(s):                         2.89653427899000e-004

Af1(s/s):                       4.54747350886000e-012

week:                           869


******** Week 869 almanac for SV-15, slot 0 ********

ID:                             1500

Health:                         32

Eccentricity:                   2.23977675463663e-003

Time of Applicability(s):       144000

Orbital Inclination(rad):       1.14653193639322e+000

Rate of Right Ascen(r/s):       0.00000000000000e+000

SQRT(A)  (m 1/2):               5.05071089313078e+003

Right Ascen at Week(rad):       2.85323904698924e+000
```

```
Argument of Perigee(rad):       -8.70289850291570e-002

Mean Anom(rad):                 -3.08905125954067e+000

Af0(s):                         6.49411231279000e-005

Af1(s/s):                       9.09494701773000e-013

week:                           869


******** Week 869 almanac for SV-16, slot -1 ********

ID:                             16-1

Health:                         32

Eccentricity:                   1.83550000000000e-003

Time of Applicability(s):       144000

Orbital Inclination(rad):       1.13249353707081e+000

Rate of Right Ascen(r/s):       0.00000000000000e+000

SQRT(A)  (m 1/2):               5.05054371669493e+003

Right Ascen at Week(rad):       3.09582748965045e+000

Argument of Perigee(rad):       2.66851068786122e+000

Mean Anom(rad):                 6.91782192978976e-001

Af0(s):                         5.00000000000000e-004

Af1(s/s):                       0.00000000000000e+000

week:                           869


******** Week 869 almanac for SV-17, slot 4 ********

ID:                             1704

Health:                         32

Eccentricity:                   8.84576720774307e-004

Time of Applicability(s):       144000

Orbital Inclination(rad):       1.13082917946630e+000

Rate of Right Ascen(r/s):       0.00000000000000e+000

SQRT(A)  (m 1/2):               5.05029194768975e+003

Right Ascen at Week(rad):       -1.33195554259822e+000
```

```
Argument of Perigee(rad):      -2.36958530021500e+000

Mean Anom(rad):                -2.16435670581638e+000

Af0(s):                        -2.28835269809000e-005

Af1(s/s):                      0.00000000000000e+000

week:                          869


******** Week 869 almanac for SV-18, slot -3 ********

ID:                            18-3

Health:                        32

Eccentricity:                  1.58283047580818e-003

Time of Applicability(s):      144000

Orbital Inclination(rad):      1.13537186282913e+000

Rate of Right Ascen(r/s):      0.00000000000000e+000

SQRT(A)  (m 1/2):              5.05041473916712e+003

Right Ascen at Week(rad):      -1.33706722854576e+000

Argument of Perigee(rad):      -4.70730444184711e-001

Mean Anom(rad):                1.47504581863733e+000

Af0(s):                        9.16374847293000e-005

Af1(s/s):                      9.09494701773000e-013

week:                          869


******** Week 869 almanac for SV-19, slot 3 ********

ID:                            1903

Health:                        32

Eccentricity:                  2.44352903735194e-004

Time of Applicability(s):      144000

Orbital Inclination(rad):      1.13925194401139e+000

Rate of Right Ascen(r/s):      0.00000000000000e+000

SQRT(A)  (m 1/2):              5.05068914526964e+003

Right Ascen at Week(rad):      -1.32184456573935e+000
```

```
Argument of Perigee(rad):      -1.18705963314368e+000

Mean Anom(rad):                1.36025505659405e+000

Af0(s):                        -1.49535015225000e-004

Af1(s/s):                      -0.00000000000000e+000

week:                          869


******** Week 869 almanac for SV-20, slot 2 ********

ID:                            2002

Health:                        32

Eccentricity:                  1.22842522658171e-003

Time of Applicability(s):      144000

Orbital Inclination(rad):      1.13945237991812e+000

Rate of Right Ascen(r/s):      0.00000000000000e+000

SQRT(A)  (m 1/2):              5.05054064557828e+003

Right Ascen at Week(rad):      -1.32075578560146e+000

Argument of Perigee(rad):      -3.82939381582557e-001

Mean Anom(rad):                -2.46146248236104e-001

Af0(s):                        -2.22451053560000e-004

Af1(s/s):                      -1.81898940355000e-012

week:                          869


******** Week 869 almanac for SV-21, slot 4 ********

ID:                            2104

Health:                        32

Eccentricity:                  5.31475615345574e-004

Time of Applicability(s):      144000

Orbital Inclination(rad):      1.13432115101620e+000

Rate of Right Ascen(r/s):      0.00000000000000e+000

SQRT(A)  (m 1/2):              5.05029468247230e+003

Right Ascen at Week(rad):      -1.33653498898153e+000
```

66

```
Argument of Perigee(rad):      -2.81972240040206e+000

Mean Anom(rad):                1.44889418884053e+000

Af0(s):                        5.36972656846000e-005

Af1(s/s):                      1.81898940355000e-012

week:                          869


******** Week 869 almanac for SV-22, slot -3 ********

ID:                            22-3

Health:                        32

Eccentricity:                  2.94760840310346e-003

Time of Applicability(s):      144000

Orbital Inclination(rad):      1.13760739536984e+000

Rate of Right Ascen(r/s):      0.00000000000000e+000

SQRT(A)  (m 1/2):              5.05043482102626e+003

Right Ascen at Week(rad):      -1.33642892609230e+000

Argument of Perigee(rad):      -1.03944861440644e-001

Mean Anom(rad):                -2.05717394866684e+000

Af0(s):                        1.93633139133000e-004

Af1(s/s):                      9.09494701773000e-013

week:                          869


******** Week 869 almanac for SV-23, slot 3 ********

ID:                            2303

Health:                        32

Eccentricity:                  3.94066120249689e-005

Time of Applicability(s):      144000

Orbital Inclination(rad):      1.13734058290765e+000

Rate of Right Ascen(r/s):      0.00000000000000e+000

SQRT(A)  (m 1/2):              5.05071557599688e+003

Right Ascen at Week(rad):      -1.33712871096215e+000
```

```
Argument of Perigee(rad):       -1.70246732457996e-001

Mean Anom(rad):                 -2.81819268437635e+000

Af0(s):                         -8.79149883986000e-005

Af1(s/s):                       -3.63797880709000e-012

week:                           869


******** Week 869 almanac for SV-24, slot 2 ********

ID:                             2402

Health:                         32

Eccentricity:                   6.68632423028246e-004

Time of Applicability(s):       144000

Orbital Inclination(rad):       1.13750141332033e+000

Rate of Right Ascen(r/s):       0.00000000000000e+000

SQRT(A)  (m 1/2):               5.05057594902682e+003

Right Ascen at Week(rad):       -1.33677735210199e+000

Argument of Perigee(rad):       1.12161248242197e+000

Mean Anom(rad):                 1.43907705778873e+000

Af0(s):                         -1.34304165840000e-004

Af1(s/s):                       0.00000000000000e+000

week:                           869
```
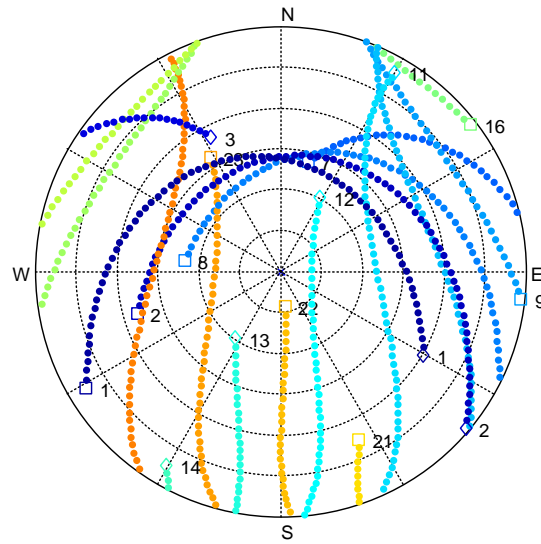
GLONASS Satellite Visibility
(SV-01 at -10 dB,
SV-02 at -20 dB)

A.10.2.3   Galileo Almanac

PRN-4 was generated at -10 dB and PRN-10 at -20 dB relative to the nominal received power levels (see Table 7). Both of these satellites are visible throughout the entire 6 hour simulation time.

```
******** Week 869 almanac for PRN-01 ********

ID:                     01

Health:                 0

Eccentricity:           0.00000000000000e+000

Time of Applicability(s):   144000

Orbital Inclination(rad):   9.77384381116824e-001

Rate of Right Ascen(r/s):   0.00000000000000e+000

SQRT(A)  (m 1/2):       5.44058820349418e+003
```

```
Right Ascen at Week(rad):      0.00000000000000e+000

Argument of Perigee(rad):      0.00000000000000e+000

Mean Anom(rad):                0.00000000000000e+000

Af0(s):                        0.00000000000000e+000

Af1(s/s):                      0.00000000000000e+000

week:                          869


******** Week 869 almanac for PRN-02 ********

ID:                            02

Health:                        0

Eccentricity:                  0.00000000000000e+000

Time of Applicability(s):      144000

Orbital Inclination(rad):      9.77384381116824e-001

Rate of Right Ascen(r/s):      0.00000000000000e+000

SQRT(A)  (m 1/2):              5.44058820349418e+003

Right Ascen at Week(rad):      0.00000000000000e+000

Argument of Perigee(rad):      0.00000000000000e+000

Mean Anom(rad):                6.98131700797731e-001

Af0(s):                        0.00000000000000e+000

Af1(s/s):                      0.00000000000000e+000

week:                          869


******** Week 869 almanac for PRN-03 ********

ID:                            03

Health:                        0

Eccentricity:                  0.00000000000000e+000

Time of Applicability(s):      144000

Orbital Inclination(rad):      9.77384381116824e-001

Rate of Right Ascen(r/s):      0.00000000000000e+000

SQRT(A)  (m 1/2):              5.44058820349418e+003
```

70

```
Right Ascen at Week(rad):      0.00000000000000e+000

Argument of Perigee(rad):      0.00000000000000e+000

Mean Anom(rad):                1.39626340159546e+000

Af0(s):                        0.00000000000000e+000

Af1(s/s):                      0.00000000000000e+000

week:                          869


******** Week 869 almanac for PRN-04 ********

ID:                            04

Health:                        0

Eccentricity:                  0.00000000000000e+000

Time of Applicability(s):      144000

Orbital Inclination(rad):      9.77384381116824e-001

Rate of Right Ascen(r/s):      0.00000000000000e+000

SQRT(A)  (m 1/2):              5.44058820349418e+003

Right Ascen at Week(rad):      0.00000000000000e+000

Argument of Perigee(rad):      0.00000000000000e+000

Mean Anom(rad):                2.09439510239320e+000

Af0(s):                        0.00000000000000e+000

Af1(s/s):                      0.00000000000000e+000

week:                          869


******** Week 869 almanac for PRN-05 ********

ID:                            05

Health:                        0

Eccentricity:                  0.00000000000000e+000

Time of Applicability(s):      144000

Orbital Inclination(rad):      9.77384381116824e-001

Rate of Right Ascen(r/s):      0.00000000000000e+000

SQRT(A)  (m 1/2):              5.44058820349418e+003
```

71

```
Right Ascen at Week(rad):      0.00000000000000e+000

Argument of Perigee(rad):      0.00000000000000e+000

Mean Anom(rad):                2.79252680319093e+000

Af0(s):                        0.00000000000000e+000

Af1(s/s):                      0.00000000000000e+000

week:                          869


******** Week 869 almanac for PRN-06 ********

ID:                            06

Health:                        0

Eccentricity:                  0.00000000000000e+000

Time of Applicability(s):      144000

Orbital Inclination(rad):      9.77384381116824e-001

Rate of Right Ascen(r/s):      0.00000000000000e+000

SQRT(A)  (m 1/2):              5.44058820349418e+003

Right Ascen at Week(rad):      0.00000000000000e+000

Argument of Perigee(rad):      0.00000000000000e+000

Mean Anom(rad):                -2.79252680319093e+000

Af0(s):                        0.00000000000000e+000

Af1(s/s):                      0.00000000000000e+000

week:                          869


******** Week 869 almanac for PRN-07 ********

ID:                            07

Health:                        0

Eccentricity:                  0.00000000000000e+000

Time of Applicability(s):      144000

Orbital Inclination(rad):      9.77384381116824e-001

Rate of Right Ascen(r/s):      0.00000000000000e+000

SQRT(A)  (m 1/2):              5.44058820349418e+003
```

```
Right Ascen at Week(rad):        0.00000000000000e+000

Argument of Perigee(rad):        0.00000000000000e+000

Mean Anom(rad):                  -2.09439510239320e+000

Af0(s):                          0.00000000000000e+000

Af1(s/s):                        0.00000000000000e+000

week:                            869


******** Week 869 almanac for PRN-08 ********

ID:                              08

Health:                          0

Eccentricity:                    0.00000000000000e+000

Time of Applicability(s):        144000

Orbital Inclination(rad):        9.77384381116824e-001

Rate of Right Ascen(r/s):        0.00000000000000e+000

SQRT(A)  (m 1/2):                5.44058820349418e+003

Right Ascen at Week(rad):        0.00000000000000e+000

Argument of Perigee(rad):        0.00000000000000e+000

Mean Anom(rad):                  -1.39626340159547e+000

Af0(s):                          0.00000000000000e+000

Af1(s/s):                        0.00000000000000e+000

week:                            869


******** Week 869 almanac for PRN-09 ********

ID:                              09

Health:                          0

Eccentricity:                    0.00000000000000e+000

Time of Applicability(s):        144000

Orbital Inclination(rad):        9.77384381116824e-001

Rate of Right Ascen(r/s):        0.00000000000000e+000

SQRT(A)  (m 1/2):                5.44058820349418e+003
```

73

```
Right Ascen at Week(rad):      0.00000000000000e+000

Argument of Perigee(rad):      0.00000000000000e+000

Mean Anom(rad):                -6.98131700797731e-001

Af0(s):                        0.00000000000000e+000

Af1(s/s):                      0.00000000000000e+000

week:                          869


******** Week 869 almanac for PRN-10 ********

ID:                            10

Health:                        0

Eccentricity:                  0.00000000000000e+000

Time of Applicability(s):      144000

Orbital Inclination(rad):      9.77384381116824e-001

Rate of Right Ascen(r/s):      0.00000000000000e+000

SQRT(A)  (m 1/2):              5.44058820349418e+003

Right Ascen at Week(rad):      2.09439510239320e+000

Argument of Perigee(rad):      0.00000000000000e+000

Mean Anom(rad):                2.32652389290844e-001

Af0(s):                        0.00000000000000e+000

Af1(s/s):                      0.00000000000000e+000

week:                          869


******** Week 869 almanac for PRN-11 ********

ID:                            11

Health:                        0

Eccentricity:                  0.00000000000000e+000

Time of Applicability(s):      144000

Orbital Inclination(rad):      9.77384381116824e-001

Rate of Right Ascen(r/s):      0.00000000000000e+000

SQRT(A)  (m 1/2):              5.44058820349418e+003
```

```
Right Ascen at Week(rad):      2.09439510239320e+000

Argument of Perigee(rad):      0.00000000000000e+000

Mean Anom(rad):                9.30784090088577e-001

Af0(s):                        0.00000000000000e+000

Af1(s/s):                      0.00000000000000e+000

week:                          869


******** Week 869 almanac for PRN-12 ********

ID:                            12

Health:                        0

Eccentricity:                  0.00000000000000e+000

Time of Applicability(s):      144000

Orbital Inclination(rad):      9.77384381116824e-001

Rate of Right Ascen(r/s):      0.00000000000000e+000

SQRT(A)  (m 1/2):              5.44058820349418e+003

Right Ascen at Week(rad):      2.09439510239320e+000

Argument of Perigee(rad):      0.00000000000000e+000

Mean Anom(rad):                1.62891579088631e+000

Af0(s):                        0.00000000000000e+000

Af1(s/s):                      0.00000000000000e+000

week:                          869


******** Week 869 almanac for PRN-13 ********

ID:                            13

Health:                        0

Eccentricity:                  0.00000000000000e+000

Time of Applicability(s):      144000

Orbital Inclination(rad):      9.77384381116824e-001

Rate of Right Ascen(r/s):      0.00000000000000e+000

SQRT(A)  (m 1/2):              5.44058820349418e+003
```

```
Right Ascen at Week(rad):        2.09439510239320e+000

Argument of Perigee(rad):        0.00000000000000e+000

Mean Anom(rad):                  2.32704749168404e+000

Af0(s):                          0.00000000000000e+000

Af1(s/s):                        0.00000000000000e+000

week:                            869


******** Week 869 almanac for PRN-14 ********

ID:                              14

Health:                          0

Eccentricity:                    0.00000000000000e+000

Time of Applicability(s):        144000

Orbital Inclination(rad):        9.77384381116824e-001

Rate of Right Ascen(r/s):        0.00000000000000e+000

SQRT(A)  (m 1/2):                5.44058820349418e+003

Right Ascen at Week(rad):        2.09439510239320e+000

Argument of Perigee(rad):        0.00000000000000e+000

Mean Anom(rad):                  3.02517919248177e+000

Af0(s):                          0.00000000000000e+000

Af1(s/s):                        0.00000000000000e+000

week:                            869


******** Week 869 almanac for PRN-15 ********

ID:                              15

Health:                          0

Eccentricity:                    0.00000000000000e+000

Time of Applicability(s):        144000

Orbital Inclination(rad):        9.77384381116824e-001

Rate of Right Ascen(r/s):        0.00000000000000e+000

SQRT(A)  (m 1/2):                5.44058820349418e+003
```

76

```
Right Ascen at Week(rad):      2.09439510239320e+000

Argument of Perigee(rad):      0.00000000000000e+000

Mean Anom(rad):                -2.55987441390008e+000

Af0(s):                        0.00000000000000e+000

Af1(s/s):                      0.00000000000000e+000

week:                          869


******** Week 869 almanac for PRN-16 ********

ID:                            16

Health:                        0

Eccentricity:                  0.00000000000000e+000

Time of Applicability(s):      144000

Orbital Inclination(rad):      9.77384381116824e-001

Rate of Right Ascen(r/s):      0.00000000000000e+000

SQRT(A)  (m 1/2):              5.44058820349418e+003

Right Ascen at Week(rad):      2.09439510239320e+000

Argument of Perigee(rad):      0.00000000000000e+000

Mean Anom(rad):                -1.86174271310235e+000

Af0(s):                        0.00000000000000e+000

Af1(s/s):                      0.00000000000000e+000

week:                          869


******** Week 869 almanac for PRN-17 ********

ID:                            17

Health:                        0

Eccentricity:                  0.00000000000000e+000

Time of Applicability(s):      144000

Orbital Inclination(rad):      9.77384381116824e-001

Rate of Right Ascen(r/s):      0.00000000000000e+000

SQRT(A)  (m 1/2):              5.44058820349418e+003
```

```
Right Ascen at Week(rad):      2.09439510239320e+000

Argument of Perigee(rad):      0.00000000000000e+000

Mean Anom(rad):                -1.16361101230462e+000

Af0(s):                        0.00000000000000e+000

Af1(s/s):                      0.00000000000000e+000

week:                          869


******** Week 869 almanac for PRN-18 ********

ID:                            18

Health:                        0

Eccentricity:                  0.00000000000000e+000

Time of Applicability(s):      144000

Orbital Inclination(rad):      9.77384381116824e-001

Rate of Right Ascen(r/s):      0.00000000000000e+000

SQRT(A)  (m 1/2):              5.44058820349418e+003

Right Ascen at Week(rad):      2.09439510239320e+000

Argument of Perigee(rad):      0.00000000000000e+000

Mean Anom(rad):                -4.65479311506889e-001

Af0(s):                        0.00000000000000e+000

Af1(s/s):                      0.00000000000000e+000

week:                          869


******** Week 869 almanac for PRN-19 ********

ID:                            19

Health:                        0

Eccentricity:                  0.00000000000000e+000

Time of Applicability(s):      144000

Orbital Inclination(rad):      9.77384381116824e-001

Rate of Right Ascen(r/s):      0.00000000000000e+000

SQRT(A)  (m 1/2):              5.44058820349418e+003
```

78

```
Right Ascen at Week(rad):       -2.09439510239320e+000

Argument of Perigee(rad):       0.00000000000000e+000

Mean Anom(rad):                 4.65304778581688e-001

Af0(s):                         0.00000000000000e+000

Af1(s/s):                       0.00000000000000e+000

week:                           869


******** Week 869 almanac for PRN-20 ********

ID:                             20

Health:                         0

Eccentricity:                   0.00000000000000e+000

Time of Applicability(s):       144000

Orbital Inclination(rad):       9.77384381116824e-001

Rate of Right Ascen(r/s):       0.00000000000000e+000

SQRT(A)  (m 1/2):               5.44058820349418e+003

Right Ascen at Week(rad):       -2.09439510239320e+000

Argument of Perigee(rad):       0.00000000000000e+000

Mean Anom(rad):                 1.16343647937942e+000

Af0(s):                         0.00000000000000e+000

Af1(s/s):                       0.00000000000000e+000

week:                           869


******** Week 869 almanac for PRN-21 ********

ID:                             21

Health:                         0

Eccentricity:                   0.00000000000000e+000

Time of Applicability(s):       144000

Orbital Inclination(rad):       9.77384381116824e-001

Rate of Right Ascen(r/s):       0.00000000000000e+000

SQRT(A)  (m 1/2):               5.44058820349418e+003
```
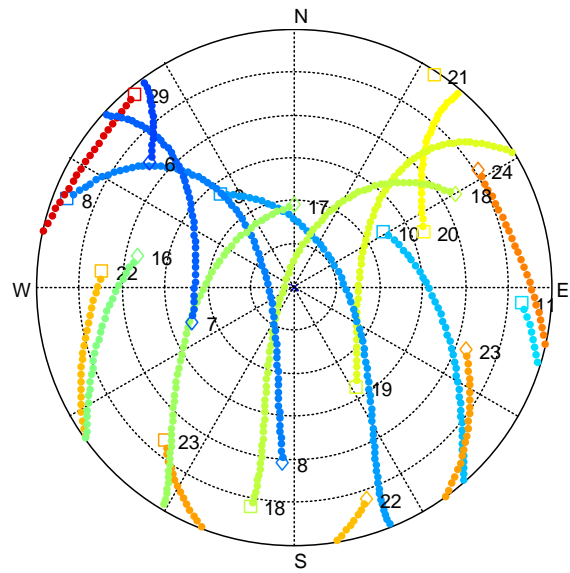
79

```
Right Ascen at Week(rad):      -2.09439510239320e+000

Argument of Perigee(rad):      0.00000000000000e+000

Mean Anom(rad):                1.86156818017715e+000

Af0(s):                        0.00000000000000e+000

Af1(s/s):                      0.00000000000000e+000

week:                          869


******** Week 869 almanac for PRN-22 ********

ID:                            22

Health:                        0

Eccentricity:                  0.00000000000000e+000

Time of Applicability(s):      144000

Orbital Inclination(rad):      9.77384381116824e-001

Rate of Right Ascen(r/s):      0.00000000000000e+000

SQRT(A)  (m 1/2):              5.44058820349418e+003

Right Ascen at Week(rad):      -2.09439510239320e+000

Argument of Perigee(rad):      0.00000000000000e+000

Mean Anom(rad):                2.55969988097488e+000

Af0(s):                        0.00000000000000e+000

Af1(s/s):                      0.00000000000000e+000

week:                          869


******** Week 869 almanac for PRN-23 ********

ID:                            23

Health:                        0

Eccentricity:                  0.00000000000000e+000

Time of Applicability(s):      144000

Orbital Inclination(rad):      9.77384381116824e-001

Rate of Right Ascen(r/s):      0.00000000000000e+000

SQRT(A)  (m 1/2):              5.44058820349418e+003
```

80

```
Right Ascen at Week(rad):        -2.09439510239320e+000

Argument of Perigee(rad):        0.00000000000000e+000

Mean Anom(rad):                  -3.02535372540697e+000

Af0(s):                          0.00000000000000e+000

Af1(s/s):                        0.00000000000000e+000

week:                            869


******** Week 869 almanac for PRN-24 ********

ID:                              24

Health:                          0

Eccentricity:                    0.00000000000000e+000

Time of Applicability(s):        144000

Orbital Inclination(rad):        9.77384381116824e-001

Rate of Right Ascen(r/s):        0.00000000000000e+000

SQRT(A)  (m 1/2):                5.44058820349418e+003

Right Ascen at Week(rad):        -2.09439510239320e+000

Argument of Perigee(rad):        0.00000000000000e+000

Mean Anom(rad):                  -2.32722202460924e+000

Af0(s):                          0.00000000000000e+000

Af1(s/s):                        0.00000000000000e+000

week:                            869


******** Week 869 almanac for PRN-25 ********

ID:                              25

Health:                          0

Eccentricity:                    0.00000000000000e+000

Time of Applicability(s):        144000

Orbital Inclination(rad):        9.77384381116824e-001

Rate of Right Ascen(r/s):        0.00000000000000e+000

SQRT(A)  (m 1/2):                5.44058820349418e+003
```

81

```
Right Ascen at Week(rad):      -2.09439510239320e+000

Argument of Perigee(rad):      0.00000000000000e+000

Mean Anom(rad):                -1.62909032381151e+000

Af0(s):                        0.00000000000000e+000

Af1(s/s):                      0.00000000000000e+000

week:                          869


******** Week 869 almanac for PRN-26 ********

ID:                            26

Health:                        0

Eccentricity:                  0.00000000000000e+000

Time of Applicability(s):      144000

Orbital Inclination(rad):      9.77384381116824e-001

Rate of Right Ascen(r/s):      0.00000000000000e+000

SQRT(A)  (m 1/2):              5.44058820349418e+003

Right Ascen at Week(rad):      -2.09439510239320e+000

Argument of Perigee(rad):      0.00000000000000e+000

Mean Anom(rad):                -9.30958623013774e-001

Af0(s):                        0.00000000000000e+000

Af1(s/s):                      0.00000000000000e+000

week:                          869


******** Week 869 almanac for PRN-27 ********

ID:                            27

Health:                        0

Eccentricity:                  0.00000000000000e+000

Time of Applicability(s):      144000

Orbital Inclination(rad):      9.77384381116824e-001

Rate of Right Ascen(r/s):      0.00000000000000e+000

SQRT(A)  (m 1/2):              5.44058820349418e+003
```

82

```
Right Ascen at Week(rad):        -2.09439510239320e+000

Argument of Perigee(rad):        0.00000000000000e+000

Mean Anom(rad):                  -2.32826922216043e-001

Af0(s):                          0.00000000000000e+000

Af1(s/s):                        0.00000000000000e+000

week:                            869
```
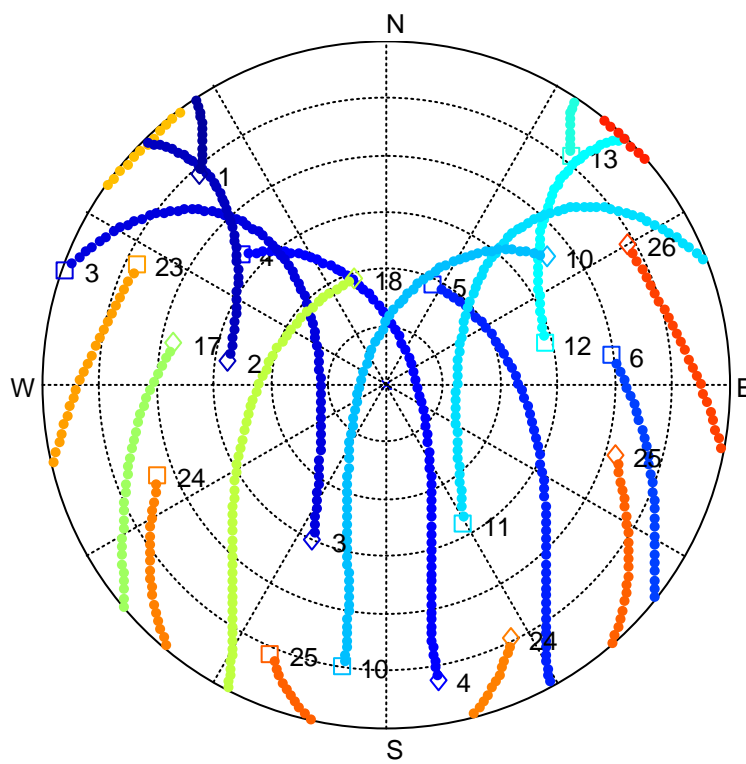

Galileo Satellite Visibility

(PRN-4 at -10 dB,

PRN-10 at -20 dB)

A.10.2.4   BeiDou Almanac

PRN-8 was generated at -10 dB and PRN-18 at -20 dB relative to the nominal received power levels (see Table 7). Both of these satellites are visible throughout the entire 6 hour simulation time.

```
******** Week 869 almanac for PRN-06 ********

ID:                       06

Health:                   0

Eccentricity:             0.00000000000000e+000

Time of Applicability(s):    144000

Orbital Inclination(rad):    9.59931088596883e-001

Rate of Right Ascen(r/s):    0.00000000000000e+000

SQRT(A)  (m 1/2):            5.27996000000000e+003

Right Ascen at Week(rad):    0.00000000000000e+000

Argument of Perigee(rad):    0.00000000000000e+000

Mean Anom(rad):              0.00000000000000e+000

Af0(s):                      0.00000000000000e+000

Af1(s/s):                    0.00000000000000e+000

week:                     869


******** Week 869 almanac for PRN-07 ********

ID:                       07

Health:                   0

Eccentricity:             0.00000000000000e+000

Time of Applicability(s):    144000

Orbital Inclination(rad):    9.59931088596883e-001

Rate of Right Ascen(r/s):    0.00000000000000e+000

SQRT(A)  (m 1/2):            5.27996000000000e+003

Right Ascen at Week(rad):    0.00000000000000e+000

Argument of Perigee(rad):    7.85398163397448e-001
```

```
Mean Anom(rad):            0.00000000000000e+000

Af0(s):                    0.00000000000000e+000

Af1(s/s):                  0.00000000000000e+000

week:                      869


******** Week 869 almanac for PRN-08 ********

ID:                        08

Health:                    0

Eccentricity:              0.00000000000000e+000

Time of Applicability(s):  144000

Orbital Inclination(rad):  9.59931088596883e-001

Rate of Right Ascen(r/s):  0.00000000000000e+000

SQRT(A)  (m 1/2):          5.27996000000000e+003

Right Ascen at Week(rad):  0.00000000000000e+000

Argument of Perigee(rad):  1.57079632679490e+000

Mean Anom(rad):            0.00000000000000e+000

Af0(s):                    0.00000000000000e+000

Af1(s/s):                  0.00000000000000e+000

week:                      869


******** Week 869 almanac for PRN-09 ********

ID:                        09

Health:                    0

Eccentricity:              0.00000000000000e+000

Time of Applicability(s):  144000

Orbital Inclination(rad):  9.59931088596883e-001

Rate of Right Ascen(r/s):  0.00000000000000e+000

SQRT(A)  (m 1/2):          5.27996000000000e+003

Right Ascen at Week(rad):  0.00000000000000e+000

Argument of Perigee(rad):  2.35619449019234e+000
```

85

```
Mean Anom(rad):              0.00000000000000e+000

Af0(s):                      0.00000000000000e+000

Af1(s/s):                    0.00000000000000e+000

week:                        869


******** Week 869 almanac for PRN-10 ********

ID:                          10

Health:                      0

Eccentricity:                0.00000000000000e+000

Time of Applicability(s):    144000

Orbital Inclination(rad):    9.59931088596883e-001

Rate of Right Ascen(r/s):    0.00000000000000e+000

SQRT(A)  (m 1/2):            5.27996000000000e+003

Right Ascen at Week(rad):    0.00000000000000e+000

Argument of Perigee(rad):    3.14159265358979e+000

Mean Anom(rad):              0.00000000000000e+000

Af0(s):                      0.00000000000000e+000

Af1(s/s):                    0.00000000000000e+000

week:                        869


******** Week 869 almanac for PRN-11 ********

ID:                          11

Health:                      0

Eccentricity:                0.00000000000000e+000

Time of Applicability(s):    144000

Orbital Inclination(rad):    9.59931088596883e-001

Rate of Right Ascen(r/s):    0.00000000000000e+000

SQRT(A)  (m 1/2):            5.27996000000000e+003

Right Ascen at Week(rad):    0.00000000000000e+000

Argument of Perigee(rad):    -2.35619449019234e+000
```

```
Mean Anom(rad):                0.00000000000000e+000

Af0(s):                        0.00000000000000e+000

Af1(s/s):                      0.00000000000000e+000

week:                          869


******** Week 869 almanac for PRN-12 ********

ID:                            12

Health:                        0

Eccentricity:                  0.00000000000000e+000

Time of Applicability(s):      144000

Orbital Inclination(rad):      9.59931088596883e-001

Rate of Right Ascen(r/s):      0.00000000000000e+000

SQRT(A)  (m 1/2):              5.27996000000000e+003

Right Ascen at Week(rad):      0.00000000000000e+000

Argument of Perigee(rad):      -1.57079632679490e+000

Mean Anom(rad):                0.00000000000000e+000

Af0(s):                        0.00000000000000e+000

Af1(s/s):                      0.00000000000000e+000

week:                          869


******** Week 869 almanac for PRN-13 ********

ID:                            13

Health:                        0

Eccentricity:                  0.00000000000000e+000

Time of Applicability(s):      144000

Orbital Inclination(rad):      9.59931088596883e-001

Rate of Right Ascen(r/s):      0.00000000000000e+000

SQRT(A)  (m 1/2):              5.27996000000000e+003

Right Ascen at Week(rad):      0.00000000000000e+000

Argument of Perigee(rad):      -7.85398163397448e-001
```

```
Mean Anom(rad):              0.00000000000000e+000

Af0(s):                      0.00000000000000e+000

Af1(s/s):                    0.00000000000000e+000

week:                        869


******** Week 869 almanac for PRN-14 ********

ID:                          14

Health:                      0

Eccentricity:                0.00000000000000e+000

Time of Applicability(s):    144000

Orbital Inclination(rad):    9.59931088596883e-001

Rate of Right Ascen(r/s):    0.00000000000000e+000

SQRT(A)  (m 1/2):            5.27996000000000e+003

Right Ascen at Week(rad):    2.09439510239320e+000

Argument of Perigee(rad):    -2.87979326579064e+000

Mean Anom(rad):              0.00000000000000e+000

Af0(s):                      0.00000000000000e+000

Af1(s/s):                    0.00000000000000e+000

week:                        869


******** Week 869 almanac for PRN-15 ********

ID:                          15

Health:                      0

Eccentricity:                0.00000000000000e+000

Time of Applicability(s):    144000

Orbital Inclination(rad):    9.59931088596883e-001

Rate of Right Ascen(r/s):    0.00000000000000e+000

SQRT(A)  (m 1/2):            5.27996000000000e+003

Right Ascen at Week(rad):    2.09439510239320e+000

Argument of Perigee(rad):    -2.09439510239321e+000
```

Mean Anom(rad):   0.00000000000000e+000

Af0(s):   0.00000000000000e+000

Af1(s/s):   0.00000000000000e+000

week: 869

******** Week 869 almanac for PRN-16 ********

ID: 16

Health: 0

Eccentricity: 0.00000000000000e+000

Time of Applicability(s):   144000

Orbital Inclination(rad):   9.59931088596883e-001

Rate of Right Ascen(r/s):   0.00000000000000e+000

SQRT(A) (m 1/2):   5.27996000000000e+003

Right Ascen at Week(rad):   2.09439510239320e+000

Argument of Perigee(rad):   -1.30899693899576e+000

Mean Anom(rad):   0.00000000000000e+000

Af0(s):   0.00000000000000e+000

Af1(s/s):   0.00000000000000e+000

week: 869

******** Week 869 almanac for PRN-17 ********

ID: 17

Health: 0

Eccentricity: 0.00000000000000e+000

Time of Applicability(s):   144000

Orbital Inclination(rad):   9.59931088596883e-001

Rate of Right Ascen(r/s):   0.00000000000000e+000

SQRT(A) (m 1/2):   5.27996000000000e+003

Right Ascen at Week(rad):   2.09439510239320e+000

Argument of Perigee(rad):   -5.23598775598309e-001

89

```
Mean Anom(rad):              0.00000000000000e+000

Af0(s):                      0.00000000000000e+000

Af1(s/s):                    0.00000000000000e+000

week:                        869


******** Week 869 almanac for PRN-18 ********

ID:                          18

Health:                      0

Eccentricity:                0.00000000000000e+000

Time of Applicability(s):    144000

Orbital Inclination(rad):    9.59931088596883e-001

Rate of Right Ascen(r/s):    0.00000000000000e+000

SQRT(A)  (m 1/2):            5.27996000000000e+003

Right Ascen at Week(rad):    2.09439510239320e+000

Argument of Perigee(rad):    2.61799387799148e-001

Mean Anom(rad):              0.00000000000000e+000

Af0(s):                      0.00000000000000e+000

Af1(s/s):                    0.00000000000000e+000

week:                        869


******** Week 869 almanac for PRN-19 ********

ID:                          19

Health:                      0

Eccentricity:                0.00000000000000e+000

Time of Applicability(s):    144000

Orbital Inclination(rad):    9.59931088596883e-001

Rate of Right Ascen(r/s):    0.00000000000000e+000

SQRT(A)  (m 1/2):            5.27996000000000e+003

Right Ascen at Week(rad):    2.09439510239320e+000

Argument of Perigee(rad):    1.04719755119660e+000
```

```
Mean Anom(rad):              0.00000000000000e+000

Af0(s):                      0.00000000000000e+000

Af1(s/s):                    0.00000000000000e+000

week:                        869


******** Week 869 almanac for PRN-20 ********

ID:                          20

Health:                      0

Eccentricity:                0.00000000000000e+000

Time of Applicability(s):    144000

Orbital Inclination(rad):    9.59931088596883e-001

Rate of Right Ascen(r/s):    0.00000000000000e+000

SQRT(A)  (m 1/2):            5.27996000000000e+003

Right Ascen at Week(rad):    2.09439510239320e+000

Argument of Perigee(rad):    1.83259571459405e+000

Mean Anom(rad):              0.00000000000000e+000

Af0(s):                      0.00000000000000e+000

Af1(s/s):                    0.00000000000000e+000

week:                        869


******** Week 869 almanac for PRN-21 ********

ID:                          21

Health:                      0

Eccentricity:                0.00000000000000e+000

Time of Applicability(s):    144000

Orbital Inclination(rad):    9.59931088596883e-001

Rate of Right Ascen(r/s):    0.00000000000000e+000

SQRT(A)  (m 1/2):            5.27996000000000e+003

Right Ascen at Week(rad):    2.09439510239320e+000

Argument of Perigee(rad):    2.61799387799149e+000
```

```
Mean Anom(rad):              0.00000000000000e+000

Af0(s):                      0.00000000000000e+000

Af1(s/s):                    0.00000000000000e+000

week:                        869


******** Week 869 almanac for PRN-22 ********

ID:                          22

Health:                      0

Eccentricity:                0.00000000000000e+000

Time of Applicability(s):    144000

Orbital Inclination(rad):    9.59931088596883e-001

Rate of Right Ascen(r/s):    0.00000000000000e+000

SQRT(A)  (m 1/2):            5.27996000000000e+003

Right Ascen at Week(rad):    -2.09439510239320e+000

Argument of Perigee(rad):    -2.61799387799148e+000

Mean Anom(rad):              0.00000000000000e+000

Af0(s):                      0.00000000000000e+000

Af1(s/s):                    0.00000000000000e+000

week:                        869


******** Week 869 almanac for PRN-23 ********

ID:                          23

Health:                      0

Eccentricity:                0.00000000000000e+000

Time of Applicability(s):    144000

Orbital Inclination(rad):    9.59931088596883e-001

Rate of Right Ascen(r/s):    0.00000000000000e+000

SQRT(A)  (m 1/2):            5.27996000000000e+003

Right Ascen at Week(rad):    -2.09439510239321e+000

Argument of Perigee(rad):    -1.83259571459404e+000
```

92

```
Mean Anom(rad):            0.00000000000000e+000

Af0(s):                    0.00000000000000e+000

Af1(s/s):                  0.00000000000000e+000

week:                      869


******** Week 869 almanac for PRN-24 ********

ID:                        24

Health:                    0

Eccentricity:              0.00000000000000e+000

Time of Applicability(s):  144000

Orbital Inclination(rad):  9.59931088596883e-001

Rate of Right Ascen(r/s):  0.00000000000000e+000

SQRT(A)  (m 1/2):          5.27996000000000e+003

Right Ascen at Week(rad):  -2.09439510239320e+000

Argument of Perigee(rad):  -1.04719755119660e+000

Mean Anom(rad):            0.00000000000000e+000

Af0(s):                    0.00000000000000e+000

Af1(s/s):                  0.00000000000000e+000

week:                      869


******** Week 869 almanac for PRN-25 ********

ID:                        25

Health:                    0

Eccentricity:              0.00000000000000e+000

Time of Applicability(s):  144000

Orbital Inclination(rad):  9.59931088596883e-001

Rate of Right Ascen(r/s):  0.00000000000000e+000

SQRT(A)  (m 1/2):          5.27996000000000e+003

Right Ascen at Week(rad):  -2.09439510239321e+000

Argument of Perigee(rad):  -2.61799387799148e-001
```

93

Mean Anom(rad):   0.00000000000000e+000

Af0(s):   0.00000000000000e+000

Af1(s/s):   0.00000000000000e+000

week: 869

******** Week 869 almanac for PRN-26 ********

ID: 26

Health: 0

Eccentricity: 0.00000000000000e+000

Time of Applicability(s):   144000

Orbital Inclination(rad):   9.59931088596883e-001

Rate of Right Ascen(r/s):   0.00000000000000e+000

SQRT(A) (m 1/2):   5.27996000000000e+003

Right Ascen at Week(rad):   -2.09439510239321e+000

Argument of Perigee(rad):   5.23598775598300e-001

Mean Anom(rad):   0.00000000000000e+000

Af0(s):   0.00000000000000e+000

Af1(s/s):   0.00000000000000e+000

week: 869

******** Week 869 almanac for PRN-27 ********

ID: 27

Health: 0

Eccentricity: 0.00000000000000e+000

Time of Applicability(s):   144000

Orbital Inclination(rad):   9.59931088596883e-001

Rate of Right Ascen(r/s):   0.00000000000000e+000

SQRT(A) (m 1/2):   5.27996000000000e+003

Right Ascen at Week(rad):   -2.09439510239321e+000

Argument of Perigee(rad):   1.30899693899575e+000

94

```
Mean Anom(rad):            0.00000000000000e+000

Af0(s):                    0.00000000000000e+000

Af1(s/s):                  0.00000000000000e+000

week:                      869


******** Week 869 almanac for PRN-28 ********

ID:                        28

Health:                    0

Eccentricity:              0.00000000000000e+000

Time of Applicability(s):  144000

Orbital Inclination(rad):  9.59931088596883e-001

Rate of Right Ascen(r/s):  0.00000000000000e+000

SQRT(A)  (m 1/2):          5.27996000000000e+003

Right Ascen at Week(rad):  -2.09439510239321e+000

Argument of Perigee(rad):  2.09439510239320e+000

Mean Anom(rad):            0.00000000000000e+000

Af0(s):                    0.00000000000000e+000

Af1(s/s):                  0.00000000000000e+000

week:                      869


******** Week 869 almanac for PRN-29 ********

ID:                        29

Health:                    0

Eccentricity:              0.00000000000000e+000

Time of Applicability(s):  144000

Orbital Inclination(rad):  9.59931088596883e-001

Rate of Right Ascen(r/s):  0.00000000000000e+000

SQRT(A)  (m 1/2):          5.27996000000000e+003

Right Ascen at Week(rad):  -2.09439510239321e+000

Argument of Perigee(rad):  2.87979326579064e+000
```

95

```
Mean Anom(rad):               0.00000000000000e+000

Af0(s):                       0.00000000000000e+000

Af1(s/s):                     0.00000000000000e+000

week:                         869
```


BeiDou Visibility
(PRN-08 at -10 dB,
PRN-18 at -20 dB)

A.10.2.5   SBAS Satellites

The two SBAS satellites were emulated in the geostationary satellite arc above 133W and 108W with PRNs 135 and 138, respectively.

A.10.3 Emulated errors

The Spirent RTCA06 tropospheric model was utilized to generate tropospheric errors on the pseudorange and carrier phase measurements as appropriate for the emulated user location and date (32N, 106W, April 18, 2016).

Ionospheric errors were emulated using the GPS single-frequency ionospheric delay model (i.e., the Klobuchar model). The following 8 coefficients were utilized:

ALPHA0: 5.58793544769E-009

ALPHA1: 1.49011611938E-008

ALPHA2: -5.96046447754E-008

ALPHA3: -1.19209289551E-007

BETA0: 83968

BETA1: 98304

BETA2: -65536

BETA3: -524288

Galileo uses a different single-frequency ionospheric correction model known as NeQuick. NeQuick coefficients were generated, using a Spirent GSS8000 simulator software utility, to best match ionospheric delay corrections per the GPS Klobuchar model with the coefficients listed above.

A.10.4

APPENDIX B

AGGREGATE ITM RESULTS

TABLE OF CONTENTS

LIST OF FIGURES

LIST OF TABLES

REFERENCES

There are no sources in the current document.

APPENDIX

Appendix B. Aggregate ITM Results

B.1   Statistical and Bounding ITMs for 1MHz and 10 MHz LTE Interference Signals

B.1.1   Interference Test Results for 1-MHz AWGN
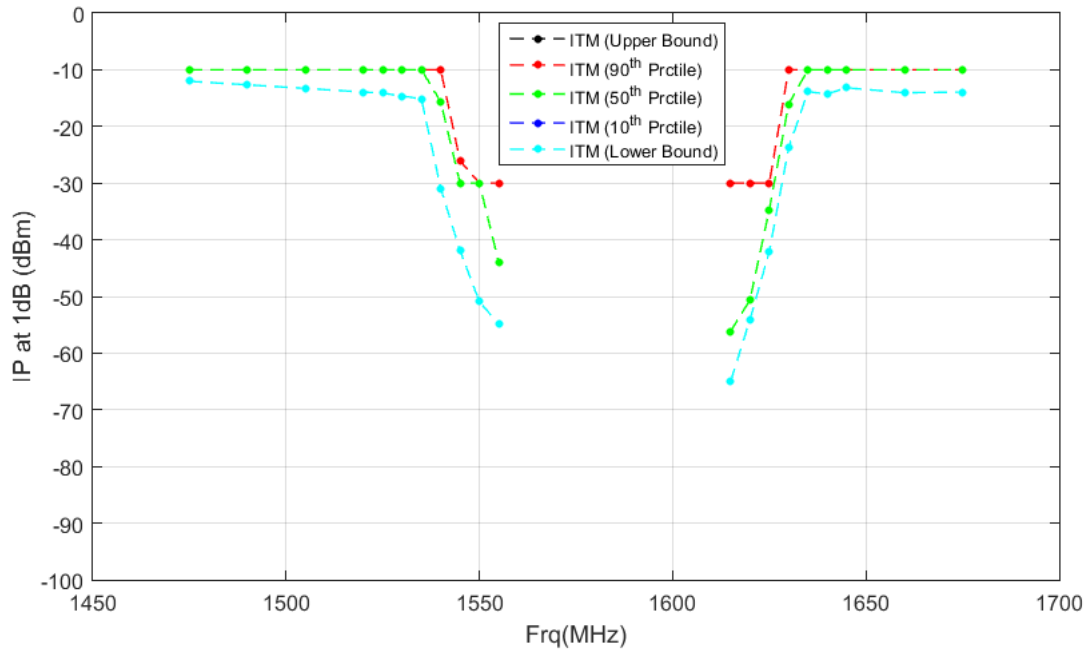
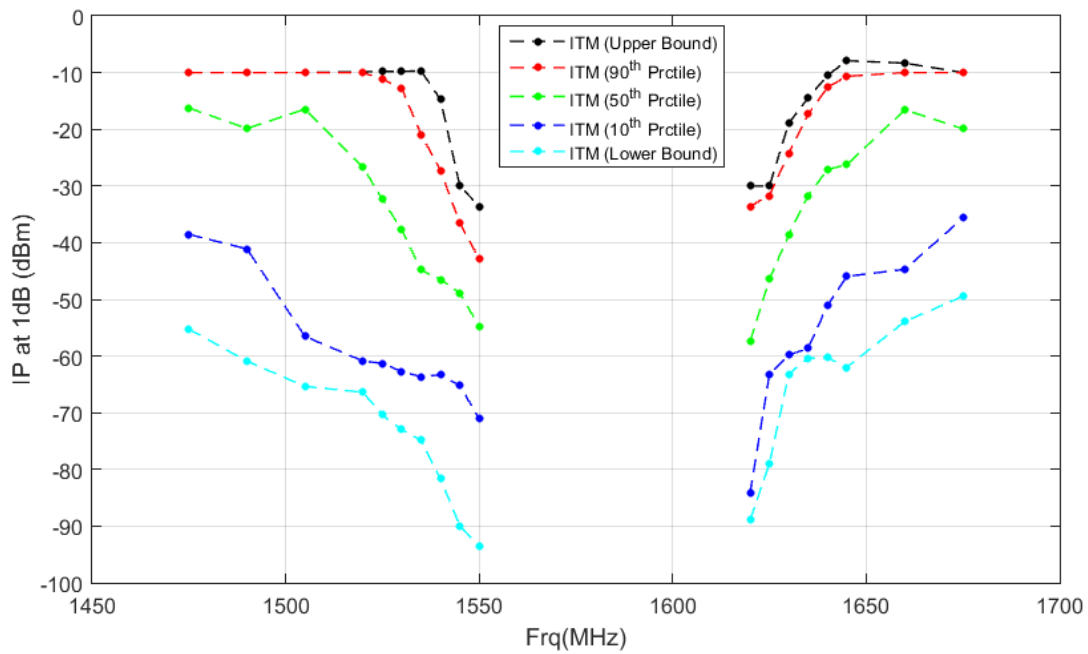**Figure B-1: 1 MHz GPS L1 C/A Statistical Mask Results for Cellular receivers**
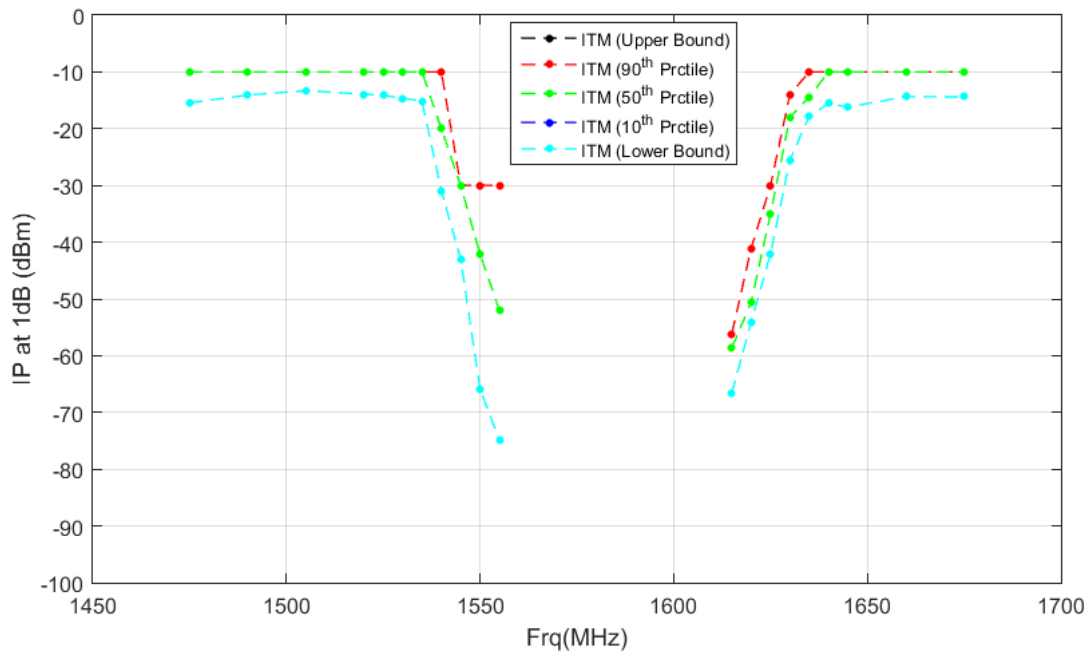
Figure B-2: 1 MHz All GNSS Aggregated Minimum Statistical Mask Results for Cellular receivers
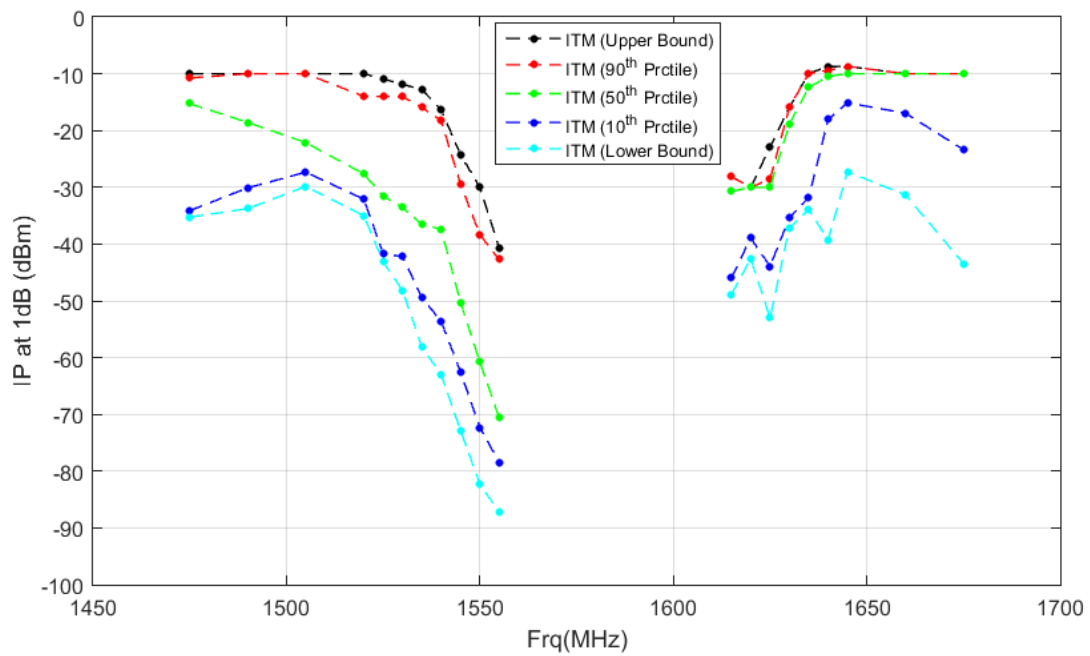
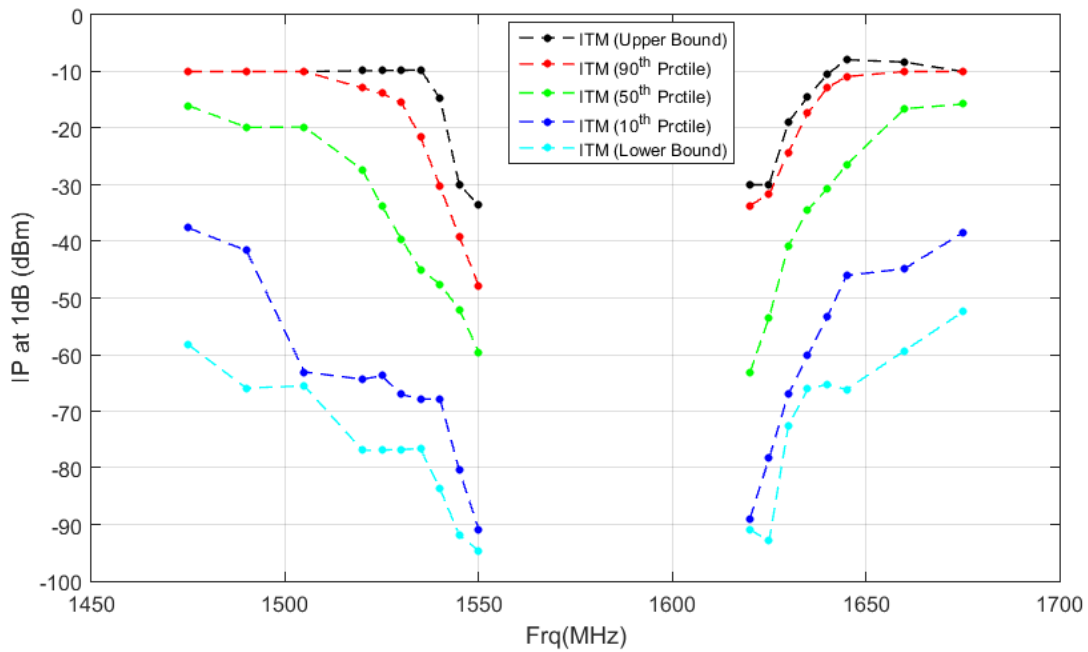**Figure B-3: 1 MHz GPS L1 C/A Statistical Mask Results for General Aviation receivers**
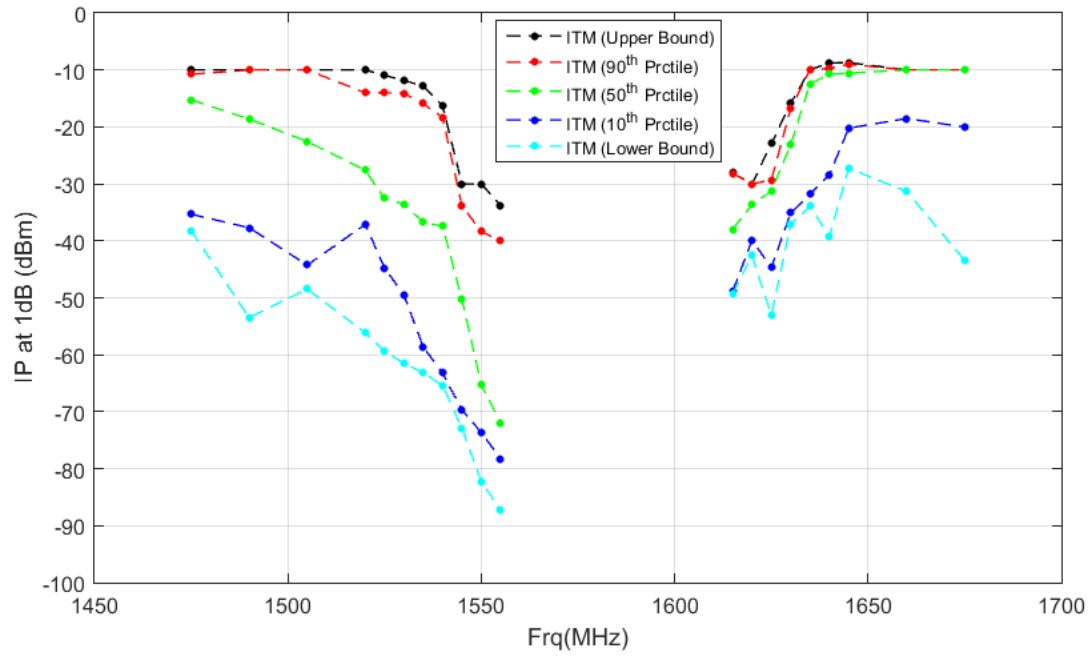
Figure B-4: 1 MHz All GNSS Aggregated Minimum Statistical Mask Results for General Aviation receivers
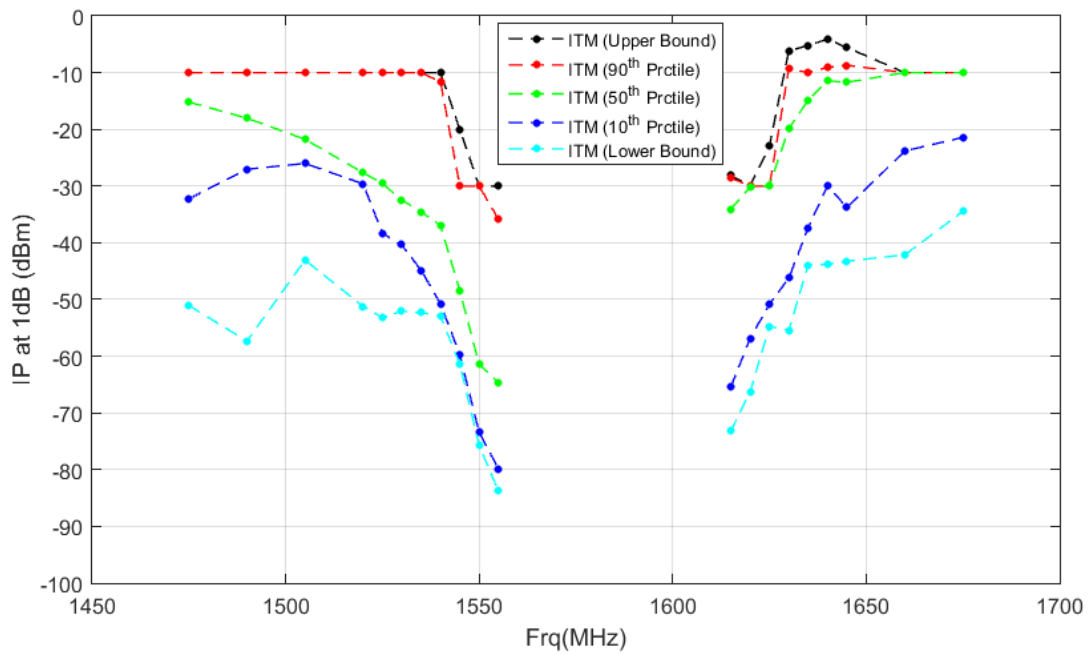
Figure B-5: 1 MHz GPS L1 C/A Statistical Mask Results for General Location Navigation receivers
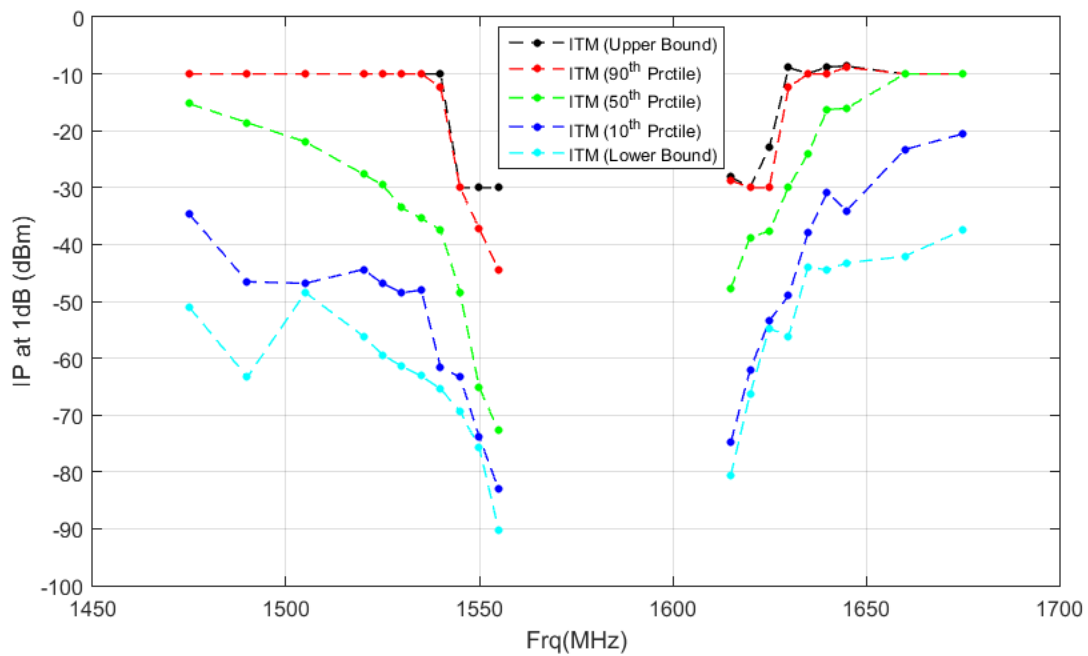
Figure B-6: 1 MHz All GNSS Aggregated Minimum Statistical Mask Results for General Location Navigation receivers
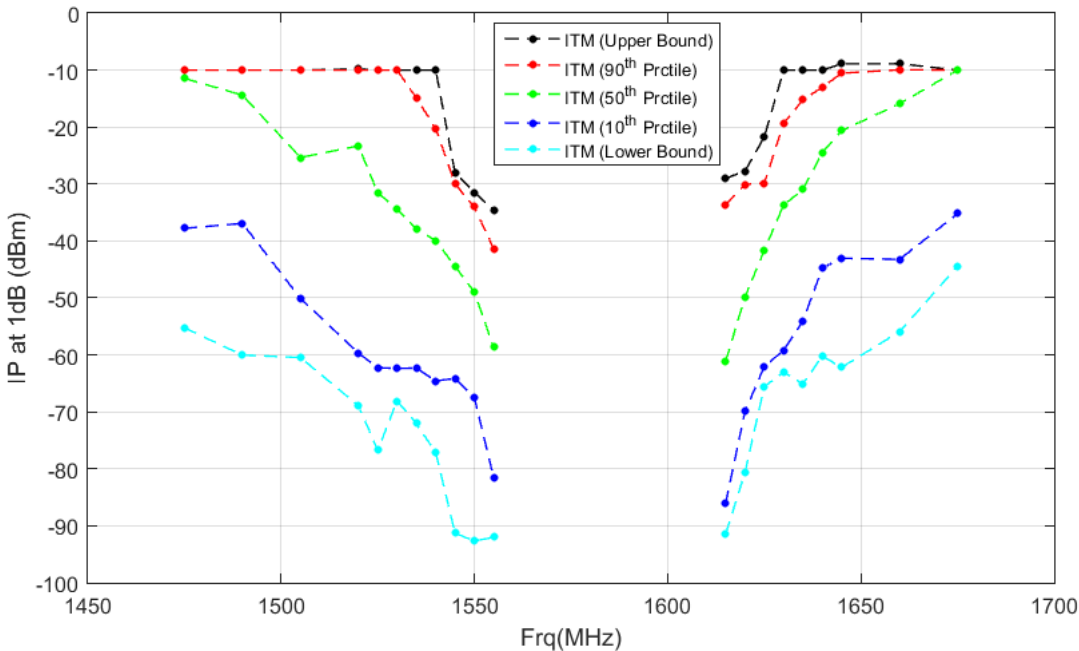
Figure B-7: 1 MHz GPS L1 C/A Statistical Mask Results for High Precision receivers
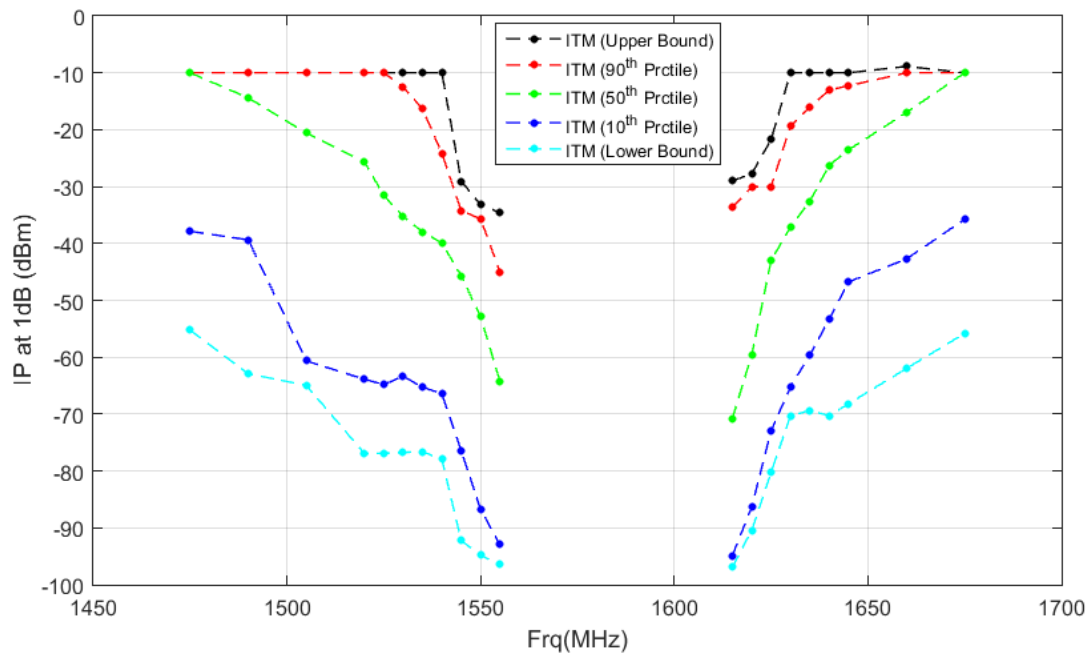
Figure B-8: 1 MHz All GNSS Aggregated Minimum Statistical Mask Results for High Precision receivers
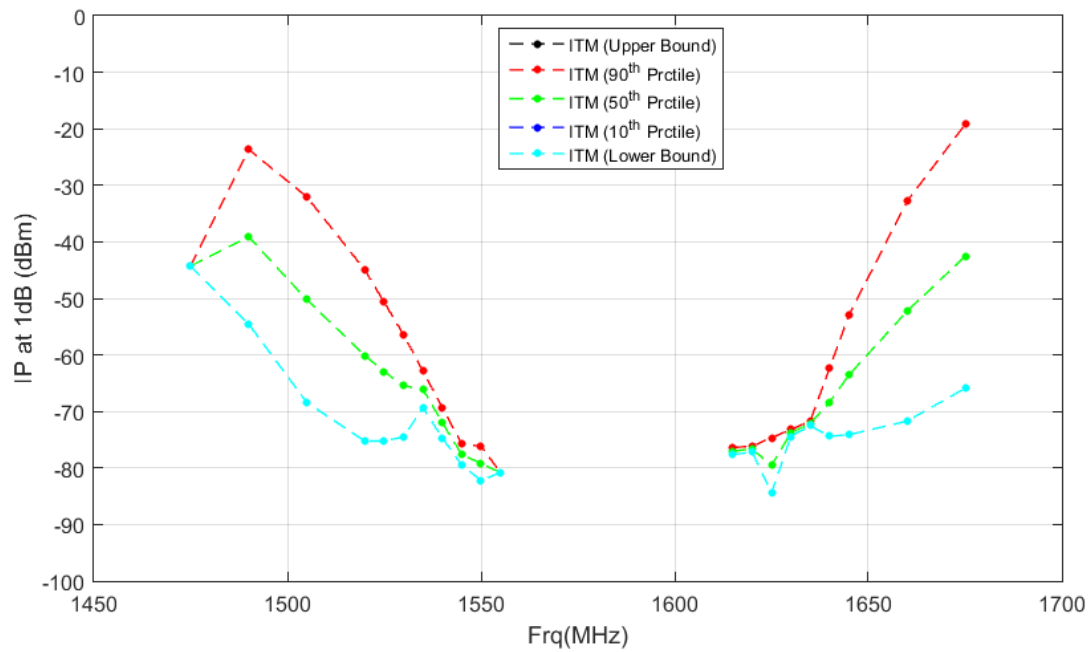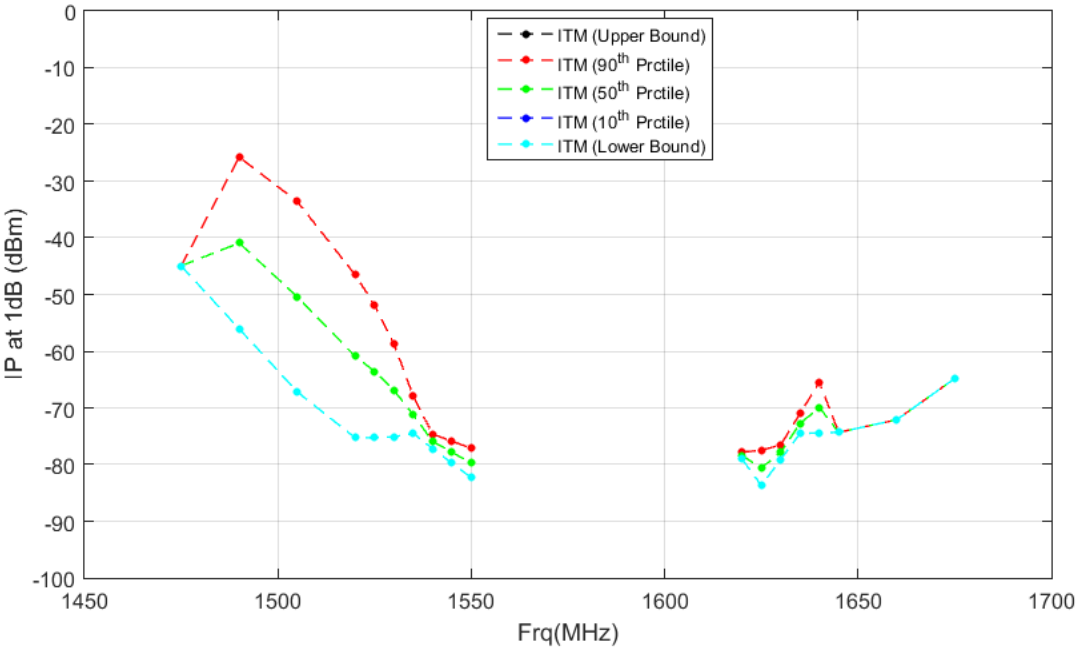
**Figure B-9: 1 MHz GPS L1 C/A Statistical Mask Results for
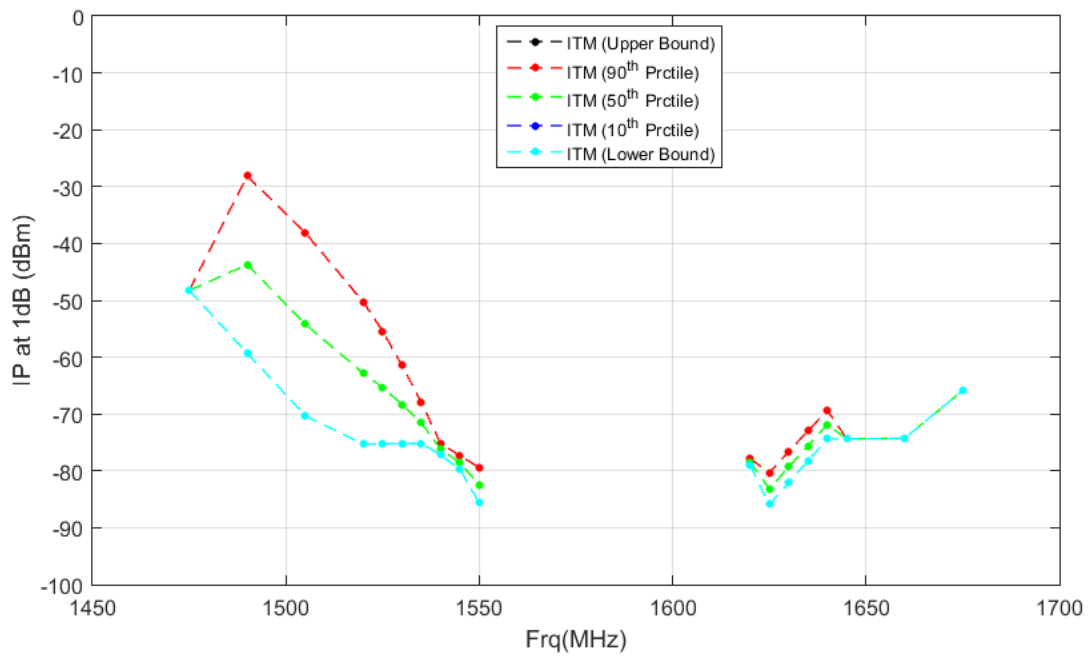Space Based receivers**
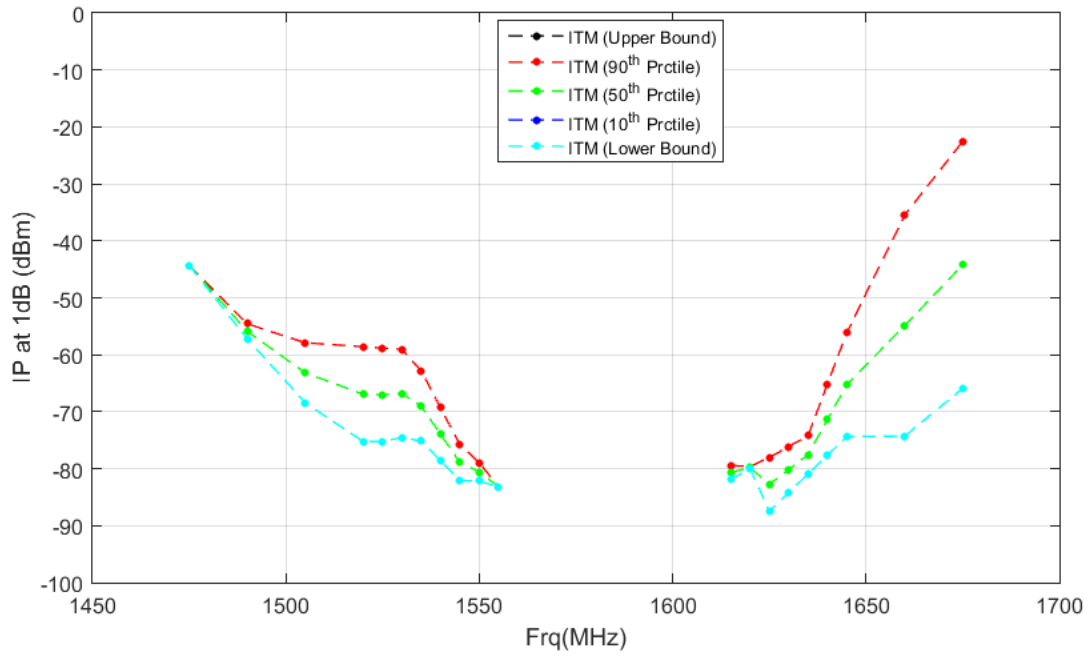
**Figure B-10: 1 MHz All GNSS Aggregated Minimum Statistical Mask Results for
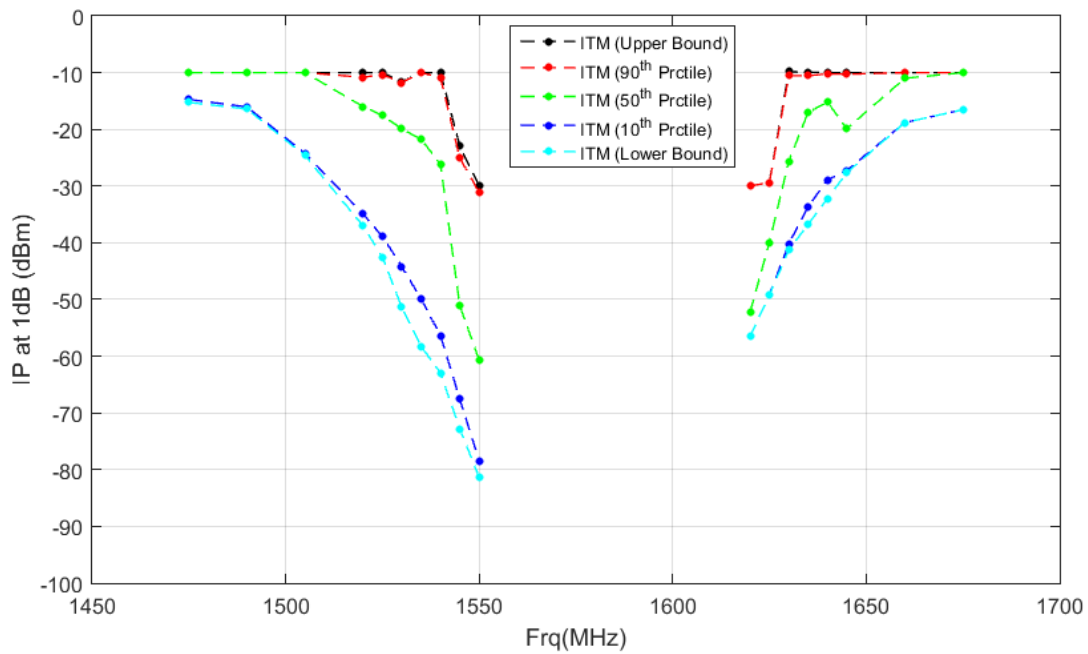Space Based receivers**
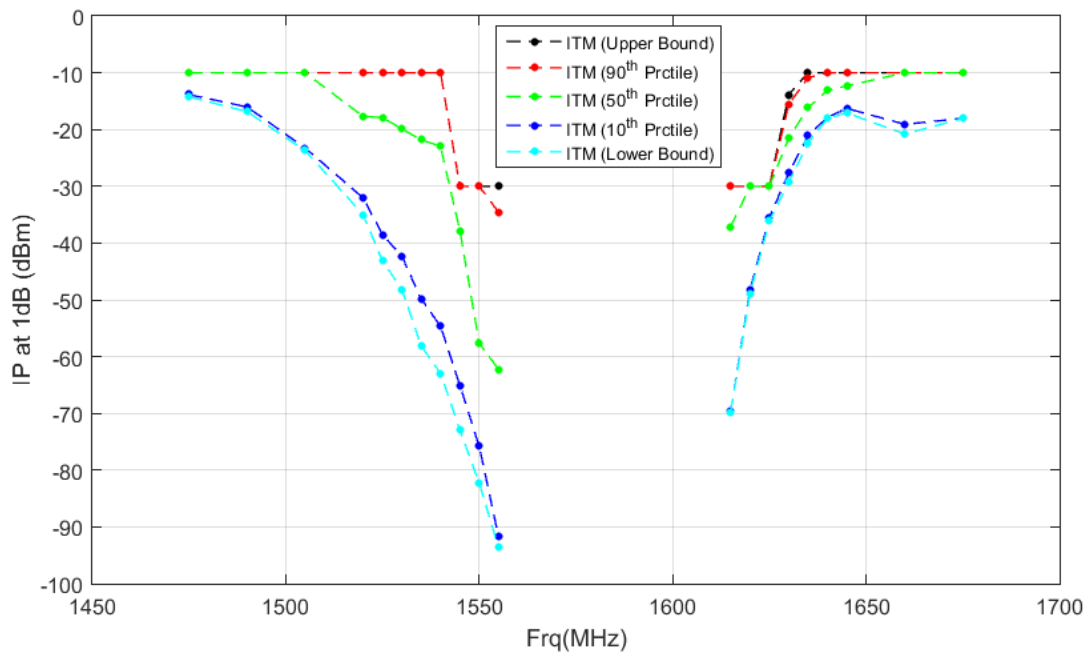
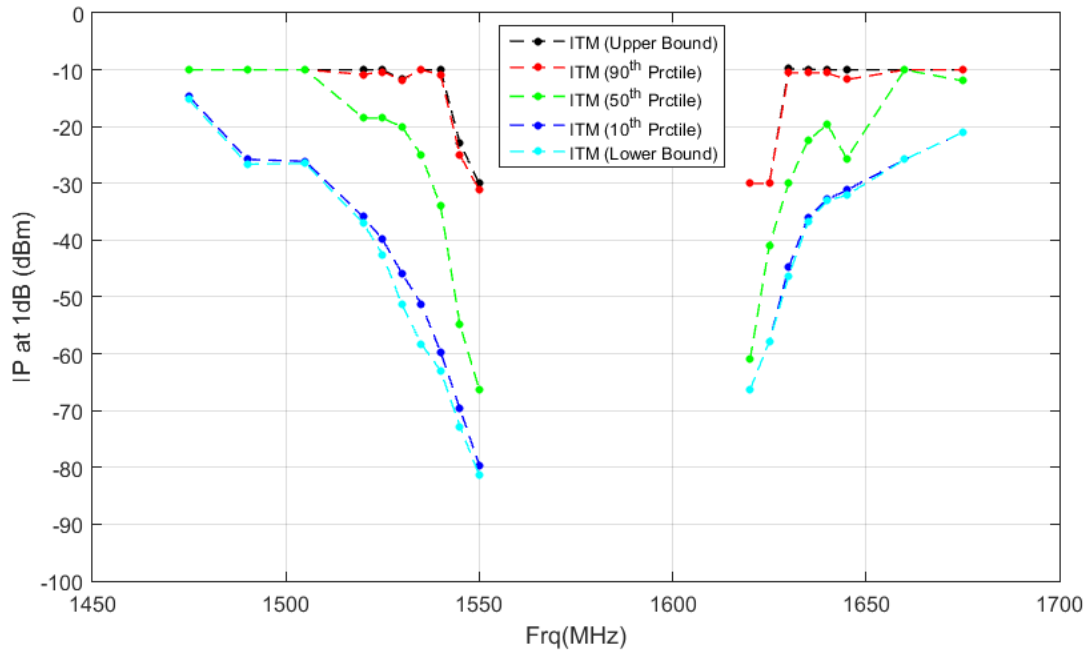**Figure B-11: 1 MHz GPS L1 C/A Statistical Mask Results for Timing receivers**
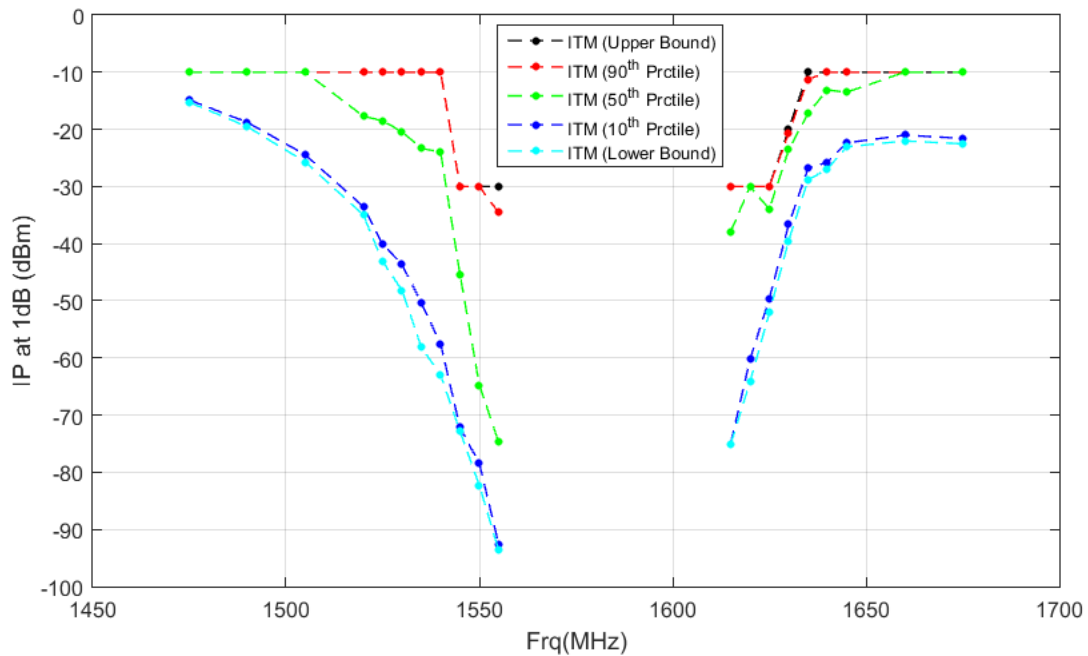
Figure B-12: 1 MHz All GNSS Aggregated Minimum Statistical Mask Results for Timing receivers

Table B-1: 1 MHz and 1 MHz In-band* GPS L1 C/A Bounding Masks (dBm)

| Frequency (MHz)	GAV	GLN	HPR	TIM	SPB	CEL
1475	-35.2559	-51.0577	-55.2458	-14.2455	-44.2989	-12.0223
1490	-33.7621	-57.3312	-60.0236	-16.8303	-54.552	-12.6553
1505	-29.8401	-43.0491	-60.4615	-23.7082	-68.4079	-13.2884
1520	-34.9844	-51.2192	-68.9024	-34.9844	-75.2401	-13.9214
1525	-43.1501	-53.1671	-76.7213	-43.1501	-75.2341	-14.1324
1530	-48.1543	-52.0402	-68.0809	-48.1543	-74.5091	-14.6318
1535	-58.124	-52.322	-72.0429	-58.124	-69.3135	-15.1311
1540	-62.9739	-52.9021	-77.1205	-62.9739	-74.6895	-30.9017
1545	-72.8509	-61.3673	-91.2872	-72.8509	-79.5006	-41.9222
1550	-82.2979	-75.7539	-92.663	-82.2979	-82.1933	-50.8924
1555	-87.2361	-83.7667	-92.0068	-93.6384	-80.8092	-54.9029
1575*	-119.066	-119.066	-116.191	-115.066	-110.143	-113.425
1595*	-82.7539	-83.6945	-99.8672	-82.7539	-81.6271	-75.4419
1615	-48.8394	-73.2344	-91.4798	-69.7614	-77.6033	-65.0079
1620	-42.5903	-66.3442	-80.6362	-48.8434	-77.2055	-54.0767
1625	-52.9903	-54.7378	-65.5759	-36.1468	-84.4141	-42.0742
1630	-37.111	-55.4588	-63.0348	-29.2349	-74.4229	-23.7846
1635	-33.9518	-43.9075	-65.1038	-22.3593	-72.5191	-13.8657
1640	-39.2495	-43.7996	-60.2043	-18.0435	-74.405	-14.2567
1645	-27.2708	-43.2334	-62.1873	-17.0656	-74.1188	-13.18
1660	-31.3256	-42.1121	-55.9123	-20.8014	-71.7159	-14.0507
1675	-43.4325	-34.4705	-44.4567	-18.0372	-65.8974	-13.9362

16
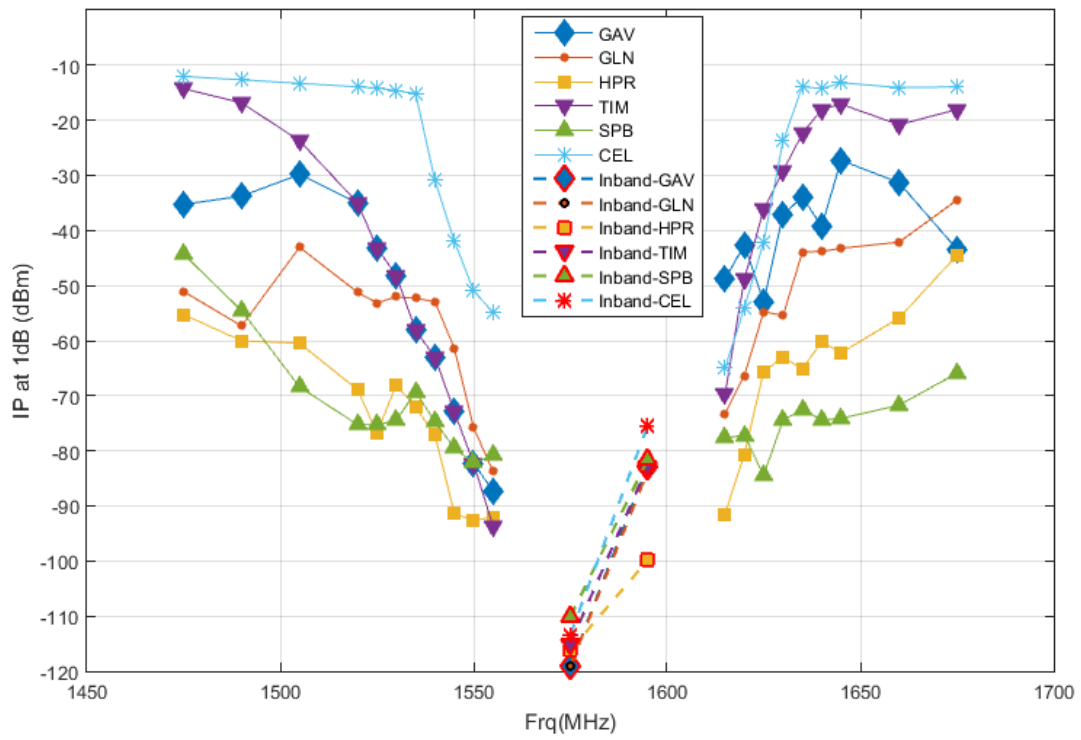
Figure B-13: Summary of 1 MHz and 1 MHz In-band GPS L1 C/A Bounding Masks

Table B-2: 1 MHz and 1 MHz In-band* GPS L1 P Bounding Masks (dBm)

| Frequency (MHz)	GLN	HPR	SPB	CEL
1475	-9.999	-54.6169	-16.4489	-12.0223
1490	-9.999	-60.4599	-57.1999	-12.6553
1505	-9.999	-62.3551	-57.8913	-13.2884
1520	-9.999	-65.2899	-58.5827	-13.9214
1525	-9.999	-62.0257	-58.8132	-14.1324
1530	-9.999	-62.0352	-59.7591	-14.6318
1535	-10.5239	-62.5546	-75.151	-15.1311
1540	-13.6638	-62.5322	-78.6008	-19.999
1545	-29.999	-62.6246	-82.0506	-29.999
1550	-40.4331	-64.2835	-78.9579	-29.999
1555	-50.8672	-66.7664	-83.1592	-29.999
1575*	-111.658	-108.025	-112.731	-113.227
1595*	-70.3132	-66.6468	NaN	-75.4419
1615	-66.3527	-63.5333	-81.9033	-65.0079
1620	-58.9925	-62.7395	-79.9751	-50.6889
1625	-43.759	-62.5091	-87.4391	-35.3214
1630	-30.4904	-61.0547	-84.1715	-23.7846
1635	-27.0752	-61.7723	-80.9039	-13.8657
1640	-23.66	-61.6717	-77.6363	-14.2567
1645	-20.2447	-62.4248	-74.3688	-13.18
1660	-9.999	-50.8114	-74.2659	-14.0507
1675	-9.999	-40.097	-65.4474	-13.9362
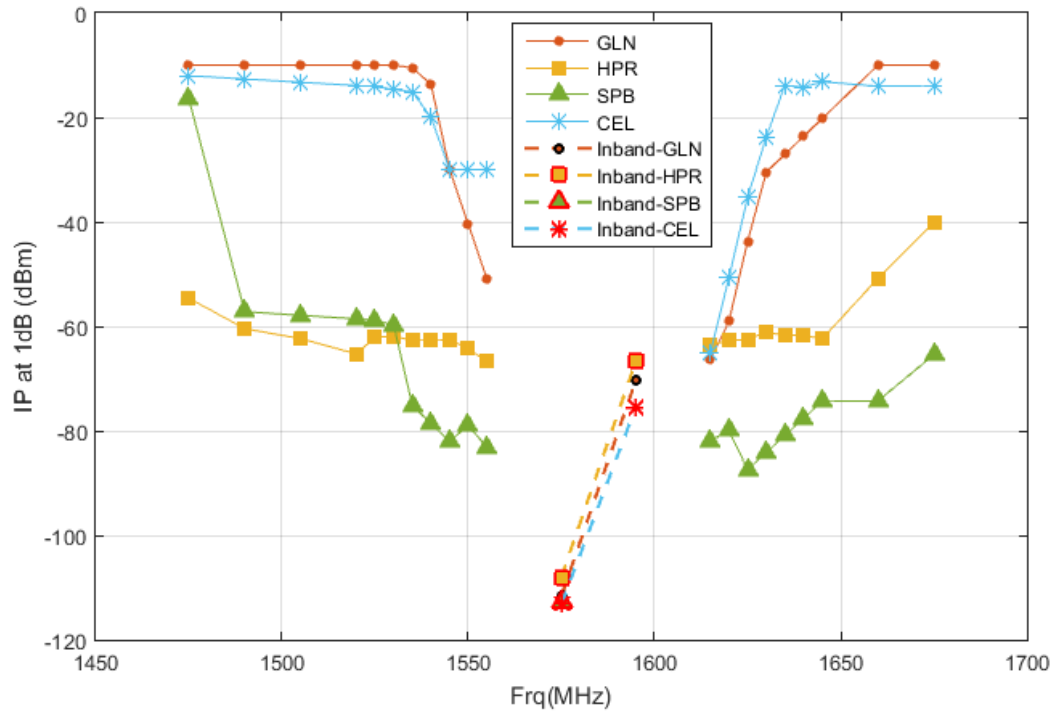
Figure B-14: Summary of 1 MHz and 1 MHz In-band GPS L1 P Bounding Masks

Table B-3: 1 MHz and 1 MHz In-band* GPS L1 C Bounding Masks (dBm)

Frequency (MHz)	GLN	CEL
1475	-9.999	-12.0223
1490	-9.999	-12.6553
1505	-9.999	-13.2884
1520	-9.999	-13.9214
1525	-9.999	-14.1324
1530	-9.999	-14.6318
1535	-10.5239	-15.1311
1540	-13.6638	-19.999
1545	-29.999	-29.999
1550	-33.2037	-29.999
1555	-50.8672	-29.999
1575*	-111.658	-113.227
1595*	-70.3132	-75.4419
1615	-66.3527	-65.0079
1620	-58.9925	-50.6889
1625	-43.759	-35.3214
1630	-30.4904	-23.7846
1635	-27.0752	-13.8657
1640	-23.66	-14.2567
1645	-20.2447	-13.18
1660	-9.999	-14.0507
1675	-9.999	-13.9362
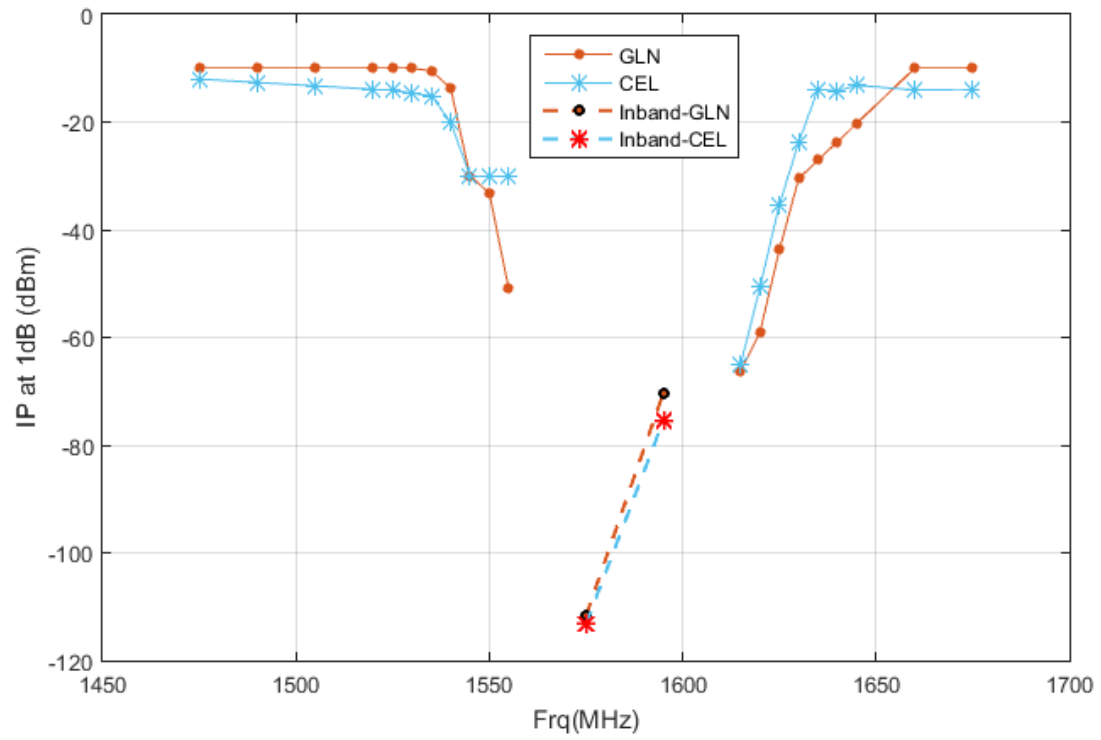
Figure B-15: Summary of 1 MHz and 1 MHz In-band GPS L1 C Bounding Masks

Table B-4: 1 MHz and 1 MHz In-band* GLONASS L1 C Bounding Masks (dBm)

| Frequency (MHz)	GAV	GLN	HPR	TIM	CEL
1475	-38.2559	-44.7577	-54.6169	-15.2559	-15.4348
1490	-53.4803	-53.4803	-62.9099	-19.5303	-14.0758
1505	-48.4582	-48.4582	-64.9422	-25.7082	-12.7169
1520	-56.1318	-56.1318	-76.9467	-31.3318	-11.3579
1525	-59.3929	-59.3929	-76.8713	-35.5429	-10.905
1530	-61.4793	-61.4793	-76.7309	-36.8043	-10.452
1535	-63.145	-63.145	-76.5364	-38.695	-9.999
1540	-65.4252	-65.4252	-76.3935	-49.3752	-21.2267
1545	-69.3673	-69.3673	-79.0175	-71.1694	-38.8222
1550	-72.6693	-72.6693	-86.7862	-72.6693	-42.0942
1555	-77.2525	-77.2525	-92.9286	-90.0964	-50.9955
1575*	-74.1159	-77.5833	-106.008	-90.6933	-73.3266
1595*	-98.5561	-101.975	-113.167	-110.561	-79.5011
1615	-49.3102	-75.1443	-96.917	-75.1443	-66.5954
1620	-39.5942	-64.2107	-90.419	-64.2107	-47.9014
1625	-43.7848	-52.0968	-80.2284	-52.0968	-37.3339
1630	-30.8828	-44.72	-70.3042	-39.5099	-25.5447
1635	-29.1745	-42.9075	-69.3723	-28.8593	-17.7719
1640	-25.6797	-44.4996	-70.2717	-26.931	-15.5567
1645	-18.4429	-37.7709	-68.1748	-23.0656	-16.18
1660	-15.3092	-40.1121	-61.9614	-22.0264	-14.3642
1675	-9.999	-37.4705	-55.797	-22.5372	-14.3862
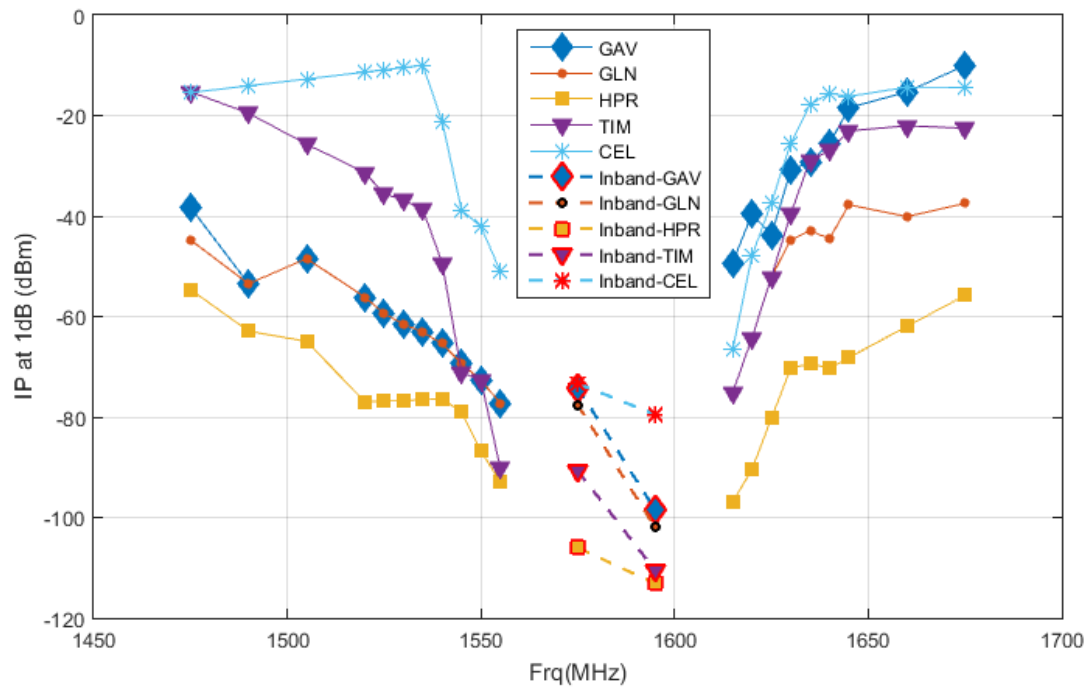
Figure B-16: Summary of 1 MHz and 1 MHz In-band GLONASS L1 C Bounding Masks

Table B-5: 1 MHz and 1 MHz In-band* GLONASS L1 P Bounding Masks (dBm)

Frequency (MHz)	GLN	HPR	CEL
1475	-9.999	-9.999	-15.4348
1490	-9.999	-9.999	-14.0758
1505	-9.999	-11.8353	-12.7169
1520	-12.0311	-13.6716	-11.3579
1525	-9.999	-18.1971	-10.905
1530	-9.999	-26.0448	-10.452
1535	-9.999	-27.7146	-9.999
1540	-12.7888	-30.2492	-19.999
1545	-29.999	-38.772	-29.999
1550	-37.5179	-51.3101	-29.999
1555	-50.9922	-58.7847	-29.999
1575*	-77.5833	-100.344	-73.3266
1595*	-101.975	-105.436	-75.3544
1615	-64.1152	-91.7591	-66.5954
1620	-59.0175	-76.0987	-47.9014
1625	-45.8712	-48.0537	-37.3339
1630	-33.3779	-30.6987	-21.0846
1635	-27.6843	-24.6631	-16.1157
1640	-12.8654	-20.8626	-15.5567
1645	-12.1488	-19.2505	-16.18
1660	-9.999	-14.6248	-14.3642
1675	-9.999	-9.999	-14.3862
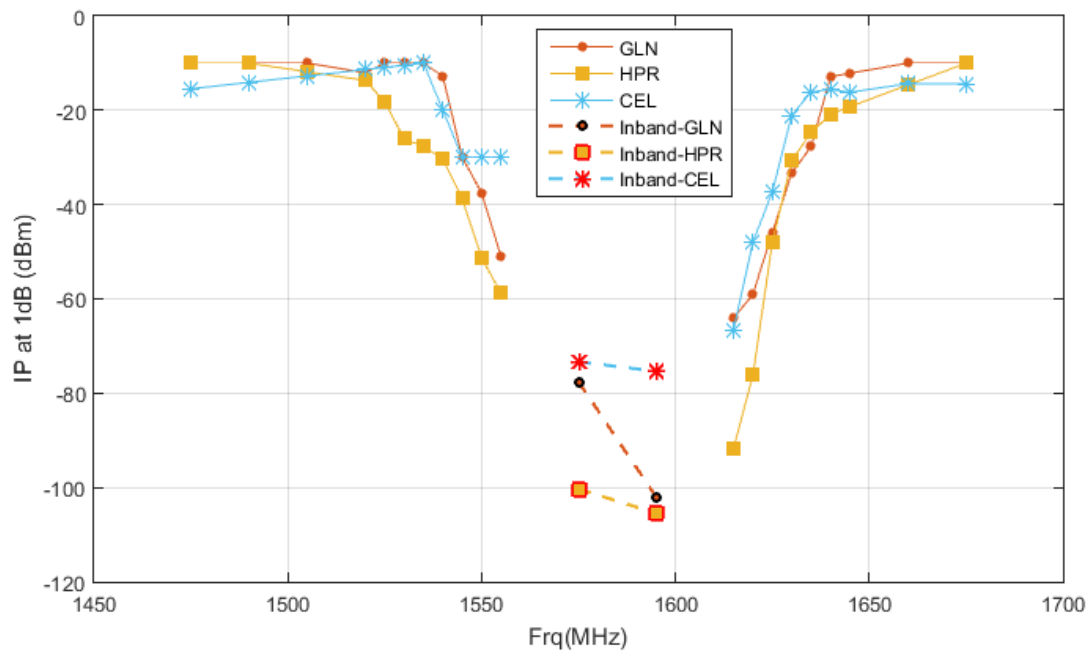
Figure B-17: Summary of 1 MHz and 1 MHz In-band GLONASS L1 P Bounding Masks

Table B-6: 1 MHz and 1 MHz In-band* BeiDou B1 I Bounding Masks (dBm)

Frequency (MHz)	GLN	HPR	CEL
1475	-15.2553	-9.999	-9.999
1490	-18.5174	-26.9935	-9.999
1505	-22.5464	-49.829	-9.999
1520	-28.4477	-63.8777	-9.999
1525	-29.3591	-71.0896	-9.999
1530	-34.3999	-76.0923	-9.999
1535	-35.2722	-76.6179	-14.7446
1540	-36.3339	-77.9462	-19.4902
1545	-61.2885	-87.3658	-42.9971
1550	-71.2057	-94.8011	-65.9259
1555	-90.2237	-96.4363	-74.9061
1575*	-78.1883	-100.556	-65.7427
1595*	-77.9432	-93.2012	NaN
1615	-80.688	-79.3254	-33.2232
1620	-53.752	-76.038	-29.999
1625	-37.6608	-68.782	-29.999
1630	-36.7556	-59.2317	-9.999
1635	-32.3209	-48.1514	-9.999
1640	-22.7274	-41.544	-9.999
1645	-17.6939	-34.8068	-9.999
1660	-9.999	-15.0115	-9.999
1675	-9.999	-9.999	-9.999
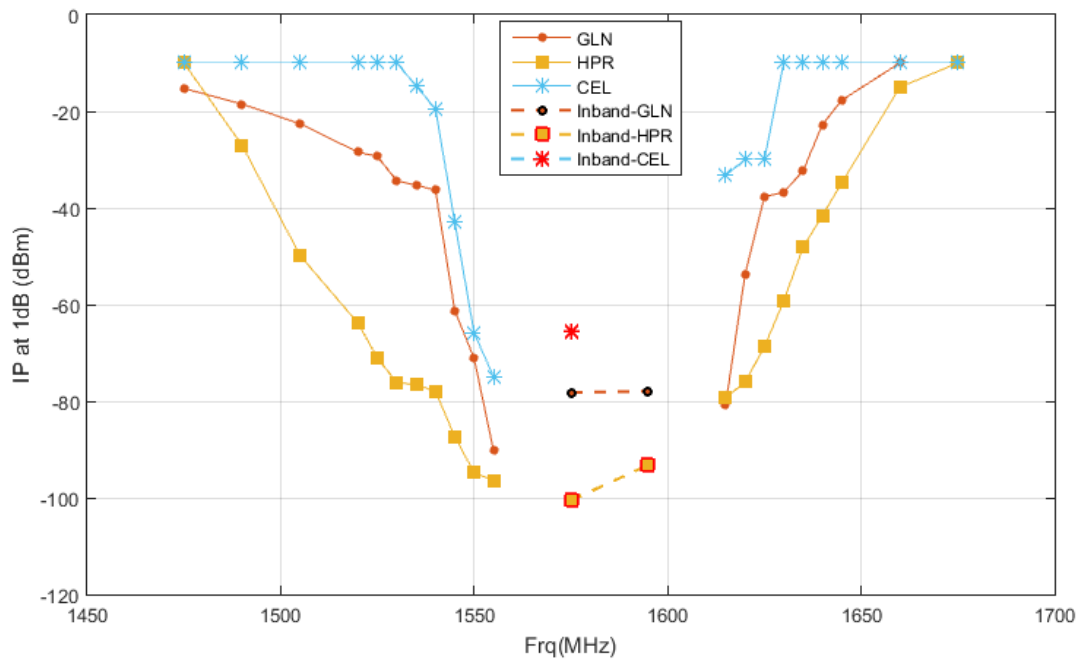
Figure B-18: Summary of 1 MHz and 1 MHz In-band BeiDou B1 I Bounding Masks

Table B-7: 1 MHz and 1 MHz In-band* Galileo E1 BC Bounding Masks (dBm)

Frequency (MHz)	HPR
1475	-35.2548
1490	-40.5603
1505	-54.5503
1520	-67.9842
1525	-73.9463
1530	-71.4059
1535	-71.6929
1540	-76.3935
1545	-90.805
1550	-93.463
1555	-93.9953
1575*	-111.593
1595*	-98.7922
1615	-91.4673
1620	-86.9953
1625	-72.9294
1630	-66.8658
1635	-59.6178
1640	-53.3542
1645	-46.7501
1660	-40.3065
1675	-36.0584
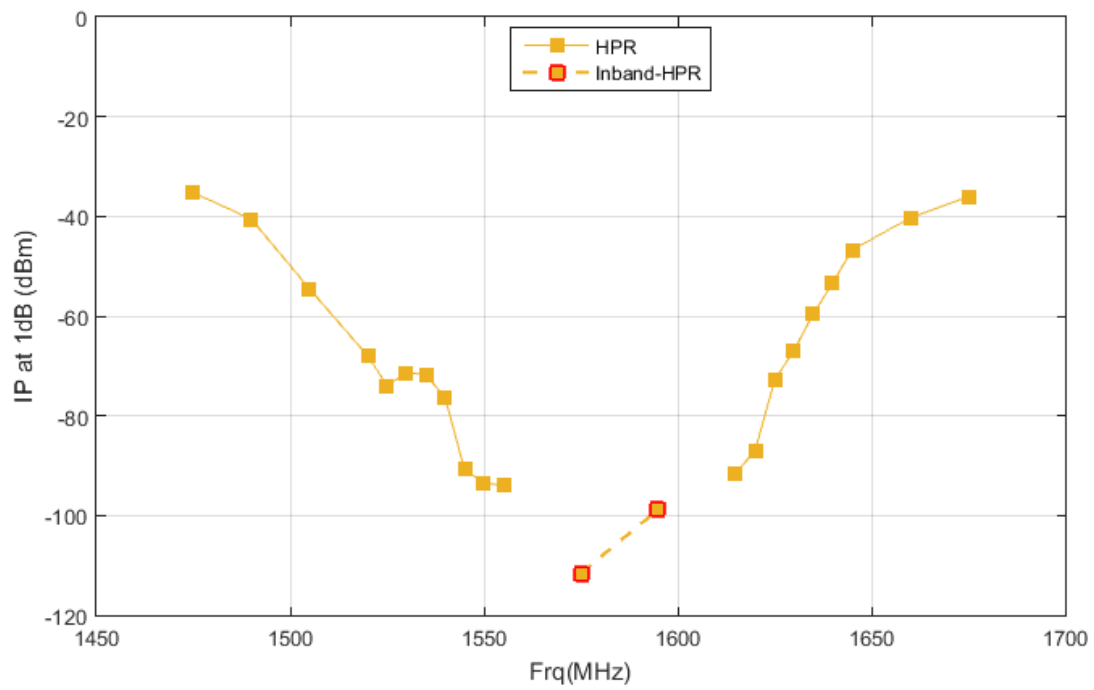
Figure B-19: Summary of 1 MHz and 1 MHz In-band Galileo E1 BC Bounding Masks

Table B-8: 1 MHz and 1 MHz In-band* SBAS L1 C/A Bounding Masks (dBm)

Frequency (MHz)	GLN	HPR	TIM
1475	-51.0577	-36.3048	-9.999
1490	-63.3312	-36.2106	-9.999
1505	-43.0991	-54.7003	-9.999
1520	-51.2192	-66.2717	-18.1846
1525	-53.1171	-68.445	-17.8801
1530	-52.0402	-70.6184	-19.9122
1535	-52.3345	-72.0554	-21.82
1540	-52.9021	-76.3935	-27.8443
1545	-57.8562	-92.255	-36.8048
1550	-75.2539	-92.7255	-60.008
1555	-83.7667	-92.7703	-64.5788
1575*	-118.108	-116.304	-111.015
1595*	-71.7432	-98.7297	-65.1566
1615	-74.2469	-91.5423	-45.1318
1620	-66.3442	-82.5362	-46.3982
1625	-54.2824	-66.4259	-37.1343
1630	-56.1713	-61.6283	-29.2349
1635	-43.9075	-55.9303	-22.8593
1640	-43.7996	-44.6667	-18.0685
1645	-43.1834	-48.7722	-14.134
1660	-42.1121	-40.0315	-10.9981
1675	-34.4705	-35.6063	NaN
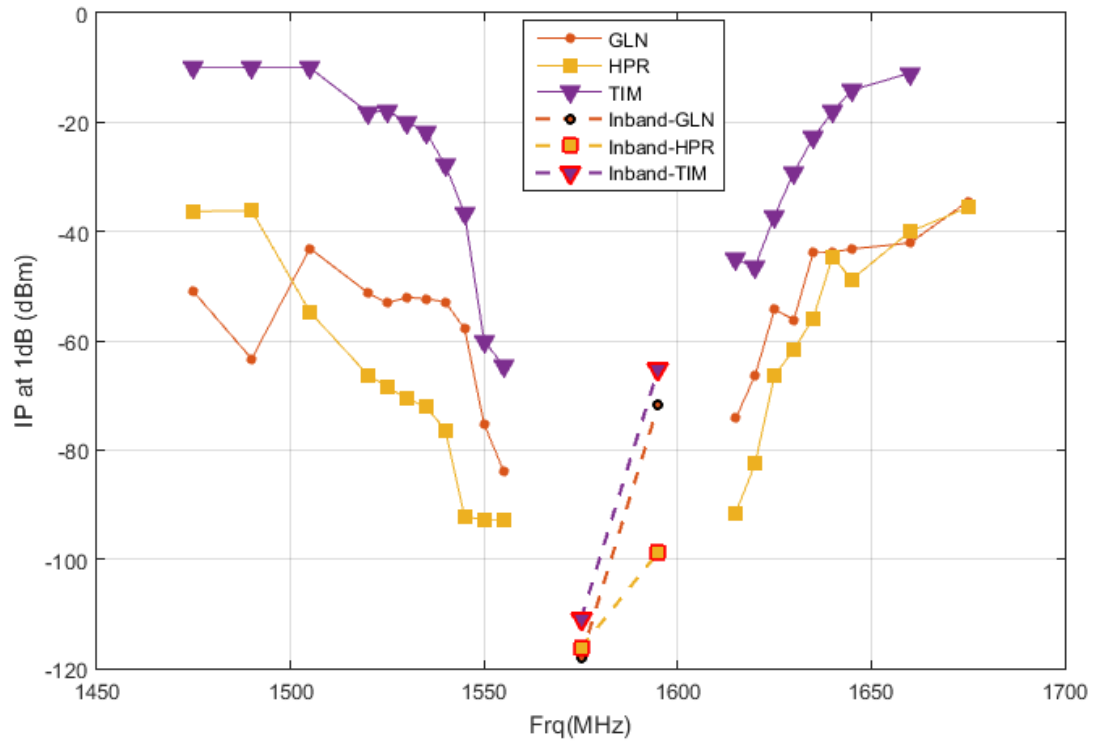
Figure B-20: Summary of 1 MHz and 1 MHz In-band SBAS L1 C/A Bounding Masks

B.1.2 Interference Test Results for 10-MHz LTE
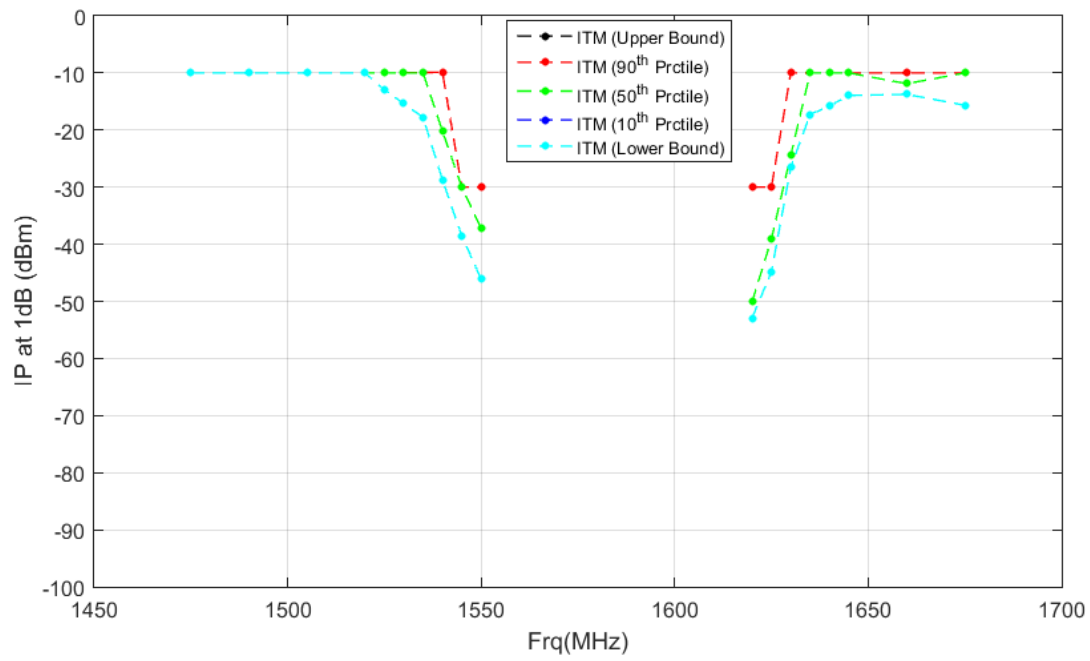
Figure B-21: 10 MHz GPS L1 C/A Statistical Mask Results for Cellular receivers
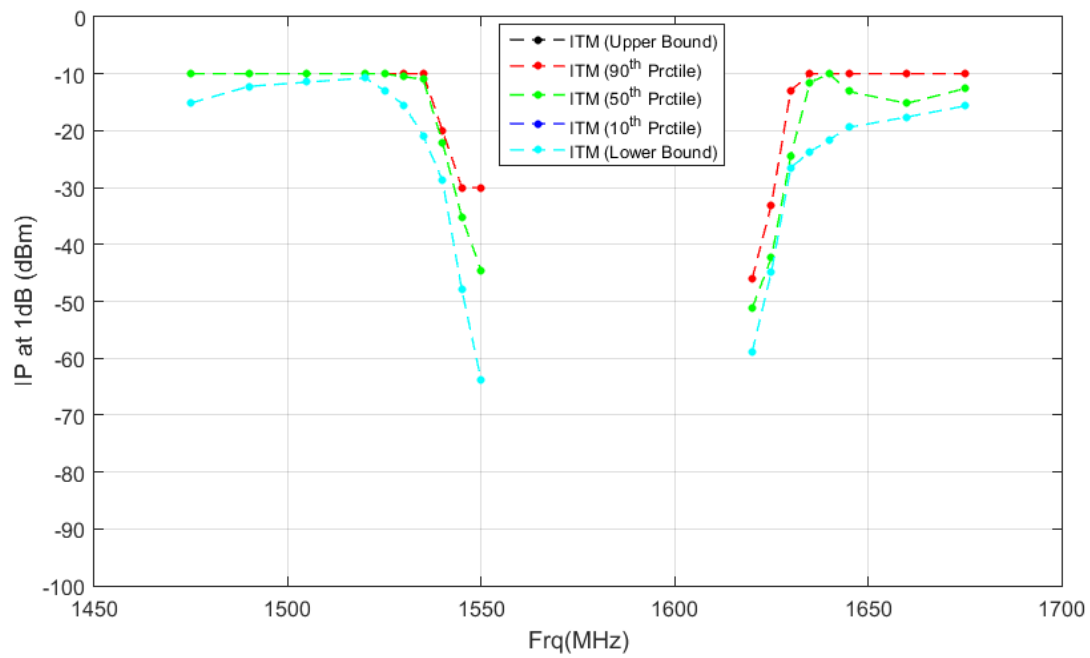
Figure B-22: 10 MHz All GNSS Aggregated Minimum Statistical Mask Results for Cellular receivers
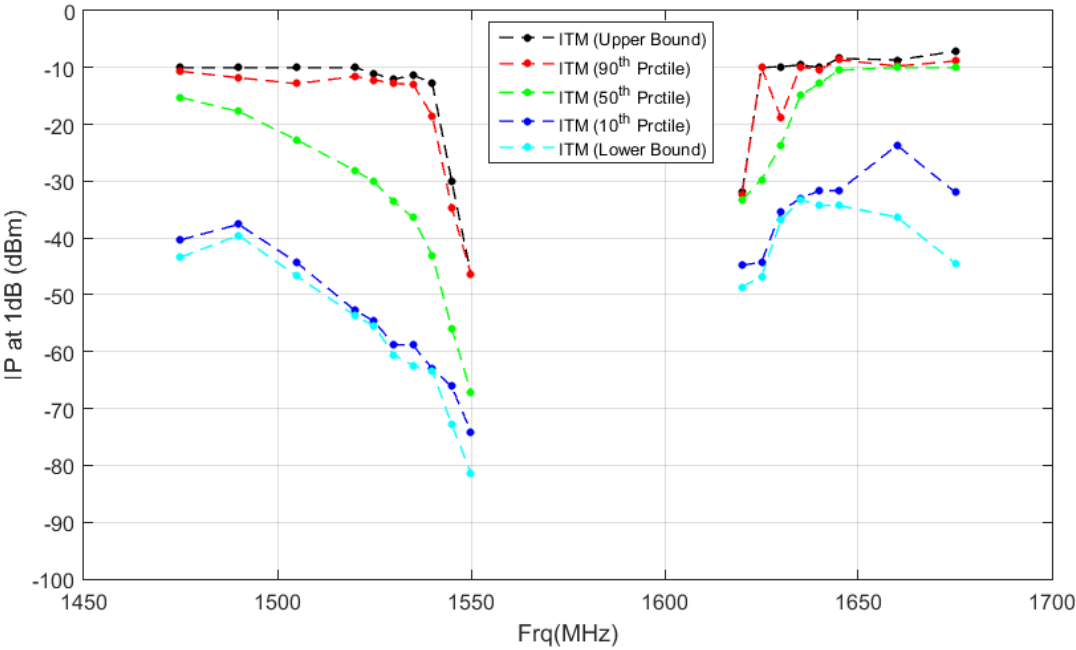
Figure B-23: 10 MHz GPS L1 C/A Statistical Mask Results for General Aviation receivers
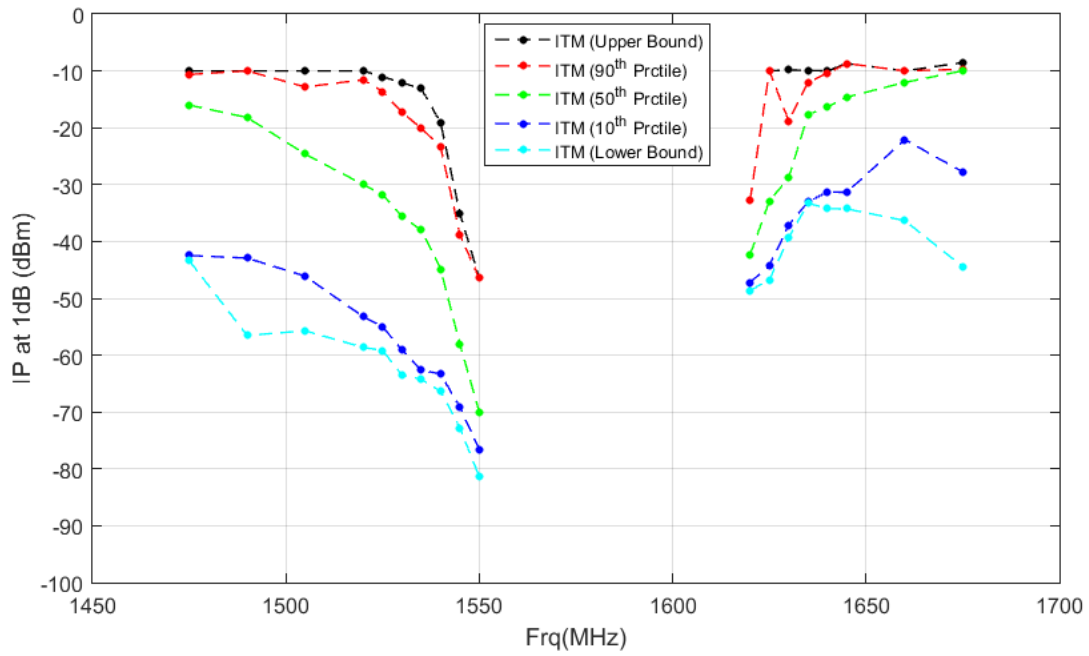
Figure B-24: 10 MHz All GNSS Aggregated Minimum Statistical Mask Results for General Aviation receivers
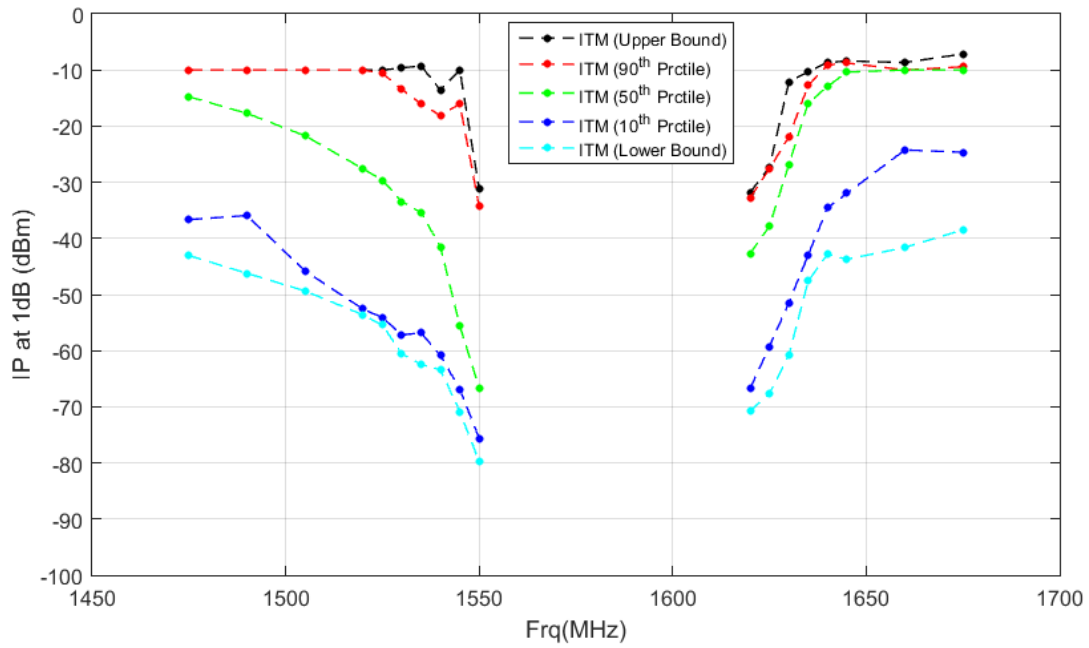
Figure B-25: 10 MHz GPS L1 C/A Statistical Mask Results for General Location Navigation receivers
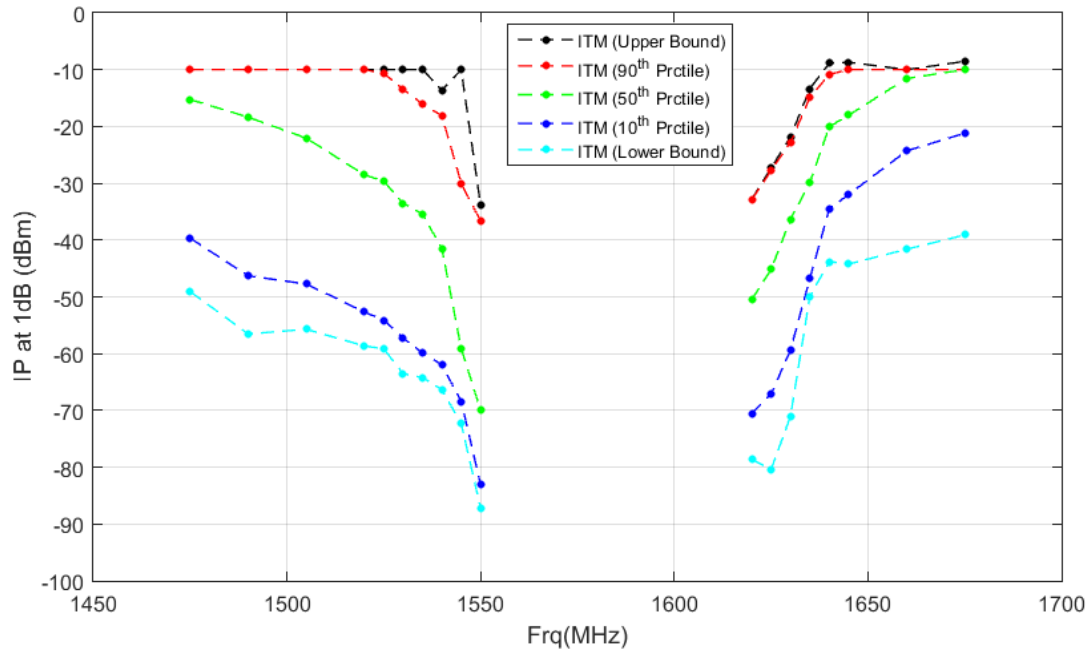
Figure B-26: 10 MHz All GNSS Aggregated Minimum Statistical Mask Results for General Location Navigation receivers

Figure B-27: 10 MHz GPS L1 C/A Statistical Mask Results for High Precision receivers

Figure B-28: 10 MHz All GNSS Aggregated Minimum Statistical Mask Results for High Precision receivers

Figure B-29: 10 MHz GPS L1 C/A Statistical Mask Results for Space Based receivers

Figure B-30: 10 MHz All GNSS Aggregated Minimum Statistical Mask Results for Space Based receivers

Figure B-31: 10 MHz GPS L1 C/A Statistical Mask Results for Timing receivers

Figure B-32: 10 MHz All GNSS Aggregated Minimum Statistical Mask Results for Timing receivers

Using this approach a bounding ITM was produced for each category and signal type combination. Figure B-33 illustrates how the L1 C/A bounding ITMs compare across the six categories of receivers. This plot shows the HPR and SPB categories to be the most susceptible in terms of received interference power levels with the cellular category generally being the most tolerant of LTE interference.

Table B-9: 10 MHz and 10 MHz Intermod* GPS L1 C/A Bounding Masks (dBm)

Frequency (MHz)	GAV	GLN	HPR	TIM	SPB	CEL
1475	-43.3646	-43.0577	-55.2458	-15.2559	-44.9489	-9.999
1490	-39.5303	-46.2115	-60.9099	-16.4053	-56.0659	-9.999
1505	-46.7082	-49.3654	-65.3551	-24.6328	-67.1829	-9.999
1520	-53.6318	-53.6318	-66.3967	-37.0094	-75.2901	-9.999
1525	-55.4429	-55.4429	-70.4213	-42.5001	-75.2341	-12.9574
1530	-60.5293	-60.5293	-72.9934	-51.3793	-75.1091	-15.3651
1530*	-73.6293	-75.91	-78.9673	-73.6293	-76.5937	-36.467
1535	-62.445	-62.445	-74.8804	-58.249	-74.501	-17.7728
1540	-63.4002	-63.4002	-81.6489	-62.9739	-77.1892	-28.7517
1545	-72.8009	-70.8562	-89.9247	-72.8009	-79.7538	-38.5472
1550	-81.3979	-79.7539	-93.538	-81.3979	-82.3183	-46.0942
1550*	-82.7979	-85.2039	-88.2261	-82.7979	-86.1433	-45.5942
1620	-48.6403	-70.7486	-88.9203	-56.5041	-79.0305	-52.9139
1625	-46.7292	-67.6878	-78.9544	-49.1718	-83.6891	-44.7992
1630	-36.8823	-60.8322	-63.1922	-41.2976	-79.1041	-26.5096
1635	-33.2516	-47.6279	-60.3723	-36.7448	-74.5191	-17.2657
1640	-34.2495	-42.7996	-60.2717	-32.192	-74.405	-15.8067
1645	-34.2708	-43.7334	-61.9748	-27.6393	-74.3188	-13.9425
1660	-36.3256	-41.6121	-53.9123	-18.8014	-72.0909	-13.7382
1675	-44.4325	-38.4705	-49.4567	-16.5372	-64.8224	-15.6612
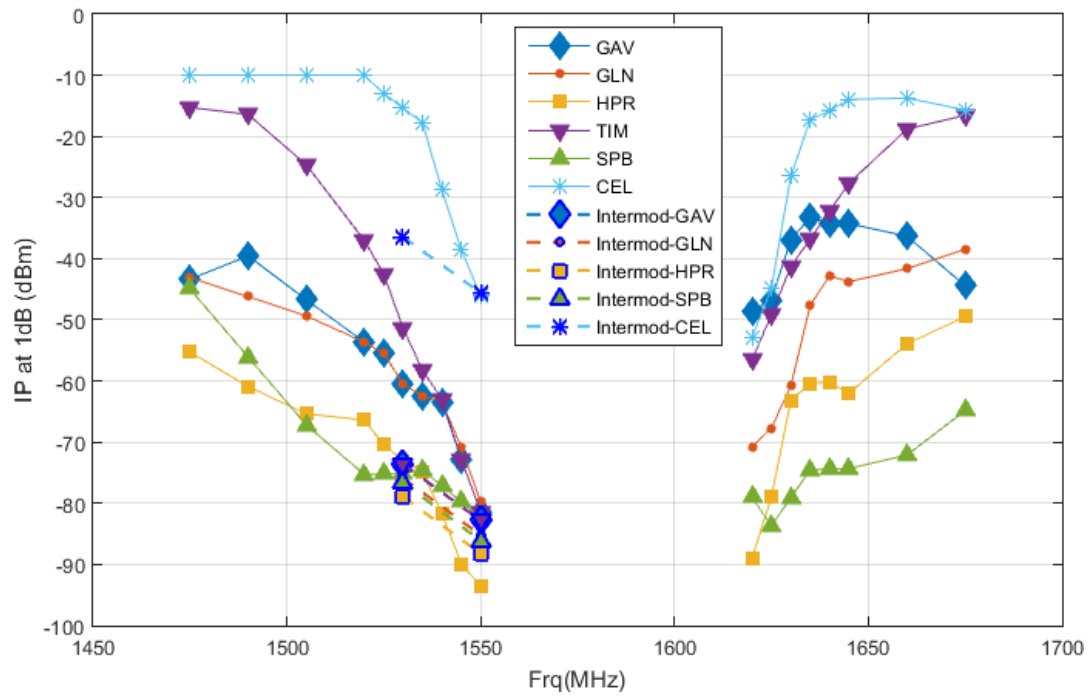
Figure B-33: Summary of 10 MHz and 10MHz Intermod GPS L1 C/A Bounding Masks

Table B-10: 10 MHz and 10 MHz Intermod* GPS L1 P Bounding Masks (dBm)

Frequency (MHz)	GLN	HPR	SPB	CEL
1475	-9.999	-58.2419	-48.2739	-9.999
1490	-9.999	-65.9099	-59.2909	-9.999
1505	-9.999	-65.5172	-70.3079	-9.999
1520	-9.999	-63.7114	-74.0025	-9.999
1525	-12.1984	-65.1348	-75.2341	-12.9574
1530	-14.3977	-64.8352	-75.2091	-15.3651
1530*	-27.9178	-68.2977	NaN	NaN
1535	-16.5971	-65.3046	-75.151	-17.7728
1540	-19.7263	-66.7822	-75.2145	-20.1804
1545	-29.999	-65.5121	-79.6059	-29.999
1550	-41.6162	-68.946	-85.6683	-29.999
1550*	-37.2516	-77.621	NaN	NaN
1620	-52.0646	-62.4395	NaN	-52.9139
1625	-48.234	-62.7591	-85.8891	-42.7839
1630	-32.0891	-62.2422	-82.0611	-26.5096
1635	-16.731	-61.4098	-78.233	-17.2657
1640	-13.365	-63.4217	-74.405	-15.8067
1645	-9.999	-62.9873	-74.3688	-13.9425
1660	-9.999	-49.5114	-74.2659	-13.7382
1675	-9.999	-46.3192	-65.8474	-15.6612
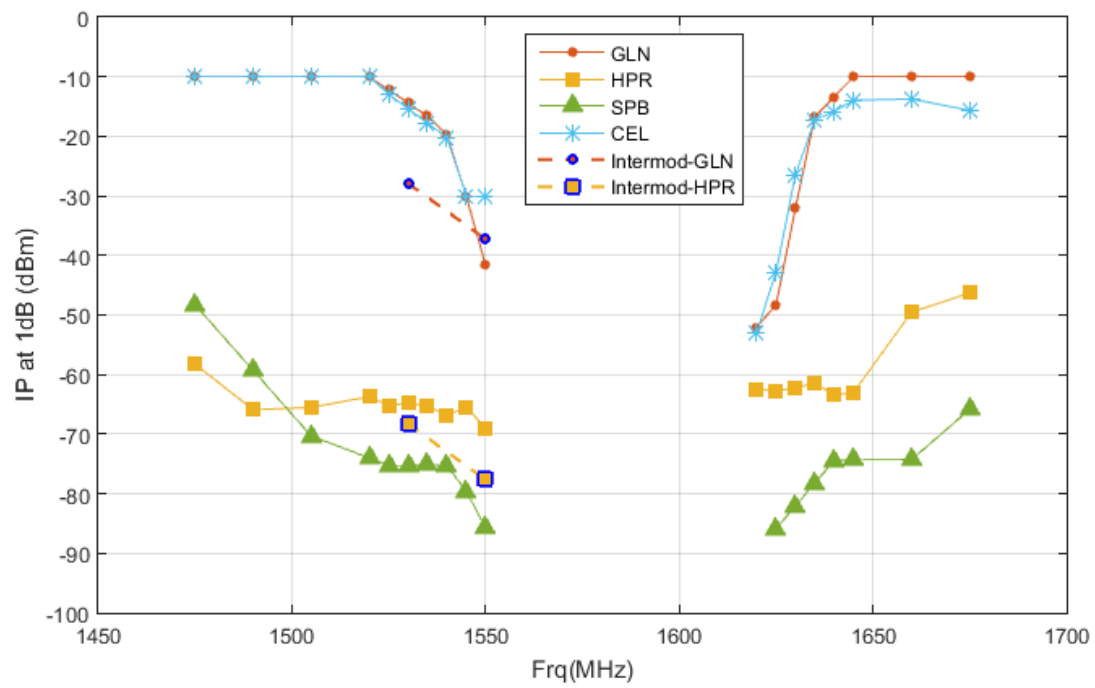
Figure B-34: Summary of 10 MHz and 10 MHz Intermod GPS L1 P Bounding Masks

Table B-11: 10 MHz and 10 MHz Intermod* GPS L1 C Bounding Masks (dBm)

Frequency (MHz)	GLN	CEL
1475	-9.999	-9.999
1490	-9.999	-9.999
1505	-9.999	-9.999
1520	-9.999	-9.999
1525	-12.1984	-12.9574
1530	-14.3977	-15.3651
1530*	-27.9178	NaN
1535	-16.5971	-17.7728
1540	-19.7263	-20.1804
1545	-29.999	-29.999
1550	-41.6162	-29.999
1550*	-37.2516	NaN
1620	-52.0646	-52.9139
1625	-48.234	-42.7839
1630	-32.0891	-26.5096
1635	-16.731	-17.2657
1640	-13.365	-15.8067
1645	-9.999	-13.9425
1660	-9.999	-13.7382
1675	-9.999	-15.6612
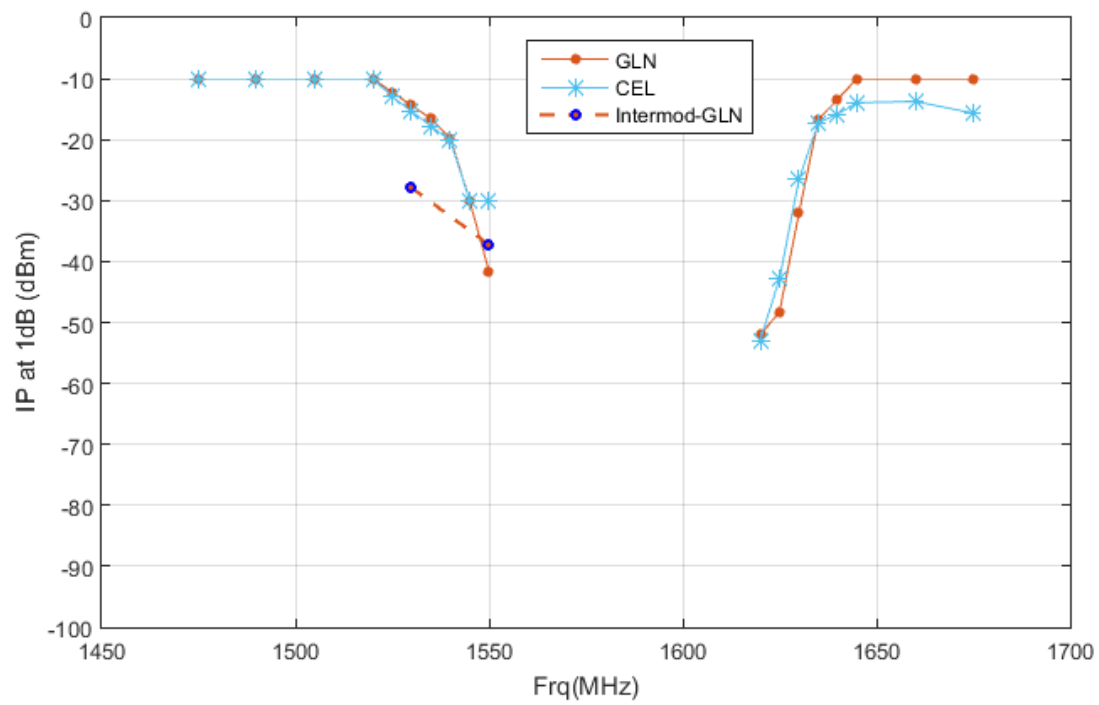
Figure B-35: Summary of 10 MHz and 10 MHz Intermod GPS L1 C Bounding Masks

Table B-12: 10 MHz and 10 MHz Intermod* GLONASS L1 C Bounding Masks (dBm)

Frequency (MHz)	GAV	GLN	HPR	TIM	CEL
1475	-41.5559	-49.0577	-57.1169	-14.6684	-15.1348
1490	-56.5303	-56.5303	-63.9099	-26.6126	-12.2023
1505	-55.7082	-55.7082	-65.1422	-26.4832	-11.4679
1520	-58.6318	-58.6318	-76.9217	-31.4068	-10.7334
1525	-59.1679	-59.1679	-76.8713	-33.7179	-10.4886
1530	-63.5043	-63.5043	-76.7309	-37.5543	-15.4582
1530*	-63.4418	-63.4418	-79.6515	-63.4418	-32.967
1535	-64.22	-64.22	-76.5364	-40.595	-20.9174
1540	-66.3502	-66.3502	-76.381	-54.7114	-26.3767
1545	-68.7673	-68.7673	-80.4122	-62.3673	-37.5972
1550	-75.3943	-75.3943	-88.6362	-75.3943	-45.0942
1550*	-72.6568	-72.6568	-89.0612	-72.6568	-42.1424
1620	-45.8192	-78.6146	-89.2958	-66.2982	-58.9889
1625	-40.1098	-80.4061	-92.9202	-57.8343	-42.9589
1630	-39.3828	-71.0266	-72.5692	-46.2599	-25.8346
1635	-30.9245	-49.925	-66.0598	-34.1262	-23.6998
1640	-27.7297	-43.7996	-65.2717	-33.0535	-21.5649
1645	-23.4929	-42.2334	-66.1748	-32.0656	-19.43
1660	-16.7459	-39.5371	-59.3114	-25.8014	-17.5882
1675	-9.999	-39.108	-52.4567	-21.0372	-15.177
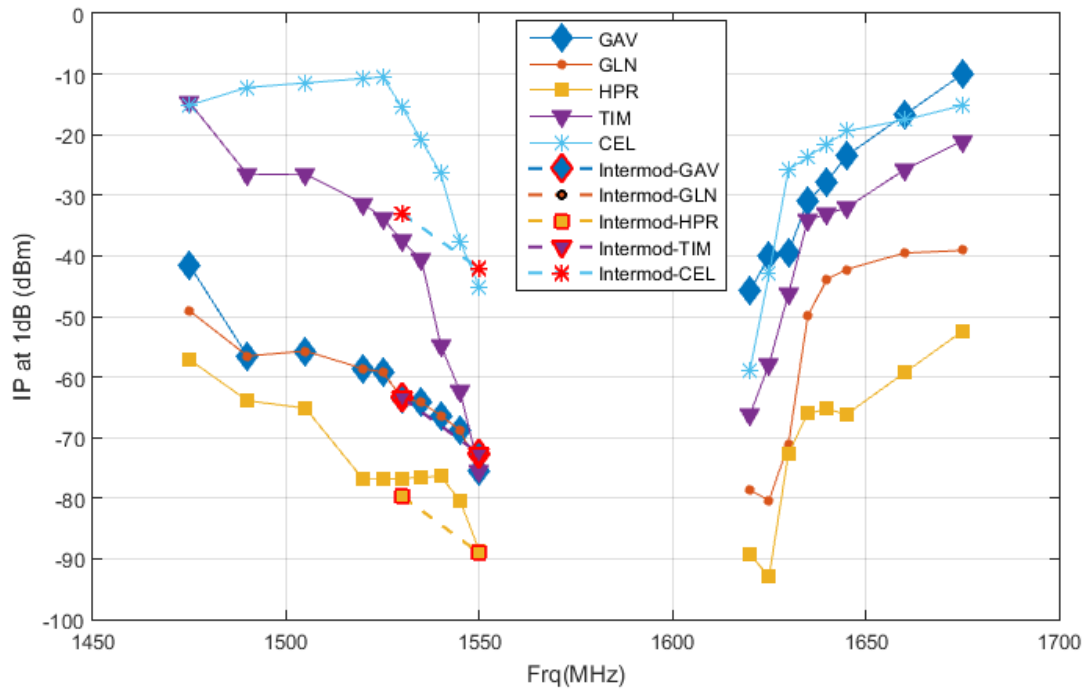
Figure B-36: Summary of 10 MHz and 10 MHz Intermod GLONASS L1 C Bounding Masks

Table B-13: 10 MHz and 10 MHz Intermod* GLONASS L1 P Bounding Masks (dBm)

Frequency (MHz)	GLN	HPR	CEL
1475	-9.999	-9.999	-15.1348
1490	-9.999	-11.2502	-12.2023
1505	-12.1713	-16.534	-11.4679
1520	-14.3436	-24.3966	-10.7334
1525	-13.6543	-29.9846	-10.4886
1530	-12.965	-35.0448	-10.2438
1530*	-29.5678	-47.5536	-9.999
1535	-12.6165	-38.3146	-9.999
1540	-16.0238	-40.9242	-19.999
1545	-29.999	-43.472	-29.999
1550	-38.8287	-56.6851	-29.999
1550*	-38.9037	-56.8351	-29.999
1620	-78.6146	-84.0237	-58.9889
1625	-80.4061	-63.1057	-42.9589
1630	-71.0266	-40.6515	-25.8346
1635	-49.925	-33.9881	-23.6998
1640	-16.666	-28.7876	-21.5649
1645	-19.0538	-24.6255	-19.43
1660	-9.999	-12.3051	-17.5882
1675	-9.999	-9.999	-15.177
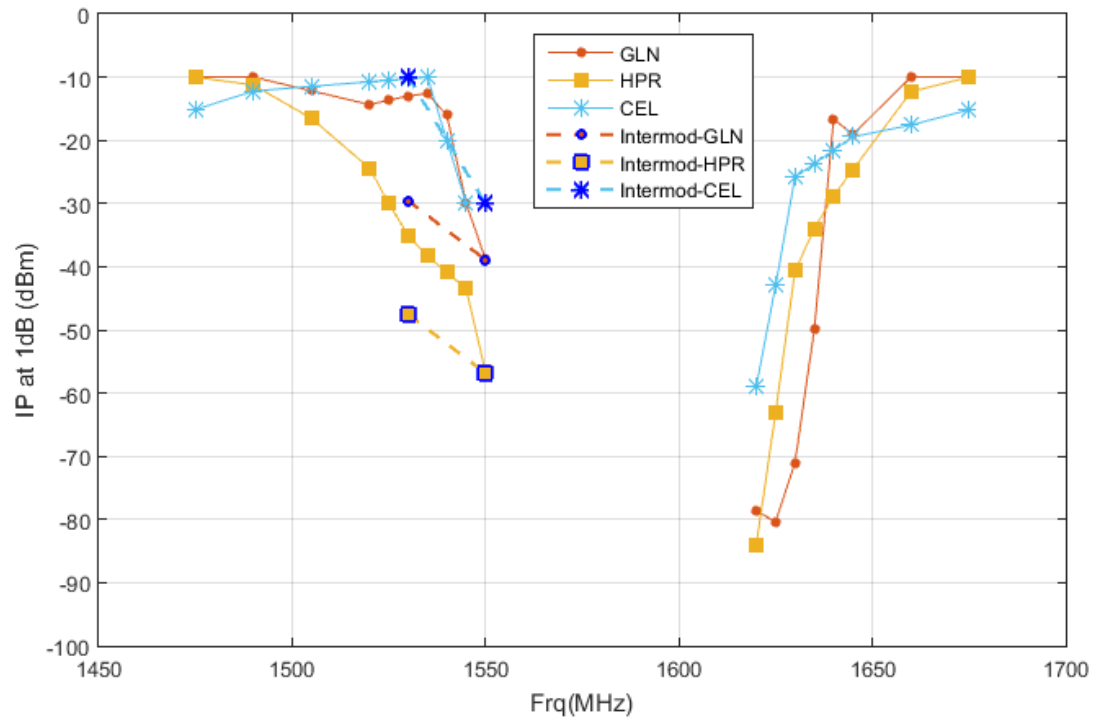
Figure B-37: Summary of 10 MHz and 10 MHz Intermod GLONASS L1 P Bounding Masks

Table B-14: 10 MHz and 10 MHz Intermod* BeiDou B1 I Bounding Masks (dBm)

Frequency (MHz)	GLN	HPR	CEL
1475	-15.2553	-19.5883	-9.999
1490	-18.5174	-27.4185	-9.999
1505	-22.5464	-51.029	-9.999
1520	-28.4227	-65.3777	-9.999
1525	-29.1841	-70.5146	-9.999
1530	-32.0749	-76.2673	-10.4945
1530*	NaN	-79.8286	-58.9725
1535	-33.6097	-76.6679	-10.9901
1540	-48.4839	-78.8212	-26.0027
1545	-64.2635	-91.9158	-47.9971
1550	-87.2057	-94.6261	-63.9259
1550*	NaN	-89.1101	-68.4259
1620	-68.727	-77.163	-29.999
1625	-53.1608	-70.407	-29.999
1630	-39.7056	-62.1942	-9.999
1635	-31.4209	-51.7889	-9.999
1640	-27.2274	-42.9315	-9.999
1645	-25.0439	-36.2818	-9.999
1660	-9.999	-14.1615	-9.999
1675	-9.999	-9.999	-9.999
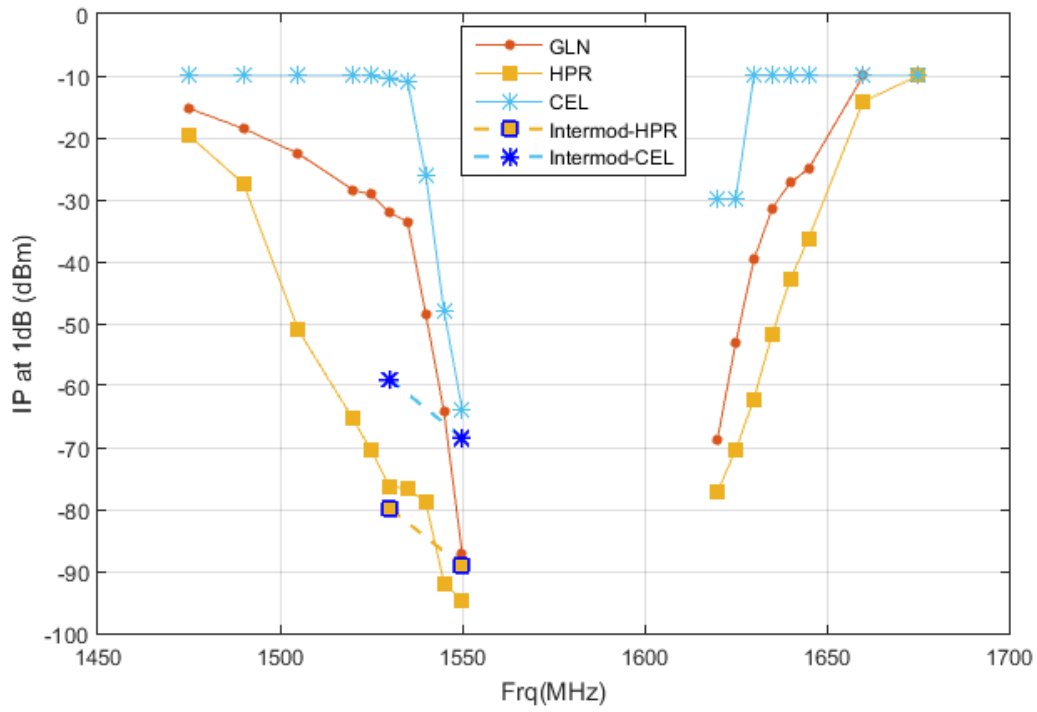
Figure B-38: Summary of 10 MHz and 10 MHz Intermod BeiDou B1 I Bounding Masks

Table B-15: 10 MHz and 10 MHz Intermod* Galileo E1 BC Bounding Masks (dBm)

Frequency (MHz)	HPR
1475	-36.1449
1490	-41.2853
1505	-56.8628
1520	-67.5092
1525	-71.2713
1530	-73.8934
1530*	-78.9423
1535	-76.5364
1540	-83.6832
1545	-90.83
1550	-91.788
1550*	-88.2011
1620	-90.8953
1625	-77.6544
1630	-60.4783
1635	-58.0303
1640	-54.8042
1645	-45.6251
1660	-41.2507
1675	-35.8563
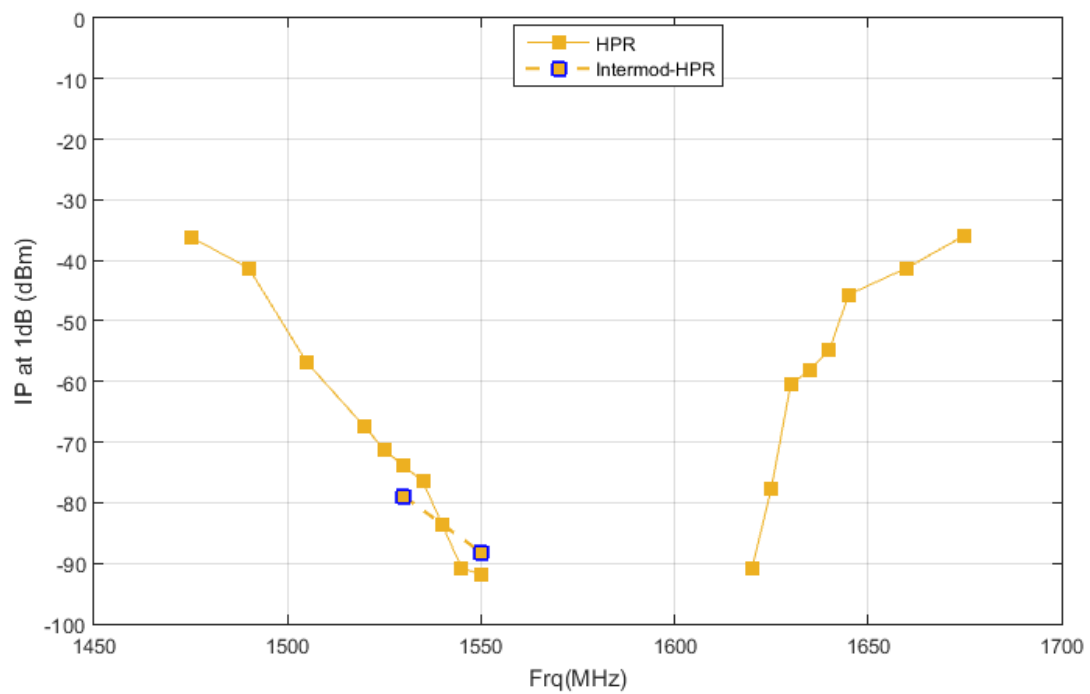
Figure B-39: Summary of 10 MHz and 10 MHz Intermod Galileo E1 BC Bounding Masks

Table B-16: 10 MHz and 10 MHz Intermod* SBAS L1 C/A Bounding Masks (dBm)

Frequency (MHz)	GLN	HPR	TIM
1475	-43.0577	-36.9968	NaN
1490	-46.2615	-39.5353	NaN
1505	-49.4654	-56.4753	NaN
1520	-52.6692	-66.8467	-15.9846
1525	-53.0921	-70.5588	-17.8801
1530	-54.2027	-74.2059	-19.9122
1530*	-72.4225	-78.9673	-55.4372
1535	-53.0595	-74.9054	-23.82
1540	-58.906	-82.4582	-30.8443
1545	-72.3562	-90.03	-52.5923
1550	-84.7539	-93.013	-63.7205
1550*	-81.7289	-88.2261	-64.7455
1620	-68.8442	-90.2953	-53.0107
1625	-61.8949	-77.5544	-49.1718
1630	-53.4838	-60.2533	-39.5099
1635	-47.6279	-56.6803	-26.3593
1640	-42.7996	-49.4667	-21.231
1645	-44.2334	-46.0279	-20.184
1660	-41.6121	-42.1585	-11.4981
1675	-38.4705	-38.5679	NaN
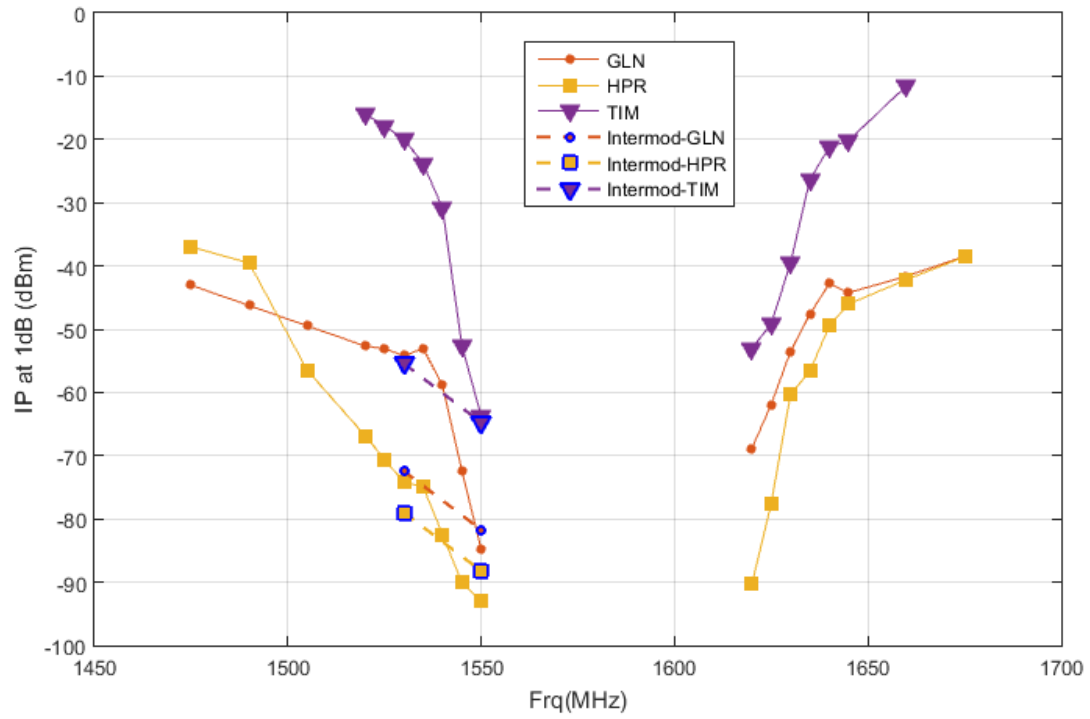
Figure B-40: Summary of 10 MHz and 10 MHz Intermod SBAS L1 C/A Bounding Masks

B.1.3   Combined 1 MHz AWGN Test Results and 10 MHz LTE Test Results
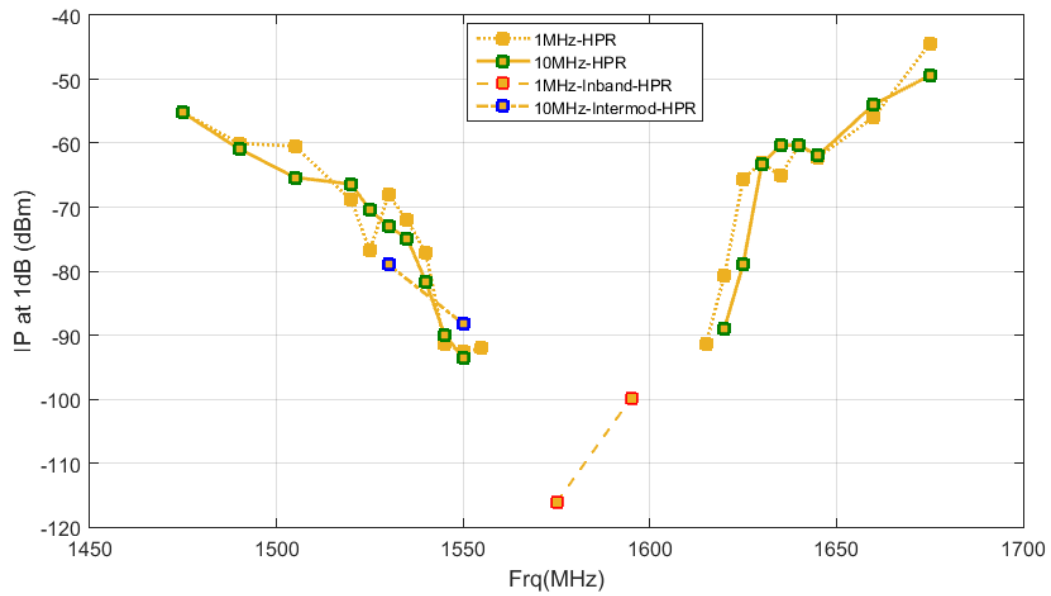
Figure B-41: Summary of 1&10 MHz, 1 MHz In-band, and 10 MHz Intermod GPS L1 C/A – HPR Bounding Masks
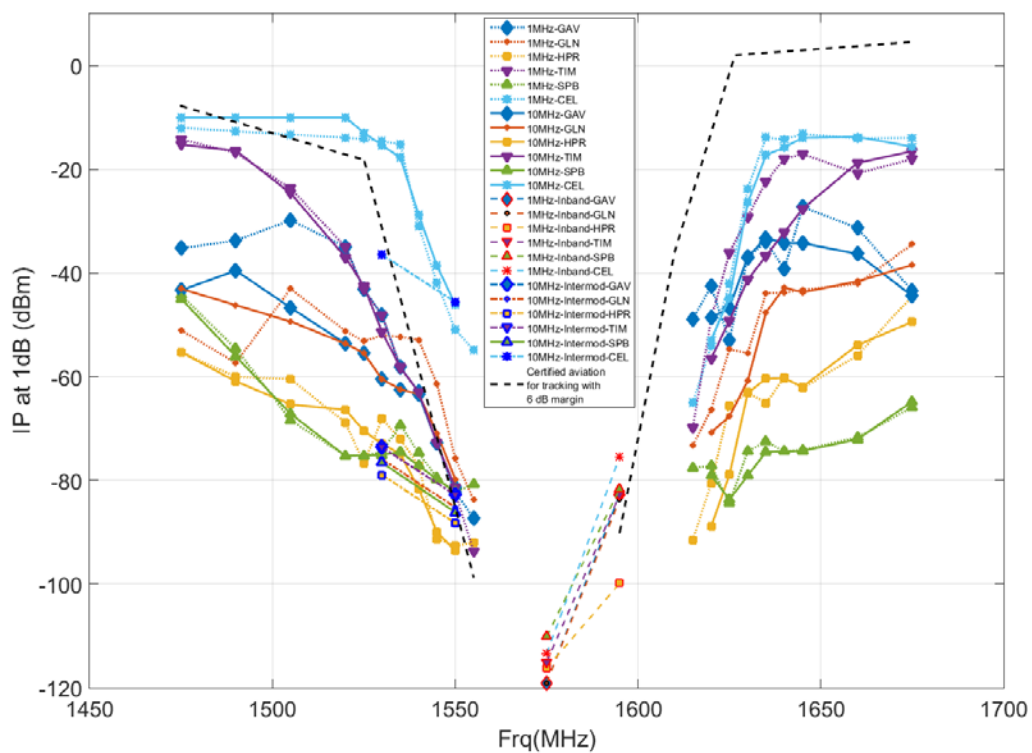
**Figure B-42: Summary of 1&10 MHz, 1 MHz In-band, and 10 MHz Intermod
with Certified Aviation GPS L1 C/A Bounding Masks**

Note: Certified Aviation Mask has a value of -110 dBm for 1 MHz in band interference
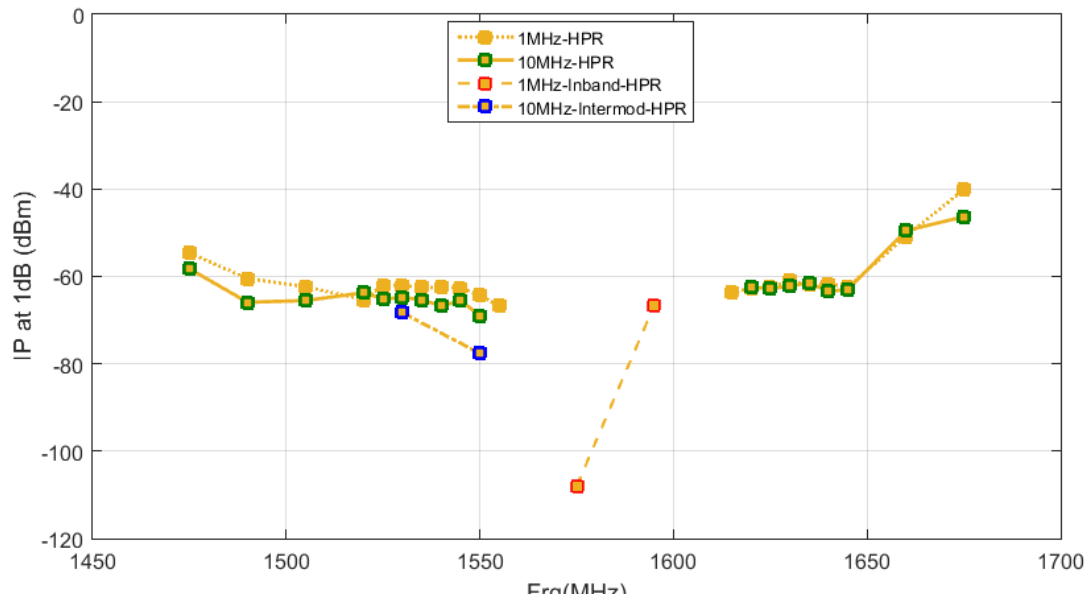
Figure B-43: Summary of 1&10 MHz, 1 MHz In-band, and 10 MHz Intermod GPS L1 P – HPR Bounding Masks
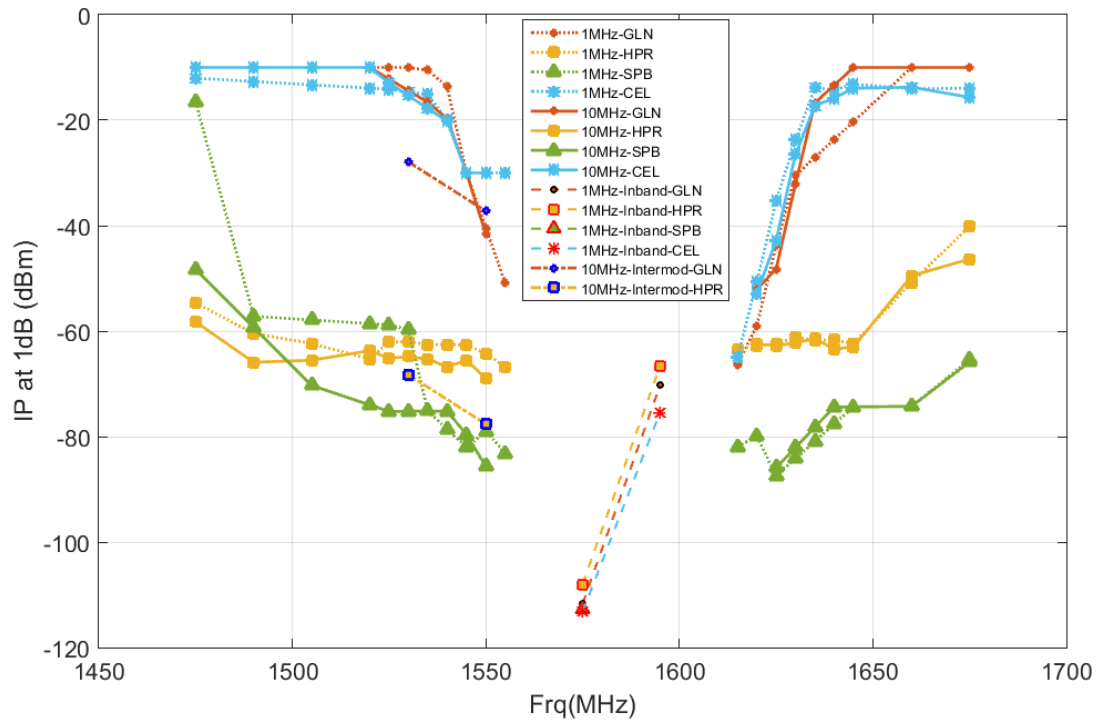
Figure B-44: Summary of 1&10 MHz, 1 MHz In-band, and 10 MHz Intermod GPS L1 P Bounding Masks
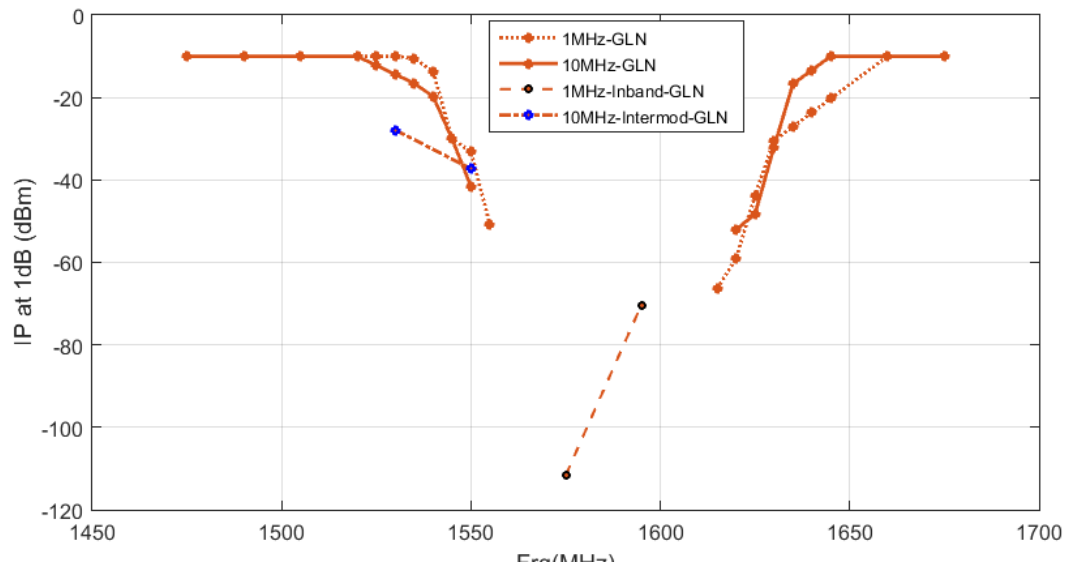
Figure B-45: Summary of 1&10 MHz, 1 MHz In-band, and 10 MHz Intermod GPS L1 C - GLN Bounding Masks
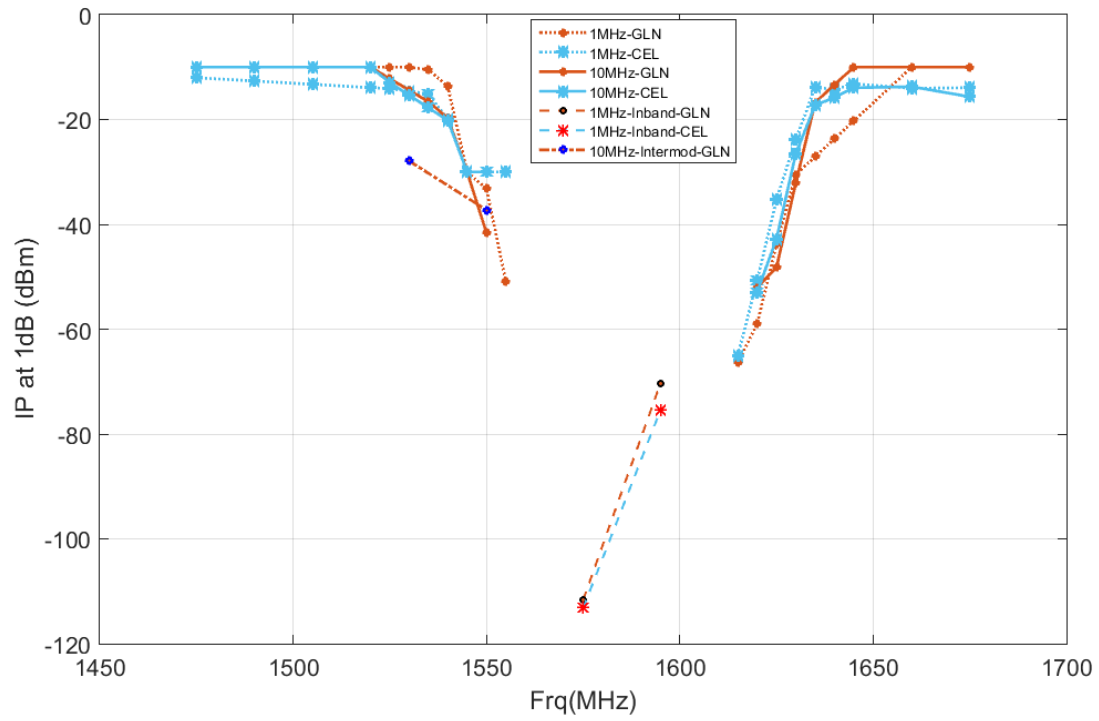
Figure B-46: Summary of 1&10 MHz, 1 MHz In-band, and 10 MHz Intermod GPS L1 C Bounding Masks
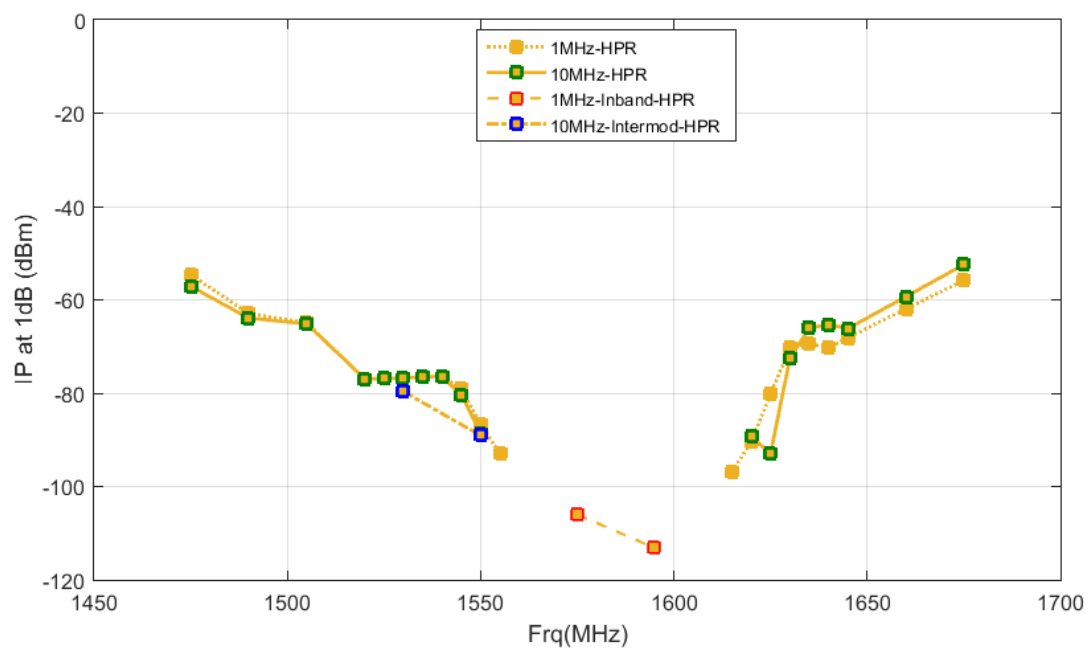
Figure B-47: Summary of 1&10 MHz, 1 MHz In-band, and 10 MHz Intermod GLONASS L1 C - HPR Bounding Masks
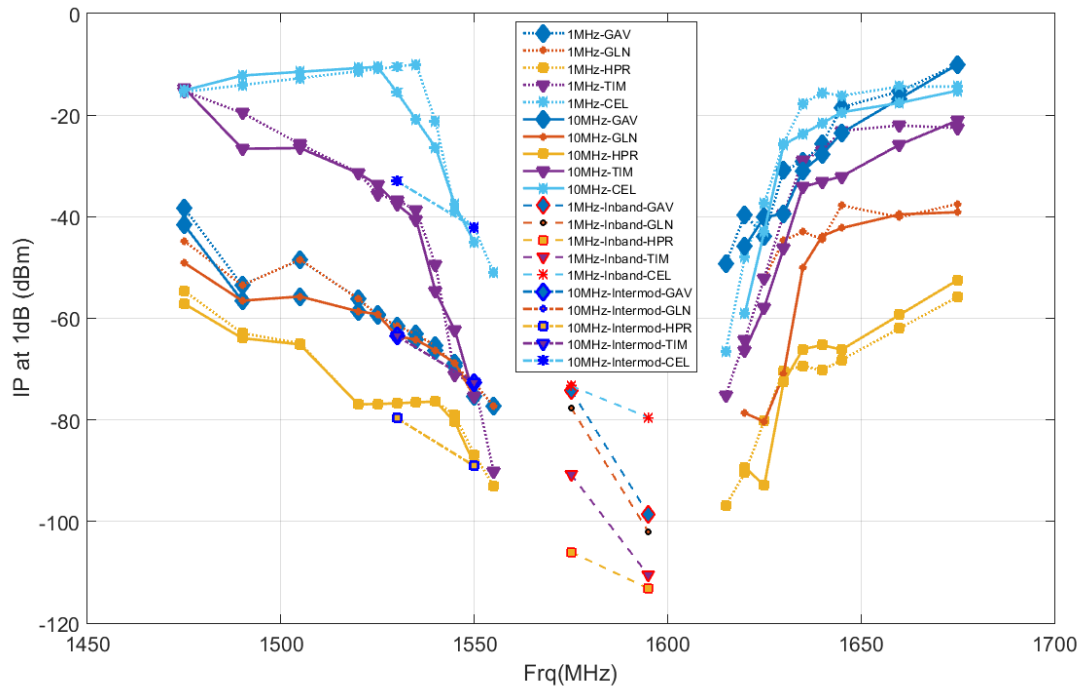
Figure B-48: Summary of 1&10 MHz, 1 MHz In-band, and 10 MHz Intermod GLONASS L1 C Bounding Masks
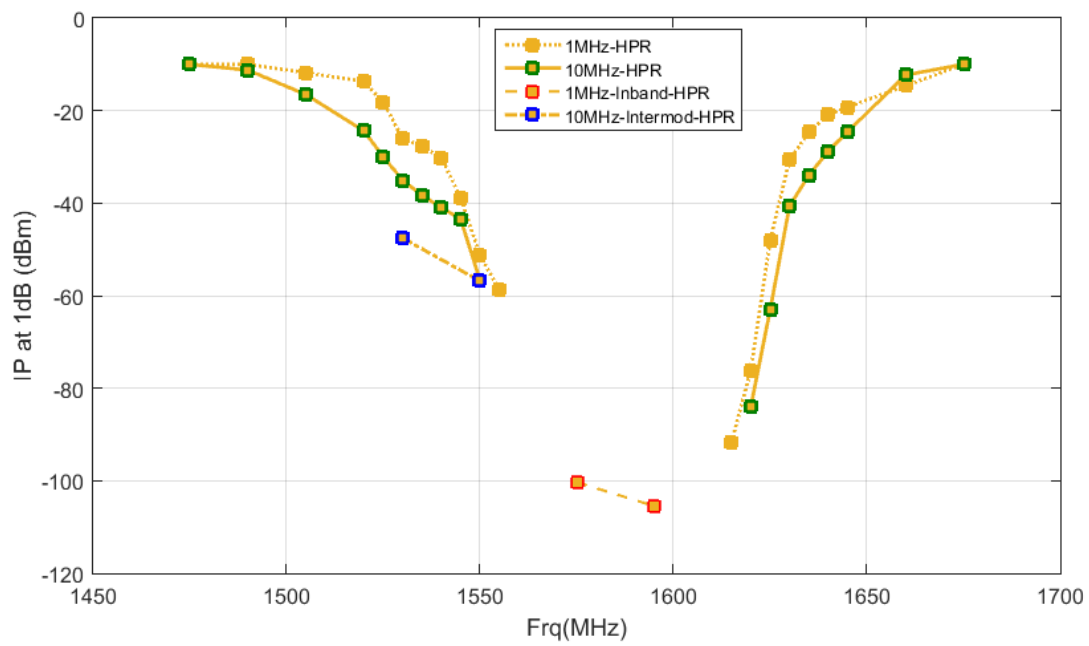
Figure B-49: Summary of 1&10 MHz, 1 MHz In-band, and 10 MHz Intermod GLONASS L1 P - HPR Bounding Masks
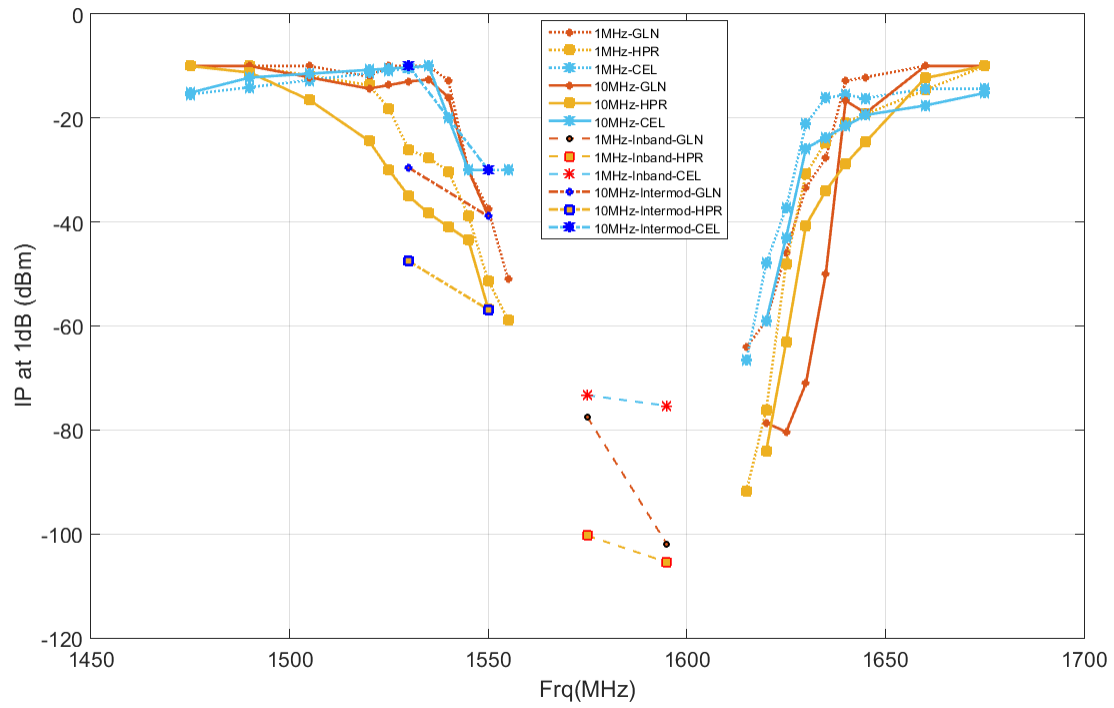
Figure B-50: Summary of 1&10 MHz, 1 MHz In-band, and 10 MHz Intermod GLONASS L1 P Bounding Masks
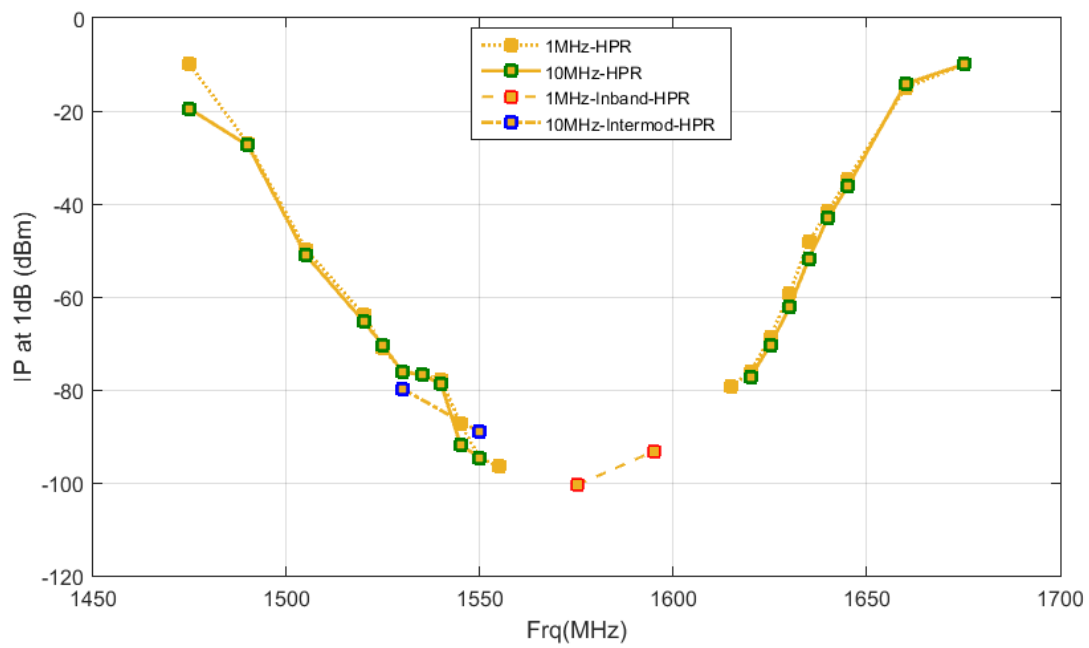
Figure B-51: Summary of 1&10 MHz, 1 MHz In-band, and 10 MHz Intermod BeiDou B1 I - HPR Bounding Masks
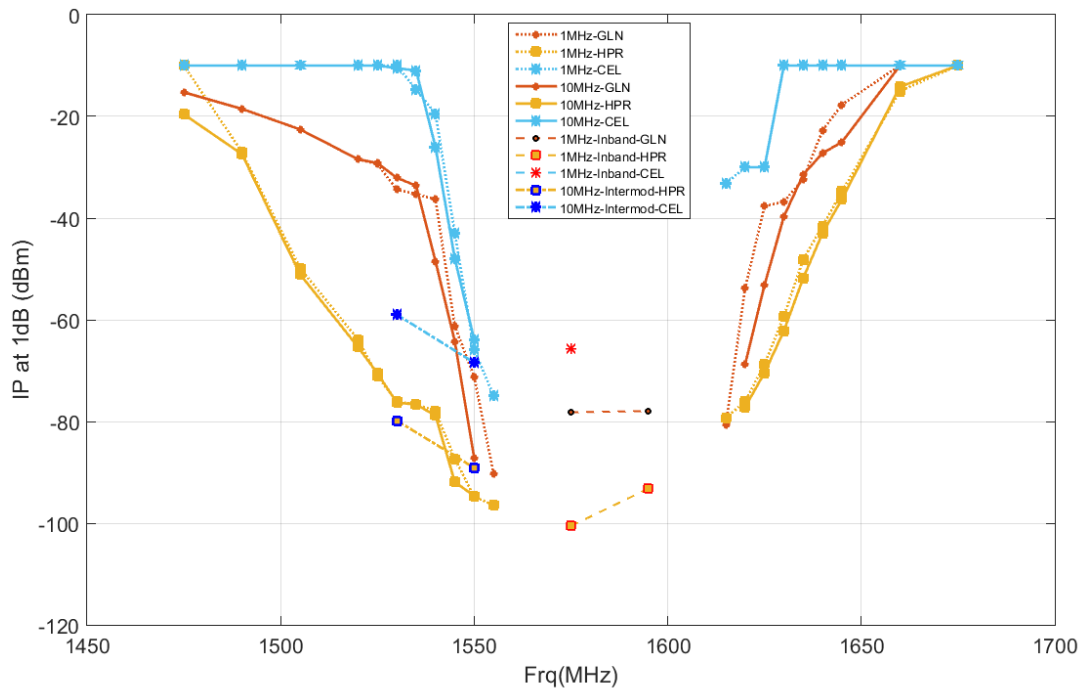
Figure B-52: Summary of 1&10 MHz, 1 MHz In-band, and 10 MHz Intermod BeiDou B1 I Bounding Masks
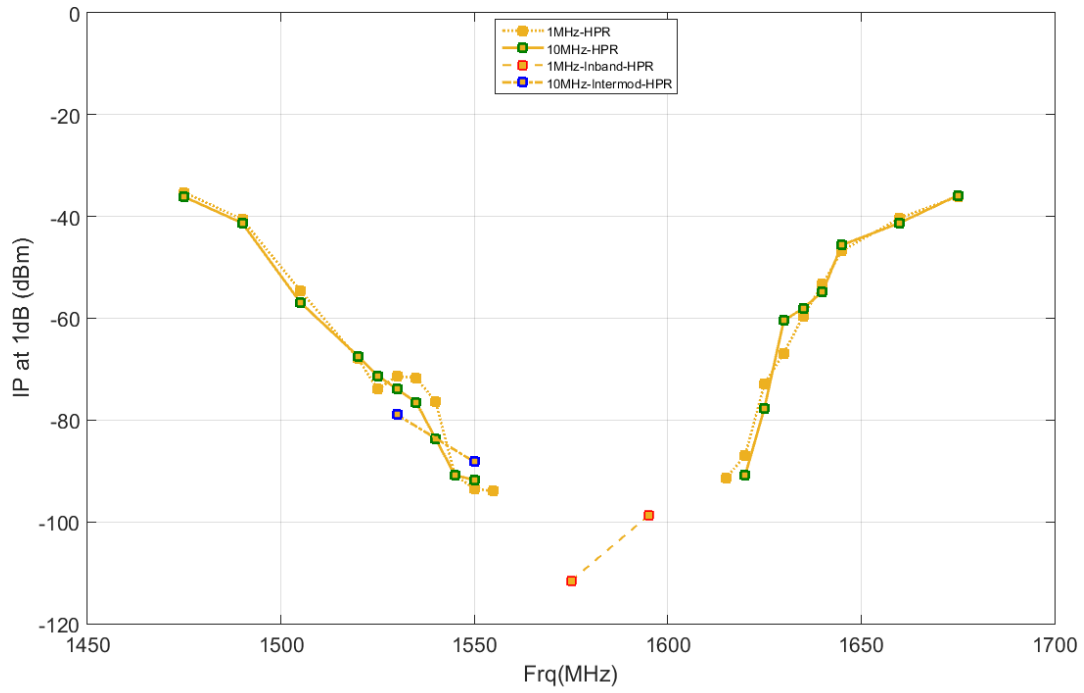
Figure B-53: Summary of 1&10 MHz, 1 MHz In-band, and 10 MHz Intermod Galileo E1 BC Bounding Masks
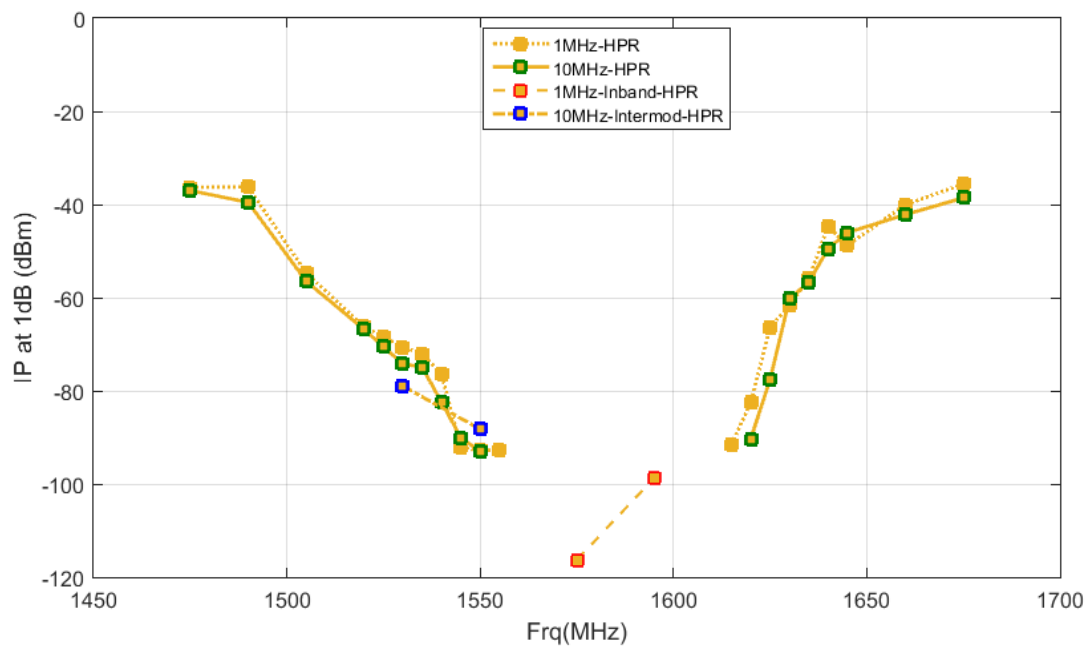
Figure B-54: Summary of 1&10 MHz, 1 MHz In-band, and 10 MHz Intermod SBAS L1 C/A - HPR Bounding Masks
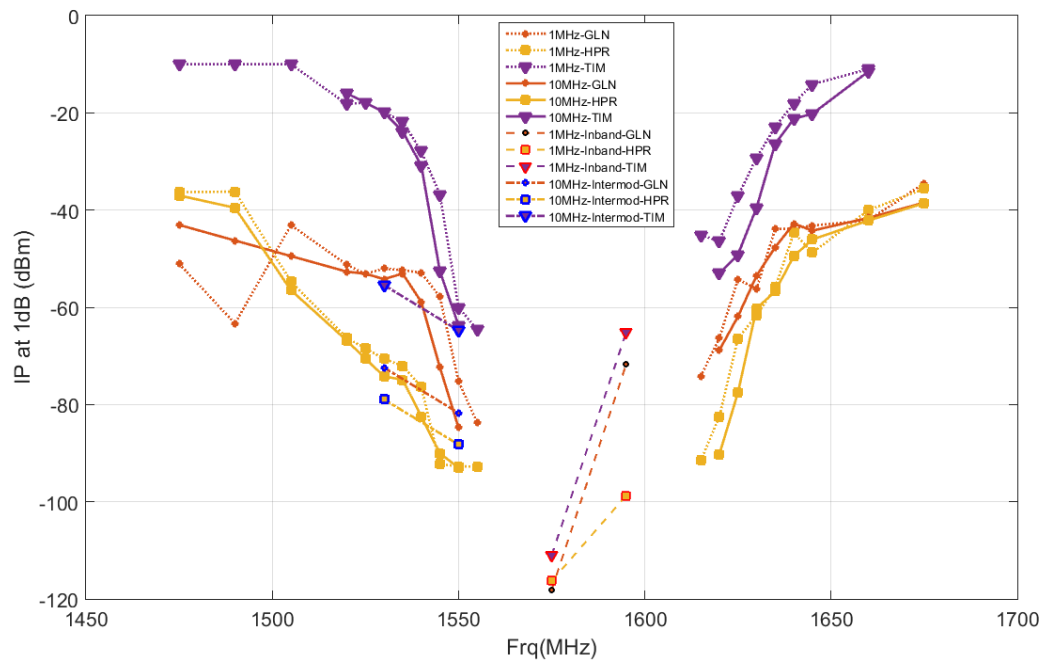
Figure B-55: Summary of 1&10 MHz, 1 MHz In-band, and 10 MHz Intermod SBAS L1 C/A Bounding Masks
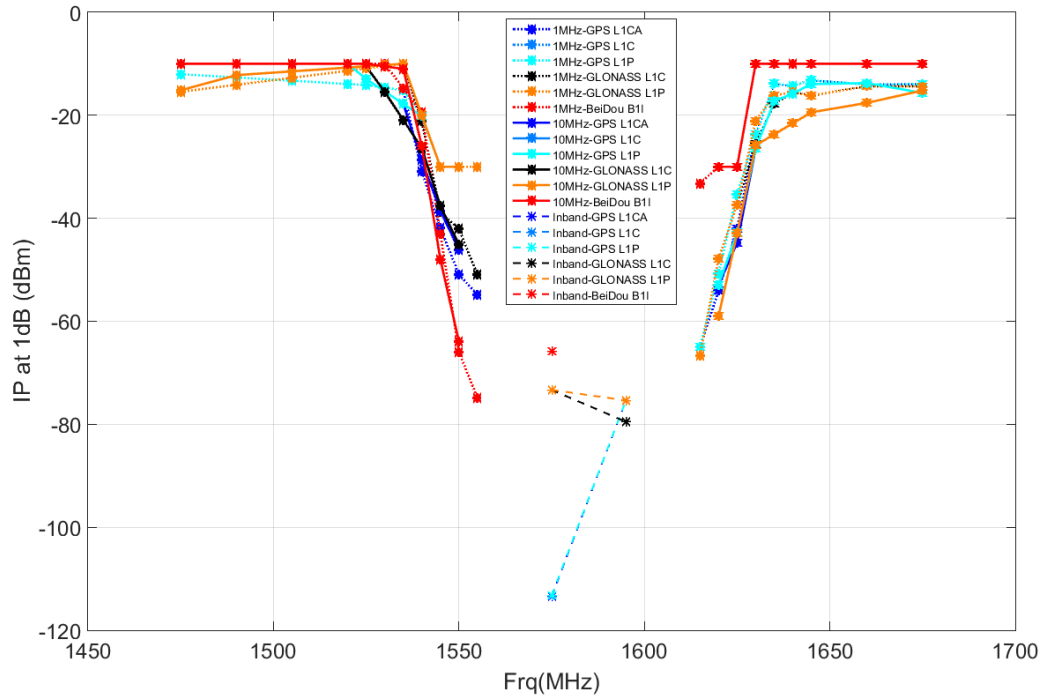
**Figure B-56: Summary of Cellular Bounding Masks for
1 & 10 MHz, 1 MHz In-band, and 10 MHz Intermod**
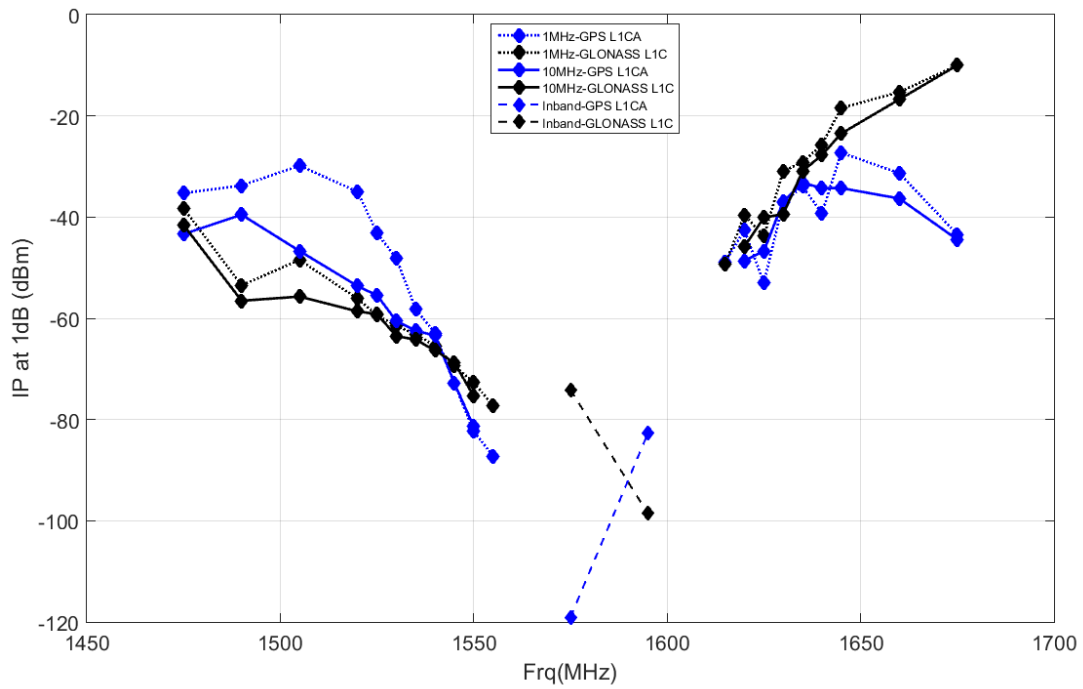
**Figure B-57: Summary of General Aviation Bounding Masks for
1 & 10 MHz, 1 MHz In-band, and 10 MHz Intermod**
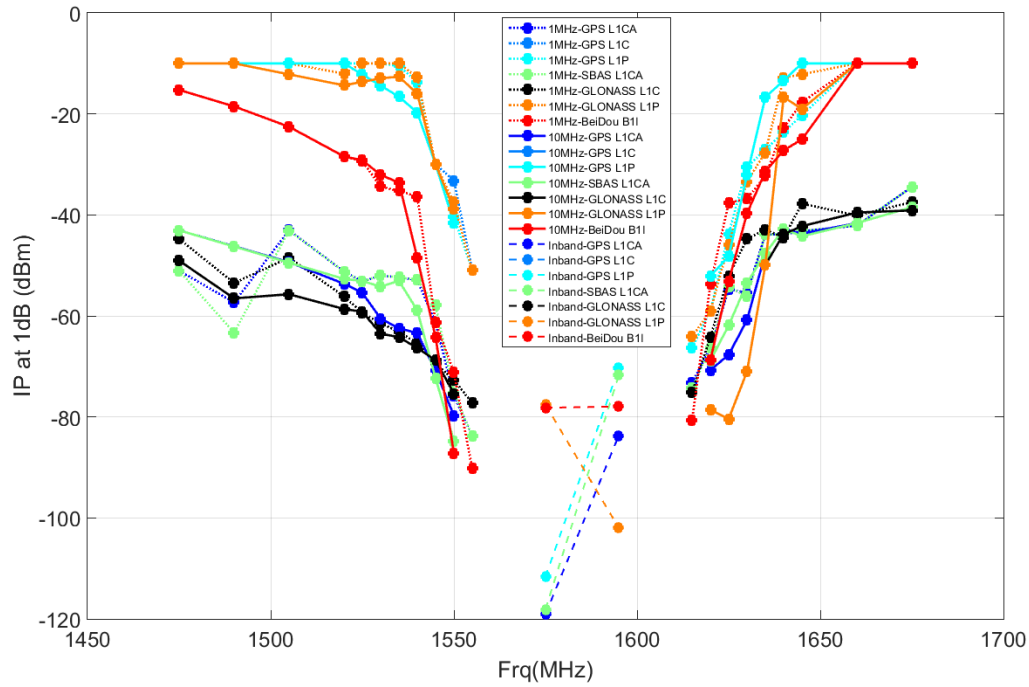
Figure B-58: Summary of General Location Navigation Bounding Masks for 1 & 10 MHz, 1 MHz In-band, and 10 MHz Intermod

Figure B-59 compares the ITMs across all emulated GNSS signal types for the HPR receiver category. The receive interference level from an LTE type signal should not exceed any of the masks in if all GNSS operation is to be ensured for the HPR category.
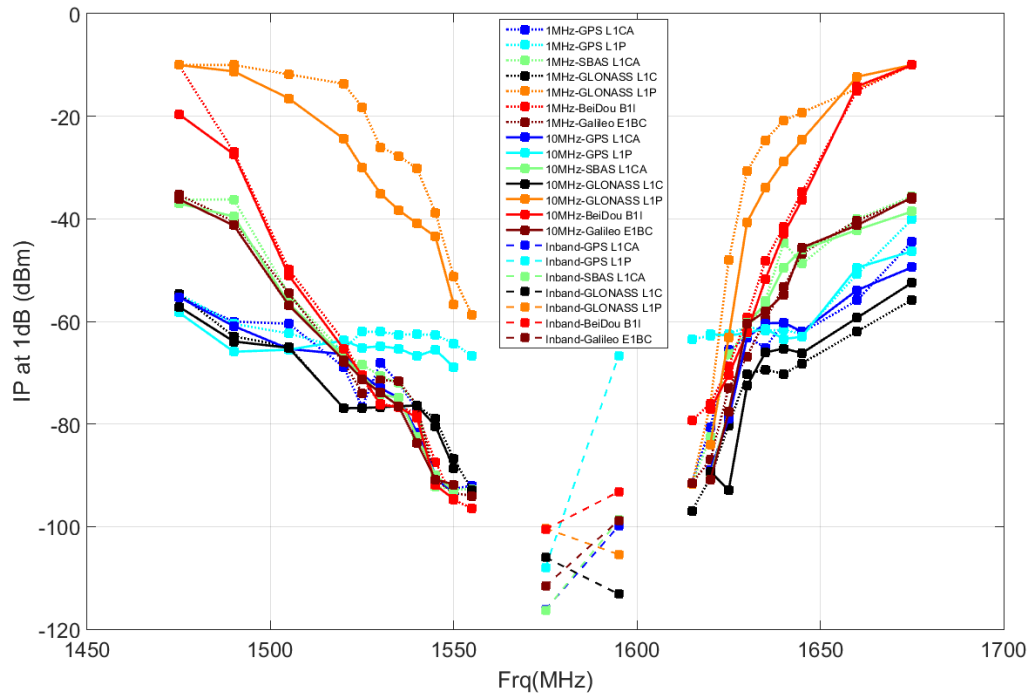
**Figure B-59: Summary of High Precision Bounding Masks for
1 & 10 MHz, 1 MHz In-band, and 10 MHz Intermod**
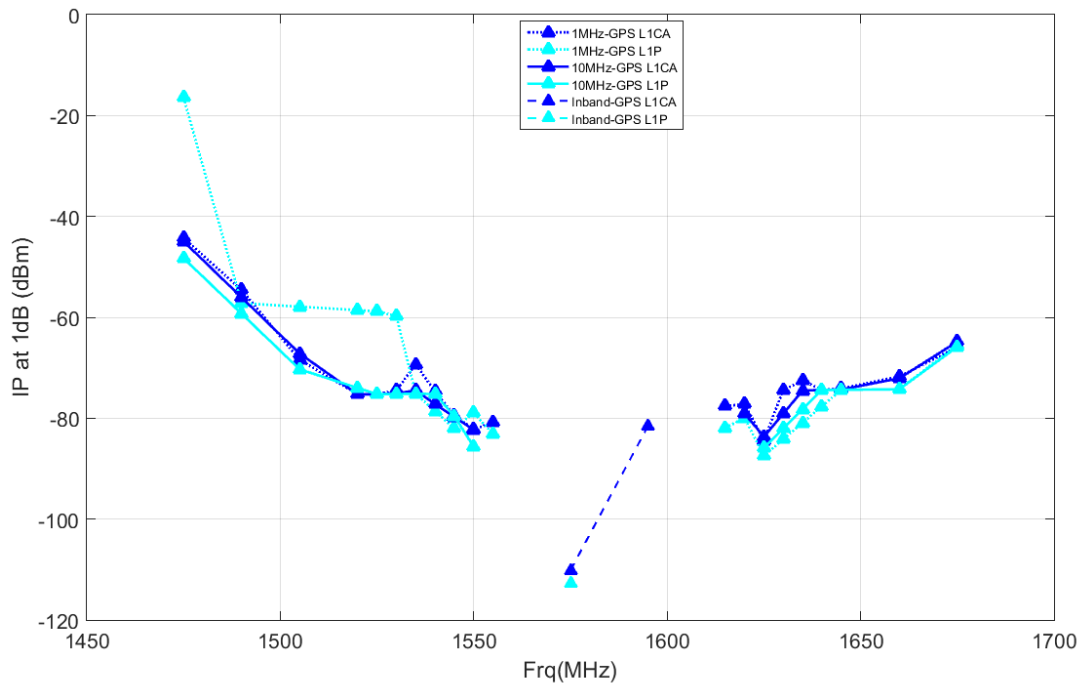
**Figure B-60: Summary of Space Based Bounding Masks for
1 & 10 MHz, 1 MHz In-band, and 10 MHz Intermod**
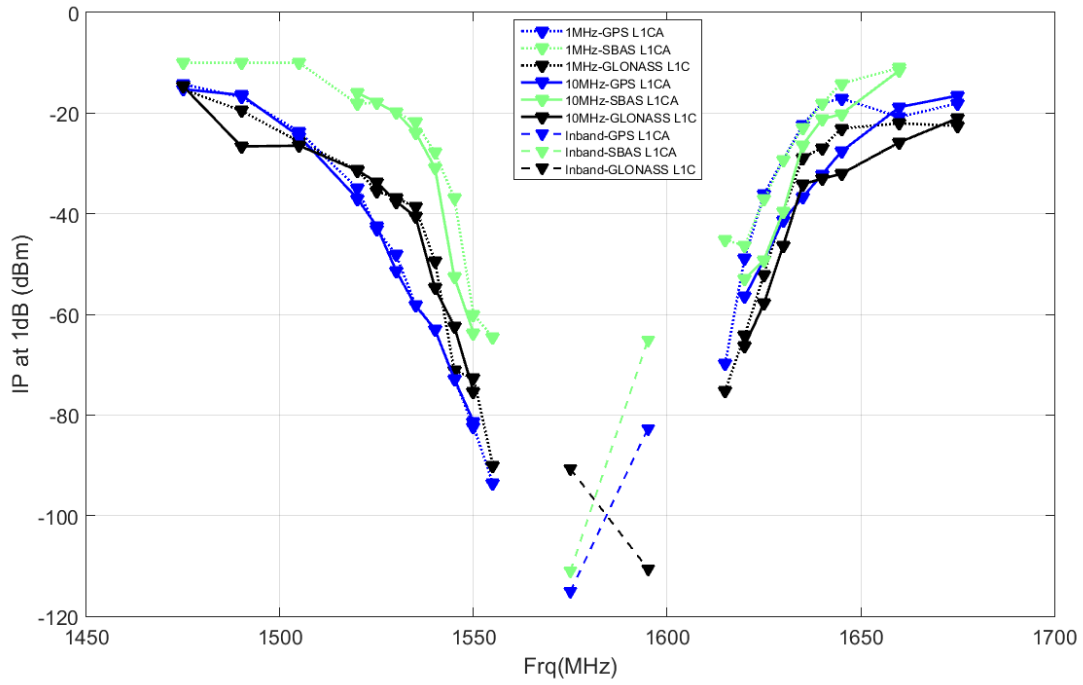
**Figure B-61: Summary of Timing Bounding Masks for
1 & 10 MHz, 1 MHz In-band, and 10 MHz Intermod**

APPENDIX C

LOSS OF LOCK RESULTS

TABLE OF CONTENTS

LIST OF FIGURES

LIST OF TABLES

REFERENCES

There are no sources in the current document.

APPENDIX

Appendix C. Loss of Lock Results

C.1 Summary of Bounding Masks

C.1.1 GPS L1 C/A
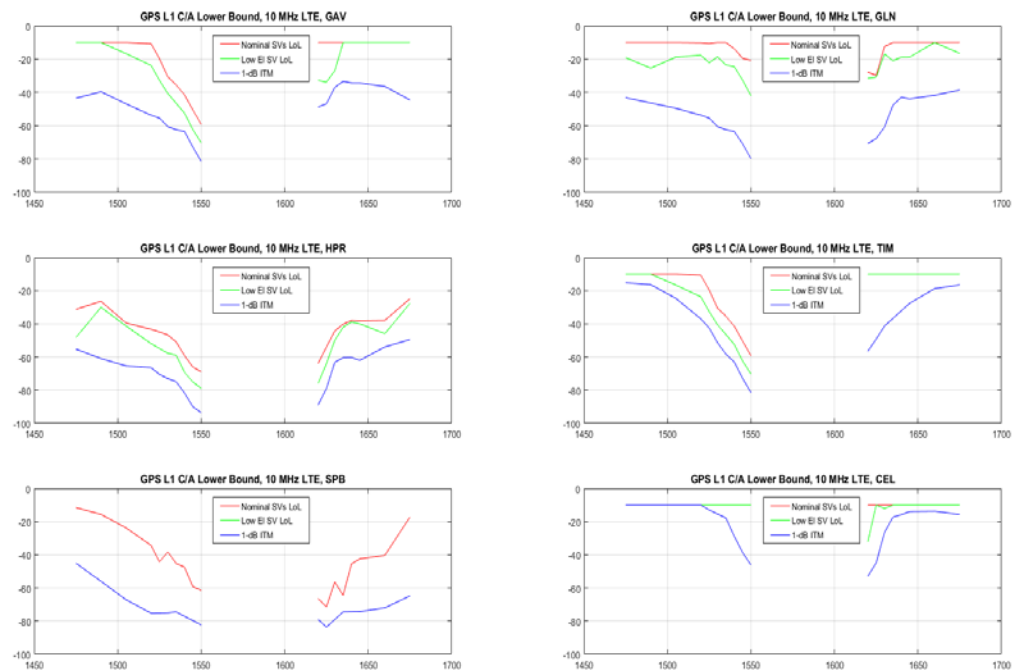
Figure C-1: Bounding Masks for GPS L1 C/A with 10 MHz LTE Interference

C.1.2 GPS L1 P
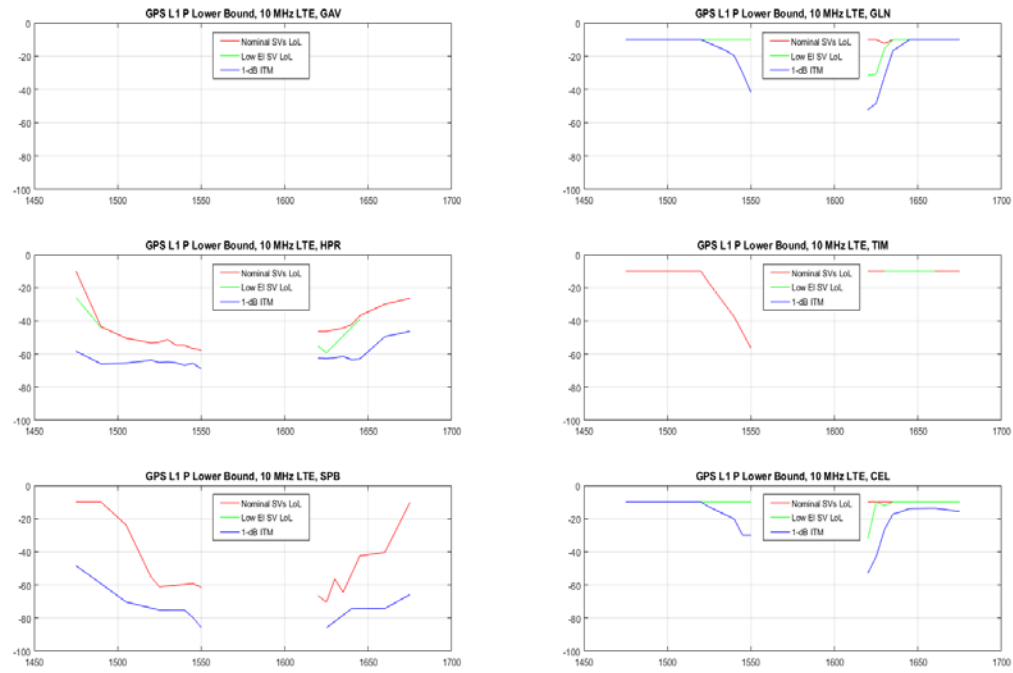
Figure C-2: Bounding Masks for GPS L1 P with 10 MHz LTE Interference

C.1.3   GPS L1 C
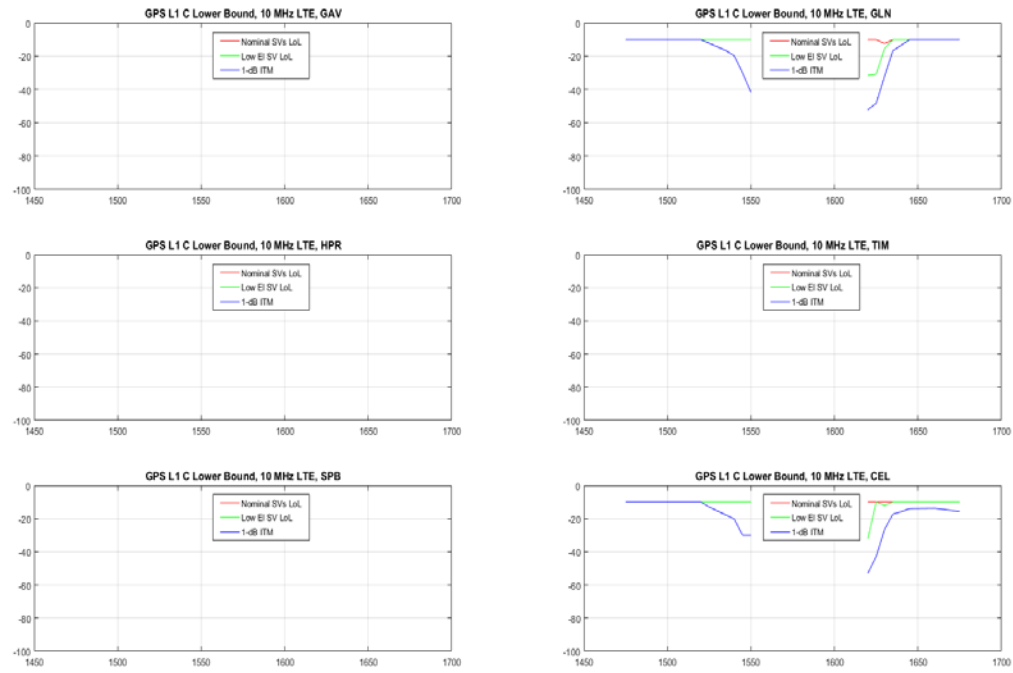
Figure C-3: Bounding Masks for GPS L1 C with 10 MHz LTE Interference

C.1.4 GLONASS L1 C
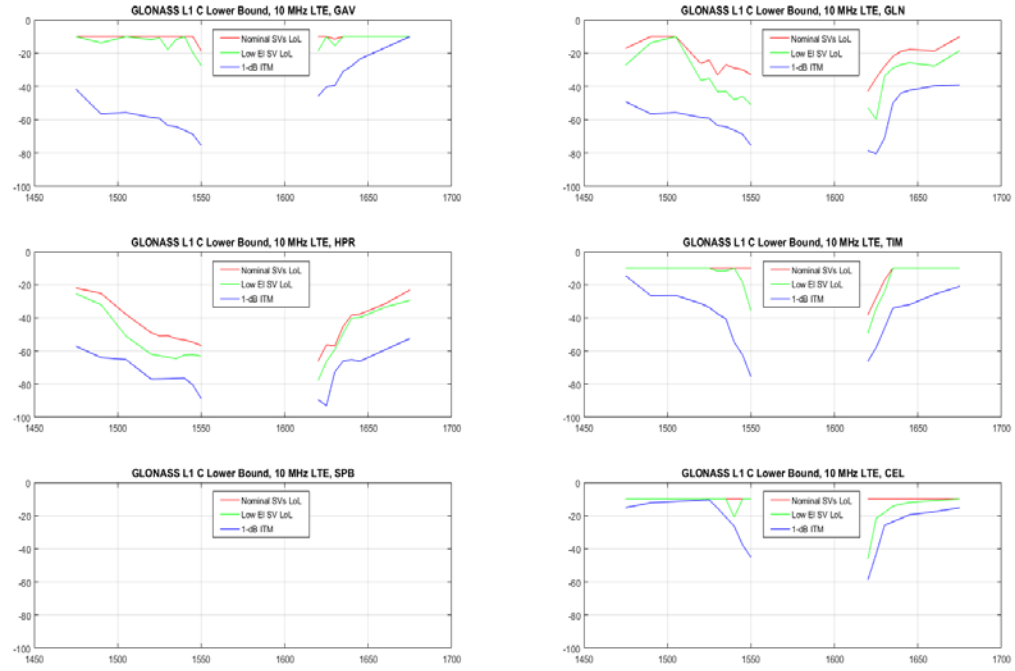
Figure C-4: Bounding Masks for GLONASS L1 C with 10 MHz LTE Interference

C.1.5　GLONASS L1 P
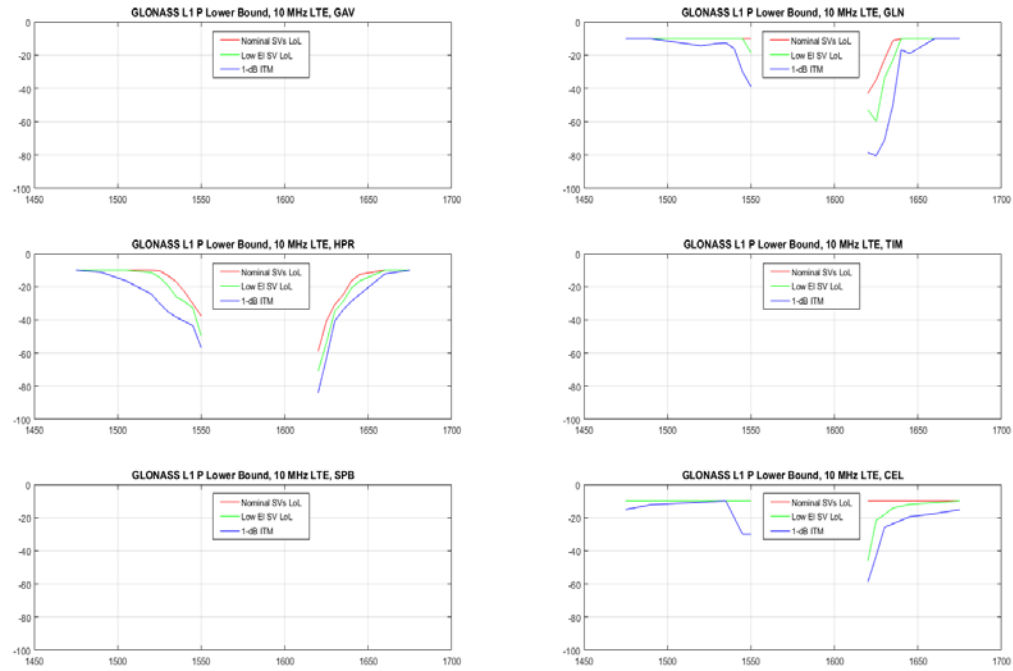
Figure C-5: Bounding Masks for GLONASS L1 P with 10 MHz LTE Interference

C.1.6   BeiDou B1I
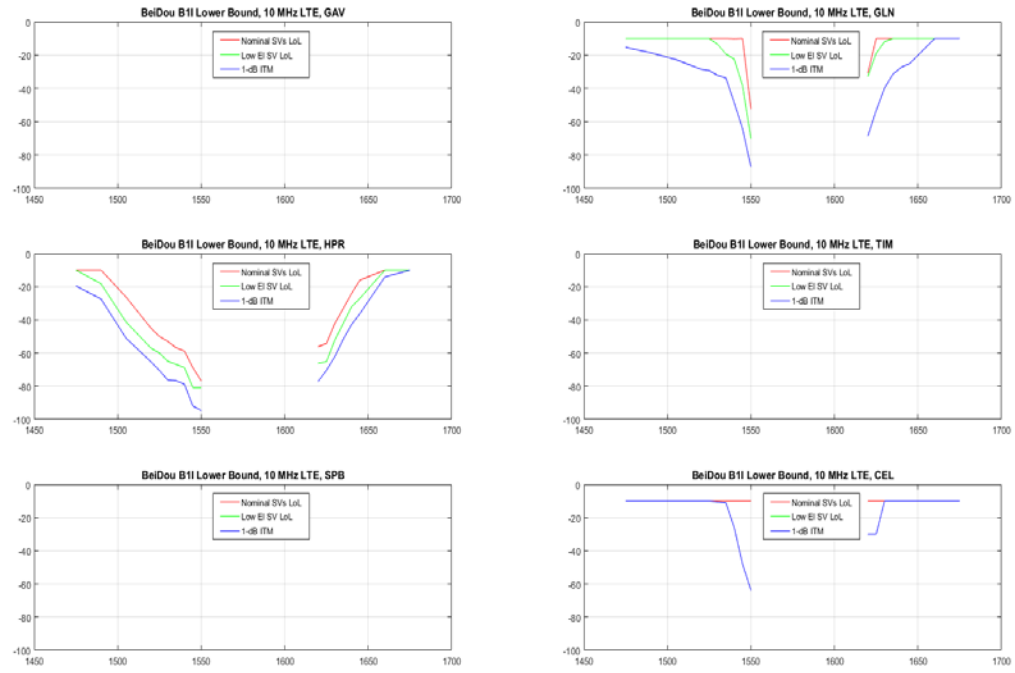
Figure C-6: Bounding Masks for BeiDou B1I with 10 MHz LTE Interference

C.1.7   Galileo E1 BC
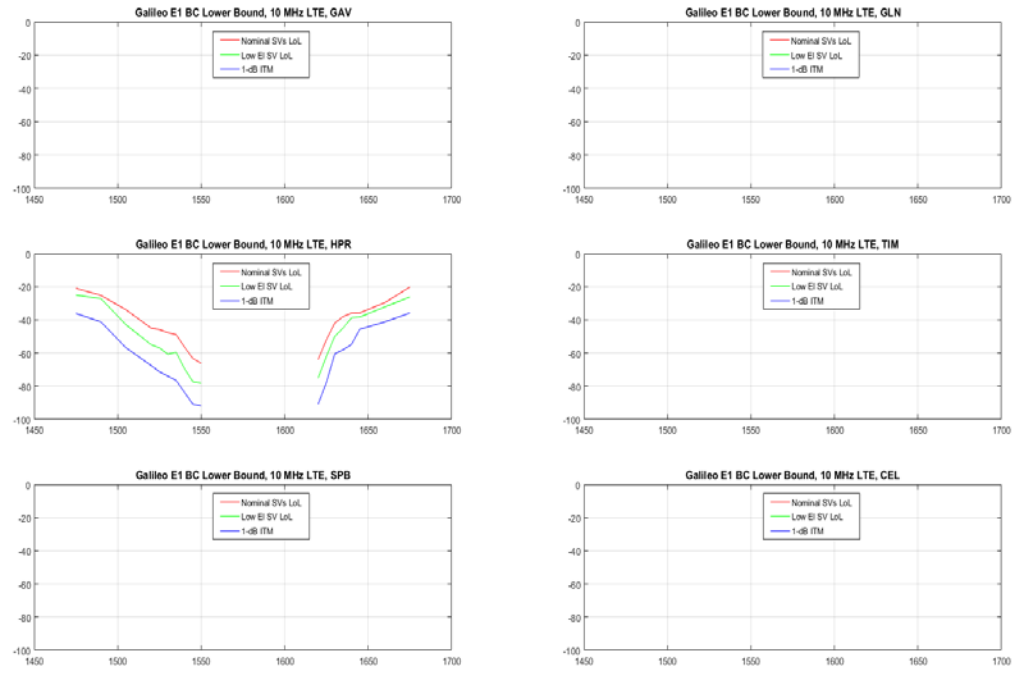
Figure C-7: Bounding Masks for Galileo E1 BC with 10 MHz LTE Interference

C.1.8   SBAS L1 C/A
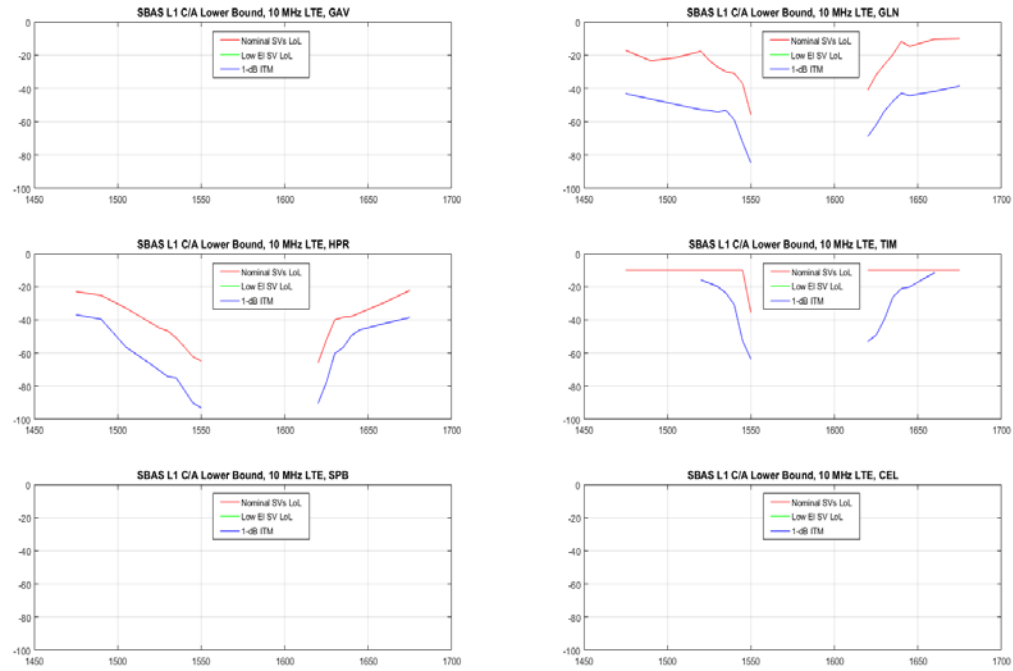
Figure C-8: Bounding Masks for SBAS L1 C/A with 10 MHz LTE Interference

C.2 Summary of Loss-of-Lock Analysis

C.2.1 GPS L1 C/A

C.2.1.1 Nominal SVs

Loss-of-Lock ITM computed using only "nominally" powered GPS signals

Table C-1: Nominal SVs GPS L1 C/A Bounding Masks (dBm)

Frequency (MHz)	GAV	GLN	HPR	TIM	SPB	CEL
1475	-9.999	-9.999	-31.2458	-9.999	-11.5239	-9.999
1490	-9.999	-9.999	-26.4447	-9.999	-15.602	-9.999
1505	-9.999	-9.999	-39.4615	-9.999	-23.7284	-9.999
1520	-10.7094	-10.2192	-43.3004	-10.7094	-34.2901	-9.999
1525	-19.6251	-10.5456	-44.8713	-19.6251	-44.2341	-9.999
1530	-30.5543	-9.999	-46.7309	-30.5543	-38.2091	-9.999
1535	-35.399	-9.999	-50.8679	-35.399	-45.151	-9.999
1540	-41.3614	-13.7121	-59.1205	-41.3614	-47.3892	-9.999
1545	-50.3634	-19.4403	-66.0247	-50.3634	-59.2506	-9.999
1550	-59.2229	-20.705	-68.8667	-59.2229	-61.4683	-9.999
1620	-9.999	-27.7486	-63.9203	-9.999	-66.5055	-9.999
1625	-9.999	-29.7378	-53.9544	-9.999	-71.4891	-9.999
1630	-9.999	-12.4154	-44.3042	-9.999	-56.4729	-9.999
1635	-9.999	-9.999	-40.1698	-9.999	-64.5191	-9.999
1640	-9.999	-9.999	-37.9451	-9.999	-45.405	-9.999
1645	-9.999	-9.999	-38.1748	-9.999	-42.3688	-9.999
1660	-9.999	-9.999	-37.9123	-9.999	-40.2659	-9.999
1675	-9.999	-9.999	-24.847	-9.999	-17.1974	-9.999

Table C-2: Nominal SVs GPS L1 C/A Median (dBm)

Frequency (MHz)	GAV	GLN	HPR	TIM	SPB	CEL
1475	-9.999	-9.999	-9.999	-9.999	-10.7615	-9.999
1490	-9.999	-9.999	-9.999	-9.999	-12.8005	-9.999
1505	-9.999	-9.999	-9.999	-9.999	-16.8637	-9.999
1520	-9.999	-9.999	-13.4422	-9.999	-22.8703	-9.999
1525	-9.999	-9.999	-16.8264	-9.999	-31.8007	-9.999
1530	-9.999	-9.999	-21.2618	-9.999	-32.8139	-9.999
1535	-9.999	-9.999	-26.9407	-9.999	-45.151	-9.999
1540	-9.999	-9.999	-31.4524	-9.999	-45.8019	-9.999
1545	-9.999	-9.999	-34.4658	-9.999	-59.2506	-9.999
1550	-9.999	-9.999	-40.9653	-9.999	-59.3381	-9.999
1620	-9.999	-9.999	-36.5694	-9.999	-56.5085	-9.999
1625	-9.999	-9.999	-31.9266	-9.999	-59.0085	-9.999
1630	-9.999	-9.999	-22.2095	-9.999	-50.5324	-9.999
1635	-9.999	-9.999	-14.6811	-9.999	-64.5191	-9.999
1640	-9.999	-9.999	-10.551	-9.999	-38.9629	-9.999
1645	-9.999	-9.999	-9.999	-9.999	-42.3688	-9.999
1660	-9.999	-9.999	-9.999	-9.999	-26.3502	-9.999
1675	-9.999	-9.999	-9.999	-9.999	-13.5982	-9.999
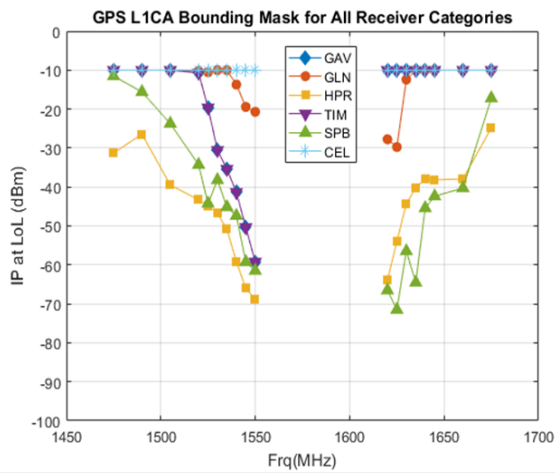
(a)
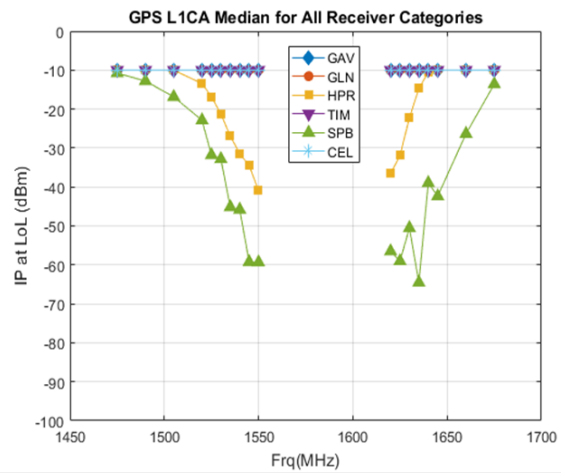
(b)

Figure C-9: Nominal SVs (a) GPS L1 C/A Bounding Masks and (b) GPS L1 C/A Median

16

C.2.1.2 Low Elevation SVs
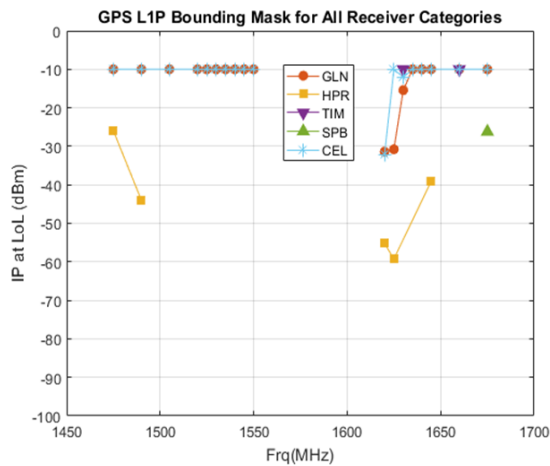
Loss-of-Lock ITM computed using only PRN-24 fixed at -10 dB relative to the nominal received power levels.

Table C-3: Low Elevation SVs GPS L1 C/A Bounding Masks (dBm)

Frequency (MHz)	GAV	GLN	HPR	TIM	SPB	CEL
1475	-9.999	-19.0577	-48.2458	-9.999	NaN	-9.999
1490	-9.999	-25.3312	-30.0449	-9.999	NaN	-9.999
1505	-16.6328	-18.724	-41.279	-16.6328	NaN	-9.999
1520	-23.7094	-17.6091	-51.9467	-23.7094	NaN	-9.999
1525	-32.6251	-22.0921	-54.8713	-32.6251	NaN	-9.999
1530	-40.5543	-18.5543	-57.7309	-40.5543	NaN	-9.999
1535	-46.399	-23.445	-58.8679	-46.399	NaN	-9.999
1540	-52.3614	-24.4252	-69.1205	-52.3614	NaN	-9.999
1545	-62.3634	-32.507	-75.0247	-62.3634	NaN	-9.999
1550	-70.2229	-41.8765	-78.8667	-70.2229	NaN	-9.999
1620	-32.6403	-31.3943	-75.9203	-9.999	NaN	-32.1514
1625	-33.7292	-30.7686	-63.9544	-9.999	NaN	-9.999
1630	-26.8823	-16.82	-49.9352	-9.999	NaN	-12.0846
1635	-9.999	-20.9075	-42.0443	-9.999	NaN	-9.999
1640	-9.999	-18.7996	-38.8251	-9.999	NaN	-9.999
1645	-9.999	-18.7334	-40.0116	-9.999	NaN	-9.999
1660	-9.999	-9.999	-45.9123	-9.999	NaN	-9.999
1675	-9.999	-16.4705	-27.6572	-9.999	NaN	-9.999

Table C-4: Low Elevation SVs GPS L1 C/A Median (dBm)

Frequency (MHz)	GAV	GLN	HPR	TIM	SPB	CEL
1475	-9.999	-9.999	-9.999	-9.999	NaN	-9.999
1490	-9.999	-9.999	-9.999	-9.999	NaN	-9.999
1505	-9.999	-9.999	-9.999	-9.999	NaN	-9.999
1520	-9.999	-9.999	-11.8129	-9.999	NaN	-9.999
1525	-9.999	-9.999	-17.1529	-9.999	NaN	-9.999
1530	-9.999	-9.999	-23.1472	-9.999	NaN	-9.999
1535	-9.999	-9.999	-31.1458	-9.999	NaN	-9.999
1540	-9.999	-9.999	-32.9976	-9.999	NaN	-9.999
1545	-9.999	-9.999	-38.5907	-9.999	NaN	-9.999
1550	-9.999	-9.999	-45.0672	-9.999	NaN	-9.999
1620	-9.999	-9.999	-38.8637	-9.999	NaN	-9.999
1625	-9.999	-9.999	-37.3521	-9.999	NaN	-9.999
1630	-9.999	-9.999	-28.4308	-9.999	NaN	-9.999
1635	-9.999	-9.999	-16.5783	-9.999	NaN	-9.999
1640	-9.999	-9.999	-14.5126	-9.999	NaN	-9.999
1645	-9.999	-9.999	-10.2873	-9.999	NaN	-9.999
1660	-9.999	-9.999	-9.999	-9.999	NaN	-9.999
1675	-9.999	-9.999	-9.999	-9.999	NaN	-9.999
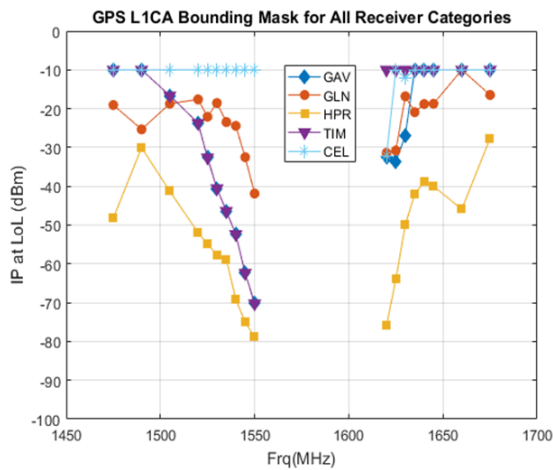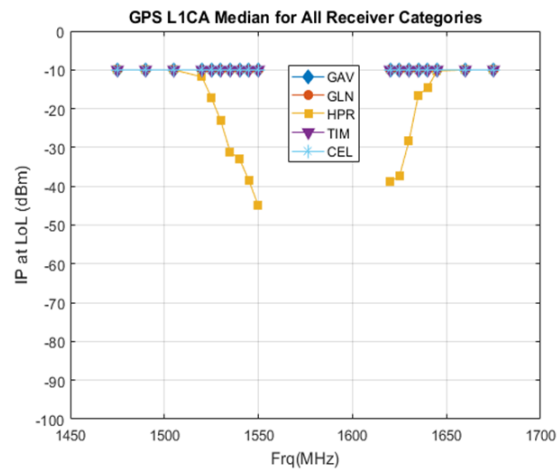
(a)   (b)

Figure C-10: Low Elevation SVs (a) GPS L1 C/A Bounding Masks and (b) GPS L1 C/A Median

18

C.2.2 GPS L1 P

C.2.2.1 Nominal SVs

Loss-of-Lock ITM computed using only "nominally" powered GPS signals

Table C-5: Nominal SVs GPS L1 P Bounding Masks (dBm)

Frequency (MHz)	GAV	GLN	HPR	TIM	SPB	CEL
1475	NaN	-9.999	-9.999	-9.999	-9.999	-9.999
1490	NaN	-9.999	-43.5111	-9.999	-9.999	-9.999
1505	NaN	-9.999	-50.4615	-9.999	-23.7284	-9.999
1520	NaN	-9.999	-53.3004	-9.999	-55.2901	-9.999
1525	NaN	-9.999	-52.8098	-17.4427	-61.2341	-9.999
1530	NaN	-9.999	-51.2816	NaN	NaN	-9.999
1535	NaN	-9.999	-54.8046	NaN	NaN	-9.999
1540	NaN	-9.999	-54.7822	-37.657	NaN	-9.999
1545	NaN	-9.999	-56.7246	NaN	-59.2506	-9.999
1550	NaN	-9.999	-57.6585	-56.4707	-61.4683	-9.999
1620	NaN	-9.999	-46.3395	-9.999	-66.5055	-9.999
1625	NaN	-9.999	-46.3261	-9.999	-70.4891	-9.999
1630	NaN	-12.4154	-45.3042	-9.999	-56.4729	-9.999
1635	NaN	-9.999	-44.3723	-9.999	-64.5191	-9.999
1640	NaN	-9.999	-42.2717	-9.999	NaN	-9.999
1645	NaN	-9.999	-36.8869	-9.999	-42.3688	-9.999
1660	NaN	-9.999	-29.9614	-9.999	-40.2659	-9.999
1675	NaN	-9.999	-26.4567	-9.999	-10.1974	-9.999

19

Table C-6: Nominal SVs GPS L1 P Median (dBm)

| Frequency (MHz)	GAV	GLN	HPR	TIM	SPB	CEL
1475	NaN	-9.999	-9.999	-9.999	-9.999	-9.999
1490	NaN	-9.999	-42.9099	-9.999	-9.999	-9.999
1505	NaN	-9.999	-47.9422	-9.999	-16.8637	-9.999
1520	NaN	-9.999	-52.8489	-9.999	-33.3703	-9.999
1525	NaN	-9.999	-51.2298	-17.4427	-40.3007	-9.999
1530	NaN	-9.999	-49.8352	NaN	NaN	-9.999
1535	NaN	-9.999	-53.2823	NaN	NaN	-9.999
1540	NaN	-9.999	-53.3135	-37.657	NaN	-9.999
1545	NaN	-9.999	-55.2629	NaN	-59.2506	-9.999
1550	NaN	-9.999	-57.2322	-56.4707	-59.3381	-9.999
1620	NaN	-9.999	-45.2663	-9.999	-66.5055	-9.999
1625	NaN	-9.999	-45.2341	-9.999	-58.5085	-9.999
1630	NaN	-9.999	-44.1922	-9.999	-56.4729	-9.999
1635	NaN	-9.999	-41.1038	-9.999	-64.5191	-9.999
1640	NaN	-9.999	-39.0043	-9.999	NaN	-9.999
1645	NaN	-9.999	-31.9579	-9.999	-42.3688	-9.999
1660	NaN	-9.999	-29.6232	-9.999	-40.2659	-9.999
1675	NaN	-9.999	-25.847	-9.999	-10.0982	-9.999
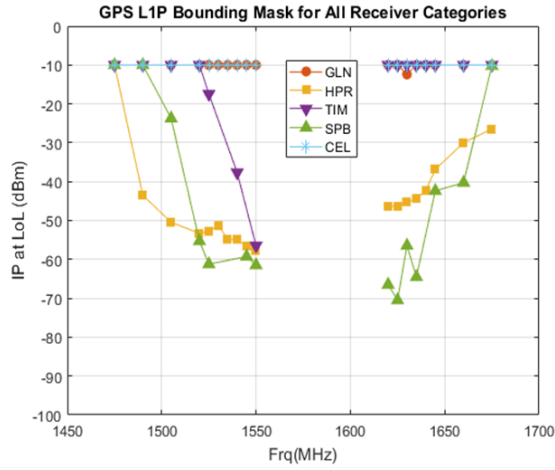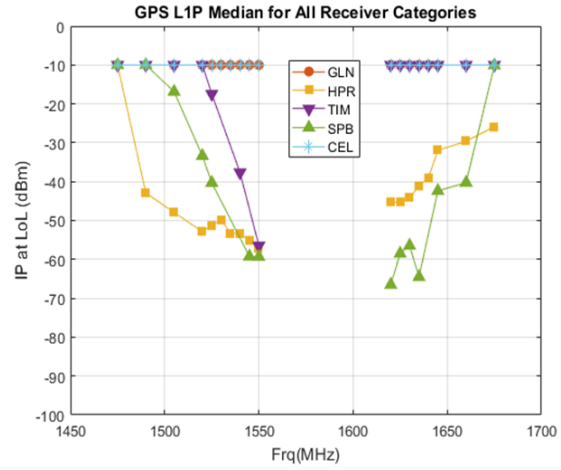
Figure C-11: Nominal SVs (a) GPS L1 P Bounding Masks and (b) GPS L1 P Median

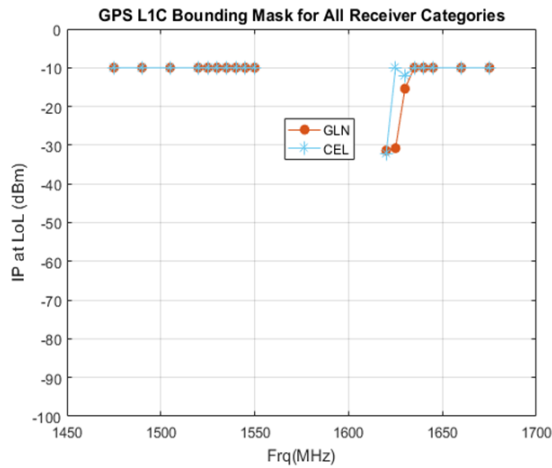### C.2.2.2   Low Elevation SVs

Loss-of-Lock ITM computed using only PRN-24 fixed at -10 dB relative to the nominal received power levels.

21

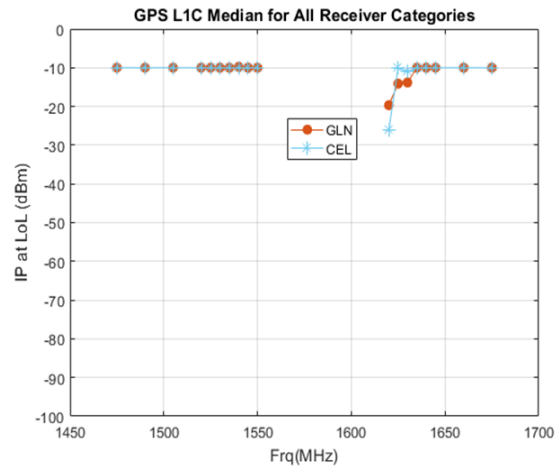**Table C-7: Low Elevation SVs GPS L1 P Bounding Masks (dBm)**

Frequency (MHz)	GAV	GLN	HPR	TIM	SPB	CEL
1475	NaN	-9.999	-25.96	NaN	NaN	-9.999
1490	NaN	-9.999	-44.0449	NaN	NaN	-9.999
1505	NaN	-9.999	NaN	NaN	NaN	-9.999
1520	NaN	-9.999	NaN	NaN	NaN	-9.999
1525	NaN	-9.999	NaN	NaN	NaN	-9.999
1530	NaN	-9.999	NaN	NaN	NaN	-9.999
1535	NaN	-9.999	NaN	NaN	NaN	-9.999
1540	NaN	-9.999	NaN	NaN	NaN	-9.999
1545	NaN	-9.999	NaN	NaN	NaN	-9.999
1550	NaN	-9.999	NaN	NaN	NaN	-9.999
1620	NaN	-31.3943	-55.2663	NaN	NaN	-32.1514
1625	NaN	-30.7686	-59.2341	NaN	NaN	-9.999
1630	NaN	-15.4154	NaN	-9.999	NaN	-12.0846
1635	NaN	-9.999	NaN	NaN	NaN	-9.999
1640	NaN	-9.999	NaN	NaN	NaN	-9.999
1645	NaN	-9.999	-39.029	NaN	NaN	-9.999
1660	NaN	-9.999	NaN	-9.999	NaN	-9.999
1675	NaN	-9.999	NaN	NaN	-26.1974	-9.999

Table C-8: Low Elevation SVs GPS L1 P Median (dBm)

Frequency (MHz)	GAV	GLN	HPR	TIM	SPB	CEL
1475	NaN	-9.999	-25.96	NaN	NaN	-9.999
1490	NaN	-9.999	-44.0449	NaN	NaN	-9.999
1505	NaN	-9.999	NaN	NaN	NaN	-9.999
1520	NaN	-9.999	NaN	NaN	NaN	-9.999
1525	NaN	-9.999	NaN	NaN	NaN	-9.999
1530	NaN	-9.999	NaN	NaN	NaN	-9.999
1535	NaN	-9.999	NaN	NaN	NaN	-9.999
1540	NaN	-9.77771	NaN	NaN	NaN	-9.999
1545	NaN	-9.999	NaN	NaN	NaN	-9.999
1550	NaN	-9.999	NaN	NaN	NaN	-9.999
1620	NaN	-19.675	-55.2663	NaN	NaN	-26.0967
1625	NaN	-14.0983	-59.2341	NaN	NaN	-9.999
1630	NaN	-13.8262	NaN	-9.999	NaN	-11.0418
1635	NaN	-9.999	NaN	NaN	NaN	-9.999
1640	NaN	-9.999	NaN	NaN	NaN	-9.999
1645	NaN	-9.999	-39.029	NaN	NaN	-9.999
1660	NaN	-9.999	NaN	-9.999	NaN	-9.999
1675	NaN	-9.999	NaN	NaN	-18.0982	-9.999
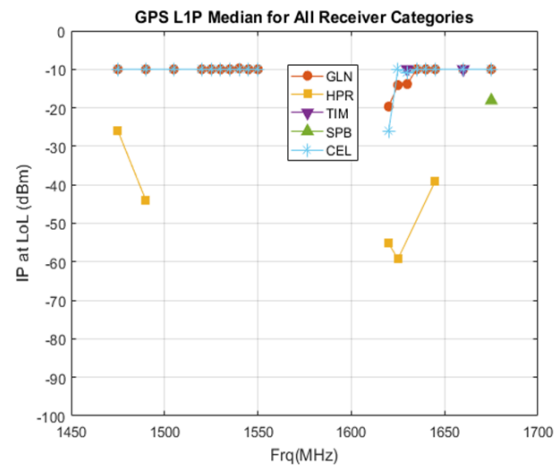
Figure C-12: Low Elevation SVs (a) GPS L1 P Bounding Masks and (b) GPS L1 P Median

23

C.2.3 GPS L1 C

C.2.3.1 Nominal SVs

Loss-of-Lock ITM computed using only "nominally" powered GPS signals

Table C-9: Nominal SVs GPS L1 C Bounding Masks (dBm)

Frequency (MHz)	GAV	GLN	HPR	TIM	SPB	CEL
1475	NaN	-9.999	NaN	NaN	NaN	-9.999
1490	NaN	-9.999	NaN	NaN	NaN	-9.999
1505	NaN	-9.999	NaN	NaN	NaN	-9.999
1520	NaN	-9.999	NaN	NaN	NaN	-9.999
1525	NaN	-9.999	NaN	NaN	NaN	-9.999
1530	NaN	-9.999	NaN	NaN	NaN	-9.999
1535	NaN	-9.999	NaN	NaN	NaN	-9.999
1540	NaN	-9.999	NaN	NaN	NaN	-9.999
1545	NaN	-9.999	NaN	NaN	NaN	-9.999
1550	NaN	-9.999	NaN	NaN	NaN	-9.999
1620	NaN	-9.999	NaN	NaN	NaN	-9.999
1625	NaN	-9.999	NaN	NaN	NaN	-9.999
1630	NaN	-12.4154	NaN	NaN	NaN	-9.999
1635	NaN	-9.999	NaN	NaN	NaN	-9.999
1640	NaN	-9.999	NaN	NaN	NaN	-9.999
1645	NaN	-9.999	NaN	NaN	NaN	-9.999
1660	NaN	-9.999	NaN	NaN	NaN	-9.999
1675	NaN	-9.999	NaN	NaN	NaN	-9.999

Table C-10: Nominal SVs GPS L1 C Median (dBm)

Frequency (MHz)	GAV	GLN	HPR	TIM	SPB	CEL
1475	NaN	-9.999	NaN	NaN	NaN	-9.999
1490	NaN	-9.999	NaN	NaN	NaN	-9.999
1505	NaN	-9.999	NaN	NaN	NaN	-9.999
1520	NaN	-9.999	NaN	NaN	NaN	-9.999
1525	NaN	-9.999	NaN	NaN	NaN	-9.999
1530	NaN	-9.999	NaN	NaN	NaN	-9.999
1535	NaN	-9.999	NaN	NaN	NaN	-9.999
1540	NaN	-9.999	NaN	NaN	NaN	-9.999
1545	NaN	-9.999	NaN	NaN	NaN	-9.999
1550	NaN	-9.999	NaN	NaN	NaN	-9.999
1620	NaN	-9.999	NaN	NaN	NaN	-9.999
1625	NaN	-9.999	NaN	NaN	NaN	-9.999
1630	NaN	-9.999	NaN	NaN	NaN	-9.999
1635	NaN	-9.999	NaN	NaN	NaN	-9.999
1640	NaN	-9.999	NaN	NaN	NaN	-9.999
1645	NaN	-9.999	NaN	NaN	NaN	-9.999
1660	NaN	-9.999	NaN	NaN	NaN	-9.999
1675	NaN	-9.999	NaN	NaN	NaN	-9.999
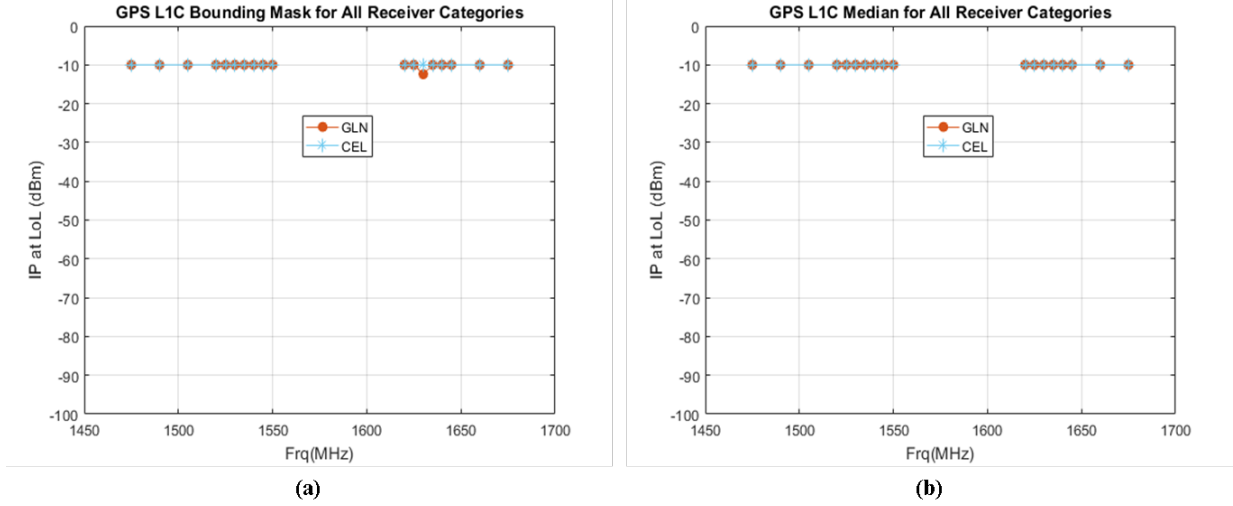
**Figure C-13: Nominal SVs (a) GPS L1 C Bounding Masks and
(b) GPS L1 C Median**

C.2.3.2   Low Elevation SVs

Loss-of-Lock ITM computed using only PRN-24 fixed at -10 dB relative to the nominal received power levels.

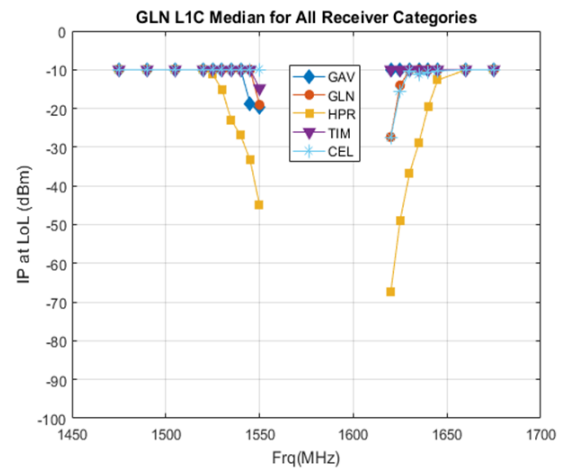**Table C-11: Low Elevation SVs GPS L1 C Bounding Masks (dBm)**

Frequency (MHz)	GAV	GLN	HPR	TIM	SPB	CEL
1475	NaN	-9.999	NaN	NaN	NaN	-9.999
1490	NaN	-9.999	NaN	NaN	NaN	-9.999
1505	NaN	-9.999	NaN	NaN	NaN	-9.999
1520	NaN	-9.999	NaN	NaN	NaN	-9.999
1525	NaN	-9.999	NaN	NaN	NaN	-9.999
1530	NaN	-9.999	NaN	NaN	NaN	-9.999
1535	NaN	-9.999	NaN	NaN	NaN	-9.999
1540	NaN	-9.999	NaN	NaN	NaN	-9.999
1545	NaN	-9.999	NaN	NaN	NaN	-9.999
1550	NaN	-9.999	NaN	NaN	NaN	-9.999
1620	NaN	-31.3943	NaN	NaN	NaN	-32.1514
1625	NaN	-30.7686	NaN	NaN	NaN	-9.999
1630	NaN	-15.4154	NaN	NaN	NaN	-12.0846
1635	NaN	-9.999	NaN	NaN	NaN	-9.999
1640	NaN	-9.999	NaN	NaN	NaN	-9.999
1645	NaN	-9.999	NaN	NaN	NaN	-9.999
1660	NaN	-9.999	NaN	NaN	NaN	-9.999
1675	NaN	-9.999	NaN	NaN	NaN	-9.999

Table C-12: Low Elevation SVs GPS L1 P Median (dBm)

Frequency (MHz)	GAV	GLN	HPR	TIM	SPB	CEL
1475	NaN	-9.999	NaN	NaN	NaN	-9.999
1490	NaN	-9.999	NaN	NaN	NaN	-9.999
1505	NaN	-9.999	NaN	NaN	NaN	-9.999
1520	NaN	-9.999	NaN	NaN	NaN	-9.999
1525	NaN	-9.999	NaN	NaN	NaN	-9.999
1530	NaN	-9.999	NaN	NaN	NaN	-9.999
1535	NaN	-9.999	NaN	NaN	NaN	-9.999
1540	NaN	-9.77771	NaN	NaN	NaN	-9.999
1545	NaN	-9.999	NaN	NaN	NaN	-9.999
1550	NaN	-9.999	NaN	NaN	NaN	-9.999
1620	NaN	-19.675	NaN	NaN	NaN	-26.0967
1625	NaN	-14.0983	NaN	NaN	NaN	-9.999
1630	NaN	-13.8262	NaN	NaN	NaN	-11.0418
1635	NaN	-9.999	NaN	NaN	NaN	-9.999
1640	NaN	-9.999	NaN	NaN	NaN	-9.999
1645	NaN	-9.999	NaN	NaN	NaN	-9.999
1660	NaN	-9.999	NaN	NaN	NaN	-9.999
1675	NaN	-9.999	NaN	NaN	NaN	-9.999

(a)

(b)

Figure C-14: Low Elevation SVs (a) GPS L1 C Bounding Masks and (b) GPS L1 C Median

28

C.2.4   GLONASS L1 C

C.2.4.1   Nominal SVs

Loss-of-Lock ITM computed using only "nominally" powered GPS signals

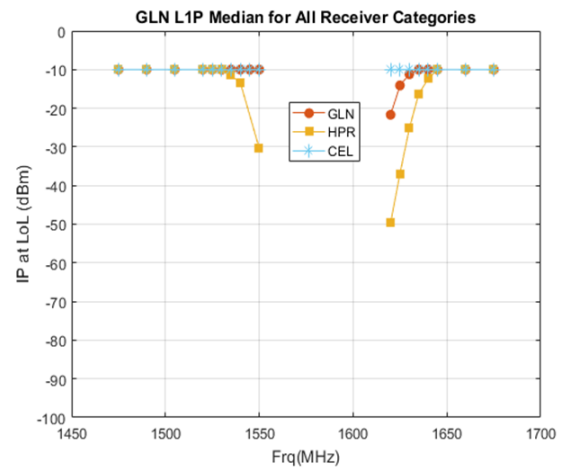**Table C-13: Nominal SVs GLONASS L1 C Bounding Masks (dBm)**

Frequency (MHz)	GAV	GLN	HPR	TIM	SPB	CEL
1475	-9.999	-17.0577	-22.0199	-9.999	NaN	-9.999
1490	-9.999	-9.999	-25.2549	-9.999	NaN	-9.999
1505	-9.999	-9.999	-37.9422	-9.999	NaN	-9.999
1520	-9.999	-26.2192	-48.9467	-9.999	NaN	-9.999
1525	-9.999	-24.0921	-50.8713	-9.999	NaN	-9.999
1530	-9.999	-33.0652	-50.7309	-9.999	NaN	-9.999
1535	-9.999	-26.897	-52.5364	-9.999	NaN	-9.999
1540	-9.999	-28.9021	-53.3135	-9.999	NaN	-9.999
1545	-9.999	-29.8816	-54.7246	-9.999	NaN	-9.999
1550	-18.6341	-32.884	-56.6585	-9.999	NaN	-9.999
1620	-9.999	-42.7896	-66.188	-38.2107	NaN	-9.999
1625	-9.999	-34.7686	-56.207	NaN	NaN	-9.999
1630	-11.4378	-27.82	-57.0348	-17.2599	NaN	-9.999
1635	-9.999	-21.9075	-45.1698	-9.999	NaN	-9.999
1640	-9.999	-18.7996	-38.3831	-9.999	NaN	-9.999
1645	-9.999	-17.7334	-37.8222	-9.999	NaN	-9.999
1660	-9.999	-18.6121	-31.6007	-9.999	NaN	-9.999
1675	-9.999	-9.999	-23.2063	-9.999	NaN	-9.999

Table C-14: Nominal SVs GLONASS L1 C Median (dBm)

Frequency (MHz)	GAV	GLN	HPR	TIM	SPB	CEL
1475	-9.999	-9.999	-9.999	-9.999	NaN	-9.999
1490	-9.999	-9.999	-9.999	-9.999	NaN	-9.999
1505	-9.999	-9.999	-9.999	-9.999	NaN	-9.999
1520	-9.999	-9.999	-16.3549	-9.999	NaN	-9.999
1525	-9.999	-9.999	-16.3513	-9.999	NaN	-9.999
1530	-9.999	-9.999	-20.7887	-9.999	NaN	-9.999
1535	-9.999	-9.999	-25.2012	-9.999	NaN	-9.999
1540	-9.999	-9.999	-23.0492	-9.999	NaN	-9.999
1545	-9.999	-9.999	-9.999	-9.999	NaN	-9.999
1550	-9.999	-9.999	-38.8832	-9.999	NaN	-9.999
1620	-9.999	-15.0761	-53.4166	-9.999	NaN	-9.999
1625	-9.999	-9.999	-37.9896	NaN	NaN	-9.999
1630	-9.999	-9.999	-33.3659	-9.999	NaN	-9.999
1635	-9.999	-9.999	-23.4376	-9.999	NaN	-9.999
1640	-9.999	-9.999	-15.6777	-9.999	NaN	-9.999
1645	-9.999	-9.999	-9.999	-9.999	NaN	-9.999
1660	-9.999	-9.999	-9.999	-9.999	NaN	-9.999
1675	-9.999	-9.999	-9.999	-9.999	NaN	-9.999
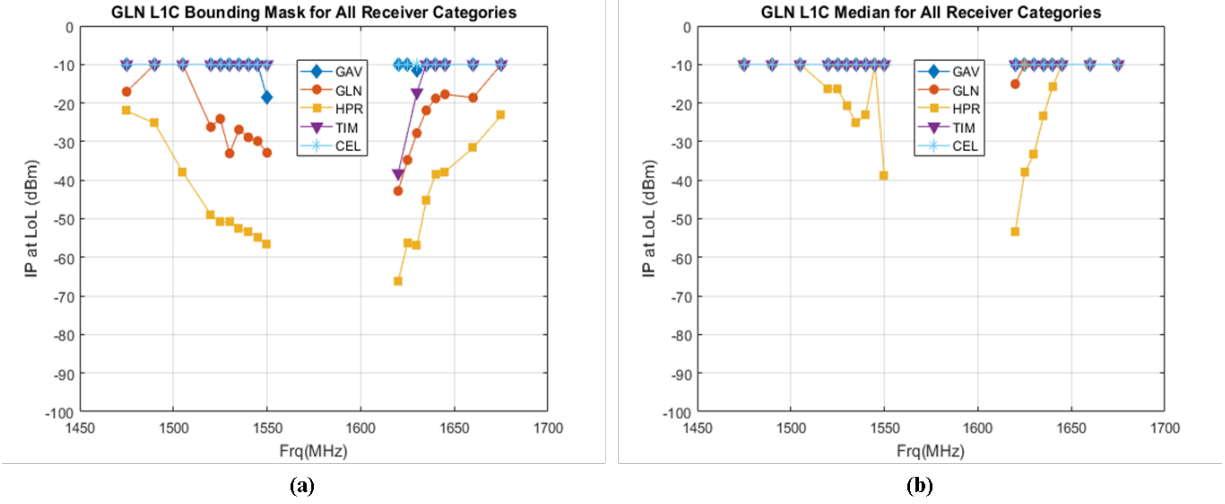
Figure C-15: Nominal SVs (a) GLONASS L1 C Bounding Masks and (b) GLONASS L1 C Median

C.2.4.2 Low Elevation SVs

Loss-of-Lock ITM computed using only SV-01 fixed at -10 dB relative to the nominal received power levels.

Table C-15: Low Elevation SVs GLONASS L1 C Bounding Masks (dBm)

Frequency (MHz)	GAV	GLN	HPR	TIM	SPB	CEL
1475	-9.999	-27.0577	-25.4968	-9.999	NaN	-9.999
1490	-13.7647	-13.7647	-32.0449	-9.999	NaN	-9.999
1505	-9.999	-9.999	-51.0301	-9.999	NaN	-9.999
1520	-11.8154	-36.2192	-61.9467	-9.999	NaN	-9.999
1525	-10.771	-35.0921	-62.8713	-9.999	NaN	-9.999
1530	-17.7766	-43.0652	-63.7309	-11.7766	NaN	-9.999
1535	-11.722	-42.897	-64.5364	-11.722	NaN	-9.999
1540	-9.999	-47.9021	-62.3935	-9.999	NaN	-20.9017
1545	-19.6831	-45.8816	-62.2675	-18.6831	NaN	-9.999
1550	-27.2693	-50.884	-63.138	-35.7205	NaN	-9.999
1620	-18.6707	-52.7896	-77.7669	-49.2107	NaN	-46.1514
1625	-9.999	-59.7686	-66.207	-34.1718	NaN	-21.579
1630	-15.4378	-33.7641	-59.1922	-24.2599	NaN	-18.0846
1635	-9.999	-28.9075	-49.3014	-9.999	NaN	-14.2157
1640	-9.999	-26.7996	-40.194	-9.999	NaN	-13.0403
1645	-9.999	-25.7334	-39.8279	-9.999	NaN	-12.005
1660	-9.999	-27.6121	-33.6007	-9.999	NaN	-10.9311
1675	-9.999	-18.4705	-29.4429	-9.999	NaN	-9.999

Table C-16: Low Elevation SVs GLONASS L1 C Median (dBm)

Frequency (MHz)	GAV	GLN	HPR	TIM	SPB	CEL
1475	-9.999	-9.999	-9.999	-9.999	NaN	-9.999
1490	-9.999	-9.999	-9.999	-9.999	NaN	-9.999
1505	-9.999	-9.999	-9.999	-9.999	NaN	-9.999
1520	-9.999	-9.999	-9.999	-9.999	NaN	-9.999
1525	-9.999	-9.999	-11.1529	-9.999	NaN	-9.999
1530	-9.999	-9.999	-15.1472	-9.999	NaN	-9.999
1535	-9.999	-9.999	-23.0548	-9.999	NaN	-9.999
1540	-9.999	-9.999	-26.9976	-9.999	NaN	-9.999
1545	-18.6831	-9.999	-33.3833	-9.999	NaN	-9.999
1550	-19.6341	-19.0674	-44.8832	-14.8166	NaN	-9.999
1620	-9.999	-27.3583	-67.4381	-9.999	NaN	-27.5419
1625	-9.999	-14.064	-48.9016	-9.999	NaN	-15.5228
1630	-9.999	-10.0739	-36.8036	-9.999	NaN	-10.2921
1635	-9.999	-9.999	-28.9246	-9.999	NaN	-11.1461
1640	-9.999	-9.999	-19.5126	-9.999	NaN	-10.7826
1645	-9.999	-9.999	-12.6969	-9.999	NaN	-10.2662
1660	-9.999	-9.999	-9.999	-9.999	NaN	-9.999
1675	-9.999	-9.999	-9.999	-9.999	NaN	-9.999
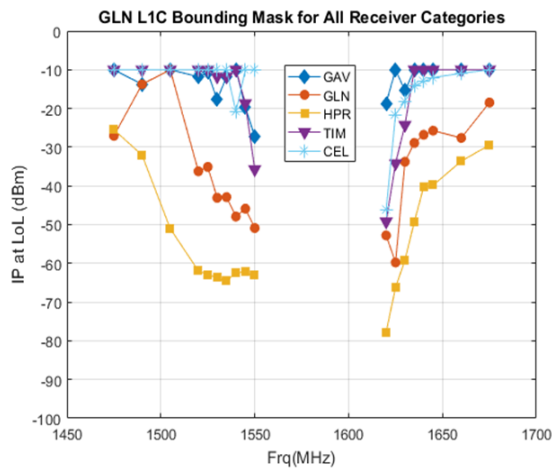
(a)

(b)

Figure C-16: Low Elevation SVs (a) GLONASS L1 C Bounding Masks and (b) GLONASS L1 C Median

33

C.2.5 GLONASS L1 P

C.2.5.1 Nominal SVs
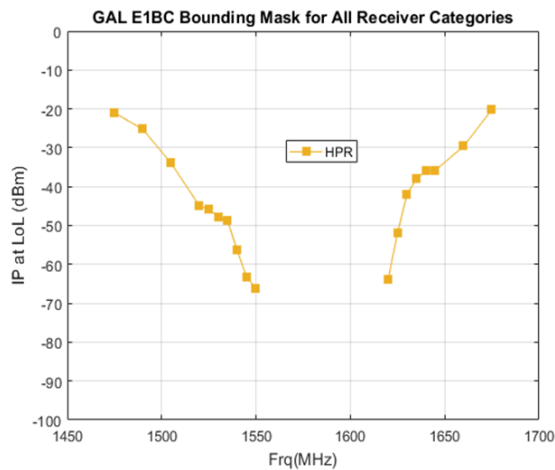Loss-of-Lock ITM computed using only "nominally" powered GPS signals

Table C-17: Nominal SVs GLONASS L1 P Bounding Masks (dBm)

Frequency (MHz)	GAV	GLN	HPR	TIM	SPB	CEL
1475	NaN	-9.999	-9.999	NaN	NaN	-9.999
1490	NaN	-9.999	-9.999	NaN	NaN	-9.999
1505	NaN	-9.999	-9.999	NaN	NaN	-9.999
1520	NaN	-9.999	-9.999	NaN	NaN	-9.999
1525	NaN	-9.999	-10.3721	NaN	NaN	-9.999
1530	NaN	-9.999	-13.2698	NaN	NaN	-9.999
1535	NaN	-9.999	-17.1146	NaN	NaN	-9.999
1540	NaN	-9.999	-23.0492	NaN	NaN	-9.999
1545	NaN	-9.999	NaN	NaN	NaN	-9.999
1550	NaN	-9.999	-37.6101	NaN	NaN	-9.999
1620	NaN	-42.7896	-59.0987	NaN	NaN	-9.999
1625	NaN	-34.7686	-40.7037	NaN	NaN	-9.999
1630	NaN	-22.4154	-30.8015	NaN	NaN	-9.999
1635	NaN	-11.24	-24.9246	NaN	NaN	-9.999
1640	NaN	-9.999	-16.5126	NaN	NaN	-9.999
1645	NaN	-9.999	-12.5755	NaN	NaN	-9.999
1660	NaN	-9.999	-9.999	NaN	NaN	-9.999
1675	NaN	-9.999	-9.999	NaN	NaN	-9.999

Table C-18: Nominal SVs GLONASS L1 P Median (dBm)

Frequency (MHz)	GAV	GLN	HPR	TIM	SPB	CEL
1475	NaN	-9.999	-9.999	NaN	NaN	-9.999
1490	NaN	-9.999	-9.999	NaN	NaN	-9.999
1505	NaN	-9.999	-9.999	NaN	NaN	-9.999
1520	NaN	-9.999	-9.999	NaN	NaN	-9.999
1525	NaN	-9.999	-9.999	NaN	NaN	-9.999
1530	NaN	-9.999	-9.999	NaN	NaN	-9.999
1535	NaN	-9.999	-11.5269	NaN	NaN	-9.999
1540	NaN	-9.999	-13.4983	NaN	NaN	-9.999
1545	NaN	-9.999	NaN	NaN	NaN	-9.999
1550	NaN	-9.999	-30.364	NaN	NaN	-9.999
1620	NaN	-21.685	-49.7287	NaN	NaN	-9.999
1625	NaN	-14.0983	-36.9373	NaN	NaN	-9.999
1630	NaN	-11.1903	-25.1865	NaN	NaN	-9.999
1635	NaN	-9.999	-16.2811	NaN	NaN	-9.999
1640	NaN	-9.999	-12.4209	NaN	NaN	-9.999
1645	NaN	-9.999	-9.999	NaN	NaN	-9.999
1660	NaN	-9.999	-9.999	NaN	NaN	-9.999
1675	NaN	-9.999	-9.999	NaN	NaN	-9.999
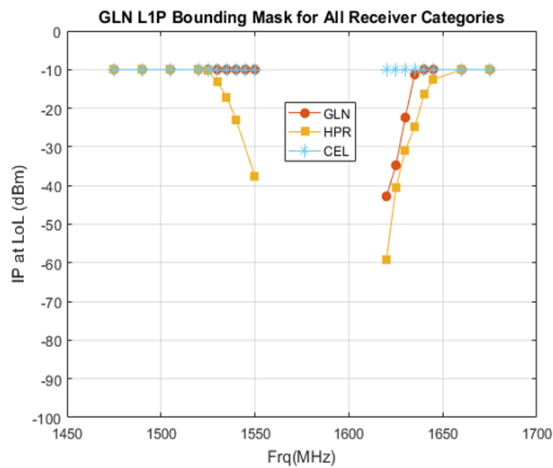
(a)

(b)

Figure C-17: Nominal SVs (a) GLONASS L1 P Bounding Masks and (b) GLONASS L1 P Median

35

C.2.5.2 Low Elevation SVs

Loss-of-Lock ITM computed using only SV-01 fixed at -10 dB relative to the nominal received power levels.

**Table C-19: Low Elevation SVs GLONASS L1 P Bounding Masks (dBm)**

Frequency (MHz)	GAV	GLN	HPR	TIM	SPB	CEL
1475	NaN	-9.999	-9.999	NaN	NaN	-9.999
1490	NaN	-9.999	-9.999	NaN	NaN	-9.999
1505	NaN	-9.999	-9.999	NaN	NaN	-9.999
1520	NaN	-9.999	-11.4466	NaN	NaN	-9.999
1525	NaN	-9.999	-14.3721	NaN	NaN	-9.999
1530	NaN	-9.999	-19.2698	NaN	NaN	-9.999
1535	NaN	-9.999	-26.1146	NaN	NaN	-9.999
1540	NaN	-9.999	-29.0492	NaN	NaN	-9.999
1545	NaN	-9.999	-32.772	NaN	NaN	-9.999
1550	NaN	-18.5007	-49.6101	NaN	NaN	-9.999
1620	NaN	-52.7896	-71.0987	NaN	NaN	-46.1514
1625	NaN	-59.7686	-53.7037	NaN	NaN	-21.579
1630	NaN	-33.7641	-34.8015	NaN	NaN	-18.0846
1635	NaN	-22.8	-28.9246	NaN	NaN	-14.2157
1640	NaN	-9.999	-20.8429	NaN	NaN	-13.0403
1645	NaN	-9.999	-16.5755	NaN	NaN	-12.005
1660	NaN	-9.999	-9.999	NaN	NaN	-10.9311
1675	NaN	-9.999	-9.999	NaN	NaN	-9.999

Table C-20: Low Elevation SVs GLONASS L1 P Median (dBm)

Frequency (MHz)	GAV	GLN	HPR	TIM	SPB	CEL
1475	NaN	-9.999	-9.999	NaN	NaN	-9.999
1490	NaN	-9.999	-9.999	NaN	NaN	-9.999
1505	NaN	-9.999	-9.999	NaN	NaN	-9.999
1520	NaN	-9.999	-9.999	NaN	NaN	-9.999
1525	NaN	-9.999	-11.5759	NaN	NaN	-9.999
1530	NaN	-9.999	-9.999	NaN	NaN	-9.999
1535	NaN	-9.999	-16.5269	NaN	NaN	-9.999
1540	NaN	-9.999	-22.4202	NaN	NaN	-9.999
1545	NaN	-9.999	-31.4723	NaN	NaN	-9.999
1550	NaN	-9.999	-36.364	NaN	NaN	-9.999
1620	NaN	-36.371	-57.7287	NaN	NaN	-45.6181
1625	NaN	-24.7626	-45.4373	NaN	NaN	-21.3128
1630	NaN	-18.2821	-31.1865	NaN	NaN	-14.3349
1635	NaN	-11.74	-21.7009	NaN	NaN	-13.2545
1640	NaN	-9.999	-15.2558	NaN	NaN	-12.3033
1645	NaN	-9.999	-10.4087	NaN	NaN	-11.2692
1660	NaN	-9.999	-9.999	NaN	NaN	-10.4651
1675	NaN	-9.999	-9.999	NaN	NaN	-9.91455
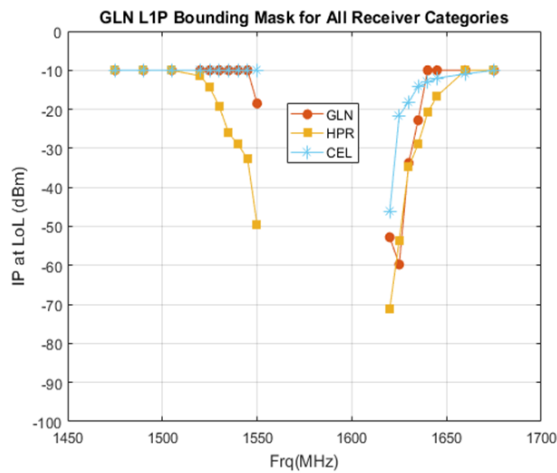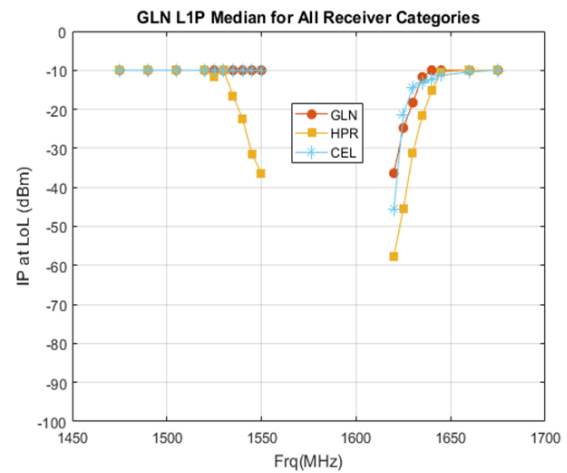
(a)   (b)

Figure C-18: Low Elevation SVs (a) GLONASS L1 P Bounding Masks and (b) GLONASS L1 P Median

37

C.2.6 BeiDou B1I

C.2.6.1 Nominal SVs

Loss-of-Lock ITM computed using only "nominally" powered GPS signals

Table C-21: Nominal SVs BeiDou B1I Bounding Masks (dBm)

Frequency (MHz)	GAV	GLN	HPR	TIM	SPB	CEL
1475	NaN	-9.999	-9.999	NaN	NaN	-9.999
1490	NaN	-9.999	-9.999	NaN	NaN	-9.999
1505	NaN	-9.999	-26.279	NaN	NaN	-9.999
1520	NaN	-9.999	-45.1027	NaN	NaN	-9.999
1525	NaN	NaN	-50.0021	NaN	NaN	-9.999
1530	NaN	-9.999	-52.9673	NaN	NaN	-9.999
1535	NaN	-9.999	-56.8679	NaN	NaN	-9.999
1540	NaN	-10.1664	-58.8462	NaN	NaN	-9.999
1545	NaN	-9.999	-68.8158	NaN	NaN	-9.999
1550	NaN	-52.2057	-76.7261	NaN	NaN	-9.999
1620	NaN	-30.752	-56.188	NaN	NaN	-9.999
1625	NaN	-9.999	-54.207	NaN	NaN	-9.999
1630	NaN	-9.999	-42.2442	NaN	NaN	-9.999
1635	NaN	-9.999	-33.3014	NaN	NaN	-9.999
1640	NaN	-9.999	-24.194	NaN	NaN	-9.999
1645	NaN	-9.999	-16.1068	NaN	NaN	-9.999
1660	NaN	-9.999	-9.999	NaN	NaN	-9.999
1675	NaN	-9.999	-9.999	NaN	NaN	-9.999

Table C-22: Nominal SVs BeiDou B1I Median (dBm)

Frequency (MHz)	GAV	GLN	HPR	TIM	SPB	CEL
1475	NaN	-9.999	-9.999	NaN	NaN	-9.999
1490	NaN	-9.999	-9.999	NaN	NaN	-9.999
1505	NaN	-9.999	-9.999	NaN	NaN	-9.999
1520	NaN	-9.999	-9.999	NaN	NaN	-9.999
1525	NaN	NaN	-9.999	NaN	NaN	-9.999
1530	NaN	-9.999	-9.999	NaN	NaN	-9.999
1535	NaN	-9.999	-9.999	NaN	NaN	-9.999
1540	NaN	-10.1664	-19.99	NaN	NaN	-9.999
1545	NaN	-9.999	-43.4035	NaN	NaN	-9.999
1550	NaN	-52.2057	-69.2392	NaN	NaN	-9.999
1620	NaN	-30.752	-9.999	NaN	NaN	-9.999
1625	NaN	-9.999	-9.999	NaN	NaN	-9.999
1630	NaN	-9.999	-9.999	NaN	NaN	-9.999
1635	NaN	-9.999	-9.999	NaN	NaN	-9.999
1640	NaN	-9.999	-9.999	NaN	NaN	-9.999
1645	NaN	-9.999	-9.999	NaN	NaN	-9.999
1660	NaN	-9.999	-9.999	NaN	NaN	-9.999
1675	NaN	-9.999	-9.999	NaN	NaN	-9.999
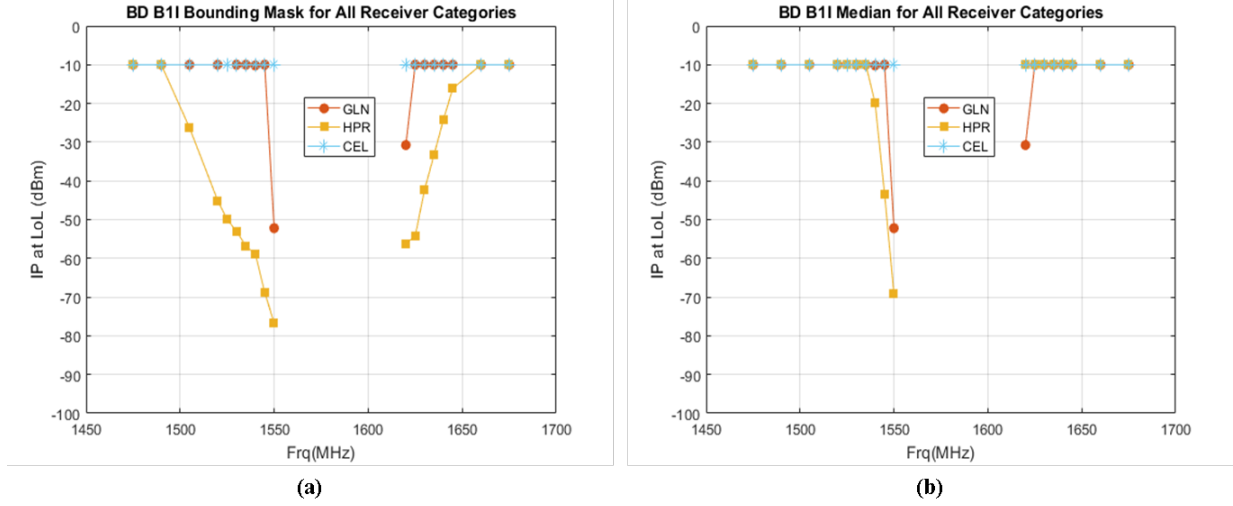
**Figure C-19: Nominal SVs (a) BeiDou B1I Bounding Masks and
(b) BeiDou B1I Median**

C.2.6.2   Low Elevation SVs

Loss-of-Lock ITM computed using only PRN-08 fixed at -10 dB relative to the nominal received power levels.

40

Table C-23: Low Elevation SVs BeiDou B1I Bounding Masks (dBm)

Frequency (MHz)	GAV	GLN	HPR	TIM	SPB	CEL
1475	NaN	-9.999	-9.999	NaN	NaN	-9.999
1490	NaN	-9.999	-18.2685	NaN	NaN	-9.999
1505	NaN	-9.999	-41.279	NaN	NaN	-9.999
1520	NaN	-9.999	-57.1027	NaN	NaN	-9.999
1525	NaN	-9.999	-60.0021	NaN	NaN	-9.999
1530	NaN	-13.3999	-64.9673	NaN	NaN	NaN
1535	NaN	-19.2972	-66.8679	NaN	NaN	NaN
1540	NaN	-22.3339	-68.8462	NaN	NaN	NaN
1545	NaN	-38.2885	-80.8158	NaN	NaN	NaN
1550	NaN	-70.2057	-80.8683	NaN	NaN	NaN
1620	NaN	-32.752	-66.188	NaN	NaN	NaN
1625	NaN	-18.8299	-65.207	NaN	NaN	NaN
1630	NaN	-11.8523	-52.2442	NaN	NaN	NaN
1635	NaN	-9.999	-42.3014	NaN	NaN	NaN
1640	NaN	-9.999	-32.194	NaN	NaN	NaN
1645	NaN	-9.999	-27.1068	NaN	NaN	NaN
1660	NaN	-9.999	-9.999	NaN	NaN	NaN
1675	NaN	-9.999	-9.999	NaN	NaN	NaN

Table C-24: Low Elevation SVs BeiDou B1I Median (dBm)

Frequency (MHz)	GAV	GLN	HPR	TIM	SPB	CEL
1475	NaN	-9.999	-9.999	NaN	NaN	-9.999
1490	NaN	-9.999	-9.999	NaN	NaN	-9.999
1505	NaN	-9.999	-9.999	NaN	NaN	-9.999
1520	NaN	-9.999	-9.999	NaN	NaN	-9.999
1525	NaN	-9.999	-9.999	NaN	NaN	-9.999
1530	NaN	-13.3999	-10.1063	NaN	NaN	NaN
1535	NaN	-19.2972	-13.0842	NaN	NaN	NaN
1540	NaN	-22.3339	-26.49	NaN	NaN	NaN
1545	NaN	-38.2885	-54.9035	NaN	NaN	NaN
1550	NaN	-70.2057	-79.9274	NaN	NaN	NaN
1620	NaN	-32.752	-44.695	NaN	NaN	NaN
1625	NaN	-18.8299	-9.999	NaN	NaN	NaN
1630	NaN	-11.8523	-17.801	NaN	NaN	NaN
1635	NaN	-9.999	-9.999	NaN	NaN	NaN
1640	NaN	-9.999	-9.999	NaN	NaN	NaN
1645	NaN	-9.999	-9.999	NaN	NaN	NaN
1660	NaN	-9.999	-9.999	NaN	NaN	NaN
1675	NaN	-9.999	-9.999	NaN	NaN	NaN
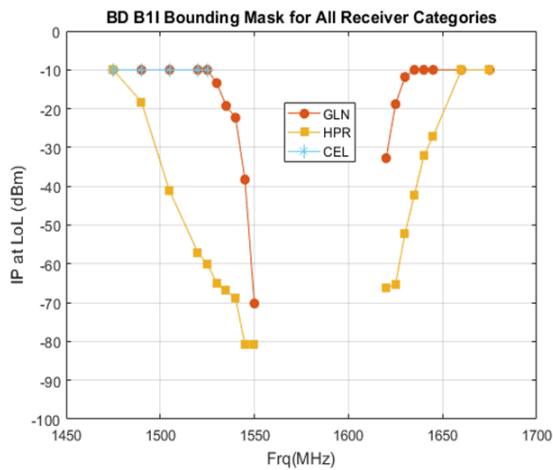
(a)
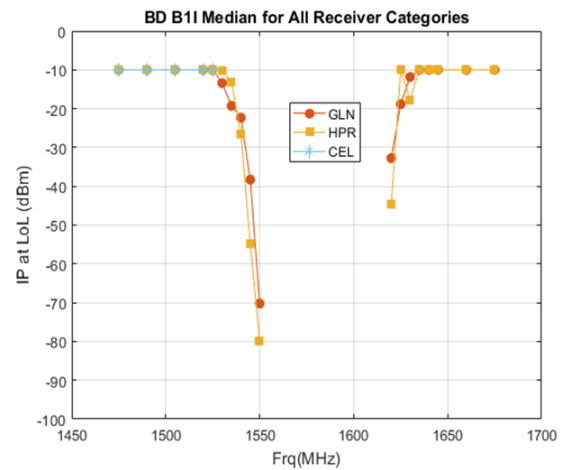
(b)

Figure C-20: Low Elevation SVs (a) BeiDou B1I Bounding Masks and (b) BeiDou B1I Median

42

C.2.7 Galileo E1 BC

C.2.7.1 Nominal SVs
Loss-of-Lock ITM computed using only "nominally" powered GPS signals

Table C-25: Nominal SVs Galileo E1 BC Bounding Masks (dBm)

Frequency (MHz)	GAV	GLN	HPR	TIM	SPB	CEL
1475	NaN	NaN	-21.0199	NaN	NaN	NaN
1490	NaN	NaN	-25.2549	NaN	NaN	NaN
1505	NaN	NaN	-33.9753	NaN	NaN	NaN
1520	NaN	NaN	-44.9467	NaN	NaN	NaN
1525	NaN	NaN	-45.8713	NaN	NaN	NaN
1530	NaN	NaN	-47.7309	NaN	NaN	NaN
1535	NaN	NaN	-48.8679	NaN	NaN	NaN
1540	NaN	NaN	-56.3935	NaN	NaN	NaN
1545	NaN	NaN	-63.2675	NaN	NaN	NaN
1550	NaN	NaN	-66.138	NaN	NaN	NaN
1620	NaN	NaN	-63.9203	NaN	NaN	NaN
1625	NaN	NaN	-51.9544	NaN	NaN	NaN
1630	NaN	NaN	-41.9352	NaN	NaN	NaN
1635	NaN	NaN	-38.0443	NaN	NaN	NaN
1640	NaN	NaN	-35.9451	NaN	NaN	NaN
1645	NaN	NaN	-35.8279	NaN	NaN	NaN
1660	NaN	NaN	-29.6007	NaN	NaN	NaN
1675	NaN	NaN	-20.2063	NaN	NaN	NaN

Table C-26: Nominal SVs Galileo E1 BC Median (dBm)

Frequency (MHz)	GAV	GLN	HPR	TIM	SPB	CEL
1475	NaN	NaN	-9.999	NaN	NaN	NaN
1490	NaN	NaN	-9.999	NaN	NaN	NaN
1505	NaN	NaN	-9.999	NaN	NaN	NaN
1520	NaN	NaN	-9.999	NaN	NaN	NaN
1525	NaN	NaN	-23.5116	NaN	NaN	NaN
1530	NaN	NaN	-17.2698	NaN	NaN	NaN
1535	NaN	NaN	-23.1146	NaN	NaN	NaN
1540	NaN	NaN	-30.0492	NaN	NaN	NaN
1545	NaN	NaN	-34.991	NaN	NaN	NaN
1550	NaN	NaN	-37.8596	NaN	NaN	NaN
1620	NaN	NaN	-38.7558	NaN	NaN	NaN
1625	NaN	NaN	-36.3017	NaN	NaN	NaN
1630	NaN	NaN	-24.8276	NaN	NaN	NaN
1635	NaN	NaN	-18.7342	NaN	NaN	NaN
1640	NaN	NaN	-10.5126	NaN	NaN	NaN
1645	NaN	NaN	-9.999	NaN	NaN	NaN
1660	NaN	NaN	-9.999	NaN	NaN	NaN
1675	NaN	NaN	-9.999	NaN	NaN	NaN
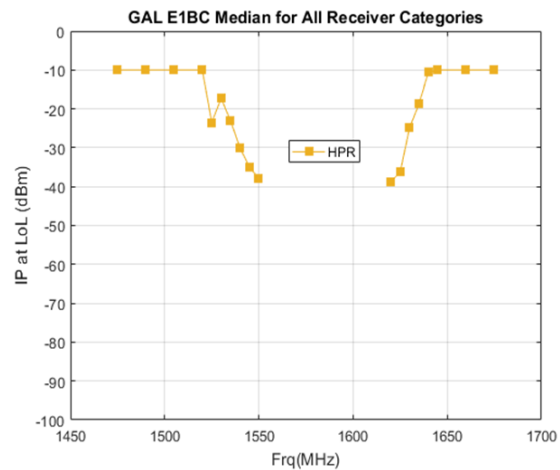
(a)　　　　　　　　　　　　　　　(b)

Figure C-21: Nominal SVs (a) Galileo E1 BC Bounding Masks and (b) Galileo E1 BC Median

44

C.2.7.2   Low Elevation SVs

Loss-of-Lock ITM computed using only PRN-04 fixed at -10 dB relative to the nominal received power levels.

Table C-27: Low Elevation SVs Galileo E1 BC Bounding Masks (dBm)

Frequency (MHz)	GAV	GLN	HPR	TIM	SPB	CEL
1475	NaN	NaN	-25.0199	NaN	NaN	NaN
1490	NaN	NaN	-27.2549	NaN	NaN	NaN
1505	NaN	NaN	-42.9753	NaN	NaN	NaN
1520	NaN	NaN	-54.9467	NaN	NaN	NaN
1525	NaN	NaN	-56.8713	NaN	NaN	NaN
1530	NaN	NaN	-60.7309	NaN	NaN	NaN
1535	NaN	NaN	-59.5364	NaN	NaN	NaN
1540	NaN	NaN	-69.3935	NaN	NaN	NaN
1545	NaN	NaN	-77.2675	NaN	NaN	NaN
1550	NaN	NaN	-78.138	NaN	NaN	NaN
1620	NaN	NaN	-75.0987	NaN	NaN	NaN
1625	NaN	NaN	-61.9544	NaN	NaN	NaN
1630	NaN	NaN	-49.9352	NaN	NaN	NaN
1635	NaN	NaN	-44.9053	NaN	NaN	NaN
1640	NaN	NaN	-38.7792	NaN	NaN	NaN
1645	NaN	NaN	-38.3086	NaN	NaN	NaN
1660	NaN	NaN	-32.2085	NaN	NaN	NaN
1675	NaN	NaN	-26.2063	NaN	NaN	NaN

Table C-28: Low Elevation SVs Galileo E1 BC Median (dBm)

Frequency (MHz)	GAV	GLN	HPR	TIM	SPB	CEL
1475	NaN	NaN	-9.999	NaN	NaN	NaN
1490	NaN	NaN	-17.2685	NaN	NaN	NaN
1505	NaN	NaN	-21.0294	NaN	NaN	NaN
1520	NaN	NaN	-22.8807	NaN	NaN	NaN
1525	NaN	NaN	-22.825	NaN	NaN	NaN
1530	NaN	NaN	-37.6765	NaN	NaN	NaN
1535	NaN	NaN	-26.9013	NaN	NaN	NaN
1540	NaN	NaN	-28.8764	NaN	NaN	NaN
1545	NaN	NaN	-27.2681	NaN	NaN	NaN
1550	NaN	NaN	-46.564	NaN	NaN	NaN
1620	NaN	NaN	-62.7254	NaN	NaN	NaN
1625	NaN	NaN	-51.8027	NaN	NaN	NaN
1630	NaN	NaN	-35.4037	NaN	NaN	NaN
1635	NaN	NaN	-26.5766	NaN	NaN	NaN
1640	NaN	NaN	-23.9544	NaN	NaN	NaN
1645	NaN	NaN	-21.3745	NaN	NaN	NaN
1660	NaN	NaN	-13.2377	NaN	NaN	NaN
1675	NaN	NaN	-9.999	NaN	NaN	NaN
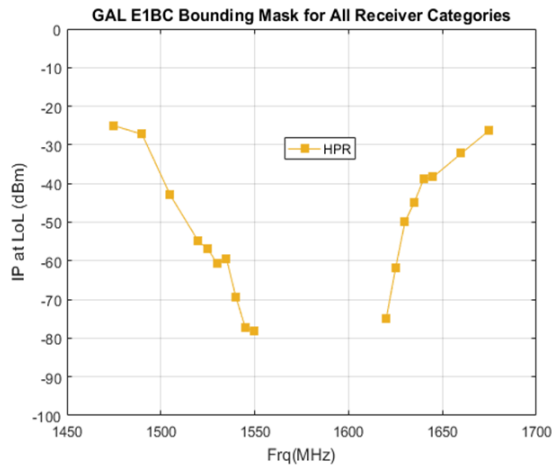
(a)
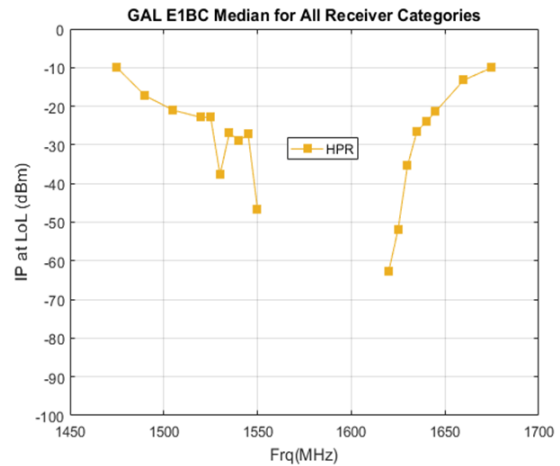
(b)

Figure C-22: Low Elevation SVs (a) Galileo E1 BC Bounding Masks and (b) Galileo E1 BC Median

C.2.8 SBAS L1 C/A

C.2.8.1 Nominal SVs

Loss-of-Lock ITM computed using only "nominally" powered GPS signals

Table C-29: Nominal SVs SBAS L1 C/A Bounding Masks (dBm)

Frequency (MHz)	GAV	GLN	HPR	TIM	SPB	CEL
1475	NaN	-17.0577	-23.0199	-9.999	NaN	NaN
1490	NaN	-23.3312	-25.2549	-9.999	NaN	NaN
1505	NaN	-21.4491	-32.9753	-9.999	NaN	NaN
1520	NaN	-17.6091	-41.9467	-9.999	NaN	NaN
1525	NaN	-23.0921	-44.8713	-9.999	NaN	NaN
1530	NaN	-27.0652	-46.7309	-9.999	NaN	NaN
1535	NaN	-29.897	-50.8679	-9.999	NaN	NaN
1540	NaN	-30.9021	-56.3935	-9.999	NaN	NaN
1545	NaN	-36.8816	-62.2675	-9.999	NaN	NaN
1550	NaN	-55.7539	-64.7261	-35.7205	NaN	NaN
1620	NaN	-40.7896	-65.9203	-9.999	NaN	NaN
1625	NaN	-31.7686	-51.9544	-9.999	NaN	NaN
1630	NaN	-25.4838	-39.9352	-9.999	NaN	NaN
1635	NaN	-19.6279	-38.4688	-9.999	NaN	NaN
1640	NaN	-11.7996	-37.9451	-9.999	NaN	NaN
1645	NaN	-14.7334	-35.8279	-9.999	NaN	NaN
1660	NaN	-10.3055	-29.4585	-9.999	NaN	NaN
1675	NaN	-9.999	-22.2063	-9.999	NaN	NaN

Table C-30: Nominal SVs SBAS L1 C/A Median (dBm)

Frequency (MHz)	GAV	GLN	HPR	TIM	SPB	CEL
1475	NaN	-9.999	-9.999	-9.999	NaN	NaN
1490	NaN	-9.999	-9.999	-9.999	NaN	NaN
1505	NaN	-9.999	-9.999	-9.999	NaN	NaN
1520	NaN	-9.999	-11.8986	-9.999	NaN	NaN
1525	NaN	-9.999	-16.8264	-9.999	NaN	NaN
1530	NaN	-9.999	-21.6315	-9.999	NaN	NaN
1535	NaN	-10.1481	-27.116	-9.999	NaN	NaN
1540	NaN	-14.1664	-31.3096	-9.999	NaN	NaN
1545	NaN	-9.999	-34.9536	-9.999	NaN	NaN
1550	NaN	-36.9631	-40.9457	-35.7205	NaN	NaN
1620	NaN	-9.999	-39.4386	-9.999	NaN	NaN
1625	NaN	-9.999	-32.9266	-9.999	NaN	NaN
1630	NaN	-11.6903	-23.4623	-9.999	NaN	NaN
1635	NaN	-9.999	-14.4376	-9.999	NaN	NaN
1640	NaN	-9.999	-10.8429	-9.999	NaN	NaN
1645	NaN	-9.999	-9.999	-9.999	NaN	NaN
1660	NaN	-9.999	-9.999	-9.999	NaN	NaN
1675	NaN	-9.999	-9.999	-9.999	NaN	NaN
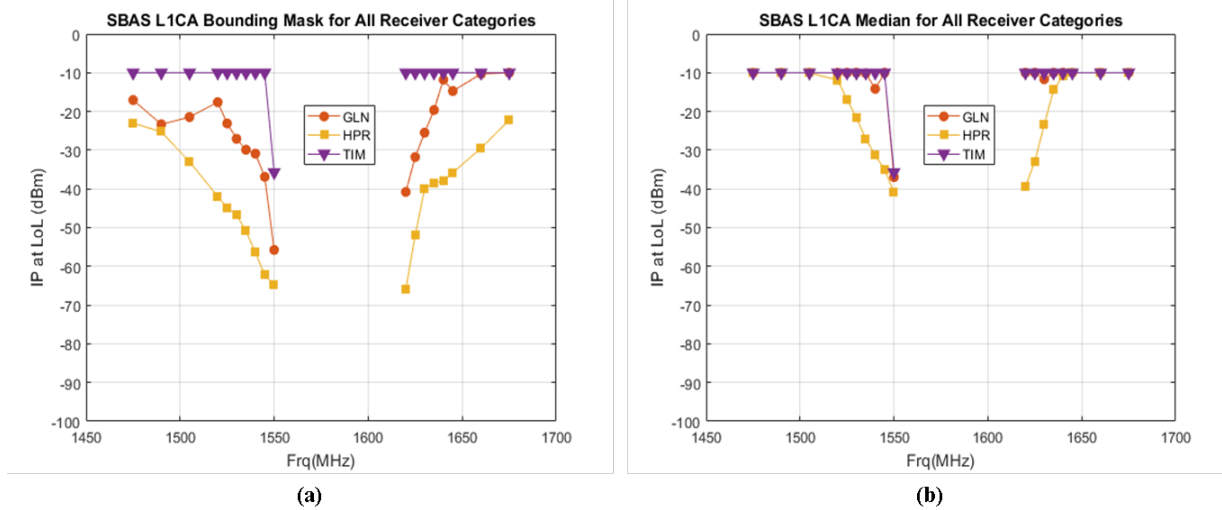
Figure C-23: Nominal SVs (a) SBAS L1 C/A Bounding Masks and (b) SBAS L1 C/A Median

APPENDIX D

CONDUCTED TEST DETAILS

TABLE OF CONTENTS

LIST OF FIGURES

No table of figures entries found.

LIST OF TABLES

4

REFERENCES

There are no sources in the current document.

APPENDIX

Appendix D. Conducted Test

D.1 OOBE Level Settings

The key points associated with wired testing were largely covered in the main body of the report or in the previous section with review of SPIGAT. One area that generated much discussion was simulation of FCC and Proposed OOBE limits in the wired testing. The OOBE levels to be generated were determined by assuming a fixed ratio between OOBE limit and LTE signal power for each of the four cases (from the combination of transmitter type and OOBE limit sponsor) as summarized in Table D-1. The appropriate ratio was applied (added) to the target LTE signal power at each point in the test to determine the corresponding OOBE level to generate. Each ratio was determined by assuming OOBE is at the limit when LTE power levels are at the specified maximums of 62 dBm (32 dBW) for base stations and 23 dBm (-7 dBW) for handsets. All limits were taken without consideration for sloping specified within (or any levels specified outside) the RNSS band. Therefore, the FCC limit was taken as -40 dBm/MHz for both handsets and base stations and the Proposed limits was taken as -70 dBm/MHz for base stations and -75 dBm/MHz for handsets.

Table D-1: Ratio of OOBE limit density to LTE power for setting OOBE testing levels

	OOBE density [dBm/MHz]	LTE power [dBm]	ratio OOBE/LTE [dB/MHz]
FCC base station	-40	62	-102
FCC handset	-40	23	-63
Proposed base station	-70	62	-132
Proposed handset	-75	23	-98

The appropriate ratio was applied to the target LTE signal power at each point in the test to determine the corresponding OOBE level to generate. For example, the LTE uplink at 1630 MHz was tested in a power range from -80 to -10 dBm. For the FCC limit (adding the ratio -63 dB/MHz), the OOBE range was -143 to -73 dBm/MHz (-233 to -163 dBW/Hz). For the Proposed limit (adding the ratio -98 dB/MHz), the corresponding OOBE range was -178 to -108 dBm/MHz (-268 to -198 dBW/Hz). Table D-2 shows the OOBE levels generated for each of the LTE test ranges.

Table D-2: OOBE levels (in dBm/MHz) for the LTE tests ranges

		LTE power [dBm]	FCC OOBE density [dBm/MHz]	Proposed OOBE density [dBm/MHz]
base station	1475	-80 To -10	-182 to -112	-212 to -142

	1490	-80	To	-10	-182	to	-112	-212	to	-142
	1505	-80	to	-10	-182	to	-112	-212	to	-142
	1520	-80	to	-10	-182	to	-112	-212	to	-142
	1525	-80	to	-10	-182	to	-112	-212	to	-142
	1530	-80	to	-10	-182	to	-112	-212	to	-142
	1535	-80	to	-10	-182	to	-112	-212	to	-142
	1540	-80	to	-10	-182	to	-112	-212	to	-142
	1545	-100	to	-30	-202	to	-132	-232	to	-162
	1550	-100	to	-30	-202	to	-132	-232	to	-162
handset	1620	-100	to	-30	-163	to	-93	-198	to	-128
	1625	-100	to	-30	-163	to	-93	-198	to	-128
	1630	-80	to	-10	-143	to	-73	-178	to	-108
	1635	-80	to	-10	-143	to	-73	-178	to	-108
	1640	-80	to	-10	-143	to	-73	-178	to	-108
	1645	-80	to	-10	-143	to	-73	-178	to	-108
	1660	-80	to	-10	-143	to	-73	-178	to	-108
base station	1675	-80	to	-10	-182	to	-112	-212	to	-142

APPENDIX E

ANTENNA CHARACTERIZATION DETAILS

TABLE OF CONTENTS

LIST OF FIGURES

LIST OF TABLES

No table of figures entries found.

REFERENCES

There are no sources in the current document.

APPENDIX

Appendix E.   Antenna Characterization Details

E.1   Anechoic Chamber Measurements
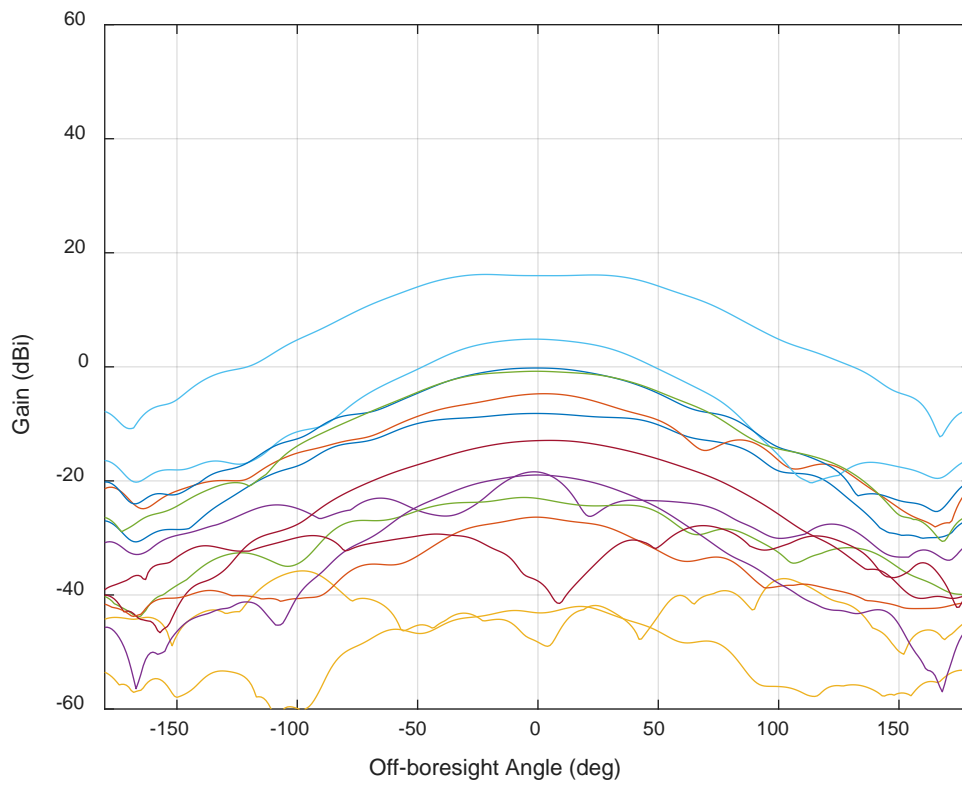
Figure E-1: VPOL Gain Patterns for 14 External Antennas (1475 MHz)
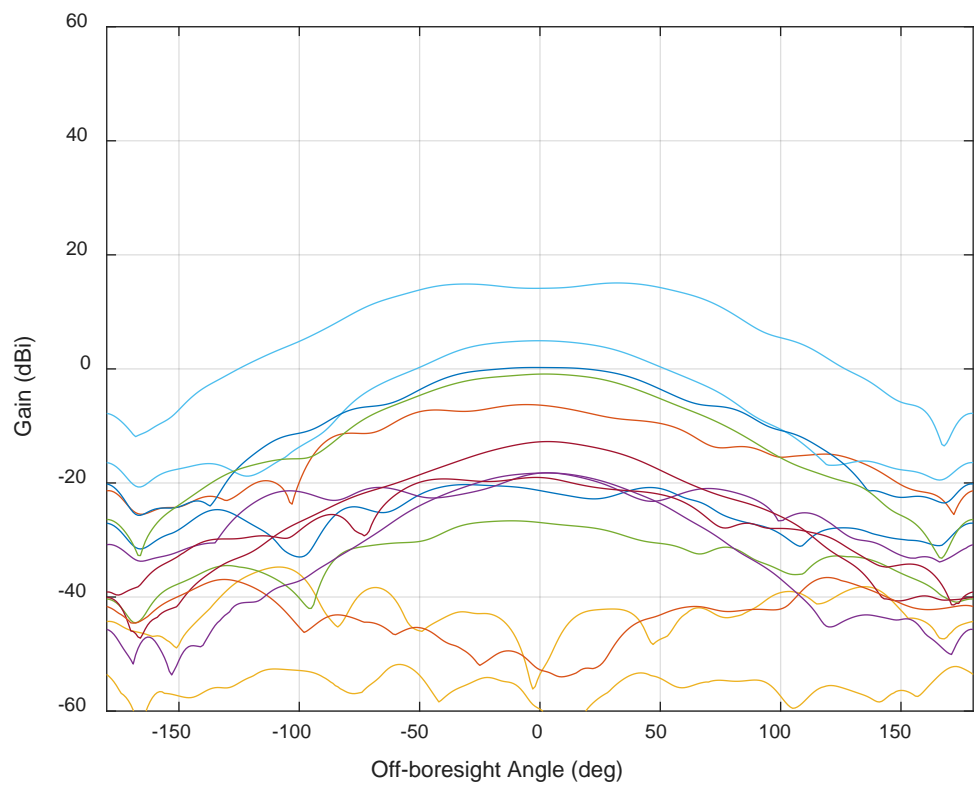
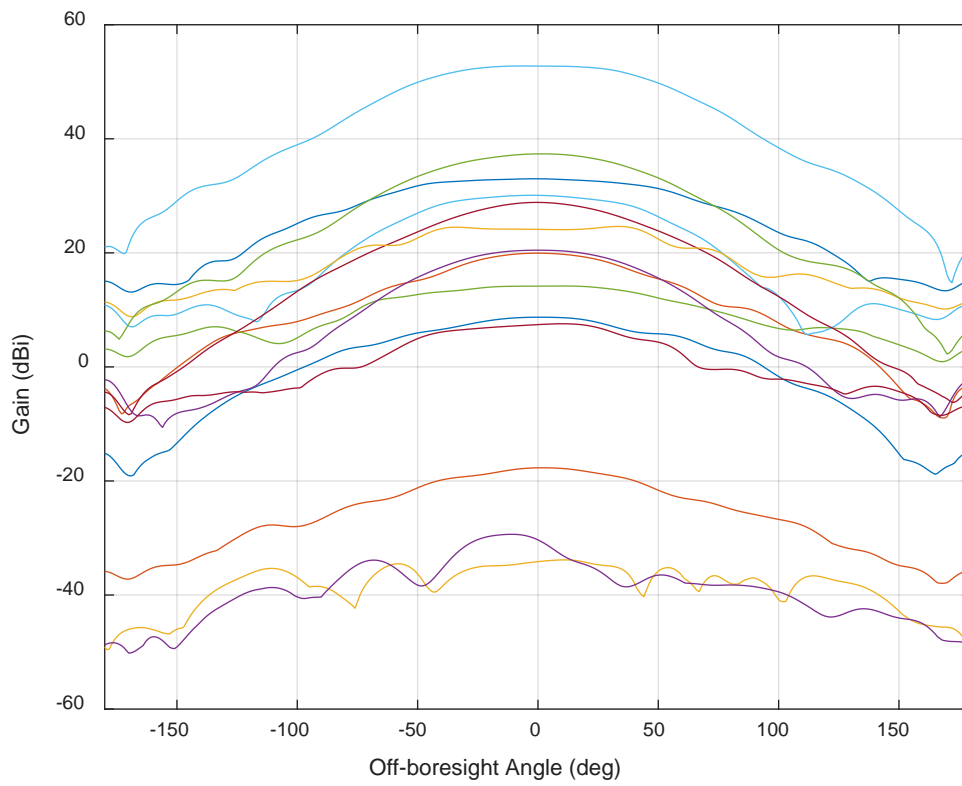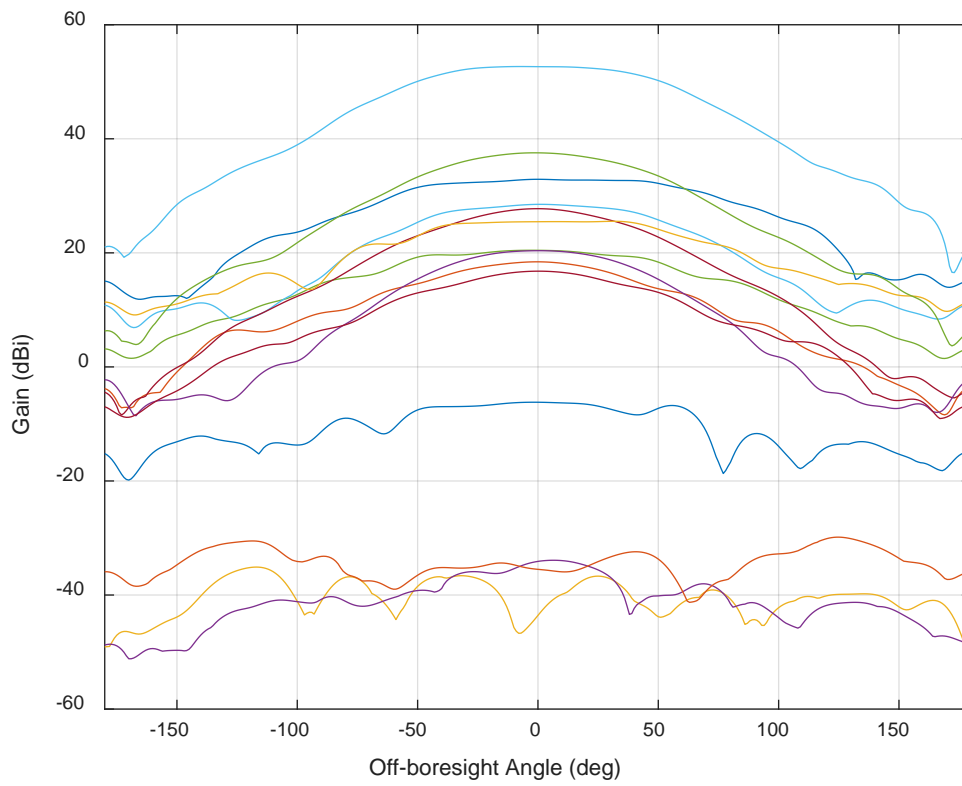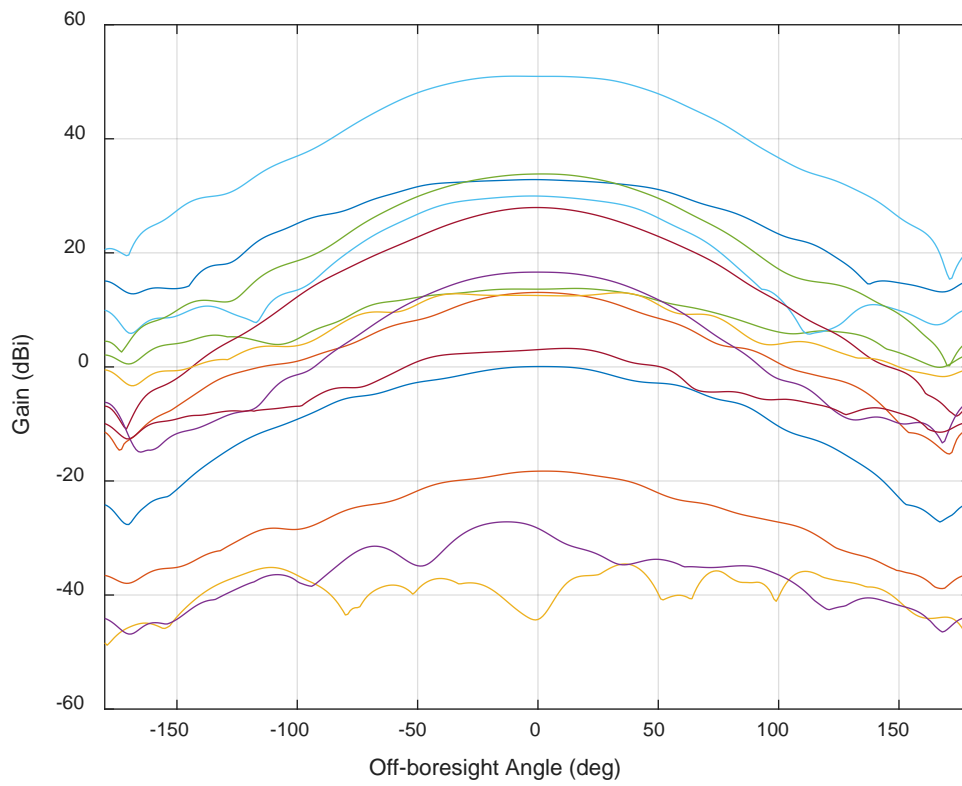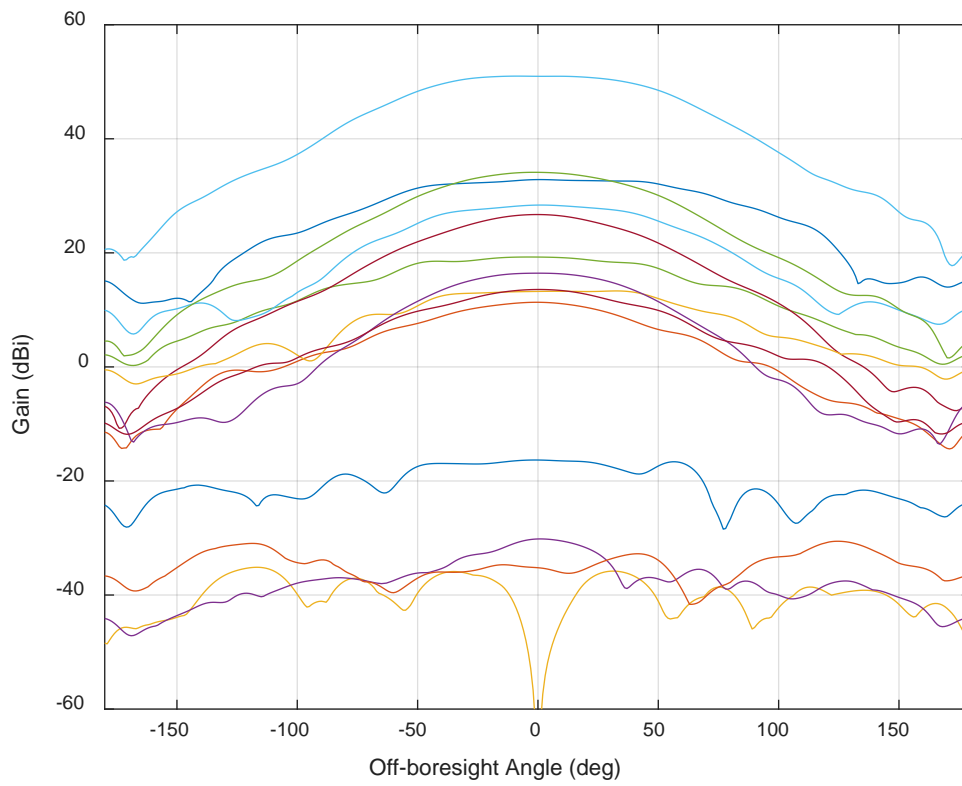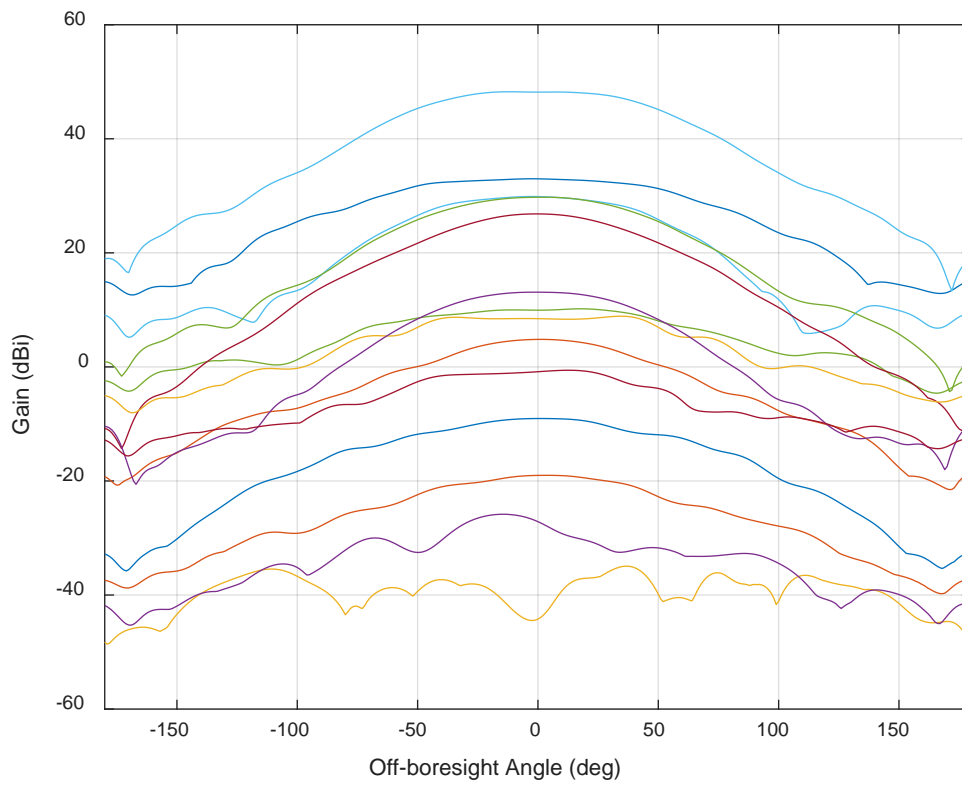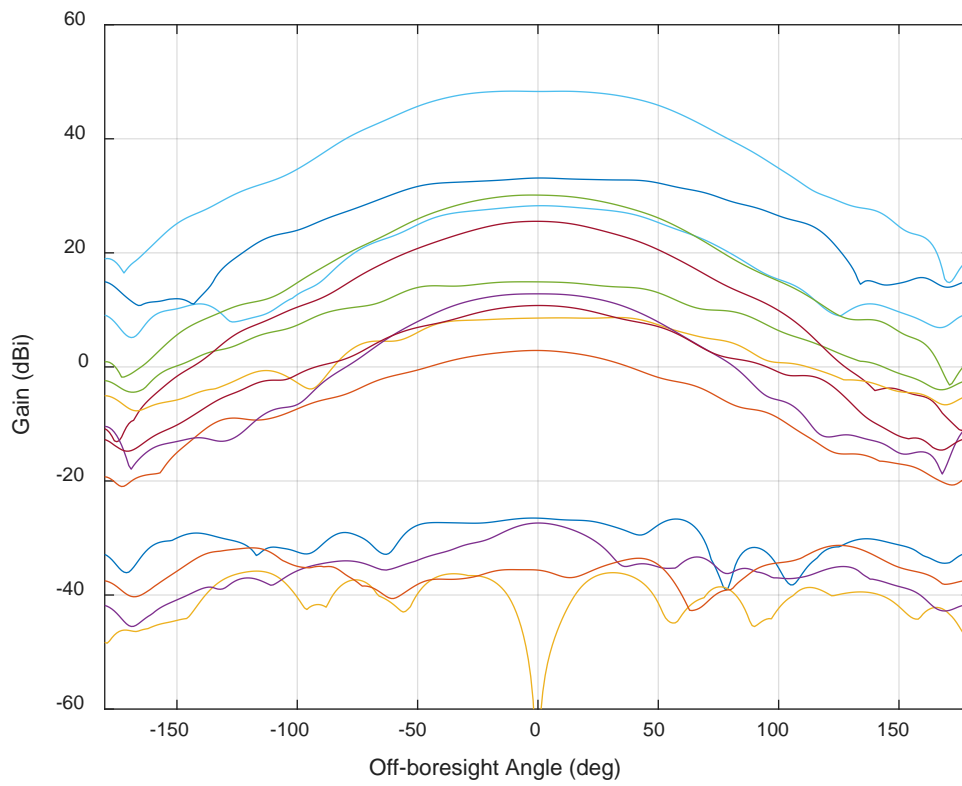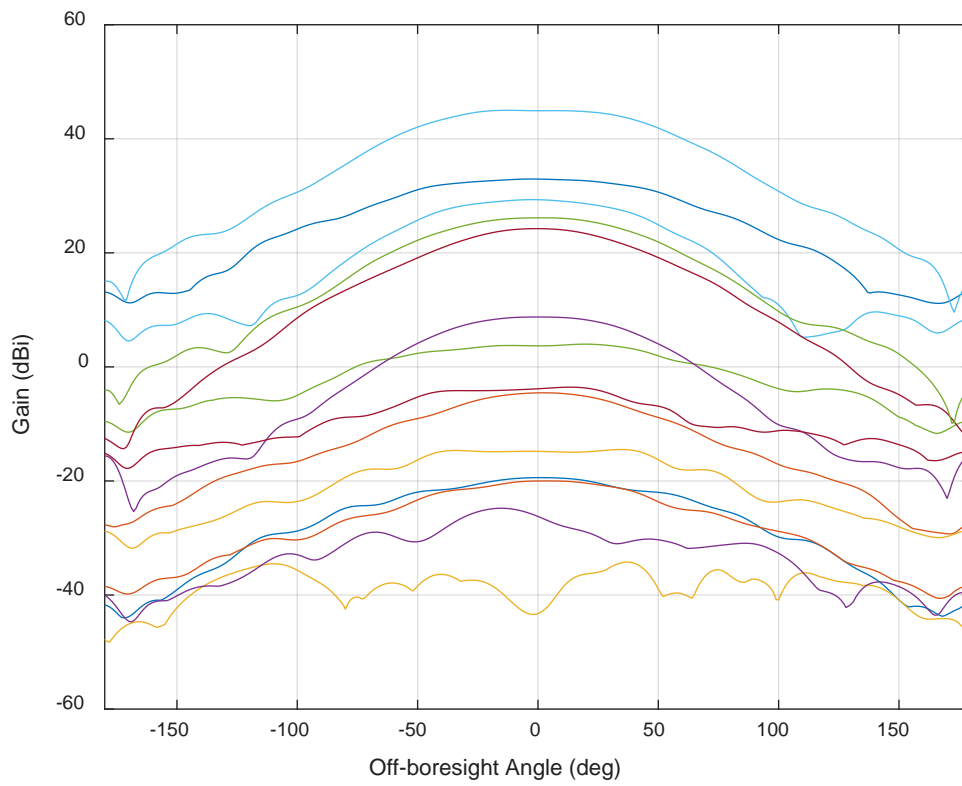**Figure E-2: HPOL Gain Patterns for 14 External Antennas (1475 MHz)**
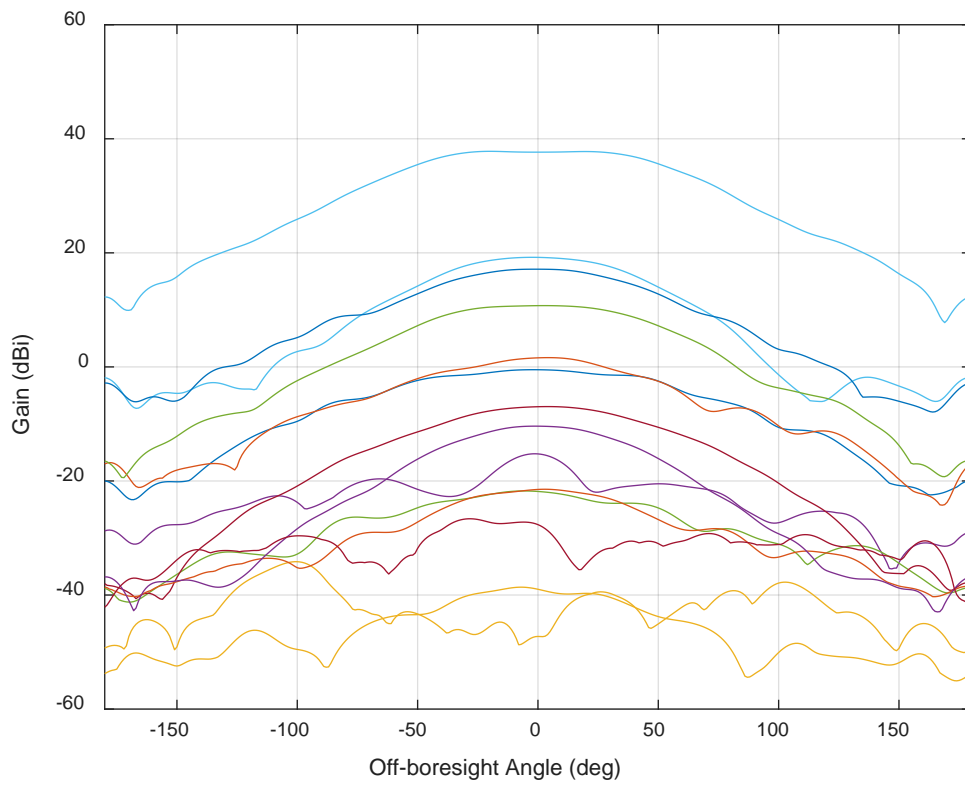
Figure E-3: VPOL Gain Patterns for 14 External Antennas (1490 MHz)
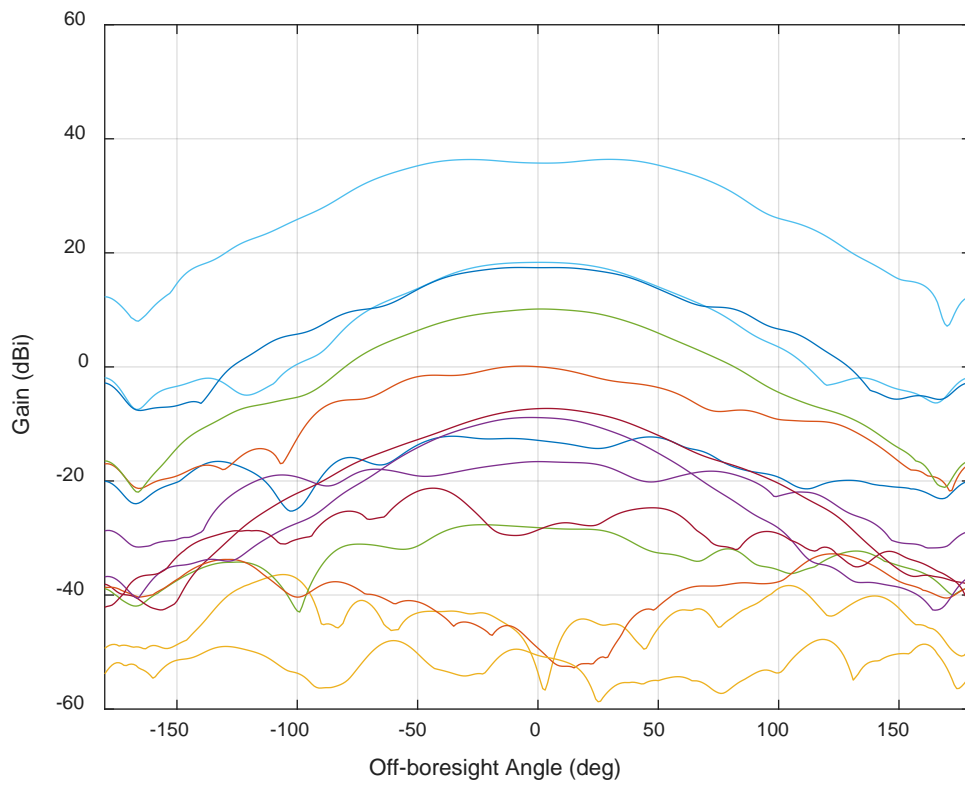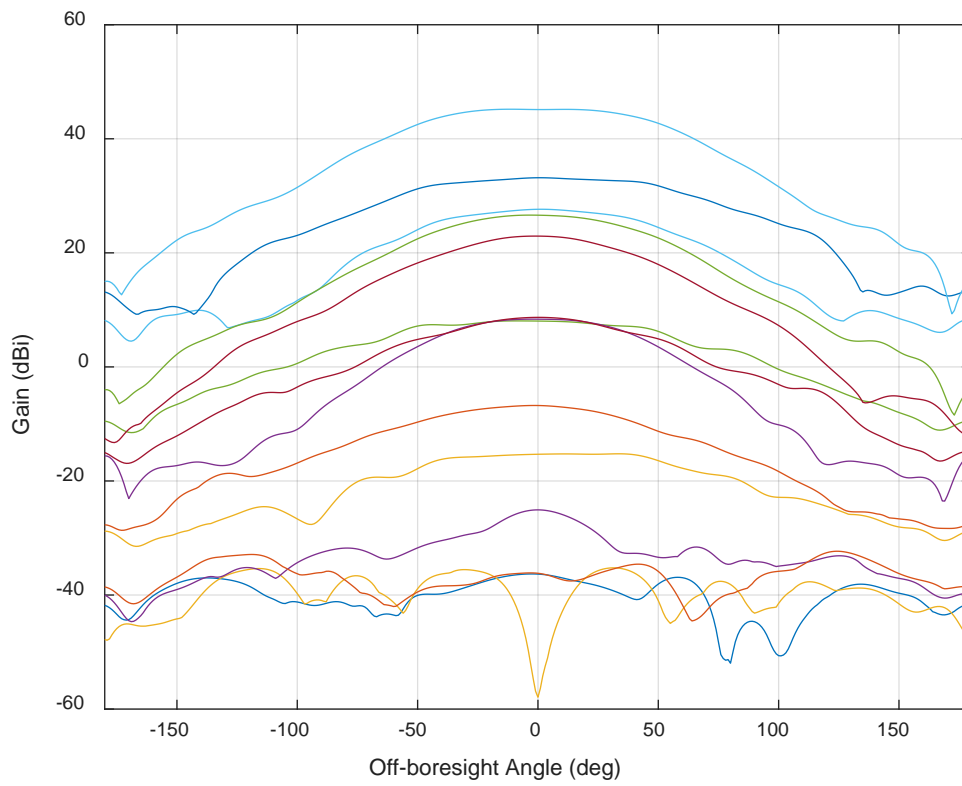
Figure E-4: HPOL Gain Patterns for 14 External Antennas (1490 MHz)
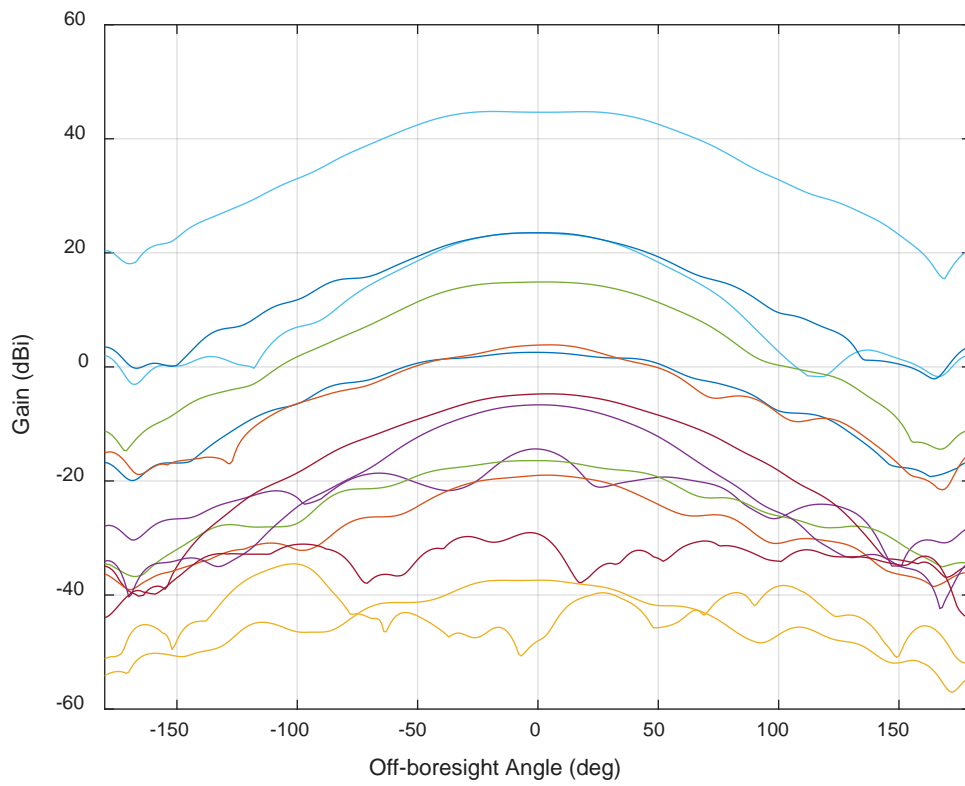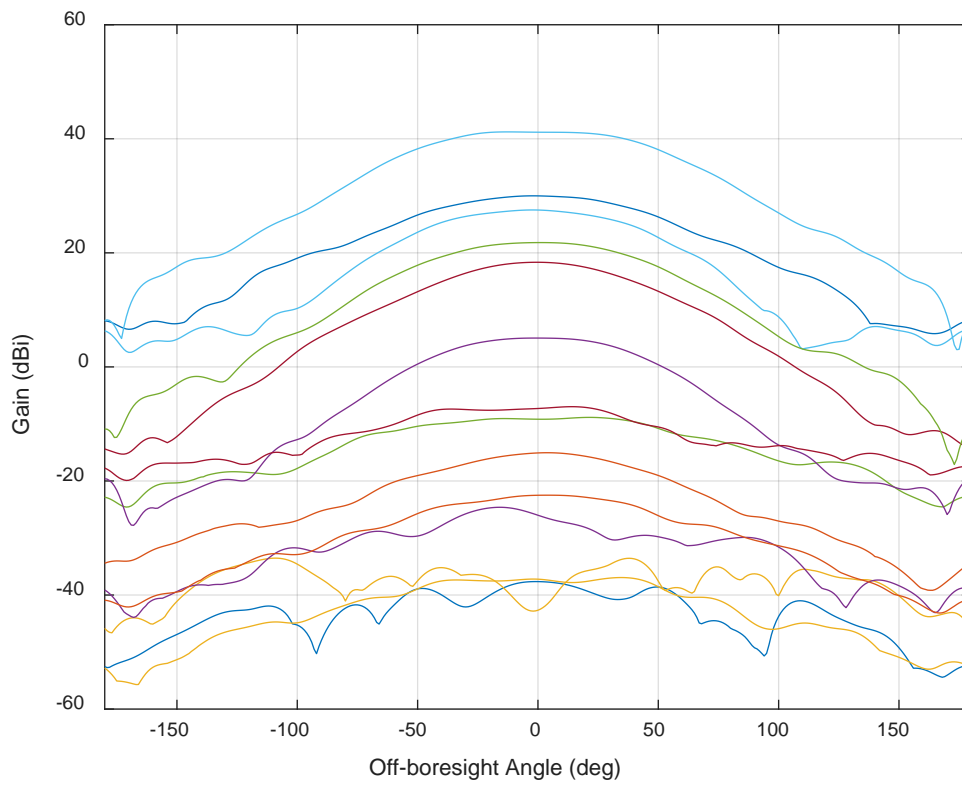
Figure E-5: VPOL Gain Patterns for 14 External Antennas (1495 MHz)
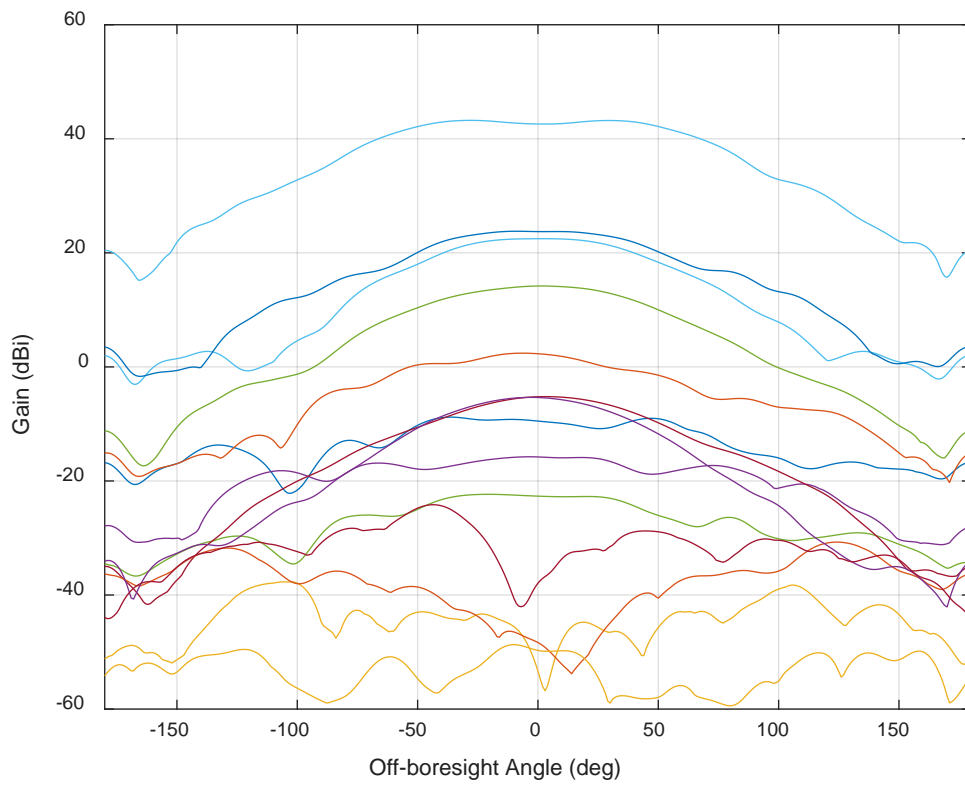
Figure E-6: HPOL Gain Patterns for 14 External Antennas (1495 MHz)
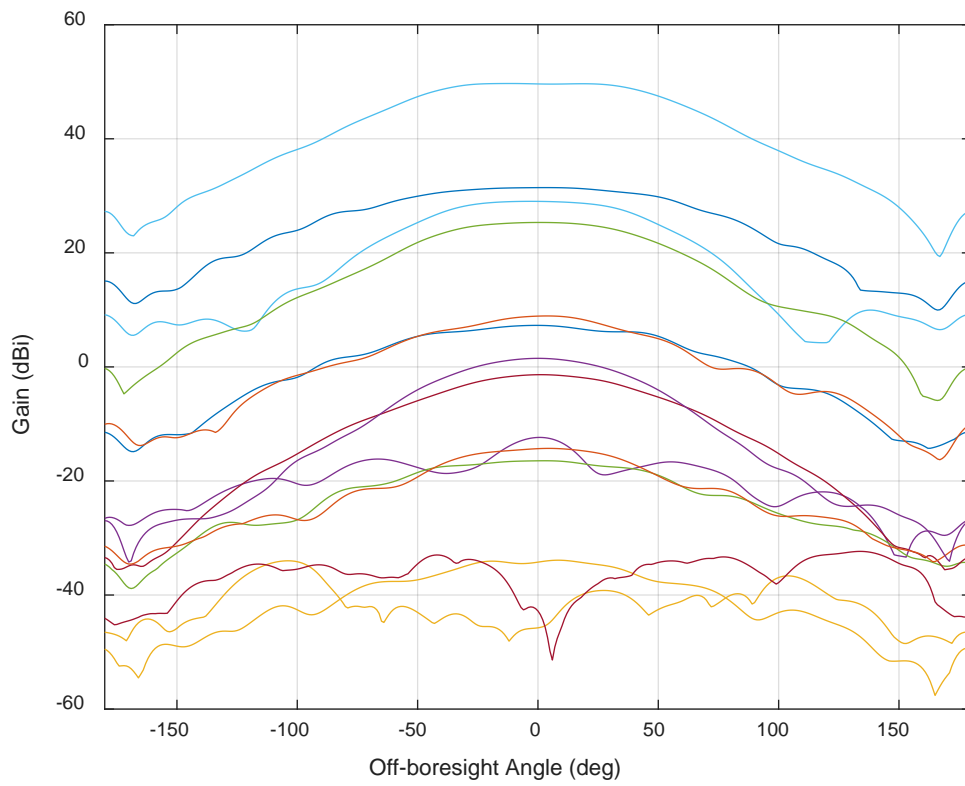
Figure E-7: VPOL Gain Patterns for 14 External Antennas (1505 MHz)

13
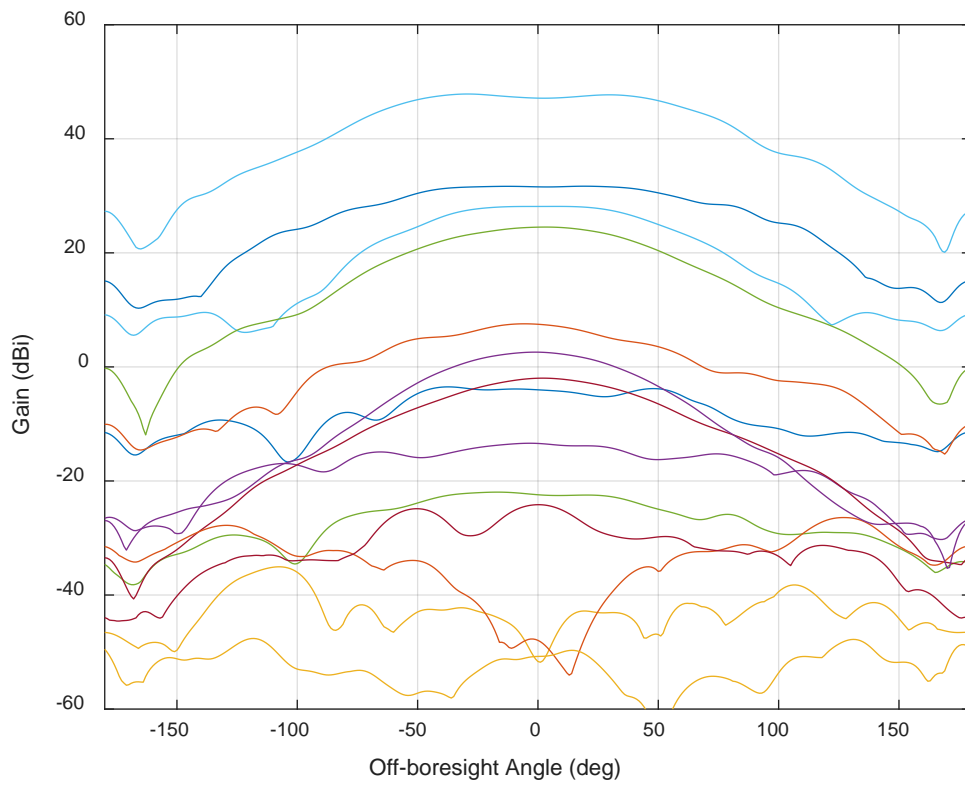
Figure E-8: HPOL Gain Patterns for 14 External Antennas (1505 MHz)
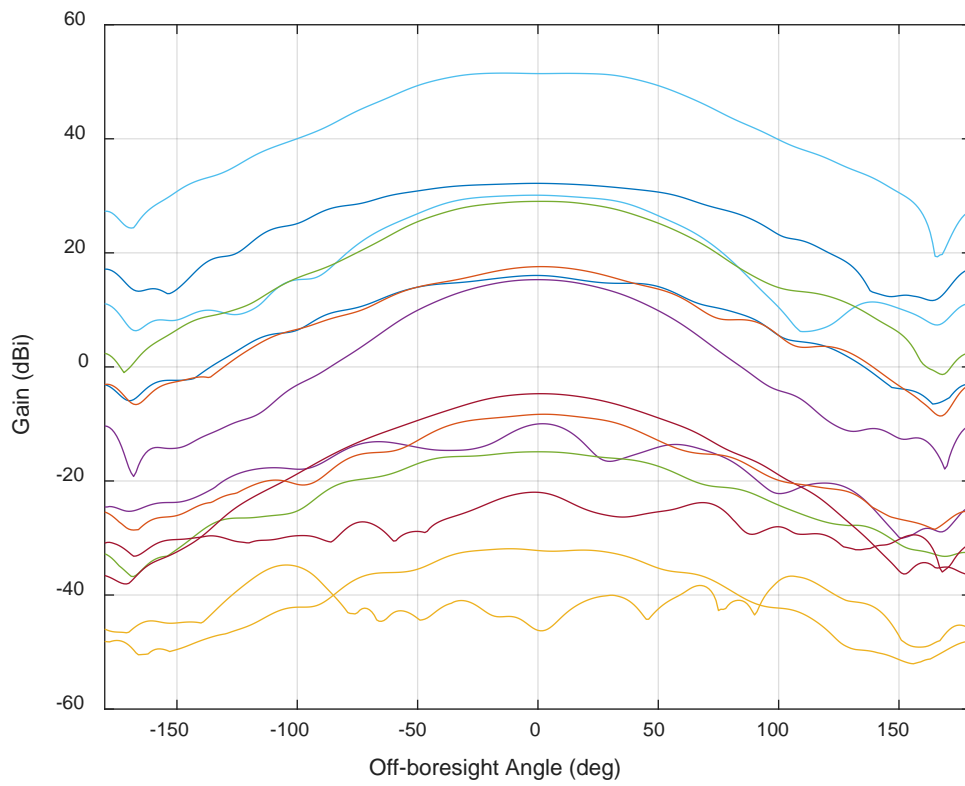
Figure E-9: VPOL Gain Patterns for 14 External Antennas (1520 MHz)
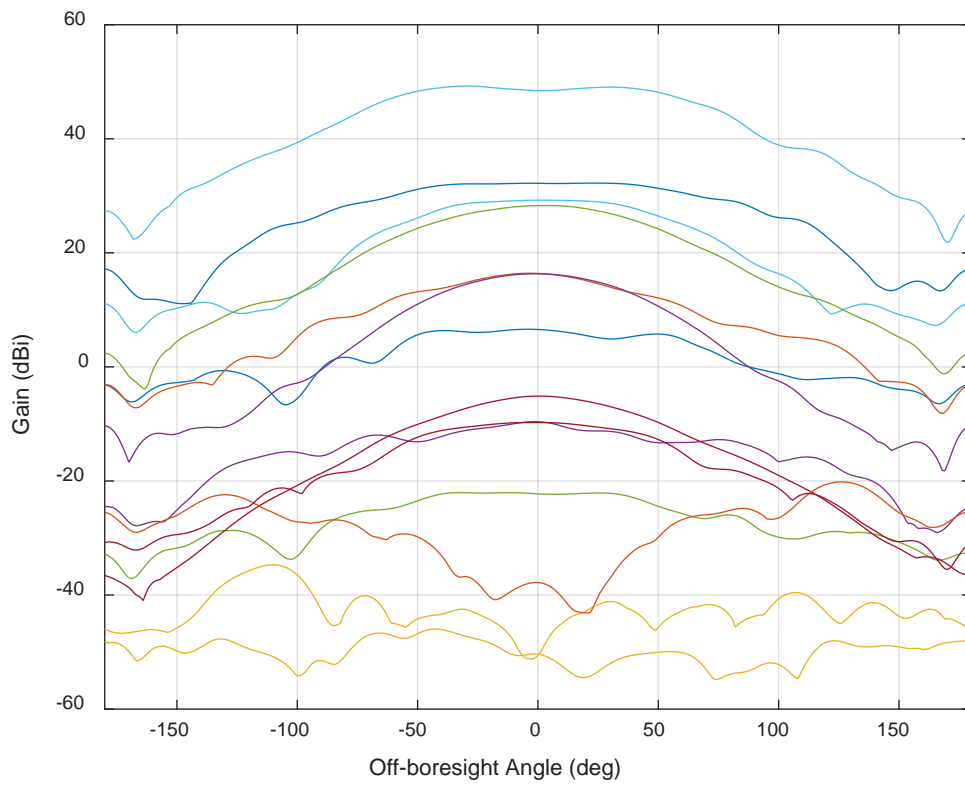
Figure E-10: HPOL Gain Patterns for 14 External Antennas (1520 MHz)
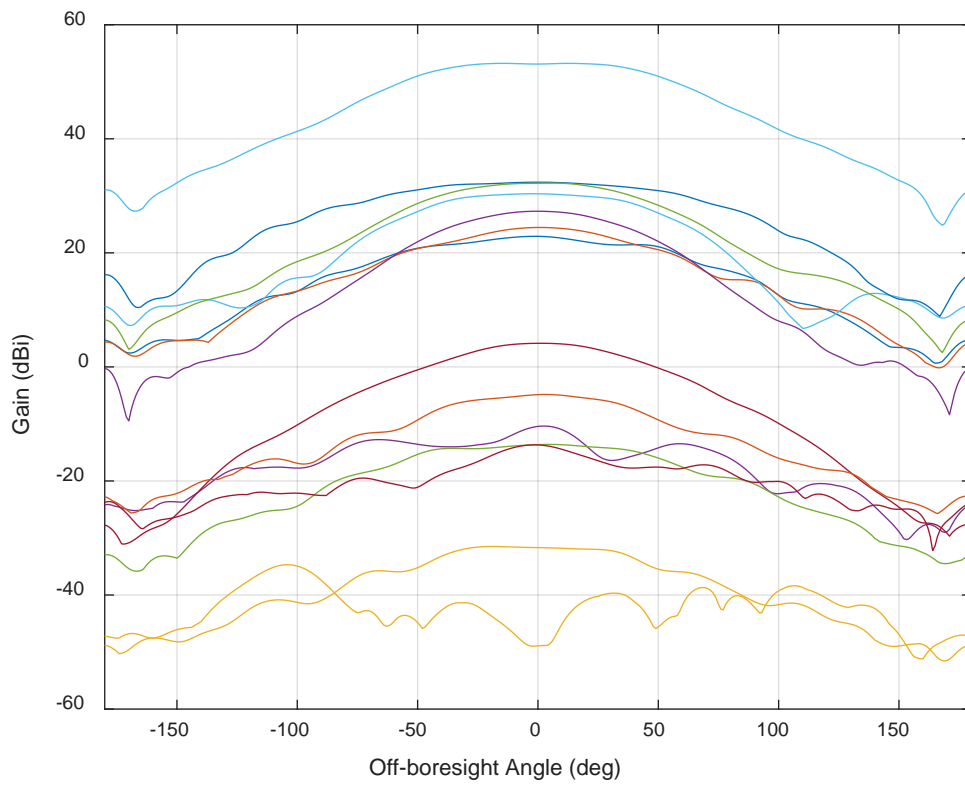
Figure E-11: VPOL Gain Patterns for 14 External Antennas (1530 MHz)
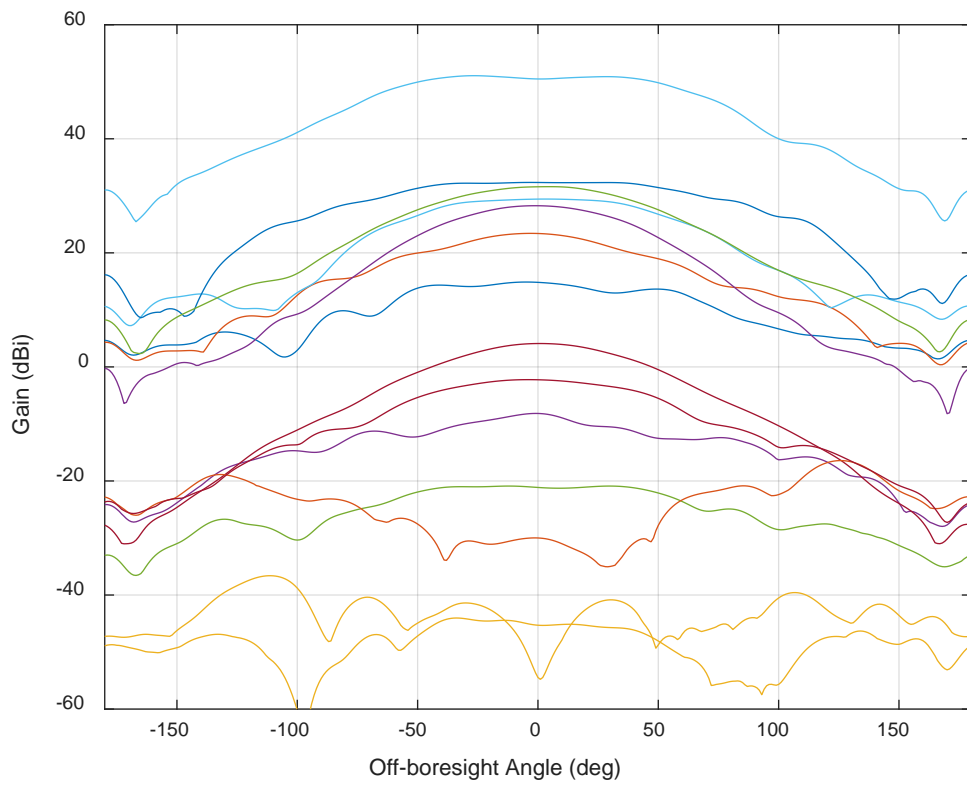
Figure E-12: HPOL Gain Patterns for 14 External Antennas (1530 MHz)
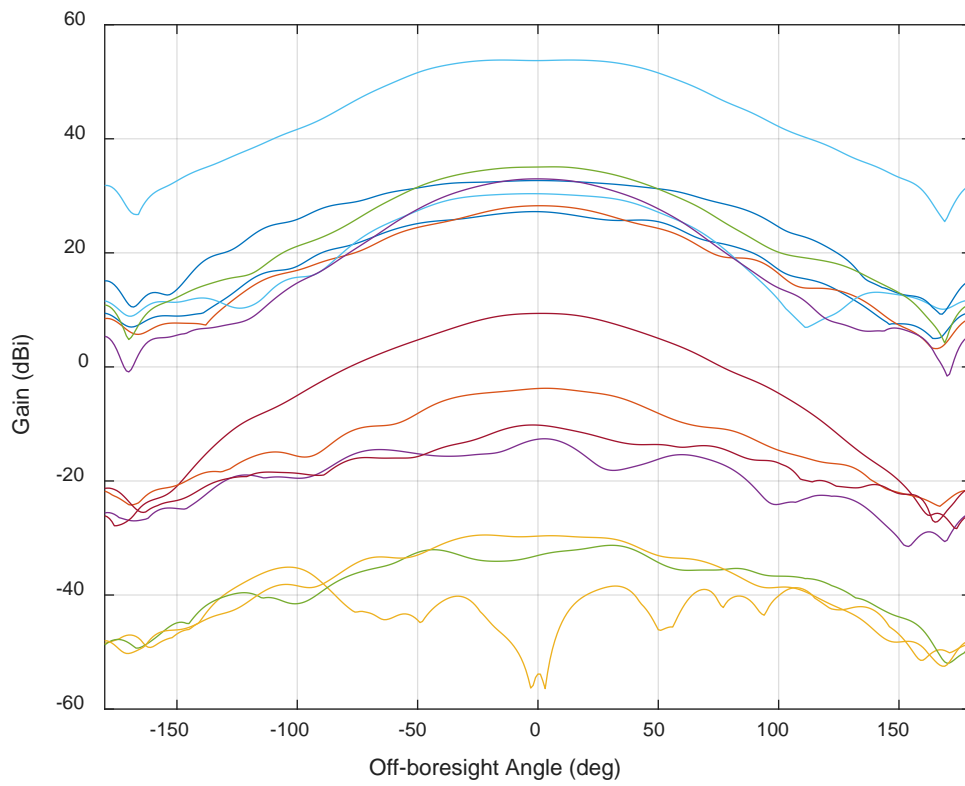
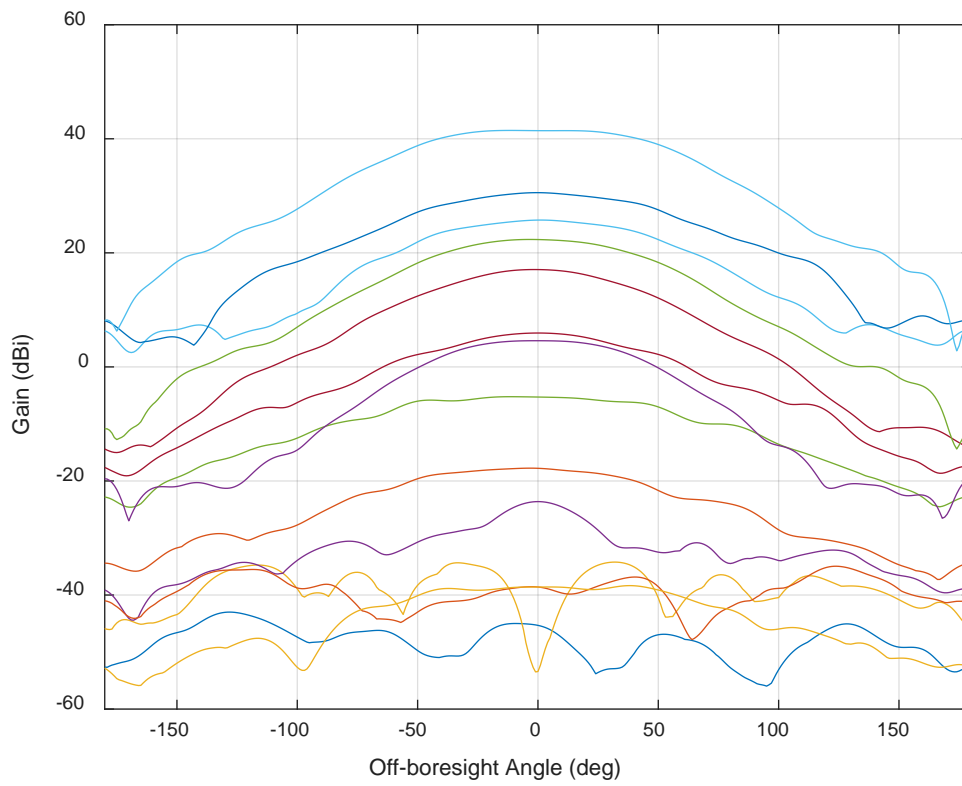**Figure E-13: VPOL Gain Patterns for 14 External Antennas (1535 MHz)**
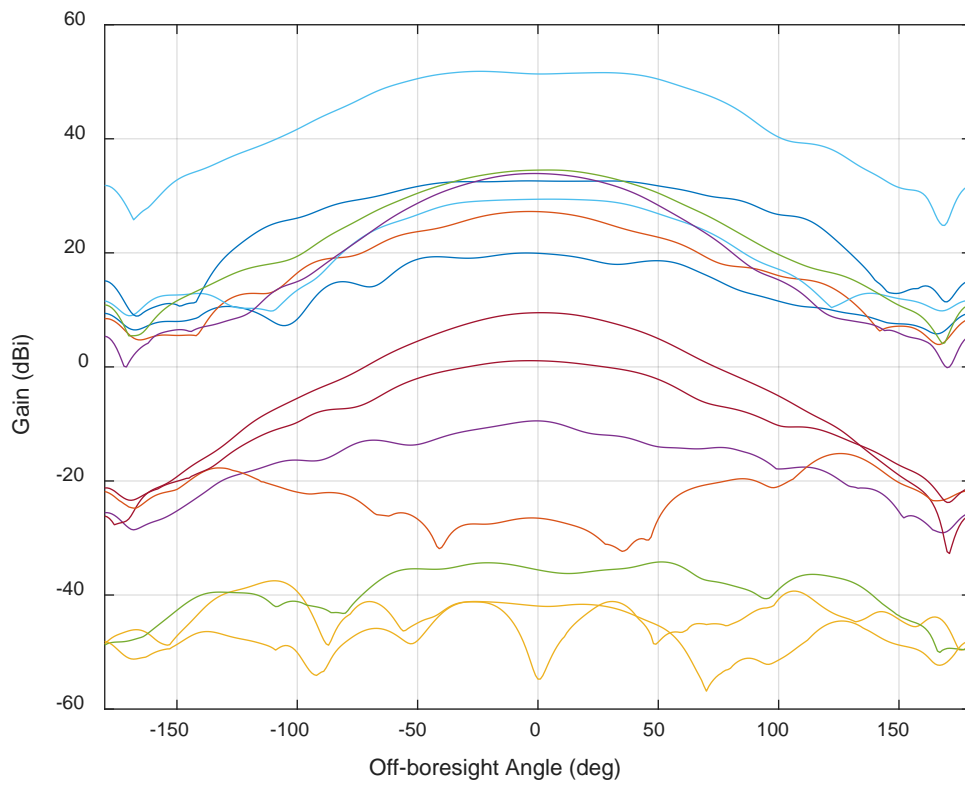
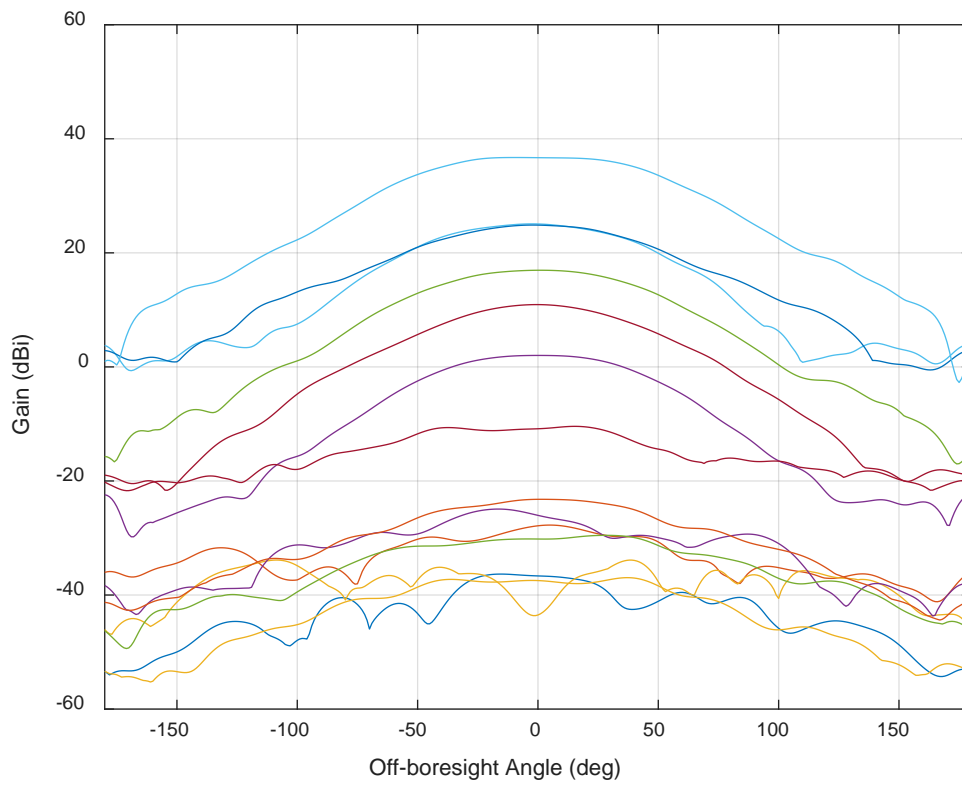**Figure E-14: HPOL Gain Patterns for 14 External Antennas (1535 MHz)**
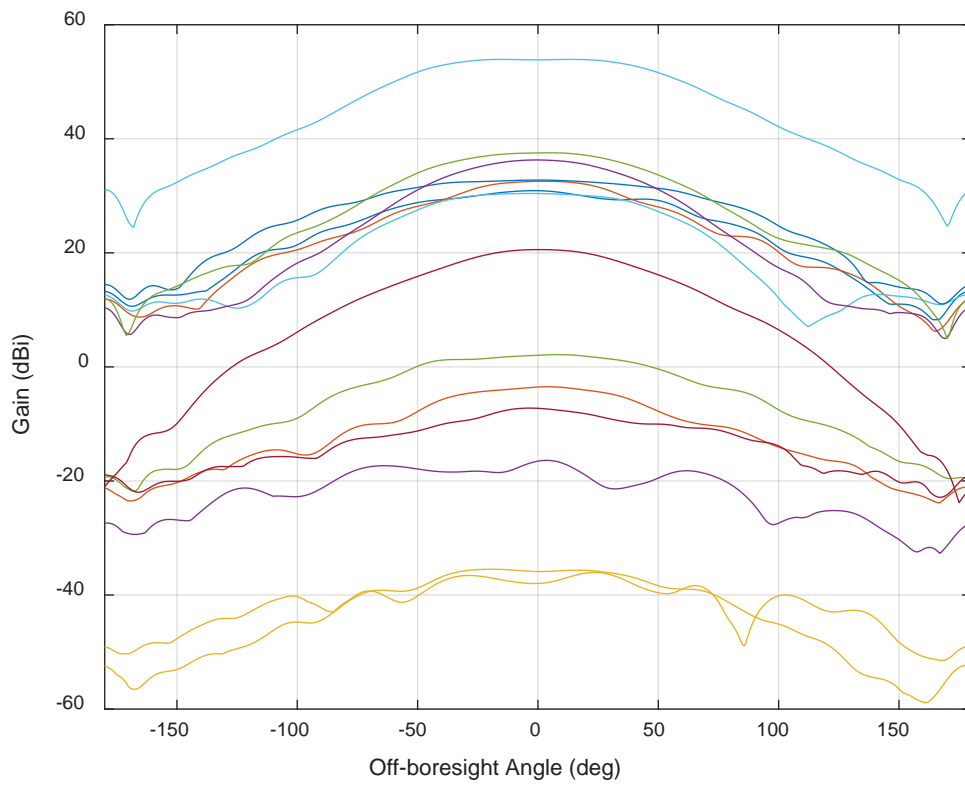
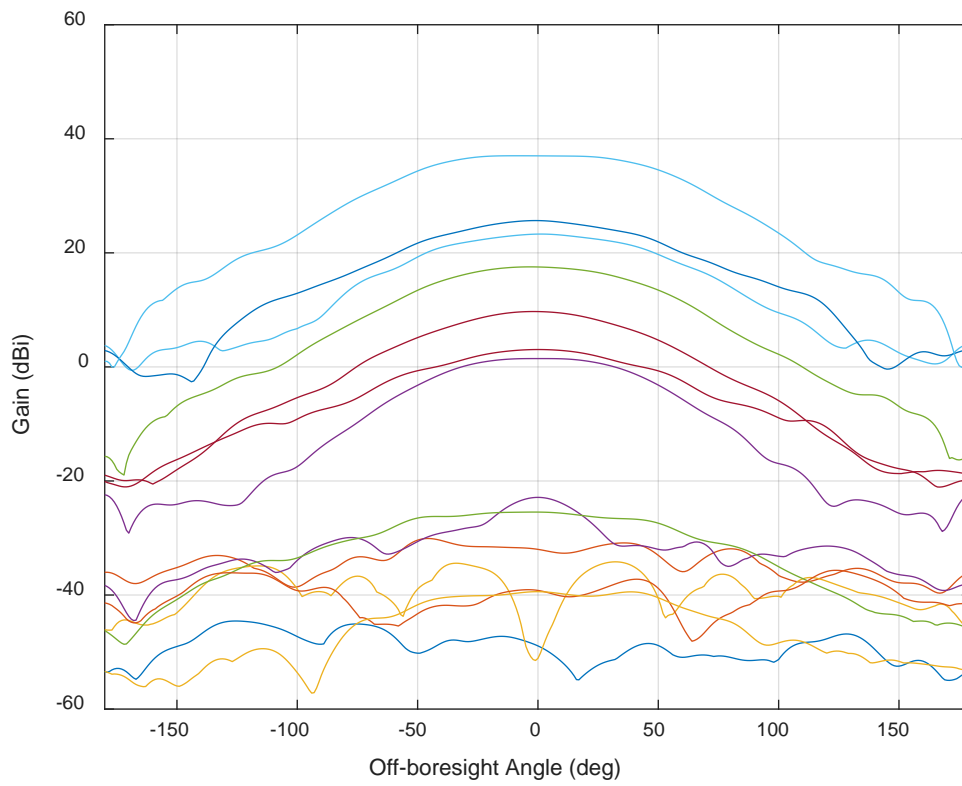**Figure E-15: VPOL Gain Patterns for 14 External Antennas (1540 MHz)**
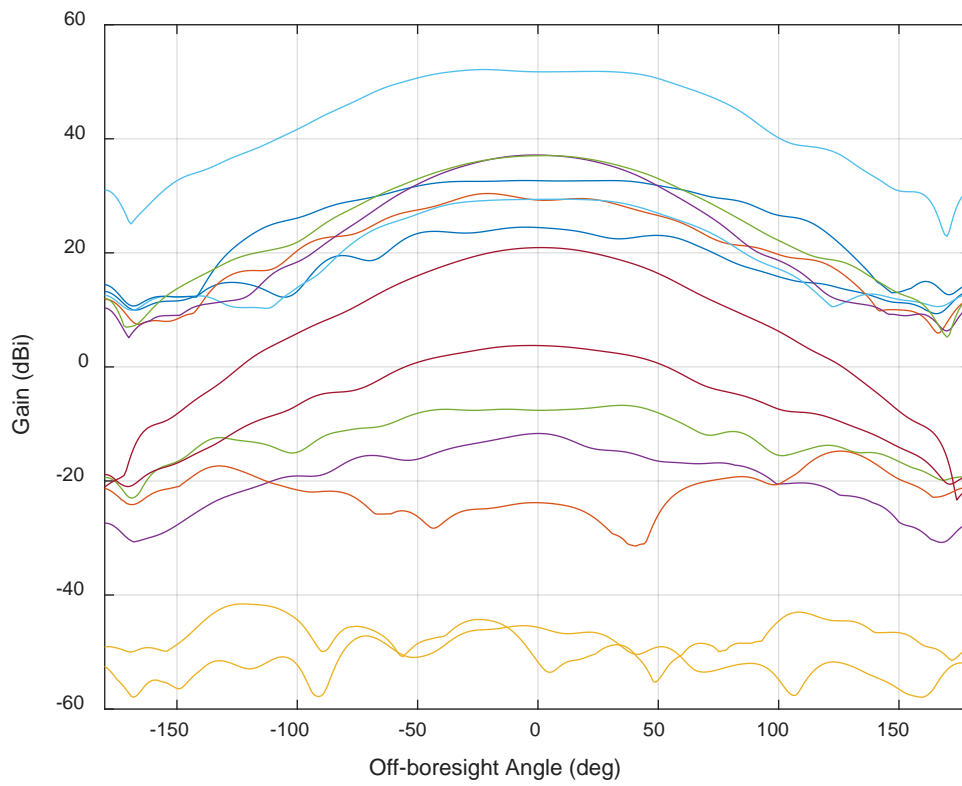
Figure E-16: HPOL Gain Patterns for 14 External Antennas (1540 MHz)
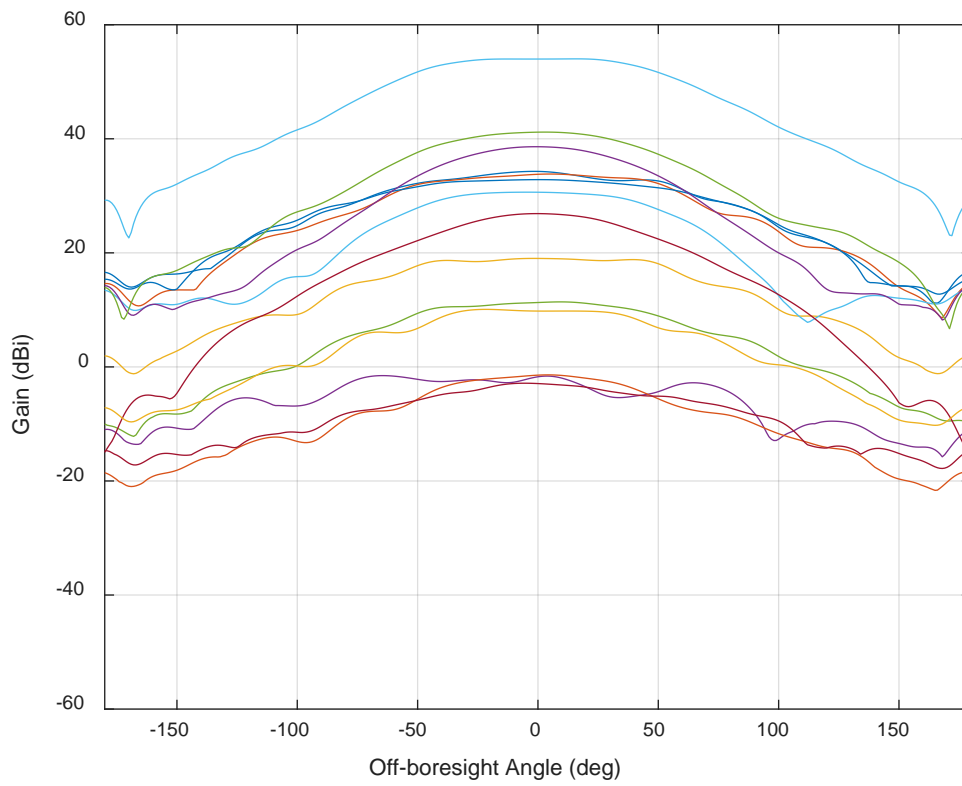
Figure E-17: VPOL Gain Patterns for 14 External Antennas (1545 MHz)
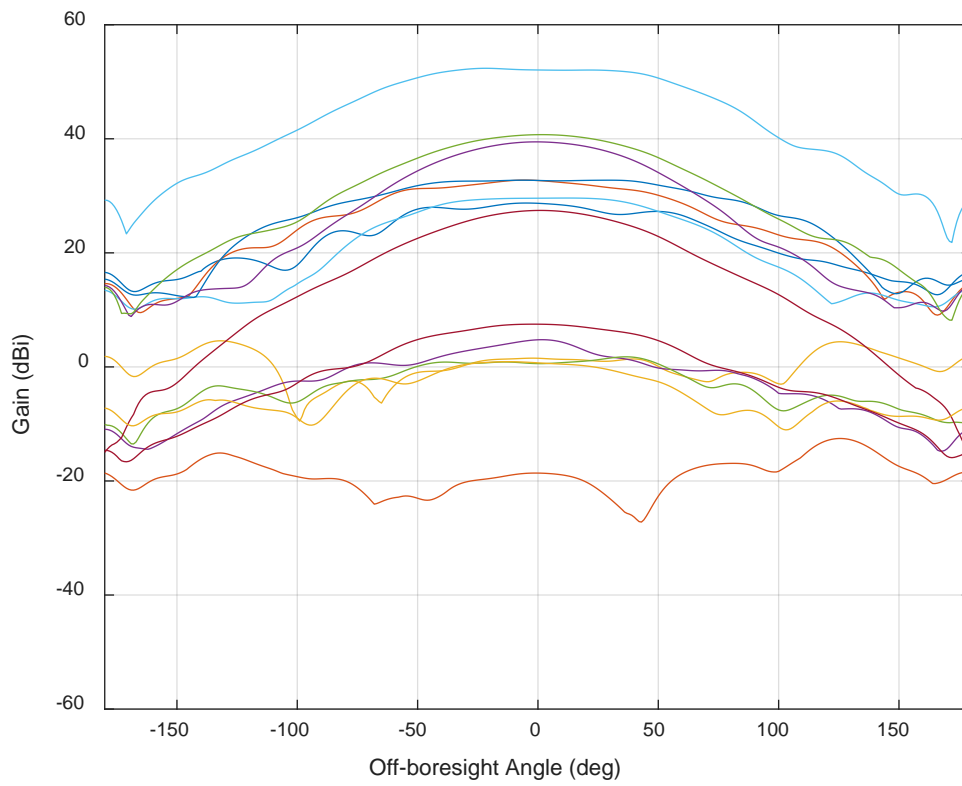
Figure E-18: HPOL Gain Patterns for 14 External Antennas (1545 MHz)
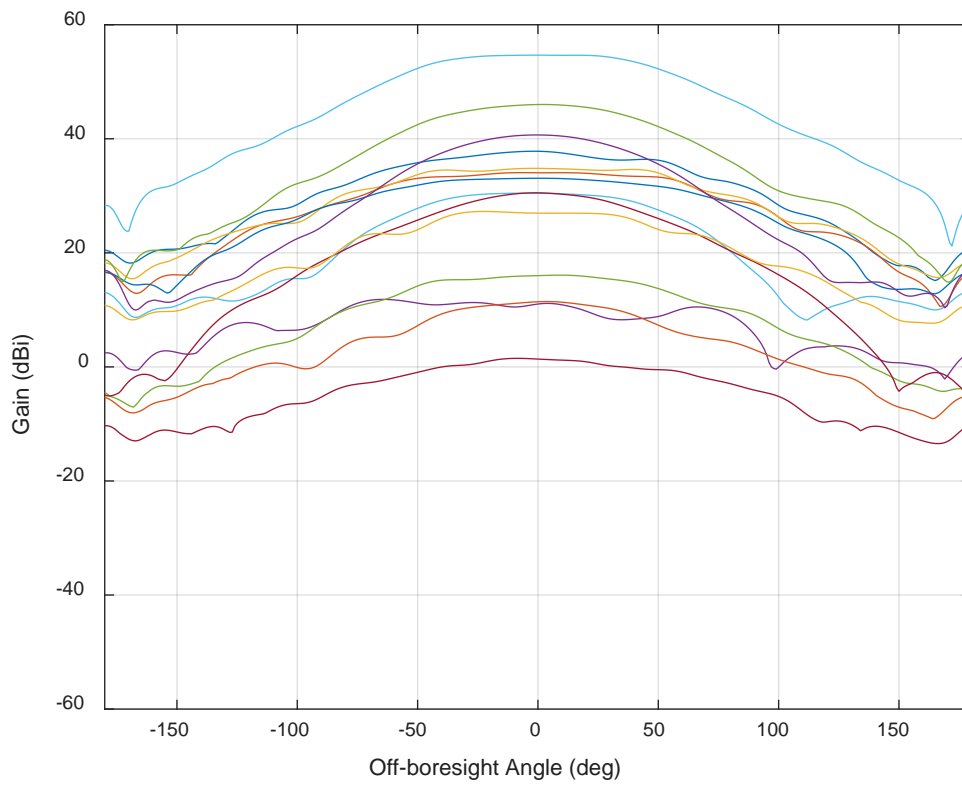
Figure E-19: VPOL Gain Patterns for 14 External Antennas (1550 MHz)
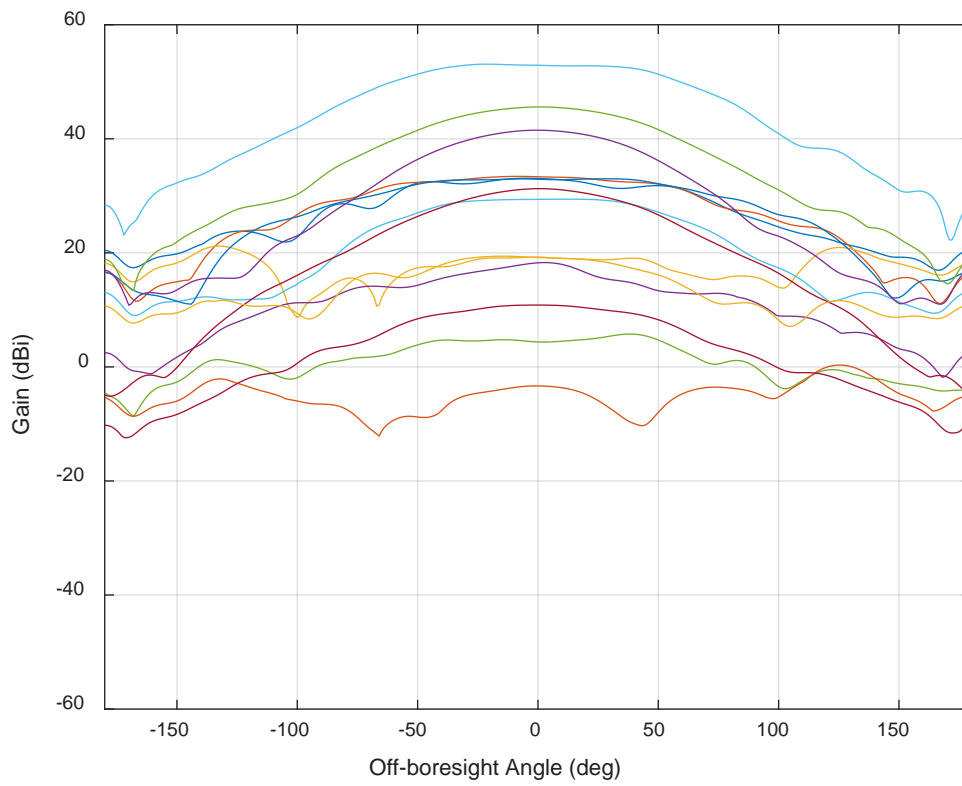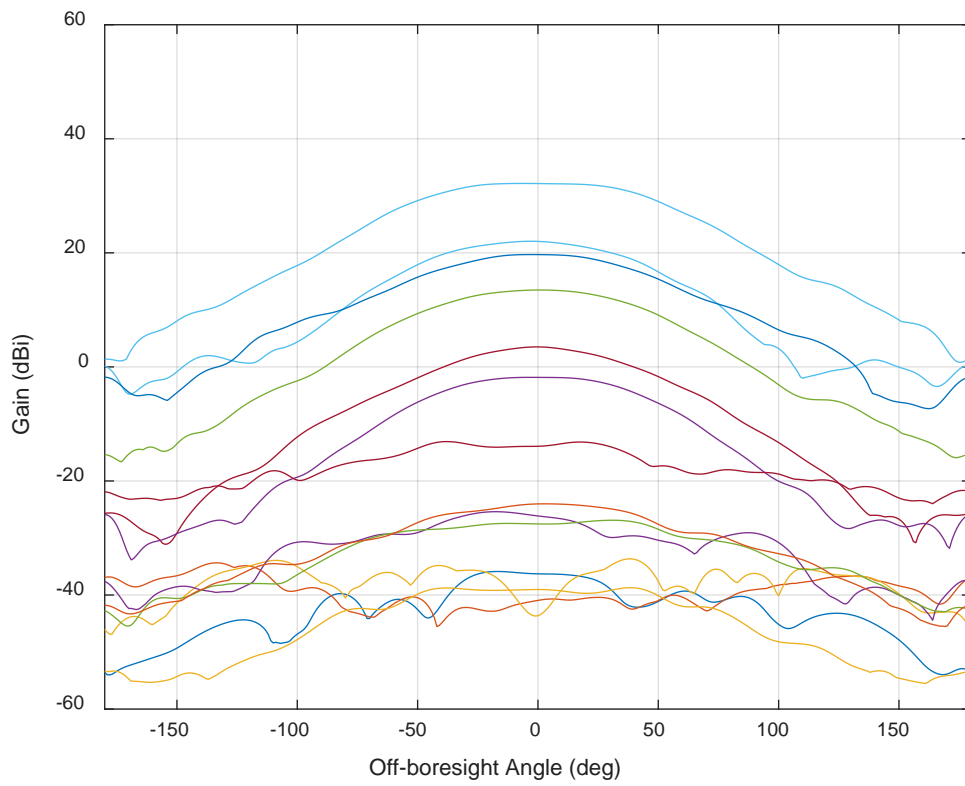
Figure E-20: HPOL Gain Patterns for 14 External Antennas (1550 MHz)
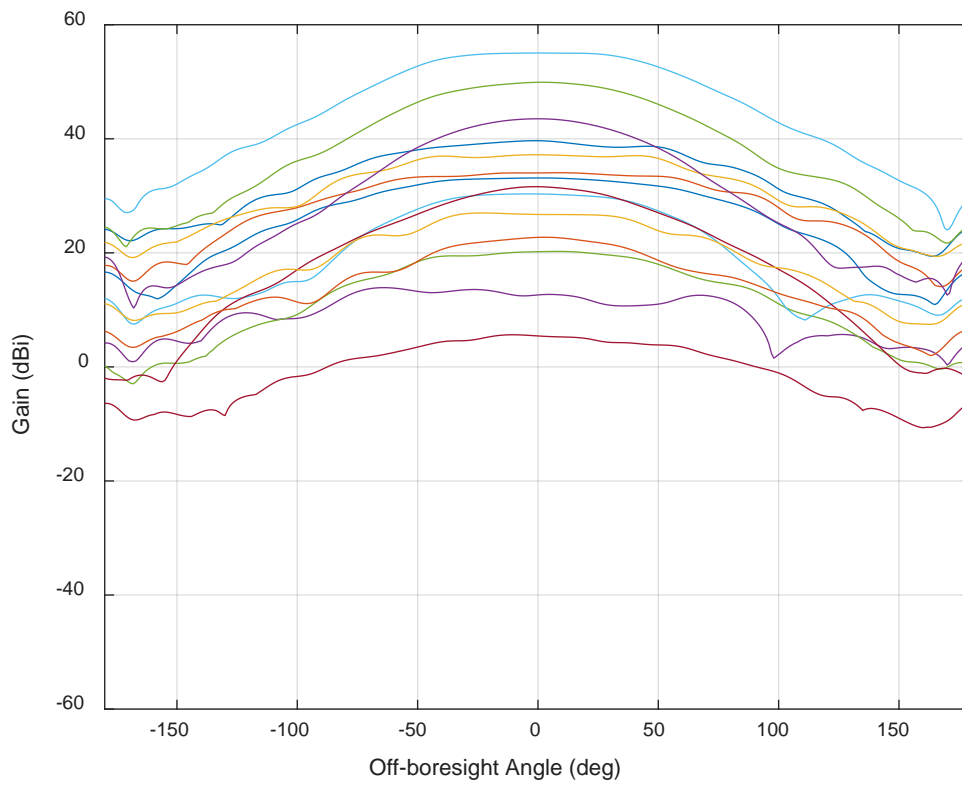
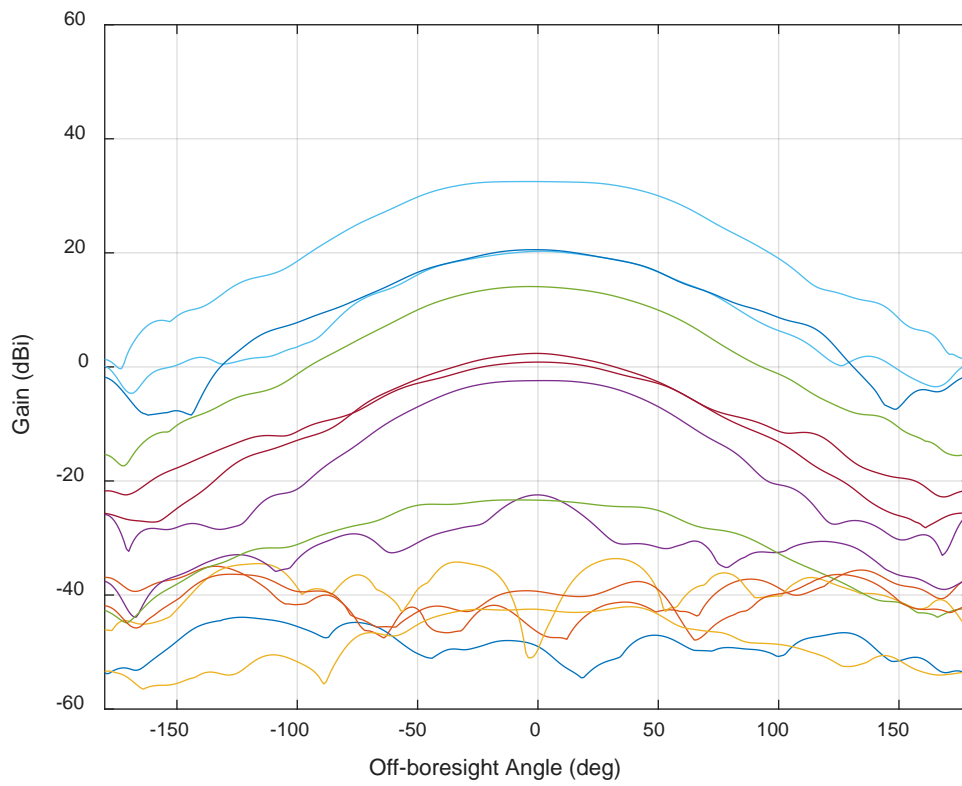**Figure E-21: VPOL Gain Patterns for 14 External Antennas (1555 MHz)**
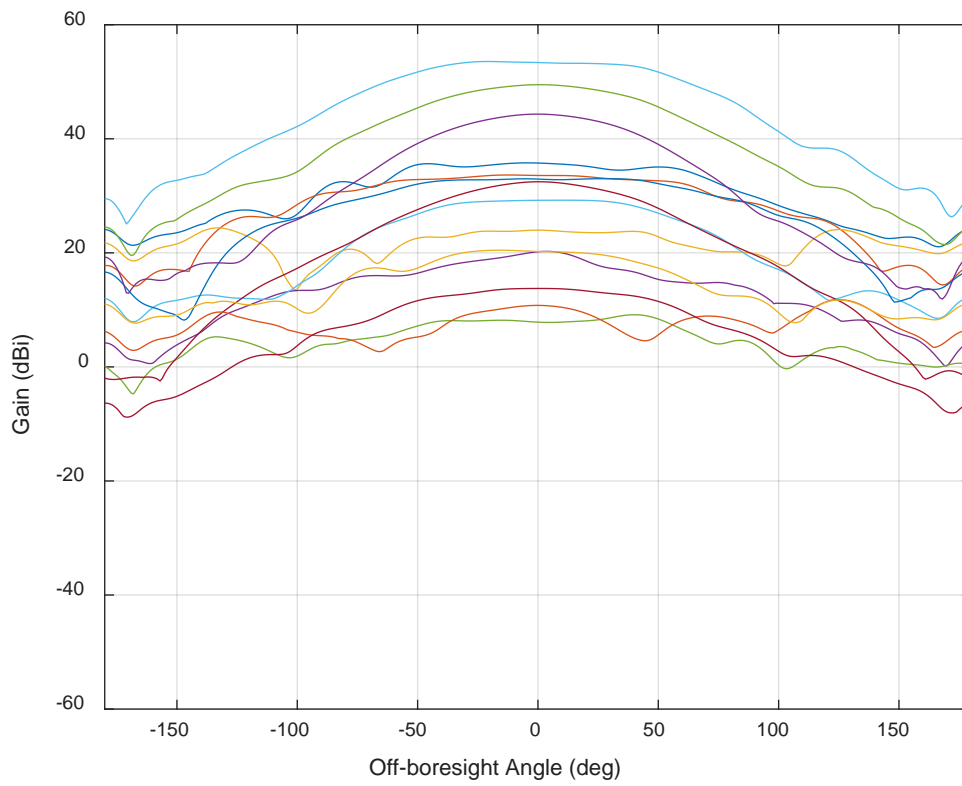
Figure E-22: HPOL Gain Patterns for 14 External Antennas (1555 MHz)
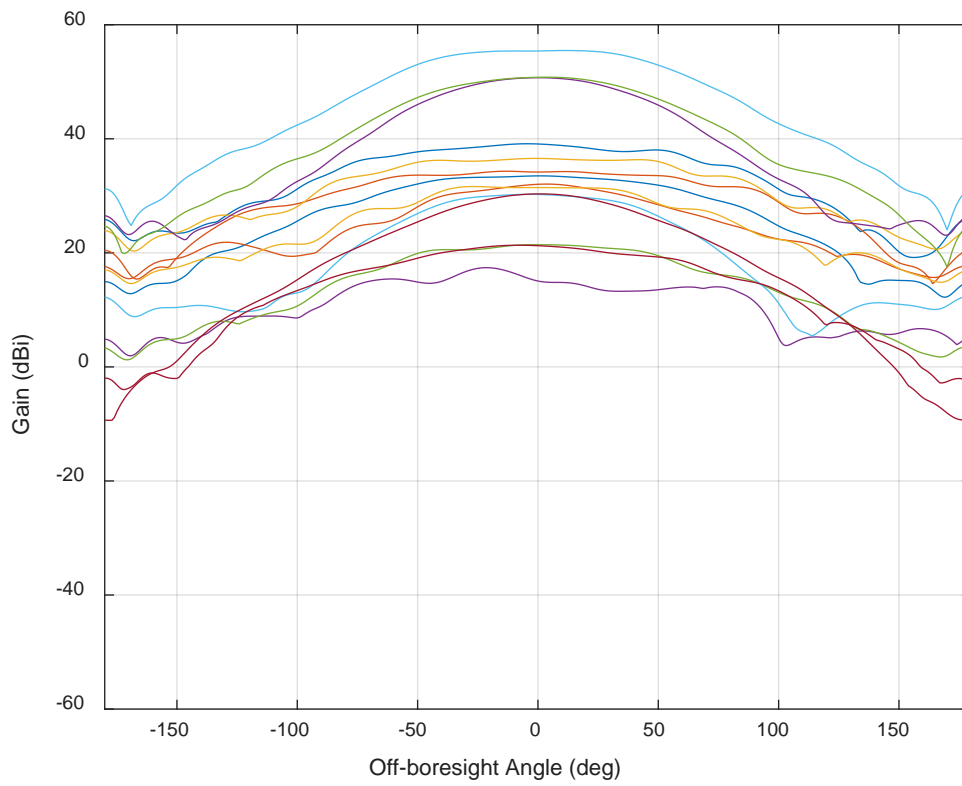
Figure E-23: VPOL Gain Patterns for 14 External Antennas (1575 MHz)
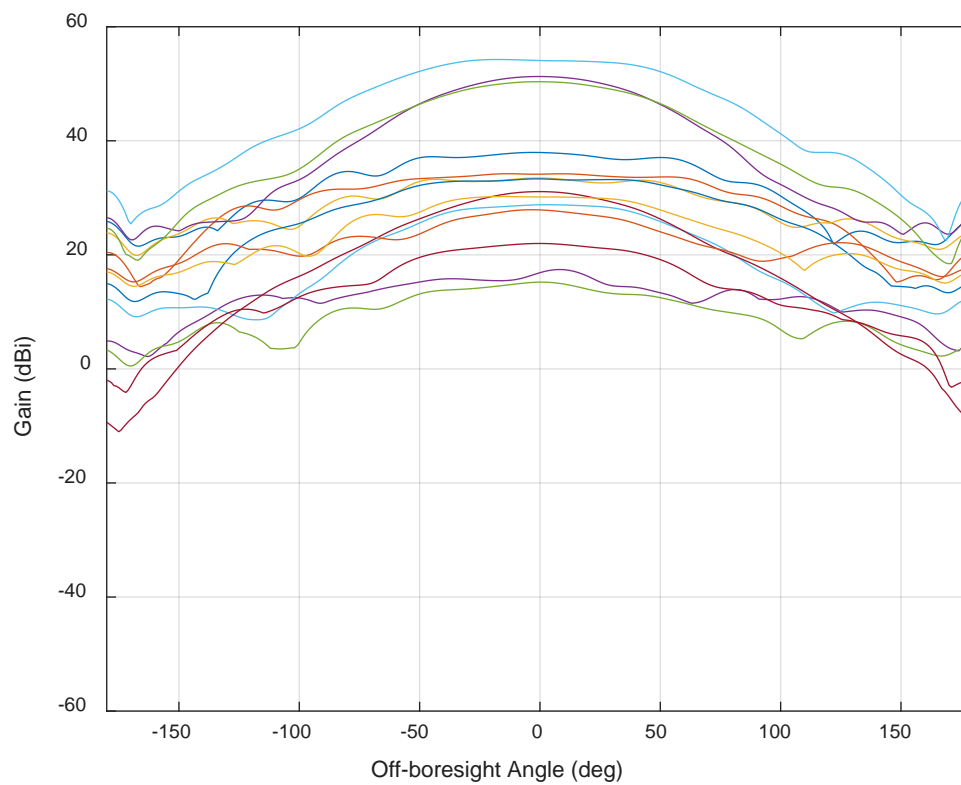
Figure E-24: HPOL Gain Patterns for 14 External Antennas (1575 MHz)
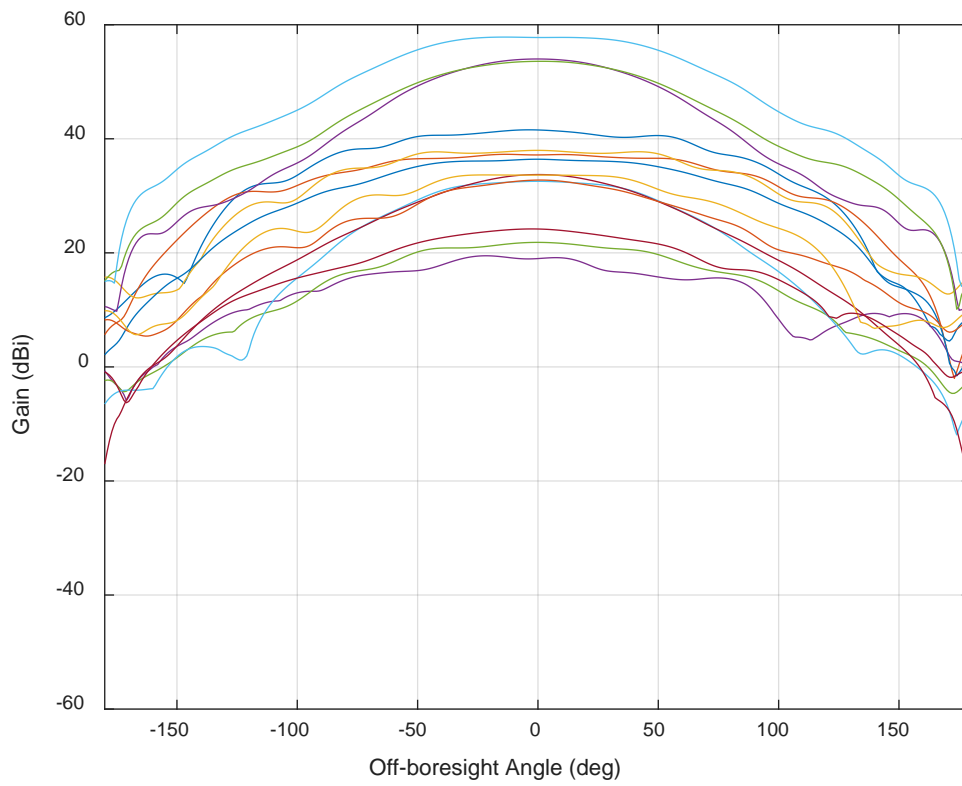
Figure E-25: RHCP Gain Patterns for 14 External Antennas (1575 MHz)
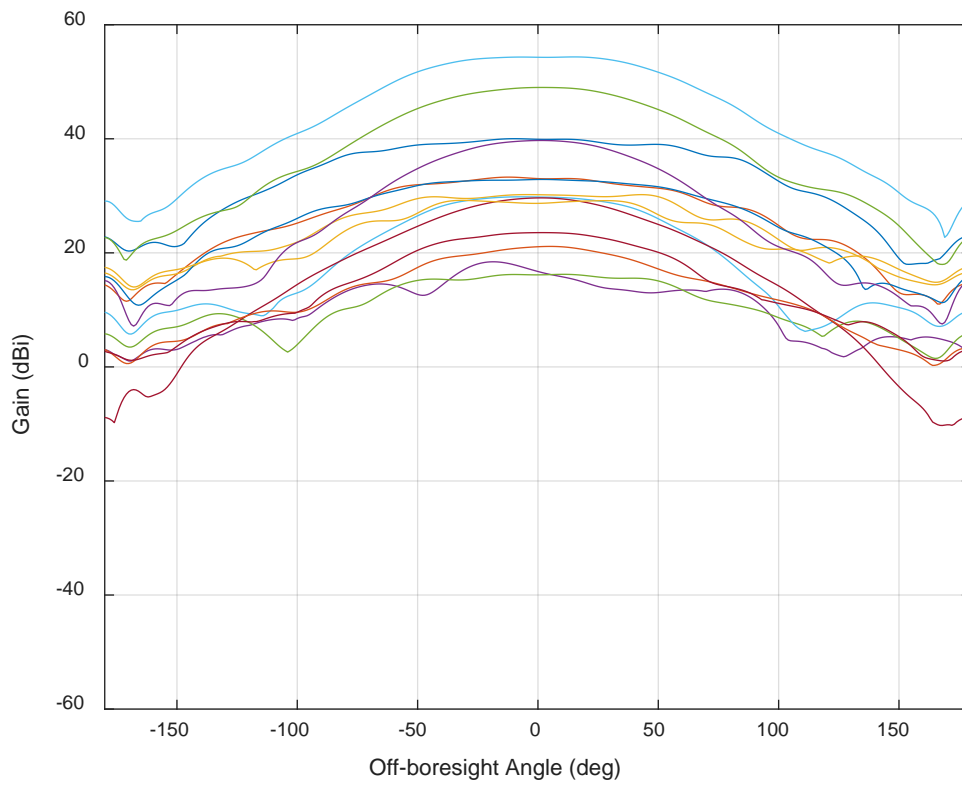
Figure E-26: VPOL Gain Patterns for 14 External Antennas (1595 MHz)
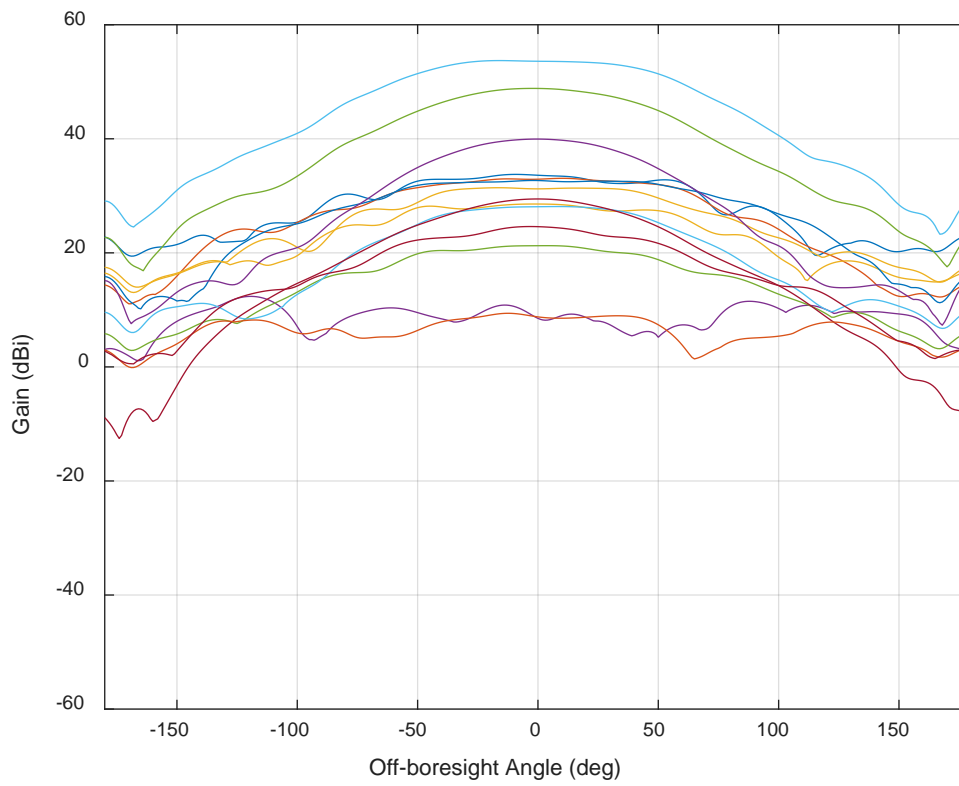
Figure E-27: HPOL Gain Patterns for 14 External Antennas (1595 MHz)

Figure E-28: VPOL Gain Patterns for 14 External Antennas (1615 MHz)

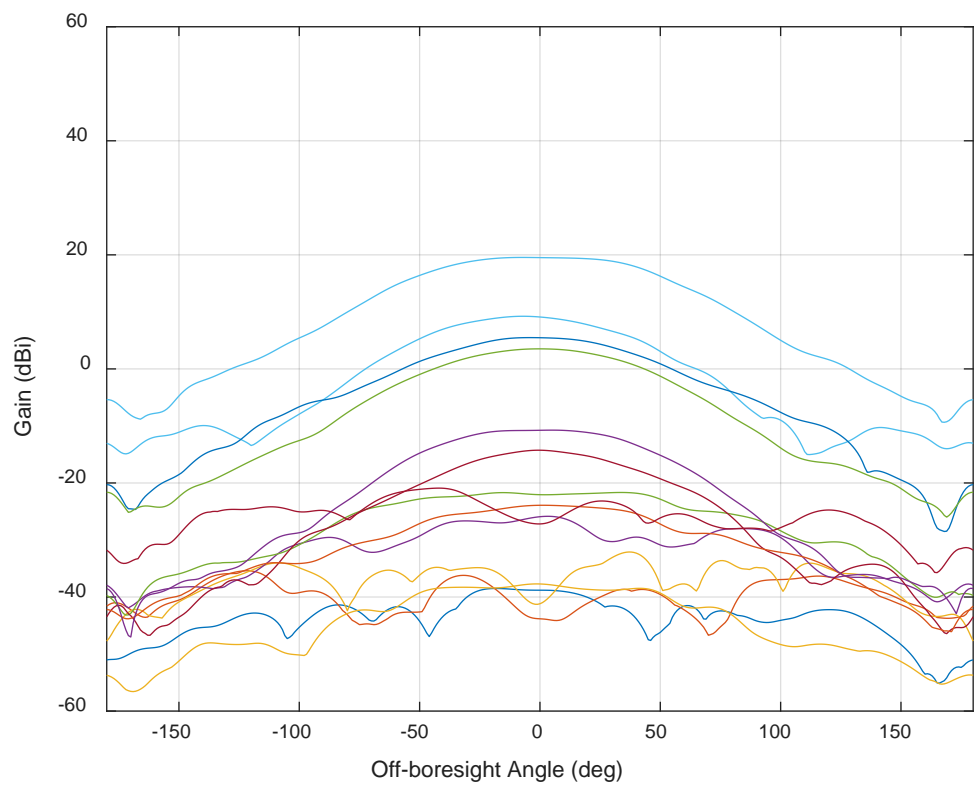**Figure E-29: HPOL Gain Patterns for 14 External Antennas (1615 MHz)**

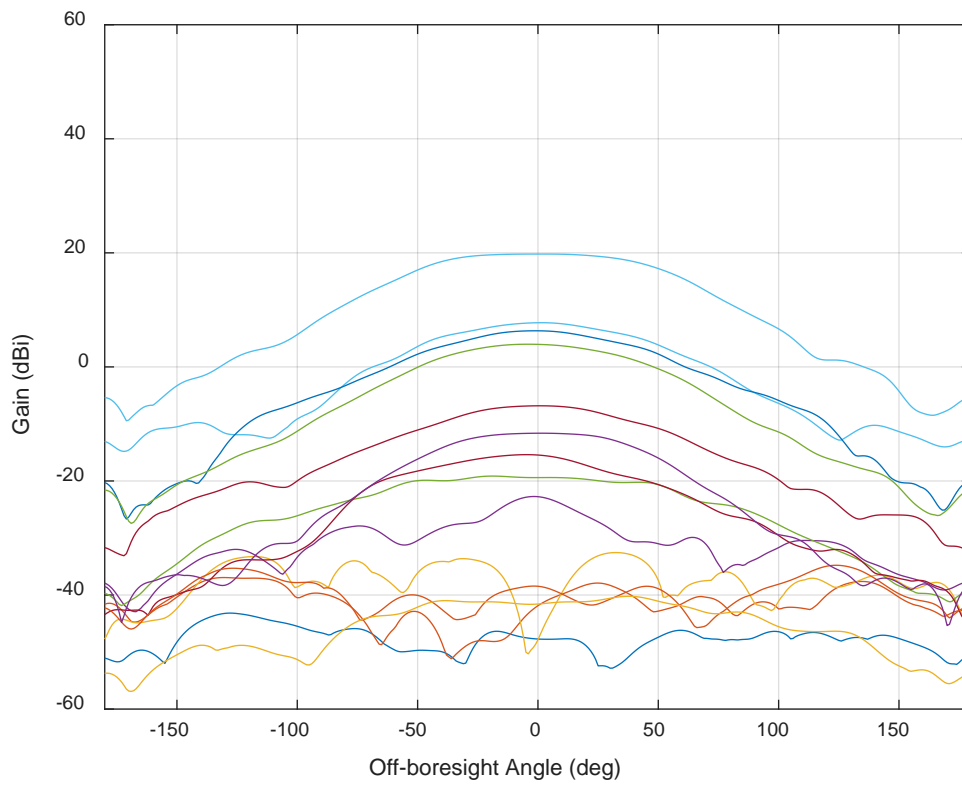**Figure E-30: VPOL Gain Patterns for 14 External Antennas (1620 MHz)**

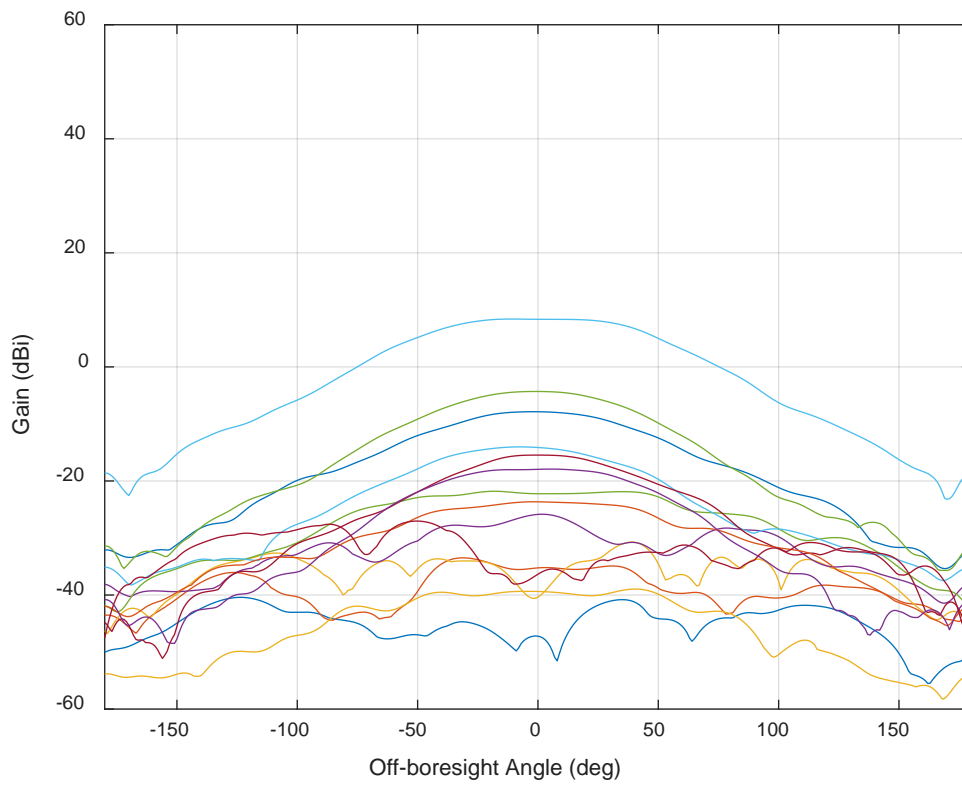**Figure E-31: HPOL Gain Patterns for 14 External Antennas (1620 MHz)**

37

Figure E-32: VPOL Gain Patterns for 14 External Antennas (1625 MHz)

Figure E-33: HPOL Gain Patterns for 14 External Antennas (1625 MHz)

Figure E-34: VPOL Gain Patterns for 14 External Antennas (1630 MHz)

Figure E-35: HPOL Gain Patterns for 14 External Antennas (1630 MHz)

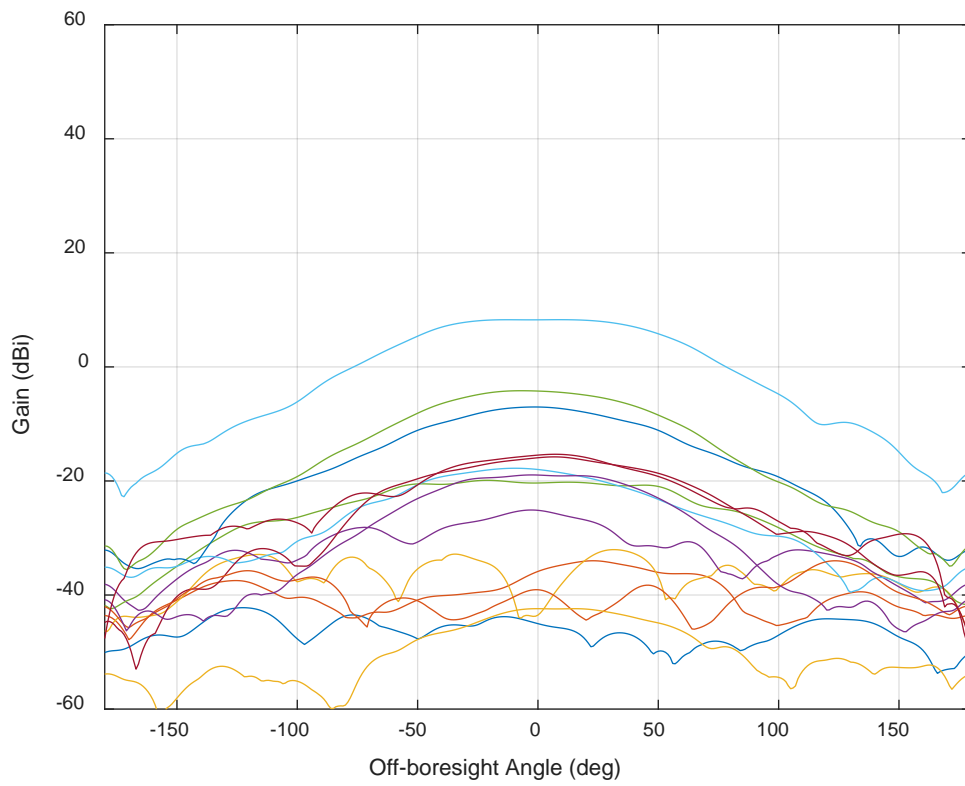**Figure E-36: VPOL Gain Patterns for 14 External Antennas (1635 MHz)**

Figure E-37: HPOL Gain Patterns for 14 External Antennas (1635 MHz)

Figure E-38: VPOL Gain Patterns for 14 External Antennas (1640 MHz)

Figure E-39: HPOL Gain Patterns for 14 External Antennas (1640 MHz)

Figure E-40: VPOL Gain Patterns for 14 External Antennas (1645 MHz)

Figure E-41: HPOL Gain Patterns for 14 External Antennas (1645 MHz)

Figure E-42: VPOL Gain Patterns for 14 External Antennas (1660 MHz)

Figure E-43: HPOL Gain Patterns for 14 External Antennas (1660 MHz)

Figure E-44: VPOL Gain Patterns for 14 External Antennas (1675 MHz)

Figure E-45: HPOL Gain Patterns for 14 External Antennas (1675 MHz)

APPENDIX F

PROPAGATION PATH AND AGGREGATE EFFECT COMPUTATION MODELS

TABLE OF CONTENTS

LIST OF FIGURES

LIST OF TABLES

No table of figures entries found.

REFERENCES

[1] M. Hata, "Empirical formula for propagation loss in land mobile radio services," *IEEE Trans. Veh. Technol.,* vol. 29, pp. 317-325, Aug. 1980.

[2] Y. Okumura, E. Ohmor, T. Kawano and K. Fukua, "Field strength and its variability in UHF and VHF land-mobile radio service," *Review of Electrical Communications Lab.,* vol. 16, no. 9, 1968.

[3] D. Parsons, The Mobile Radio Propagation Channel, Chichester, England: John Wiley & Sons, 1996.

[4] V. Erceg, L. J. Greenstein, S. Y. Tjandra, S. R. Parkoff, A. Gupta, B. Kulic, A. Julius and R. Bianchi, "An Empirically Based Path Loss Model for Wireless Channels in Suburban Environments," *IEEE Journal on Selected Areas in Communications,* vol. 17, no. 7, July 1999.

[5] Status Report: Assessment of Compatibility of Planned LightSquared Ancillary Terrestrial Component Transmissions in the 1526-1536 MHz Band with Certified Aviation GPS Receivers, FAA Report PR 25, January 25, 2012.

[6] Handout for wireless comm. graduate course, University of Illinois (ECE559), Professor V. V. Veeraldi pp. 53-56.

[7] C. Loo, "A Statistical Model for a Land Mobile Satellite Link," *IEEE Transactions on Vehicle Technology,* vol. 34, no. 3, Aug. 1985.

[8] K. M. Peterson and R. J. Erlandson, "Analytic Statistical Model for Aggregate Radio Frequency Interference to Airborne GPS Receivers from Ground-Based Emitters," *Journal of the Institute of Navigation,* vol. 59, no. 1, Spring, 2012.

[9] Final Report: A Generalized Statistical Model for Aggregate Radio Frequency Interference to Airborne GPS Receivers from Ground Based Emitters (DOT/FAA/TC-14/30, Rev. 1), August 7, 2017.

[10] J. A. Gubner, "A New Formula for Lognormal Characteristic Function," *IEEE Transactions on Vehicle Technology,* vol. 55, no. 5, pp. 1668- 1671, Sept. 2006.

[11] K. Chung, A Course In Probability Theory, New York: Academic Press, 1974.

APPENDIX

Appendix F. Propagation Path and Aggregate Effect Computation Models

F.1 Propagation Path Model General Aspects

All the RFI propagation path models used herein are based on the flat-earth approximation. In other words, the ground under the aircraft is assumed to be essentially smooth and flat out to a radio horizon from the point on the ground directly under the aircraft. In line-of-sight propagation conditions at radio frequencies near the GPS carrier, this radio horizon value depends, in general, on the aircraft GNSS and RFI source antenna heights and the amount of atmospheric refraction along the propagation path. A 4/3 Earth radius approximation for the refractive effect on the radio horizon will be used in all propagation models.

The propagation model described in this document basically consists of two different types of models. Those scenarios where blockage is a factor are typically evaluated using probabilistic models while clear line-of-sight scenarios are analyzed using free space path loss.

For scenarios that involve environments in which emissions from adjacent channel systems undergo scattering, reflections, and absorption prior to arriving at an aircraft's GPS antenna, a probabilistic propagation model must be used. These propagation environments were the subject of much research during the development of cellular radio systems. As a result, the cellular radio community has over the years developed propagation models which for the most part are applicable to the present RFI scenarios under consideration.

Generally, in this document the point at which free space propagation path model is used occurs at an aircraft antenna height of 550 meters. Above 550 meters, various parameter limits associated with the probabilistic models are exceeded thereby making the model use problematic. Also at these aircraft heights, line-of-sight conditions generally prevail which means that free space path loss is the most appropriate model to apply.

Below the 550 meter aircraft antenna height the probabilistic models developed by the cellular radio community become applicable. Each of these models have one feature in common; the probabilistic nature of the propagation path model is well approximated by the product of a slow fading process and a fast fading process. The slow fading process is very well approximated by a log-normal distribution while the fast fading process is described by a non-central Chi-Squared distribution. The log-normal component is completely determined by two parameters, μ and σ and the Chi-Squared process by the parameters L, ψ_o and ρ_o. The range dependent median path model between the GPS antenna and the interference source determines the parameter μ while the remaining parameters vary with range depending on the scenario. In some special cases below 550 m aircraft antenna height, free-space ($1/r^2$) propagation is assumed.

F.2 Single Path Model

F.2.1 Single Path Median Isotropic Propagation Model

The single path median isotropic propagation model used depends upon the GPS aircraft antenna height and emitter source antenna height above ground. For aircraft antenna heights greater than or equal to 550 meters, a free space propagation model is used. The median isotropic propagation path model for aircraft antenna heights below 550 meters consists in general of three segments, depending on the scenario, appropriately blended together. They form a continuous function of the lateral separation radius r (in meters) between the aircraft and RFI source antennas. At the shorter radial distances, conventional two-ray propagation is used. That model assumes a direct path between the two antennas interacts with one other path reflected from the ground between antennas. For radii greater than about 1 km, the Hata-Okumura suburban propagation model ([1], [2]) is used. At radii beyond 20 km, a long distance extension is made to the standard Hata-Okumura formulation. If necessary to achieve propagation path model continuity, the two-ray and Hata-Okumura model segments are connected together by one of two means. One method uses a single, constant slope exponential fit function that covers radius values in between segments. The other method, used in mobile broadband handset station scenarios with aircraft antenna heights below 80 meters and source antennas less than 2 meters, is a modified Erceg-Greenstein path loss segment. Since median isotropic propagation path model is generally a function of the aircraft and RFI source antenna heights, the path loss is adapted to each specific RFI scenario.

For convenience, this Appendix generally uses the term "path spreading factor" (*PF*), which is the algebraic reciprocal of the path loss.

F.2.1.1 Short Range Path Segment (Two-Ray) Isotropic Model

F.2.1.1.1 Short Range Path Segment (Level-Terrain Two-Ray) Isotropic Model

Measurements indicate that at short ranges, where few obstructions are present, the GPS antenna receives interference from an RFI source by both a direct and reflected path [3]. On the reflected path, the electromagnetic wave is reflected from the earth's surface with a range-dependent complex reflection coefficient $\rho_v(r)$[1]. In addition to the relative phase delay between the direct and reflected rays, the complex reflection coefficient both attenuates and adds phase shift to the reflected ray. When the two rays additively combine at the receive antenna, the resulting received power fluctuates with lateral separation range r. Figure F-1 illustrates the direct and indirect reflected ray geometry.

---

[1]The equations that follow from this model are a first-order approximation to a more complicated possible derivation. This approximation is considered acceptable for the aviation-related analyses in this report.
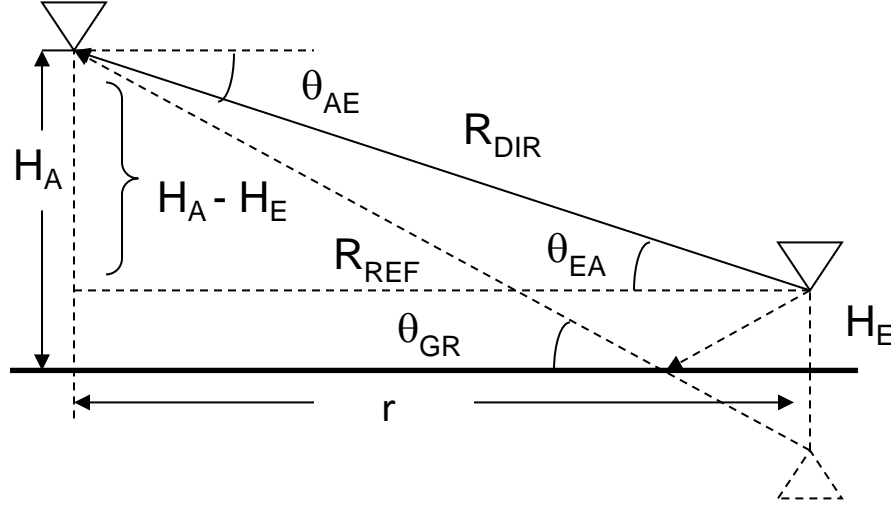
Figure F-1: Level-Terrain Two-Ray Path Model Geometry

With the aircraft antenna height denoted by H_A and the interference source antenna height by H_E the direct and reflected ray path lengths are defined respectively as: $R_{DIR}(r) = \sqrt{(H_A - H_E)^2 + (r)^2}$ and $R_{REFL}(r) = \sqrt{(H_A + H_E)^2 + (r)^2}$. The reflected ray relative phase lag is determined by

$\phi(r) = \left(\frac{2\pi}{\lambda_c(f_c)}\right)(R_{REFL}(r) - R_{DIR}(r))$, where λ_c is the free-space wavelength at the receiver center

frequency, f_c. The grazing angle, $\theta_{GR}(r)$, of the reflected ray with the concrete reflecting surface is given as $\theta_{GR}(r) = \sin^{-1}((H_A + H_E) / R_{REFL}(r))$. Two electrical parameters of concrete (relative dielectric constant, $\varepsilon_r = 7.0$, conductivity, $\sigma_{cc} = 0.15$ S/m) are used to form a constituent ratio

parameter, $x(f_c) = \frac{\sigma_{cc}}{2\pi f_c \varepsilon_0}$, where ε_0 is the free space permittivity. With the ratio parameter x

defined, the complex reflection coefficient for vertical polarized waves, $\rho_v(r)$, is given as:

$$\rho_v(r, f_c) = \frac{(\varepsilon_r - i \cdot x(f_c))\sin(\theta_{GR}(r)) - \sqrt{(\varepsilon_r - i \cdot x(f_c)) - \cos^2(\theta_{GR}(r))}}{(\varepsilon_r - i \cdot x(f_c))\sin(\theta_{GR}(r)) + \sqrt{(\varepsilon_r - i \cdot x(f_c)) - \cos^2(\theta_{GR}(r))}}$$;

where the imaginary constant, $i = \sqrt{-1}$. The complex multipath field factor at the receive antenna

is then given by $P_v(r, f_c) = 1 + \left(\frac{R_{DIR}(r)}{R_{REFL}(r)}\right)\rho_v(r, f_c) \cdot e^{-i\phi(r)}$. With these definitions the two-

ray isotropic median path spreading factor (reciprocal of path loss) is written (algebraic terms) as:

$$PF_{2Ray}(r, f_c) = \left(\frac{\lambda_c(f_c)}{4\pi} \cdot \frac{|P_v(r, f_c)|}{R_{DIR}(r)} \right)^2 \quad \text{for } 0 \le r < r_1. \tag{F-1}$$

The aircraft and source antenna gains for the direct ray path can be computed from the direct ray elevation angle, $\theta_{AE}(r) = -\sin^{-1}((H_A - H_E)/R_{DIR}(r))$. Note that $\theta_{EA} = -\theta_{AE}$. The break point r_1 is described in Section F.2.2.2. Figure F-2 shows a typical two-ray model path spreading factor plotted in dB as a function of the range r in meters for f_c.= 1575.42 MHz
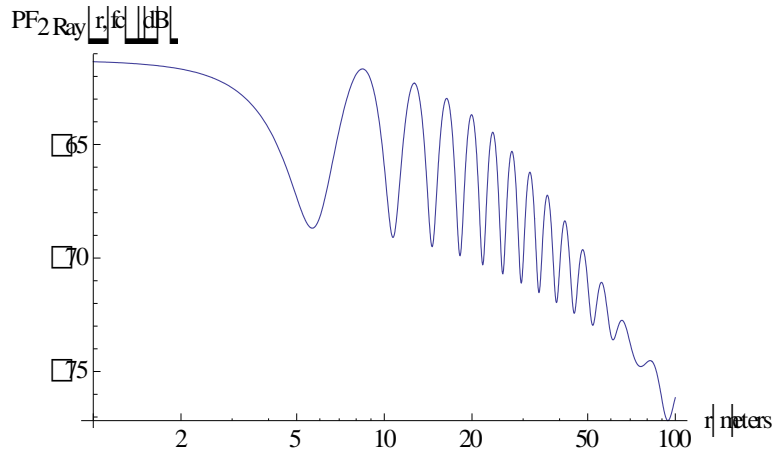
Figure F-2: Example Level Terrain Two-Ray Isotropic Median Path Spreading Factor

F.2.1.1.2 Sloping Terrain Two-Ray Isotropic Path Model

A more general purpose two-ray isotropic path model for use in some scenarios is one with sloping terrain between emitter and aircraft. The simpler two-ray level terrain model discussed in Section F.2.1.1.1 must be adjusted as shown in Figure F-3. The sloping terrain grazing angle, $\theta_{GRS}(r)$, as a function of the lateral separation radius, r, is derived in terms of known path parameters: R_{DIR}, H_E (as defined in level terrain case), terrain slope angle θ_S, and the aircraft height above the local terrain, h_A. While the triangles formed by the antennas, ray paths, and level terrain in Figure B-1 are right similar triangles, the associated triangles in Figure B-3 on sloping terrain are not right similar. Thus derivation of $\theta_{GRS}(r)$ will involve use of the Law of Sines.

Figure F-3: Sloping Terrain Two-Ray Path Model Geometry

The derivation of begins by applying the Pythagorean Theorem to four ground segments,

$$r^2 + h_S^2 = (Rs1 + Rs2)^2.$$

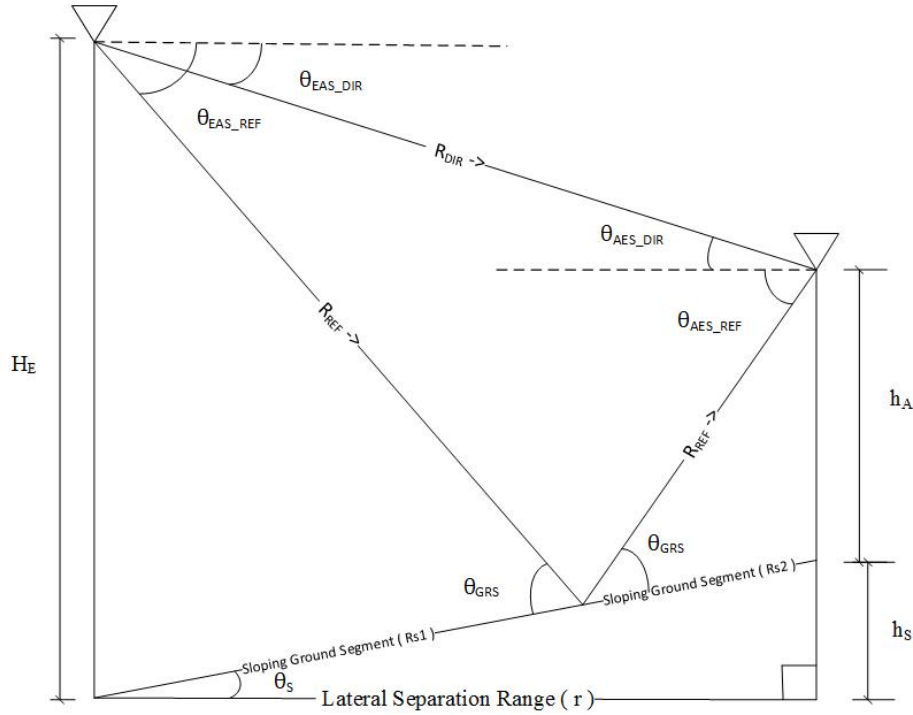Using the Law of Sines, the two sloping ground segments *Rs1* and *Rs2* can be defined in terms of ground slope and grazing angles and the closer of the emitter or aircraft height;

$$Rs1 = H_E \sin(\pi/2 - (\theta_{GRS}(r) - \theta_S))/ \sin(\theta_{GRS}(r)) \text{ and}$$
$$Rs2 = h_A \sin(\pi/2 - (\theta_{GRS}(r) + \theta_S)) / \sin(\theta_{GRS}(r)).$$

With a = $\pi/2$ and b = $(\theta_{GRS}(r) \pm \theta_S)$ used in the identity $sin(a - b) = sin(a)cos(b) - cos(a)sin(b)$, the relationships for Rs1 and Rs2 simplify to:

$$Rs1 = H_E \cos(\theta_{GRS}(r) - \theta_S) / \sin(\theta_{GRS}(r)) \text{ and}$$
$$Rs2 = h_A \cos(\theta_{GRS}(r) + \theta_S) / \sin(\theta_{GRS}(r)).$$

Applying the identity, $cos(a - b) = cos(a)cos(b) + sin(a)sin(b)$, to the expression for *Rs1* and the identity, $cos(a + b) = cos(a)cos(b) - sin(a)sin(b)$, to the expression for *Rs2*, then substituting both results back into the original Pythagorean Theorem expression of the four ground segments, and taking the square root of both sides of the expression yields:

$(r^2 + h_S^2)^{1/2} = \{H_E [\cos(\theta_{GRS}(r))\cos(\theta_S) + \sin(\theta_{GRS}(r))\sin(\theta_S)]$
$\qquad + h_A [\cos(\theta_{GRS}(r))\cos(\theta_S) - \sin(\theta_{GRS}(r))\sin(\theta_S)]\} / \sin(\theta_{GRS}(r)).$

Finally, applying the trigonometric relationship $h_s = r[\tan(\theta_S)]$ for the slope height above level terrain assumption at the aircraft nadir, and the identity, $\cos(a)/\sin(a) = 1/\tan(a)$, and performing algebraic simplifications the resulting expression is:

$$\theta_{GRS}(r) = \tan^{-1}\left(\frac{(H_E + h_A)\cos(\theta_S)}{r\sqrt{1+\tan^2(\theta_S)} - (H_E - h_A)\sin(\theta_S)}\right).$$

The direct path length, $R_{DIR,S}(r)$, needed for the sloping terrain two-ray path loss is determined by first noting that the aircraft antenna height above level terrain in Figure F-3 is given by $H_A(r) = h_A + r\tan(\theta_S)$. Then the level terrain expression, $R_{DIR}(r) = \sqrt{(H_A - H_E)^2 + r^2}$, after substitution becomes, on the sloping terrain, $R_{DIR,S}(r) = \sqrt{(h_A + r\cdot\tan(\theta_S) - H_E)^2 + r^2}$. The reflected ray path length, $R_{REF,S}(r)$, is determined from Law of Sines relations to be $R_{REF,S}(r) = (H_E + h_A)\cos(\theta_S)/\sin(\theta_{GRS}(r))$. With these revised sloping terrain parameter definitions, the remaining two-ray path loss factors can be determined from the same expression forms as in Section F.2.1.1.1.

Once $\theta_{GRS}(r)$ is determined, four elevation angles, θ_{EAS_DIR}, θ_{EAS_REF}, θ_{AES_DIR}, θ_{AES_REF}, can be derived for use to compute the antenna gains in the scenario. By definition, $\theta_S \geq 0$, $\theta_{GRS} > 0$, $\theta_{EAS\_REF} < 0$, and $\theta_{AES\_REF} < 0$. It is also true that $\theta_{AES\_DIR} = -\theta_{EAS\_DIR}$. However, the direct ray elevation angles θ_{EAS_DIR} and θ_{AES_DIR} can be either positive or negative depending on the relative heights of H_E vs. $(h_A + h_S)$. The emitter direct path elevation angle, $\theta_{EAS\_DIR}(r)$, for sloping terrain is given by: $\theta_{EAS\_DIR}(r) = -\tan^{-1}\{ [(H_E - h_A) - r\tan(\theta_S)] / r\}$ for $H_E > (h_A + h_S)$ and $r \leq r_1$. Expressions for the two reflected path elevation angles are $\theta_{EAS\_REF}(r) = -(\theta_{GRS}(r) - \theta_S)$ and $\theta_{AES\_REF}(r) = -(\theta_{GRS}(r) + \theta_S)$.

F.2.1.1.3 Two-Ray Path Model Aspects for Directive, Dual-Polarization Source Antennas

Although RFI sources in some scenarios can be modelled with vertically polarized emissions, other scenarios call for the use of relatively directive base station source antennas that transmit a ±45° cross-polarized signal. This type of signal is modelled for aviation GPS RFI analyses as a dual vertically- and horizontally-polarized signal. Each polarization component is assumed to contain half the total emission power. This signal type causes increased complexity especially in the two-ray path loss segment. Compared to the formulation in Section F.2.1.1.1, one extra parameter needed in the two-ray zone is the horizontal-polarized reflection coefficient expressed as

$$\rho_h(r, f_c) = \frac{\sin(\theta_{GR}(r)) - \sqrt{(\varepsilon_r - i\cdot x(f_c)) - \cos^2(\theta_{GR}(r))}}{\sin(\theta_{GR}(r)) + \sqrt{(\varepsilon_r - i\cdot x(f_c)) - \cos^2(\theta_{GR}(r))}}.$$

Without accounting yet for any source antenna directivity, the associated horizontal polarized

multi-path field factor is expressed in similar form to Section F.2.1.1.1 as

$$P_h(r, f_c) = 1 + \left(\frac{R_{DIR}(r)}{R_{REFL}(r)} \right) \rho_h(r, f_c) \cdot e^{-i\phi(r)} \text{; where the direct and reflected}$$

ray path lengths, $R_{DIR}(r)$ and $R_{REFL}(r)$, and the reflected ray path relative phase lag, $\phi(r)$, are the same as for vertical polarization.

To properly account for the source and receive antenna pattern effects on the reflected ray relative strength compared to the direct ray at the receive antenna, the ray angles need to be determined. The ray angle expressions in Section F.2.1.1.2 above can be adapted as needed for flat or sloping ground (flat ground has $\theta_S=0$). The source side ray angles, once determined, are then transformed as in Appendix G into the tilted beam coordinates and used to determine the source antenna power gain in the direct and reflected ray directions. The source antenna power gain in any direction is assumed to be independent of polarization. The receive side ray angles are used with the receive antenna equations in Section 4.1.2 to determine the receive antenna power gain to both direct and reflected vertical and horizontal polarization ray components.

The source transmit direct- and reflected-ray power gain values, Gtd(r) and Gtr(r), are then formed into a transmit voltage gain ratio, $VGtrd(r) = \sqrt{\frac{Gtr(r)}{Gtd(r)}}$ (same value for both v-pol. and h-pol.). Similarly the receive direct- and reflected-ray vertical- and horizontal-polarized power gain values, $Grd_v(r)$, $Grr_v(r)$, $Grd_h(r)$, and $Grr_h(r)$ are formed into receive voltage gain ratios $VGrd_v(r) = \sqrt{\frac{Grr_v(r)}{Grd_v(r)}}$ and $VGrd_h(r) = \sqrt{\frac{Grr_h(r)}{Grd_h(r)}}$. These voltage gain ratios are used to modify the multi-path field factor and yield the directive multi-path factors:

$$Pd_h(r, f_c) = 1 + VGtrd(r) \cdot VGrd_h(r) \cdot \left(\frac{R_{DIR}(r)}{R_{REFL}(r)} \right) \rho_h(r, f_c) \cdot e^{-i\phi(r)} \text{ and}$$

$$Pd_v(r, f_c) = 1 + VGtrd(r) \cdot VGrd_v(r) \cdot \left(\frac{R_{DIR}(r)}{R_{REFL}(r)} \right) \rho_v(r, f_c) \cdot e^{-i\phi(r)}.$$

Since the voltage gain ratios are less than unity, their effect in the above expressions is to diminish the magnitude of the fluctuating component in the multi-path field factor at a given radius compared to the initial value without the directivity correction.

When these modified multi-path field factor expressions are substituted into the basic two-ray path factor Equation (F-1), the resulting vertical and horizontal polarization path factors are:

$$PF_{2Ray,v}(r, f_c) = \left(\frac{\lambda_c(f_c)}{4\pi} \cdot \frac{|Pd_v(r, f_c)|}{R_{DIR}(r)} \right)^2 \text{ and } PF_{2Ray,h}(r, f_c) = \left(\frac{\lambda_c(f_c)}{4\pi} \cdot \frac{|Pd_h(r, f_c)|}{R_{DIR}(r)} \right)^2.$$

When the effects of a directive dual-polarized base station source antenna are incorporated, as discussed above, an additional complication occurs in the determination of the outer radius limit, r_1, for the two-ray path model. Investigation of the path factor expressions indicates that at any

14

particular given radius the horizontal and vertical path factors may have different values. However, there are certain radius values at which the path factors are equal, a feature which is necessary for the starting radius of the mid-range path model zone.

For sources emitting only vertically polarized signals, the r_1 value is the radius at which the complex vertical polarization reflection coefficient, $\rho_v(r, f_C)$, is purely imaginary (phase of ρ_v = -90°) very near the minimum magnitude. At this radius, the grazing angle for the reflecting surface is at a critical value, θ_{CRIT}, that depends on only the surface electrical parameters. With the critical grazing angle known along with antenna heights, the expression for grazing angle in Section F.2.1.1.2 can be inverted to solve for the associated vertical polarization radius, r_{1v}. The strategy for the dual polarization radius, r_{1d} is to determine from the path factor equations, the first radius beyond r_{1v} at which the vertical and horizontal polarization path factors are equal (usually a few centimeters beyond r_{1v}). The two-ray path factor value at r_{1d} is used in the formula for the mid-range path factor.

F.2.1.2 Medium Range Path Segment Erceg-Greenstein Isotropic Model

Median path propagation models were initially developed for cellular mobile phones at lateral separation ranges beyond 1 km and out to 20 km. This left a need for some type of model to cover ranges from 100 meters to 1 km. In the mid-1990's this need was met by researchers from ATT Laboratories who developed a mid-range model that came to be known as the Erceg-Greenstein model [4]. Their model pertains to ranges from 100 meters to 8 km with base station antenna heights between 10 and 80 meters and a mobile unit antenna height of 2 meters. The model was developed for suburban environments using three different terrain categories to make it more flexible. An operating frequency of 1.9 GHz was used in developing the model although extrapolations to other frequencies are possible. In the Erceg-Greenstein model the median path loss is proportional to $(r/r_o)^\gamma$ where r_o is usually taken to be 100 meters. The loss exponent γ changes with terrain type but is greater than 2 meaning that the path loss is more severe than that associated with a free space model. The classic Erceg-Greenstein model has the actual path loss increasing slightly as the range increases, however the modified model used in this analysis holds this constant with range.

The modified Erceg-Greenstein model has a median isotropic path spreading factor (in algebraic terms) given by:

$$PF_{EG,\text{mod}}(r, f_c) = 1/\left[A^2(f_c) \cdot \left(\frac{r}{r_0}\right)^{a - b \cdot H_A + {}^{c_{EG}}\!/\!H_A} \right] \text{, for } r_1 \le r < r_2 \tag{F-2}$$

In Equation (F-2), $A(f_c) = 4\pi r_0/\lambda_c(f_c)$ with $r_0 = 100$ m. Values for constants a (3.6), b (0.005), and c_{EG} (20.0) are chosen to represent the area in the vicinity of an airport (terrain model C (flat, light tree cover)). The break points r_1 and r_2 are described in Section F.2.2.2. Figure F-4 shows a

15

sample median path spreading factor produced by the Erceg-Greenstein model at f_c = 1575.42 MHz.
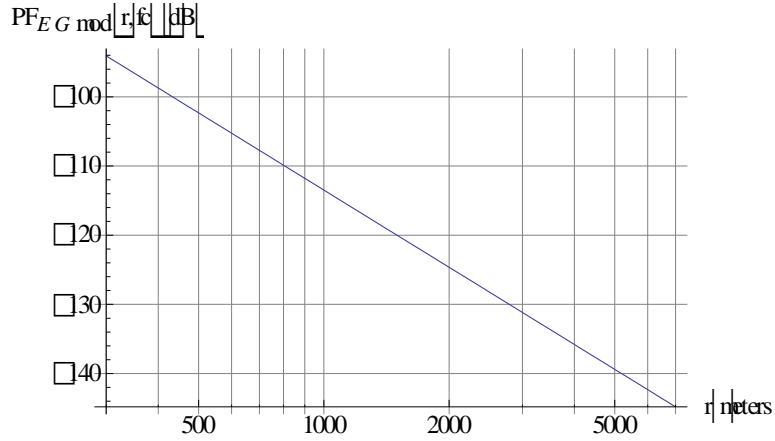

Figure F-4: Example Erceg-Greenstein Isotropic Median Path Spreading Factor

F.2.1.3 Medium Range Path Segment Exponential Fit Isotropic Model

For cases when $H_A > 80$ m (e.g., the FAF Waypoint) or $H_E > 2$ m, an exponential, constant slope blending function is used. The function's constant exponent and intercept point are chosen to achieve continuity at either end with the short- and long-range path loss functions given appropriate segment breakpoints, r_1 and r_2. For handset interference sources, the exponential constant slope path loss model is given by:

$$PF_{\exp fit1}(r, f_c) = PF_{2Ray}(r_1, f_c)(r / r_1)^{-\Gamma_1(f_c)} \qquad \text{(F-3)}$$

The exponent is expressed as:

$$\Gamma_1(r_1, r_2, f_c) = [\alpha(f_c) + \beta_c \cdot log_{10}(r_2 / 1000) + log_{10}(PF_{2Ray}(r_1, f_c))] / log_{10}(r_2 / r_1)$$

where $r_2 < 20,000$ m, and $\alpha(f_c)$, and β_c, are parameters associated with the Hata-Okumura model discussed in Section F.2.1.4.

For base station interference sources there is a single exponential constant slope model given in similar form but with different parameter values by

$$PF_{\exp fit1}(r, f_c) = PF_{2Ray}(r_1, f_c)(r / r_1)^{-\Gamma_1(r_1, r_2, f_c)} \qquad \text{(F-4)}$$

where $\Gamma_1(r_1, r_2, f_c)$ has the same form as in Equation (F-3).

F.2.1.4 Long Range Segment Path Isotropic Model

16

For propagation over "flat earth" terrain from RFI sources at distances beyond 1 km from the aircraft antenna, the Hata-Okumura median path propagation model is used. It was originally developed for predicting UHF cellular mobile telephone propagation at distances beyond 1 km from the base station for three terrain types: urban areas, suburban areas and open areas. In this Report the suburban terrain parameters are used to represent the environment around a large metropolitan airport. As with the Erceg-Greenstein model, the Hata-Okumura path median spreading factor is inversely proportional to $(r/r_o)^\gamma$ but in this case r_o is set to 1000 meters. The exponent γ varies with antenna height as well as range and for distances beyond 20 km it also varies with operating frequency. With the ITU-R extension to the original model, it is usable to ranges of 100 km. Figure F-5 shows the median path spreading factor generated by the Hata-Okumura model for an operating frequency f_c = 1575.42 MHz.
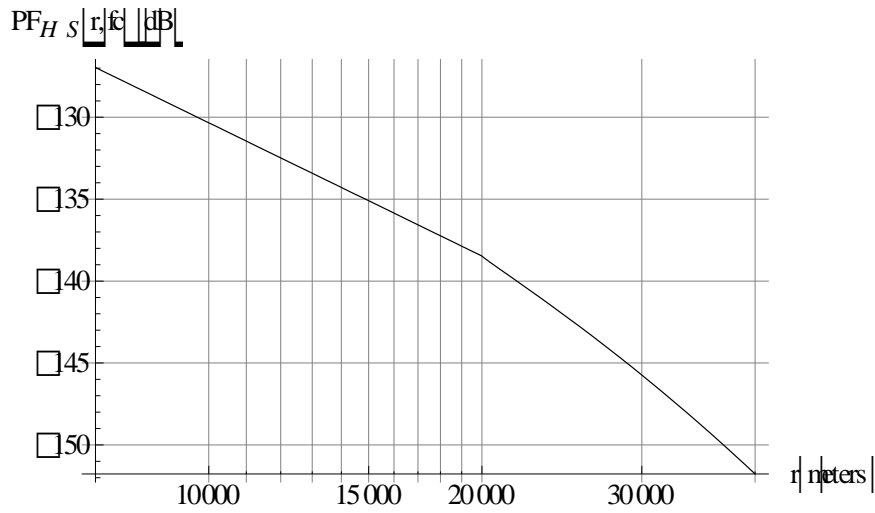
Figure F-5: Example Hata-Okumura Median Isotropic Path Spreading Factor

The Hata suburban median isotropic path spreading factor (in algebraic terms) is given by:

$$PF_{HS}(r, f_c) = 10^{\left(K_{sp}(r)/10-\left(\alpha(f_c)+\beta_c\cdot(\log(r/1000))^{F(r,f_c,H_A)}\right)\right)} \qquad \text{(F-5)}$$

for $r_2 \le r \le R_0$ as appropriate where $K_{sp}(r)$ (in dB) denotes a range-dependent slope correction factor (0 dB for "flat-earth"),

$$\alpha(f_C) = 0.1\left[69.12+26.16\cdot\log(f_C)-2\cdot\log^2\left(f_C/28\right)-13.82\cdot\log(H_A)-3.2\cdot\log^2(11.75H_E)\right],$$

$$\beta_C = 0.1\cdot\left[44.9-6.55\cdot\log(H_A)\right] \text{ and } F(r,f_c,H_A)= 1, \text{ r} \le 20 \text{ km, or:}$$

$$F(r,f_c,H_A) = 1+\left[0.14+1.87\cdot10^{-4}(f_c)+\frac{1.07\cdot10^{-3}H_A}{\left(1+7\cdot10^{-6}H_A^2\right)}\right](\log_{10}(r/2\cdot10^4))^{0.8} \text{ for r>20km.}$$

17

For the certified aviation equipment analyses in this report, the Hata "base station" antenna height, H_A, in the long range model segment is assumed to be the greater of the aircraft or interference source antenna height. The Hata "mobile station" height, H_E, is the lesser of the two antenna heights. In addition, the propagation is assumed to be reciprocal.

When applying the Hata suburban median isotropic spreading factor to certain discrete base station scenarios on irregular, sloping terrain, it may be necessary to apply a non-zero slope correction factor $K_{sp}(r)$ to the model. This correction factor, derived from the work of Okumura [2], was chosen as the principal factor and other smaller ones were considered negligible. These terrain slopes are averages computed over a significant distance (Okumura suggests distances of 5-10 km), The correction as given in [2] shows that positive (upward, away from the aircraft) slopes reduce the path loss while negative (downward) slopes yield increased path loss. Steep slopes produce increased correction whether they are positive or negative. The correction is given in dB as a function of slope angle in milliradians and distance in kilometers. Correction factor data points presented graphically in [[2], (Figure 34)] have been extracted and fit with an equation for ease of use. The Okumura data points and fit equations for several distances (10, 30 , 60 km) are plotted in Figure F-6. The fit equation $K_{sp}(\theta, d)$ in dB as a function of slope angle θ (milliradians) and distance d (m) is:

$$Ksp(\theta,d) = \begin{cases} a_1 + (a_2 + a_3(d/1000))\theta - (a_4 + a_5(d/1000))\theta^2, & \theta < 0 \\ b_1 + (b_2 + b_3(d/1000) + b_4(d/1000)^2)\theta - (b_5 + b_6(d/1000) + b_7(d/1000)^2)\theta^2, & 0 \le \theta \end{cases}$$

where $a_1 = 0.052857$, $a_2 = -0.105285$, $a_3 = 0.0288714$, $a_4 = 0.0027143$, $a_5 = 7.14265 \times 10^{-5}$, $b_1 = 0.018567$, $b_2 = 0.01394$, $b_3 = 0.0193213$, $b_4 = -9.1533 \times 10^{-5}$, $b_5 = -1.94286 \times 10^{-3}$, $b_6 = 4.25715 \times 10^{-4}$, and $b_7 = -3.14287 \times 10^{-6}$.
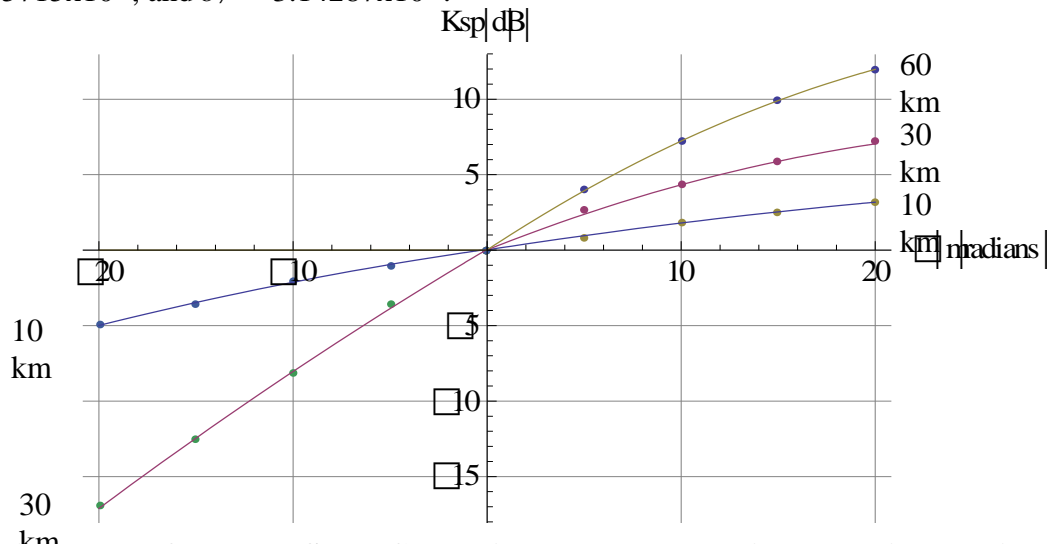

Figure F-6: Okumura Slope Correction Factor Data Points and Fit Equations

In applying this factor, it proved useful to divide the terrain into angular sectors about the aircraft nadir point. These sectors were chosen so as to provide as much terrain uniformity as possible

18

when traversing outward from aircraft nadir along any given radial line. Within a given sector, an average ground height was determined extending to some appropriate radial distance from aircraft nadir followed by a slope determination, if one exists beyond such distance.

F.2.1.5 Free Space Path Isotropic Model

For aircraft antenna heights generally greater than 550 meters and certain special cases below 550 m, there is predominately a clear line of sight to all RFI sources other than ground based mobile sources whose interference impact has been shown to be negligible at these altitudes from previous analysis [5]. In such cases, a free space path propagation model is most appropriate. Free space propagation is the most basic model in which the path isotropic spreading factor is proportional to the inverse square of the separation range. This is a deterministic model with no associated probability distribution. Hence the path spreading factor can be exactly determined once the range between GPS antenna and interfering source is known. The free space isotropic spreading factor is given by:

$$PF_{FSP}(r, f_c) = (c / 4\pi R_{DIR}(r) f_c)^2 \qquad \text{(F-6)}$$

where, as previously defined, $R_{DIR}(r) = \sqrt{(H_A - H_E)^2 + (r)^2}$ and c is the speed of light in vacuum.

F.2.2 Single Path Probabilistic Propagation Model

F.2.2.1 Single Path Probabilistic Propagation Model Basic Aspects

The probabilistic propagation channel is typically modeled as a product of a slow fading process (log-normal power distribution) and a fast fading process [3]. The fast fading portion may be either "flat" (maximum delay spread, τds << 1/W, where W=interference signal base-bandwidth) or it may be frequency selective. The simplest case to model is the case where the fast fading is flat. In that case, the received interference from a single emitter, $\gamma(t)$, may be written as $\gamma(t) = \text{Re}\{\alpha(t)\beta(t)s_E(t)\}$ where Re{ } denotes the real part, while α, β, and s_E are independent complex random processes. The term $\alpha(t)$ denotes the fast fading process, $\beta(t)$ the slow fading component, and $s_E(t)$ the portion of the interfering emitter signal arriving at the GPS receiver antenna at center frequency f$_c$, ($s_E(t) = u(t)exp(i2\pi f_c t)$, where u(t) is complex).

In the propagation model, α has independent normally distributed real and imaginary parts each with mean values that may be different from zero to account for the presence of a strong line-of-sight component at shorter ranges. Thus, $|\alpha(t)|^2$, has a non-central Chi-squared distribution with two degrees of freedom. Although $|s_E(t)|^2$ is a random process, to avoid dealing with those statistics the instantaneous power associated with the single source emission (unwanted emission in this analysis) is deemed to be constant as in most of the literature on path loss models. In the

19

model used for this analysis, power was assumed to be $2P_oW$ watts; i.e., an rms power spectral density of P_0 watts/Hz over a signal base-bandwidth, *W*. Under these assumptions, the random process $\left|\overline{\beta}(t)s_E(t)\right|^2$ is log-normally distributed and the received single emitter interference power $\left|\gamma(t)\right|^2$ becomes the product of two random variables, one having a non-central Chi-squared distribution while the other is log-normally distributed.

For a scenario with frequency selective fast fading, it is shown [6] that γ can be approximated as the sum of several independent flat fading processes. Thus, γ(t) is written as

$\gamma(t) = (\sum_{l=0}^{L-1} \overline{\alpha}_l(t)s_E(t-\tau_l))\overline{\beta}(t)$; where the channel parameter, L, is the number of resolvable fast fading paths and the τ_l are chosen such that $E[s_E(t-\tau_i)s_E(t-\tau_k)]=0$ for $k \neq l$. Then the instantaneous power, $\left|\gamma(t)\right|^2$, becomes $\left|\gamma(t)\right|^2 = (\sum_{l=0}^{L-1}\left|\alpha_l(t)\right|^2 \left|s_E(t-\tau_l)\right|^2)\left|\beta(t)\right|^2$..

Using the same assumption as above regarding the single emitter power, the received single emitter power density may be written as:

$$\left|\gamma(t)\right|^2_{density} = \underbrace{(\sum_{l=0}^{L-1}\left|\overline{\alpha}_l(t)\right|^2)}_{FastFading}\overbrace{\left|\overline{\beta}(t)\right|^2 P_o}^{SlowFading}.$$

This form for the received single emitter power density is the most flexible and is the form adopted in the present model. The slow fading portion is log-normally distributed with parameters μ and σ while the fast fading process has a non-central Chi-squared distribution with 2L degrees of freedom and parameters ρ_o and ψ_o.

The propagation model assumes each of these parameters to be range dependent hence we may express the received single emitter power spectral density as:

$$P_E(r) = \Sigma(r)\Omega(r),$$

where Σ denotes the fast fading component and Ω the slow fading. Note all time dependence has been dropped as all of the constituent processes are assumed to be stationary.

F.2.2.2 Median Path Segment Propagation Parameters and Segment Break Points

The propagation environment is modeled probabilistically with a range and height-dependent median path loss to an individual RFI source. Based on a flat-earth assumption, a continuous median path spreading factor function, *PF(r,f$_c$)*, is generated by combining three range segment models taken in part from mobile radiotelephone propagation studies. The long range segment model (*r* typically greater than 1 km) is based on the Hata-Okumura model [[1], (suburban

20

case)]. Two options are used for the mid-range segment model depending on aircraft antenna height: Erceg/Greenstein ($H_A \leq 80$ m), and an exponential constant slope blend models for $H_A > 80$ m. The short range segment model (ranges less than a few hundred meters) is the classic two-ray with concrete as the single reflecting surface. Reciprocity is assumed to hold as it relates to the probabilistic modeling of the propagation channel. The median path isotropic spreading factor is then expressed for handset interference sources as:

$$PF(r,f_c) = \begin{cases} PF_{2Ray}(r,f_c), & 0 \leq r < r_1 \\ PF_{EG,mod}(r,f_c) \, or \, PF_{\exp fit1}(r,f_c), & r_1 \leq r < r_2 \\ PF_{HS}(r,f_c), & r_2 \leq r \leq R_o \end{cases} \tag{F-7}$$

while, for base station interference, sources:

$$PF(r,f_c) = \begin{cases} PF_{2Ray}(r,f_c), & 0 \leq r < r_1 \\ PF_{\exp fit1}(r,f_c), & r_1 \leq r < r_2 \\ PF_{HS}(r,f_c), & r_2 \leq r \leq R_o \end{cases} \tag{F-8}$$

For handset interference sources, the following set of guidelines was used for the isotropic median path loss break points.

- At short ranges a two-ray median path propagation model is used up to the range r_1 where the two ray and Erceg-Greenstein and/or exponential fit models join. This break point varies with aircraft antenna height and is computed so as to produce a continuous path spreading factor function. When the Erceg-Greenstein model is used, this break point is usually near 100 meters. When the exponential fit model is used, as in the FAF scenario, this break point is near where the two ray vertically polarized component reflection coefficient is at minimum magnitude.

- The second segment uses the Erceg-Greenstein model, if applicable, up to the point r_2 where it intersects the Hata-Okumura median path propagation model. When the exponential fit model is used, to preserve some consistency with the lower height cases, the mid-range segment inner radius, r_1, is set to give a two-ray segment grazing angle, $\theta_{GR}(r)$ such that $\tan(\theta_{GR}(r_1)) \cong 0.5$. Some slight adjustment of the r_1 value may be done, if needed, to reduce the spreading factor slope change at the junction with the two-ray segment. In a similar way, the outer radius, r_2, is set to give an elevation angle from the source to the receive antenna, $\varepsilon(r)$, such that $\tan(\varepsilon(R_2)) = 1/14$ (i.e.; $\varepsilon(r_2) \cong 4°$). An exponential fit mid-range segment is also used for very low aircraft antenna heights (e.g. < 10 m). In these instances, r_1 is set for the radius at which the two ray vertically polarized component reflection coefficient is at minimum magnitude. The outer radius, r_2, is set at 1 km (the minimum applicable radius for the Hata model).

- Beyond r_2 the Hata-Okumura suburban median path propagation model is used.

- The radio horizon is given by $R_0 = 4124.12\left(\sqrt{H_A} + \sqrt{H_E}\right)$ (all dimensions in meters).

21

For base station interference sources, two basic breakpoints were defined as follows.

- At short ranges a two-ray median path propagation model is used up to the radius r_1 where the vertically polarized component reflection coefficient is at minimum magnitude. This break point varies with aircraft antenna height.
- Beyond r_1, the median path spreading factor is modelled as an exponential constant-slope blending function out to radius, r_2 (details in Section F.2.1.3), where it intersects the Hata-Okumura long range segment.
- Beyond r_2, the Hata-Okumura suburban median path propagation model is used.

F.2.2.3 Single Path Probabilistic Propagation Slow Fading Parameters, μ and σ

With the median path spreading factor, $PF(r,fc)$, defined for any individual source, the single-path slow fading parameter, $\mu(r,f_c)$, can be written in general as:

$$\mu(r, f_c) = ln[P_{xmit} \cdot G_{xmit}(\theta_{elev}(r), \phi_{az}) \cdot PF(r, f_c) \cdot G_{rcv}(\zeta_{elev}(r))]$$

This expression can be rewritten and further simplified to:

$$\mu(r, f_c) = \ln(P_0) + \mu'(r, f_c) \qquad\qquad \text{(F-9)}$$

where $\mu'(r, f_c) = ln[G_{norm}(\theta_{elev}(r), \phi_{az}) \cdot PF(r, f_c) \cdot G_{rcv}(\zeta_{elev}(r))]$ is a unitless mean fading factor, $ln()$ denotes natural logarithm and P_0 ($P_{xmit}\ \eta\ G_0$) is the RFI source effective isotropic radiated power (EIRP) or power spectra density at the transmit beam center (Appendix G.1). The antenna gain factors are: $G_{xmit}(\ )$ the interfering emitter antenna gain, $\theta_{elev}(r)$ the transmit elevation angle, and ϕ_{az} the azimuth angle toward the receive antenna, $G_{norm}()$ is the normalized transmit gain ($G_{xmt}(\ )/\eta\ G_0$), $G_{rcv}(\ )$ the receive antenna gain, and $\zeta_{elev}(r)$ the receive elevation angle toward the interfering emitter antenna. Note that $G_{norm}(\ )$ is set to unity independent of angle for handset emitters.

The single-path slow fading parameter, σ, is generally range dependent and hence is written as σ(r). Its range dependence varies with the interference scenario, i.e., whether the interference is from a base station source or from a handset source. For a handset source, a linear transition region is used between the very short range condition and the onset of significant scattering (chosen to be the mid-range segment inner radius) [5]. The transition region starting point is chosen as the radius, r_s, such that the elevation angle from the source to the receive antenna, $\varepsilon(r_s)$ is 45° (i.e.; $r_s = H_A\text{-}H_E)^2$. The transition end point is the radius, r_1, previously defined in Section B.2.2.2 for handset sources. For convenience, the single-path standard deviation, $\sigma(r)$, is

---

[2] For handset scenarios when the aircraft antenna height is very low (e.g. < 10 m), the transition region start point radius, r_s is set equal to r_1 and the end point radius is r_2.

described in decibel terms. Similar to the strategy used in [B-5], the short-range and full-scattering $\sigma(r)$ limits used in this analysis are 0.5 dB and 6.4 dB[3], respectively. Thus:

$$\sigma_{dB}(r) = \begin{cases} 0.5, & 0 \le r \le r_s \\ 0.5 + 5.9\dfrac{(r - r_s)}{(r_1 - r_s)}, & r_s < r \le r_1 \\ 6.4, & r > r_1 \end{cases} \qquad \text{(F-10)}$$

Note that $\sigma(r) = (Ln(10)/10)\sigma_{dB}(r)$.

For base station sources the method used in [5] is modified somewhat in this analysis. Instead of a stepped or polynomial function for the radial variation, a linear function for $\sigma_{dB}(r)$ similar to that used for handsets is used. A standard deviation for "light shadowing" is given as 0.5 dB, which is similar to the handset scenario is assumed for short distances ($< r_1$), in agreement with Loo's result [7]. Beyond the r1 breakpoint, $\sigma_{dB}(r)$ rises linearly in r up to 6.4 dB at the r_2 breakpoint (start of Hata Okumura path segment). (See Section F.2.2.2 for base station sources). Thus:

$$\sigma_{dB}(r) = \begin{cases} 0.5, & 0 \le r \le r_1 \\ 0.5 + 5.9\dfrac{(r - r_1)}{(r_2 - r_1)}, & r_1 < r \le r_2 \\ 6.4, & r > r_2 \end{cases} \qquad \text{(F-11)}$$

F.2.2.4 Single Path Probabilistic Propagation Fast-Fading Parameters, L, ψ_0, ρ_0

For handset interference sources, the unitless diffuse scattering parameter[4], $\psi_0(r)$, is specified in terms of a product with channel parameter, L, as:

---

[3] The 6.4 dB standard deviation value used in the Log-Normal slow fading component of the certified avionics analysis model comes from measurements made around London by M.F. Ibrahim and J.D. Parsons [3]. This 6.4 dB was applicable for London type terrain and measured at a frequency of 900 MHz. As shown in [2], the standard deviation does not change much with frequency, so a 6.4 dB standard deviation was also assumed for the certified avionics analysis around 1531 MHz. In reality the standard deviation may be around 0.5 dB greater at 1531 MHz than at 900 MHz.

[4] For handset scenarios when the aircraft antenna height is very low (e.g. < 10 m), the fast fading parameters transition region start point radius, r_s is set equal to r_1 and the end point radius is r_2.

$$2L\psi_0(r) = \begin{cases} 0.1, & 0 \le r \le r_s \\ 0.1 + 0.9\dfrac{(r - r_s)}{(r_1 - r_s)}, & r_s < r \le r_1 \\ 1.0, & r > r_1 \end{cases} \qquad \text{(F-12)}$$

Note in Equation (F-12) that the composite parameter $2L\psi_0(r)$ is non-zero at short ranges ($< r_s$). This aspect provides consistency with the assumption that $\sigma(r)$ is also non-zero over the same ranges. This result associates the small $\sigma(r)$ value with a small amount of diffuse scattering in the propagation loss at short ranges. For this analysis $L = \lceil \tau_{DS}W \rceil$ where the operator $\lceil \; \rceil$ implies rounding up the operand to the next integer, τ_{DS}, is the spread in channel delay time, and W is the channel baseband bandwidth. Thus L denotes the number of resolvable paths associated with the fast fading component (see Section F.2.2.1).

In a similar manner then have for base station interference sources:

$$2L\psi_0(r) = \begin{cases} 0.1, & 0 \le r \le r_1 \\ 0.1 + 0.9\dfrac{(r - r_1)}{(r_2 - r_1)}, & r_1 < r \le r_2 \\ 1.0, & r > r_2 \end{cases} \qquad \text{(F-13)}$$

For handset sources the unitless line-of-sight parameter, $\rho_0(r)$, is specified as:

$$\rho_0^2(r) = \begin{cases} 1.0, & 0 \le r \le r_s \\ 1.0 - \dfrac{(r - r_s)}{(r_1 - r_s)}, & r_s < r \le r_1 \\ 0, & r > r_1 \end{cases} \qquad \text{(F-14)}$$

Again, for the base station scenario using the break point definitions given in Section F.2.2.2:

$$\rho_0^2(r) = \begin{cases} 1.0, & 0 \le r \le r_1 \\ 1.0 - \dfrac{(r-r_1)}{(r_2-r_1)}, & r_1 < r \le r_2 \\ 0, & r > r_2 \end{cases} \qquad \text{(F-15)}$$

F.3 Aggregate Propagation Effects Computation Methods

Aggregate propagation effects are treated differently depending upon whether the interference sources are randomly distributed or have discrete known locations. Although there are exceptions, most handset sources use randomly distributed sources while base station sources have known locations. For uniformly-distributed, randomly-located interference sources, it is shown ([8], [9]) that once the single path interference characteristics have been determined, it is possible to determine the mean power, standard deviation, and cumulative probability distribution associated with aggregate received interference power. The same holds true for sources that have discrete known locations although the method used to determine mean power and cumulative probability distribution is different.

F.3.1 Randomly-Located Source Statistics

F.3.1.1 Randomly-Located Source Mean Aggregate Interference Power

As noted, for uniformly-distributed, randomly-located interference sources, once the single path interference characteristics have been determined, it is possible to determine the mean power, standard deviation, and cumulative probability distribution associated with aggregate received interference power by the "Analytic Statistical" method. For example, the aggregate mean power is given by:

$$\overline{P_I} = P_o \overline{n} \int_0^{R_o} (2L\psi_o(r) + \rho_o^2(r)) \exp[\sigma^2(r)/2 + \mu'(r, f_c)] f(r) dr \qquad \text{(F-16)}$$

where $\overline{n}$ is the mean number of active emitters (Poisson-distributed) within the radio horizon radius, R_0, and $f(r)$ is the radial location probability density function for uniformly distributed emitters. (More details in [9]). The expression, $(2L\psi_o(r) + \rho_o^2(r))$, is the first moment (mean) of the non-central Chi-squared fast-fading distribution and the expression, $\exp[\sigma^2(r)/2 + \mu'(r, f_c)]$, is the log-normal slow-fading distribution unitless mean.

F.3.1.2 Randomly-Located Source Aggregate Interference Power Standard Deviation

For randomly-located interference sources, the normalized standard deviation (normalized by the aggregate mean power) has been determined as in [9] by:

25

$$\sigma_I = P_0 \cdot \sqrt{n \int_0^{R_o} ((2L\psi_o(r) + \rho_o^2(r))^2 + 4L\psi_o^2(r) + 4\psi_o(r)\rho_o^2(r))exp[2\mu'(r,f_c) + 2\sigma^2(r)]f(r)dr \, / \, \overline{P_I}} \qquad \text{(F-17)}$$

where the parameters L, μ, σ, ψ$_o$, and ρ$_o$ are as defined previously.

F.3.1.3 Randomly-Located Source Aggregate Interference Power Probability Distribution

Following the methodology described in [9] for randomly-located sources, the characteristic function associated with the normalized aggregate interference power is expressed as:

$$C(\tau) = \exp[-\overline{n}(1 - \phi(\tau))] \qquad \text{(F-18)}$$

where $\phi(\tau) = E[\exp(i\tau P_E(r) / \overline{P_I})]$, i.e., $\phi(\tau)$ is the characteristic function of the interference from a single emitter normalized by the mean aggregate interference power.

It is shown in [B-9], after some manipulation it is possible to write:

$$\phi(\tau) = \int_{-\infty}^{\infty} \int_0^{R_o} (1/\sqrt{\pi})\Phi(\tau, y, r) f(r) Exp(-y^2) dr dy \; ; \text{ where}$$

$$\Phi(\tau, y, r) = [1 / (1 - 2i\tau\psi_o(r)\Gamma(r, f_c) \exp(\sqrt{2}\sigma(r)y))]^L \exp[i\tau\Gamma(r, f_c) \exp(\sqrt{2}\sigma(r)y)\rho_o^2(r) / (1 - 2i\tau\psi_o(r)\Gamma(r, f_c) \exp(\sqrt{2}\sigma(r)y))]$$

and $\Gamma(r, f_c) = P_o \cdot G_{norm}(\theta_{elev}(r), \phi_{az}) \cdot PF(r, f_c) \cdot G_{rcv}(\zeta_{elev}(r)) / \overline{P_I}$

Then as in [10], the K-point Hermite-Gauss quadrature method with weights w_k and nodes y_k may be used to write:

$$\phi(\tau) \approx \sum_{k=1}^{K} (w_k / \sqrt{\pi}) \int_0^{R_o} \Phi(\tau, y_k, r) f(r) dr \qquad \text{(F-19)}$$

A value of 65 has been used for K to obtain very good accuracy in Equation (F-19).

Finally using Equation (F-18), we obtain the desired cumulative distribution function for the random variable $P_I / \overline{P_I}$ as in [11] by the following:

$$\Pr(P_I / \overline{P_I} > z) = 1 - (1/(2\pi)) \lim_{A \to \infty} \int_{-A}^{A} ((1 - \exp(-i\tau z)) / (i\tau)) C(\tau) d\tau + (1/2)\exp(-\overline{n}) \qquad \text{(F-20)}$$

for $z > 0$.

In those instances where randomly-located handsets are considered and where there is an already established level of unwanted interference from existing baseline sources, the procedure below may be used to determine the cumulative distribution function for the total aggregate interference.

Let $P_{I_1} / \overline{P_{I_1}}$ denote the normalized aggregate interference from existing baseline sources and $P_{I_2} / \overline{P_{I_2}}$ that from the new handset sources. Also let $\overline{n} = \overline{n_1} + \overline{n_2}$ where $\overline{n_1}$ and $\overline{n_2}$ are the mean number of active emitters within the radio horizon associated with existing baseline sources and new handsets, respectively. The mean number of active emitters may be computed as described in [9] using parameters applicable to either existing sources or new handsets. The characteristic function $C_1(\tau)$ associated with existing baseline sources is then given by:

$$C_1(\tau) = Exp[-\overline{n_1}(1 - \phi_1(\overline{P_{I_1}}\tau / (\overline{P_{I_1}} + \overline{P_{I_2}})))]$$

where $\phi_1(\bullet)$ is the normalized single emitter interference characteristic function determined using the methodology described above with the parameters provided in [9]. The function $\phi_1(\bullet)$ must be computed for whatever flight scenario is applicable (see, for example, [9]).

Similarly,

$$C_2(\tau) = Exp[-\overline{n_2}(1 - \phi_2(\overline{P_{I_2}}\tau / (\overline{P_{I_1}} + \overline{P_{I_2}})))]$$

where $\phi_2(\bullet)$ is determined using parameters applicable to the new handsets under consideration.

The characteristic function $C(\tau)$ associated with the total normalized aggregate interference, $(P_{I_1} + P_{I_2}) / (\overline{P_{I_1}} + \overline{P_{I_2}})$, is then given by $C(\tau) = C_1(\tau)C_2(\tau)$, which may be inverted to give the desired cumulative distribution function using Equation (F-20).

F.3.2   Discretely-Located Source Statistics

F.3.2.1   Discrete Source Mean Aggregate Interference Power

For sources having a known discrete distribution (e.g., the relative location (range) and height parameters associated with each source are known), two possible approaches may be used to determine the aggregate interference power, its mean and cumulative distribution function. Since the single source interference power in this case is still a random variable and is described by the product of a slow fading process and a fast fading process, similar to the case with randomly-located sources, the aggregate mean power may be computed as:

$$\overline{P_I} = P_o \sum_{k=1}^{n} (2L\psi_o(r_k) + \rho_o^2(r_k)) \exp[\sigma^2(r_k)/2 + \mu'(r_k, H_{E_k}, H_A, f_c)] \qquad \text{(F-21)}$$

where r_k and H_{E_k} denote the lateral range to and height of the kth emitter antenna, H_A is the aircraft antenna height, and n is the known number of discrete interference sources (Analytic Statistical method).

27

Alternatively, it is also possible to use a Monte Carlo simulation to determine the mean aggregate interference power. In this alternative, the received power from the kth interfering emitter is modeled as the product of a slow fading process (log-normally distributed) and a fast fading process having a non-central Chi-Squared distribution. The log-normal component is generated using the same two parameters, μ and σ as in the random source distribution while the Chi-Squared process uses the parameters, L, ψ_o and ρ_o.

F.3.2.2 Discrete Source Aggregate Interference Power Probability Distribution

F.3.2.2.1 General Discrete Source Aggregate Interference Power Probability Distribution

For discretely distributed interference sources, the characteristic function, $\phi_k(\tau)$, for the kth single emitter interference power can be computed as $\phi_k(\tau) = E[\exp(i\tau P_{E_k}(r_k, H_{E_k})/\overline{P_I}]$. This characteristic function can be written as:

$$\phi_k(\tau) \approx \sum_{m=1}^{M}(w_m / \sqrt{\pi})\Phi(\tau, y_m, r_k)$$

where the weights w_m and nodes y_m are as defined previously and r_k is the distance to the kth interference source. A good value for M would be 65 as in the case of randomly-located, uniformly distributed interference sources.

The characteristic function for the normalized aggregate interference, $C(\tau)$, can then be determined from:

$$C(\tau) = \prod_{k=1}^{n}\phi_k(\tau).$$

Similar to the uniform randomly distributed interference case, the distribution function is

$$\Pr(P_I / \overline{P_I} > z) = 1 - (1/(2\pi)) \lim_{A\to\infty} \int_{-A}^{A} ((1 - \exp(-i\tau z))/(i\tau))C(\tau)d\tau \qquad \text{(F-22)}$$

F.3.2.2.2 Discrete Source Aggregate Characteristic Function with Sectorization

The previous subsection describes in general the method to compute the aggregate characteristic function $C(\tau)$ from the discretely-located individual base station characteristic functions $\phi_k(\tau)$. However, in the discrete location cases where several angular sectors are defined to enable terrain modeling, some alterations need to be made. The method described above may be used to determine the characteristic function $C_n(\tau)$ for an individual sector assuming each of these characteristic functions have been normalized using the mean received aggregate factor for the

nth sector Fd_{AGGn} (used in place of $\bar{P}_I$ in previous section). Then the composite characteristic function $C(\tau)$ is defined in terms of the individual sector characteristic functions $C_n(\tau)$ by

$$C(\tau) = \prod_{n=1}^{N} C_n((Fd_{AGGn}/MF_{AGG}) \cdot \tau)$$

where n is the individual sector number, N is the total number of sectors, and MF_{AGG} is the overall mean aggregate factor for all the sectors. Once $C(\tau)$ is determined, the desired cumulative probability distribution function for the location can be computed with the inverse Fourier transform as in Equation (F-22) above.